Polymeric Thermochromic Dye for Improvement of Asphalt Pavement Durability

Prepared by:
Xiong (Bill) Yu and Jianying Hu

Technical Report Documentation Page

1. Report No. **FHWA/OH-2017-14**	2. Government Accession No.	3. Recipient's Catalog No.
4. Title and Subtitle **Polymeric Thermochromic Dye for Improvement of Asphalt Pavement Durability**		5. Report Date **January 2017**
		6. Performing Organization Code
7. Author(s) **Xiong (Bill) Yu and Jianying Hu**		8. Performing Organization Report No.
9. Performing Organization Name and Address **Case Western Reserve University Cleveland, OH 44106**		10. Work Unit No. (TRAIS)
		11. Contract or Grant No. **SJN 134661**
12. Sponsoring Agency Name and Address **Ohio Department of Transportation 1980 West Broad Street Columbus, Ohio 43223**		13. Type of Report and Period Covered **Final report**
		14. Sponsoring Agency Code
15. Supplementary Notes		

16. Abstract

Asphalt pavements features good performance and relatively low construction and maintenance costs. However, the black color of asphalt binder implies that the sunlight is not reflected but absorbed, which raises the temperature of the asphalt pavement and impairs its long-term durability. This project investigated the use of innovative polymeric thermochromic materials into asphalt binder to develop thermochromic asphalt binder, which will reduce the surface temperature of asphalt pavement during summer and lead to improved durability. Comparison measurements have found that the surface temperature of thermochromic asphalt binder is lower than that of the conventional asphalt binder. Besides the cooling effects, study showed that the surface temperature of thermochromic asphalt was higher than regular asphalt under low temperature. This means thermochromic asphalt can delay ice formation on the surface of road than traditional asphalt, which is an important potential benefits for road safety in cold regions The project conducted a pilot study to gauge the potential of thermochromic asphalt concrete to improve the durability of the pavement, reduce the environmental impacts, and mitigate ice related safety issues on the road.

17. Keywords **Thermochromic asphalt, sustainability, environmental benign, multifunctional asphalt**	18. Distribution Statement **No restrictions. This document is available to the public through the National Technical Information Service, Springfield, Virginia 22161**

19. Security Classification (of this report) **Unclassified**	20. Security Classification (of this page) **Unclassified**	21. No. of Pages **183**	22. Price

Form DOT F 1700.7 (8-72)   **Reproduction of completed pages authorized**

Polymeric Thermochromic Dye for Improvement of Asphalt Pavement Durability

Prepared by:

Xiong (Bill) Yu, Ph.D., P.E., Professor
Jianying Hu, Graduate Research Assistant
Department of Civil Engineering,
Case Western Reserve University

January 2017

Acknowledgments

EXECUTIVE SUMMARY

Asphalt pavements features good performance and relatively low construction and maintenance costs. However, the black color of asphalt binder implies that the sunlight is not reflected but absorbed, which raises the temperature of the asphalt pavement and impairs its long-term durability. Conventional cool pavement technologies reduce the surface temperature of roads regardless of the season. While this provides benefit for the hot summer season, has a detrimental negative impact during the winter season.

Thermochromic materials are substances that can reversibly change their colors in response to temperature. They reflect solar energy at high temperature and absorb that at low temperature. This project investigated the use of innovative polymeric thermochromic materials into asphalt binder to develop thermochromic asphalt binder, which will reduce the surface temperature of asphalt pavement during summer and lead to improved durability. Comparison measurements have found that the surface temperature of thermochromic asphalt binder is lower than that of the conventional asphalt binder with maximum decrease as high as 6.6 °C during typical summer day in the northeast U.S. (i.e. Cleveland, OH). Along with the cooling effects, the study showed that the surface temperature of thermochromic asphalt was higher than regular asphalt under low temperature. This means thermochromic asphalt can delay ice formation on the surface of road than traditional asphalt, which is an important potential benefits for road safety in cold regions. The thermal, optical, and mechanical properties of the thermochromic asphalt binders were characterized. Superpave binder grading was assigned to the thermochromic binders. The plant production conditions for thermochromic asphalt were determined with thermal and pyrolysis analyses. Experiments were also conducted to assess the performance of HMA prepared with thermochromic binders. The results from the experiments indicates that thermochromic HMA can achieve the performance requirements. The performance of the thermochromic HMA upon long term exposure was evaluated in an outdoor set up. The results indicate that the effectiveness of the thermochromic HMA was retained after long term exposure.

The project conducted a pilot study to gauge the potential of thermochromic asphalt concrete to improve the durability of the pavement, reduce the environmental impacts, and mitigate ice related safety issues on the road. This demonstrates innovation for development of sustainable and environmental benign infrastructure.

TABLE OF CONTENTS

LIST OF FIGURES

LIST OF TABLES

CHAPTER ONE

INTRODUCTION

1.1 Motivation for This Project

The majority of highways in Ohio and 94% of US highways are surfaced with asphalt. The conventional asphalt has high solar absorbance due to its dark color. Consequently, the surface temperature of asphalt pavement can be considerably higher during summer than pavement with a lighter surface, i.e., concrete pavement. The dark color also means asphalt roads radiate thermal energy faster during winter and therefore cool at a fast rate. The influence of thermal loads can be translated into reduced structural strength, increased rutting, accelerated aging of binders and thermal cracks; all compromising pavement performance. Pigments and seals have become available to change the color of an asphalt surface to make it lighter. However, common types of pigments are based on metallic powder or crystal salt, which does not have good compatibility with polymeric binders. ODOT experience indicated that the use of Verglimit, a crystalline phase change materials for thermal energy storage, resulted in failure of pavement. Polymeric dye, which feature excellent compatibility with asphalt binder, has promise to overcome the limitations and significantly increase the durability of asphalt road via its multifunctional roles.

1.2 Research Objectives

The goal of this research is to evaluate the effectiveness of multifunctional polymeric thermochromic dyes to increase the longevity of asphalt pavement via multifunctional roles of both improving its optical properties and microstructure. In the optical properties side, the selected polymeric dyes will feature a unique thermal-threshold infrared reflectance, i.e., it will effectively reflect infrared solar radiation above the temperature threshold. Therefore, the longevity of asphalt pavement will be increased by reducing the surface temperature of pavement during summer. Since solar modulation occurs only in the infrared range, there will be no visual impact on drivers. Besides, at the infrared reflectance thermal thresh, it will reduce the rate of cooling of asphalt road on cold weathers. In the microstructure side, the polymeric dyes function as a polymer modifier to existing asphalt binder and therefore may further improve its durability in terms of resistance to rutting and fatigue. The effectiveness of thermochromic properties will

be evaluated by measuring the surface temperature of dye treated asphalt concrete (i.e., to assess the reduction of its surface temperature variation). The effectiveness of microstructure performance will be measured by assessing the asphalt binder and asphalt concrete in terms of fatigue and rutting performance. For both types of testing, the un-modified asphalt concrete will be used as the baseline. The durability will be directly assessed based on the extension of pavement longevity from both thermal and microstructure aspects.

1.3 Research Background and Significance of the Work

As of 2001, there are about 2.5 million miles of paved roads in the United States. Maintenance and rehabilitation of aging pavement cost billions of dollars each year (FHWA 2001). The design of pavement, which is evolving from pure empirical to mechanistic-empirical procedures, has been focusing on the mechanical aspects. The goal is to ensure the pavement structure is sufficient to support the design traffic loads. A number of field experiences demonstrate the significant role of non-mechanical environmental factors, including moisture and temperature, in pavement deterioration. The thermal aspect of pavement is being recognized as a major factor determining the durability of pavement.

About 94 percent of the roads and highways in the United States are surfaced with asphalt (NAPA). The conventional asphalt has high solar absorbance due to its dark color. Consequently, the surface temperature on asphalt pavement can be considerably higher than that of a lighter surface, i.e., concrete pavement. The dark color also means the surface of the asphalt road emits thermal radiation faster when the environmental temperature is lower (such as in winter) and therefore might accelerate the icing process. The influence of thermal loads can be translated into reduced structural strength, increased rutting, accelerated aging of binders, and thermal cracks; all compromising pavement performance. The high surface temperature also accelerates green gas volatile emission as the asphalt binder breaks down.

Pigments and seals have become available to change the color of an asphalt surface to make it lighter, i.e., architectural asphalt. They however are suitable in most cases only for architectural considerations where color is a dominant criterion (EPA 2005). Besides, the artificial color can affect the driver perception of road conditions, as most drivers are accustomed to black (i.e. asphalt) or while (i.e., concrete) road. The change of visual appearance can potentially change the drivers' perception, especially at high speeds.

Most pigments are based on metallic powder or crystal salt. Therefore, they can cause problems in the bonding deterioration in the asphalt binder. In this study, we will evaluate the use of polymeric thermochromic dye to modulate the thermal response of asphalt pavement. The polymeric dye will feature much better thermal and solution stability as well as compatibility with asphalt binder.

1.3.1 Influence of Temperature on Performance of Asphalt Pavement

A number of field and laboratory experiments demonstrate the significant role of temperature on pavement durability under both hot and cold weather conditions (Shami et al. 1997). For example, study by Huang et al. (2008) showed that the rutting typically occurred when the surface temperature of asphalt pavement is above 20°C; the higher the surface temperature the higher the potential of rutting occurrence. Low pavement temperature is related to thermal cracks, which is a major cause of pavement deterioration in cold regions such as Ohio. Figure 1.1 shows examples of measured data on the effects of pavement temperature on asphalt performance properties. The data demonstrates that higher temperature caused considerable increase of asphalt rutting and permanent shear strain.
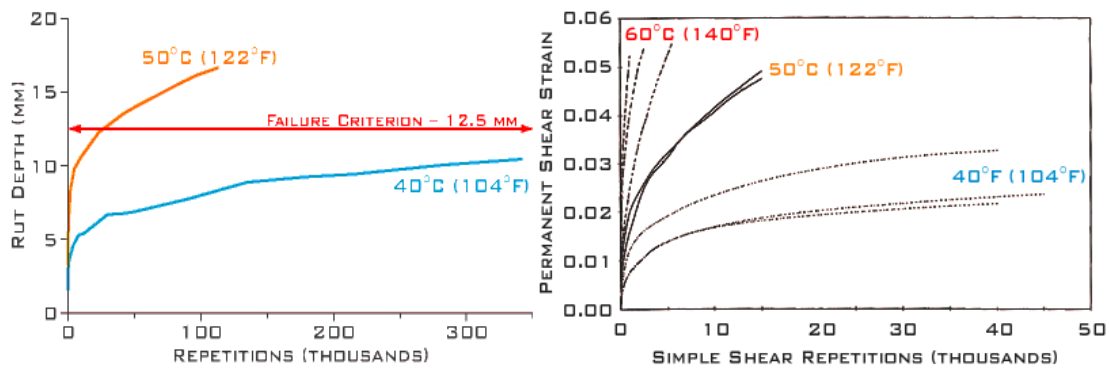
Fig. 1.1 Temperature effects on rutting and permanent shear strain of asphalt concrete[1]

1.3.2 Properties Determining Thermal Energy Balance in Pavement Surfaces

The temperature of the road surface is affected by three major thermal exchange mechanisms: absorption of the incident solar energy, thermal radiation to the atmosphere and thermal convection with the air close to the road surface (Fig. 1.2(a)). The direct source of heat for

---

[1] http://heatisland.lbl.gov/Pavements/Durability/

3

pavement comes from solar radiation. The surface temperature on roads can be unpleasantly high during summer (Fig. 1.2(b)).
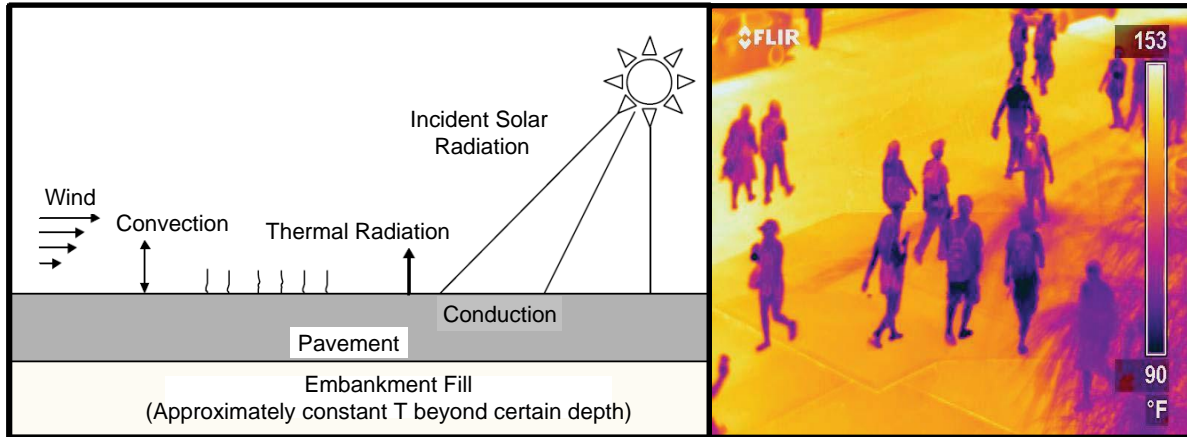
Fig. 1.2 a) Thermal balance on pavement; b) Surface temperature (EPA 2009)

There are two major properties of pavement materials affecting pavement thermal balance, i.e., solar reflectance and thermal emittance. Solar Reflectance (SR)/Solar Absorbance (SA) is the percentage of solar energy reflected/absorbed by a surface. They are the main determinant of a material's maximum surface temperature. SA and SR are dependent and are related by the following equation:

$$SA+SR=100\%$$

Thermal Emittance (SE) determines how much heat it will radiate per unit area at a given temperature. In another word, SE describes how readily a surface sheds heat.

Figure 1.3(a) is an example result produced using the thermal transfer model developed at NIST by Bentz (2000). The result shown in Figure 1.3(b) occurs when the ambient temperature is within 3 degrees below the surface temperature, the heat loss by thermal radiation/emission is the dominant factor over the heat loss by convection (assume wind speed of 5 m/s).
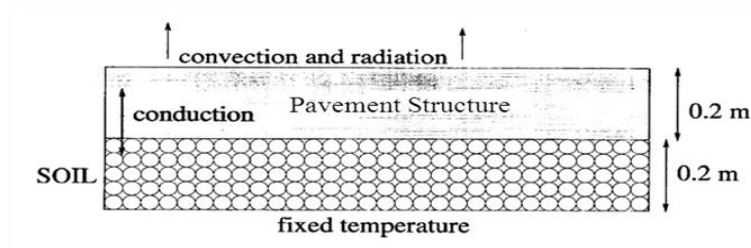
(a)
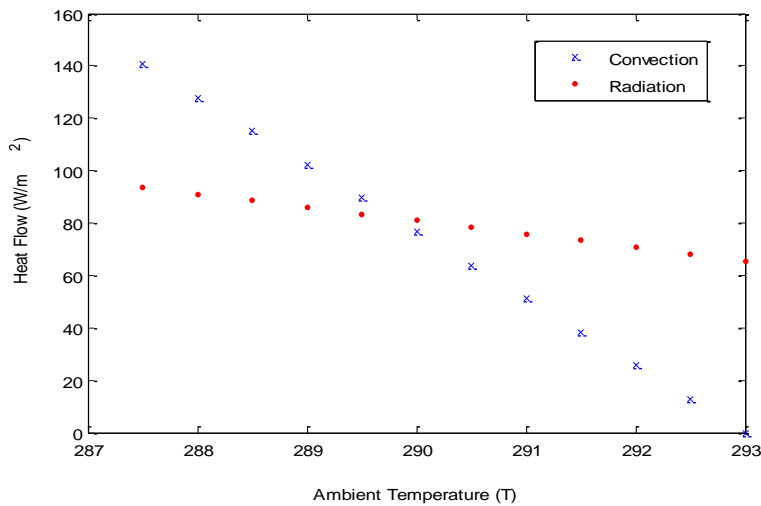
(b)

Fig. 1.3 a) Schematic of the pavement heat transfer model; b) comparison of heat loss from pavement structure by thermal radiation/emission versus by convection (assume wind speed of 5m/s) (Yu 2009, unpublished data)

Therefore, solar reflectance and thermal emittance are the most important factors in determining how pavement cools down or heats up. Solar reflectance has a major role on the maximum surface temperature while the thermal emmitance/radiation determines the minimum temperature (Levinson et al. 2002). Among these two important properties, there are only limited options to change the thermal emittance because most pavement materials inherently have high emittance values. Changing the solar reflectance can have a major impact on the surface temperature of pavements. From Figure 1.4, it can be seen that at the same solar input, changing the solar reflectance of an ordinary asphalt road to that of concrete will result in at least a 10 degree drop in the road temperature. This means a significant reduction of rutting, aging and emission of volatiles in asphalt roads.
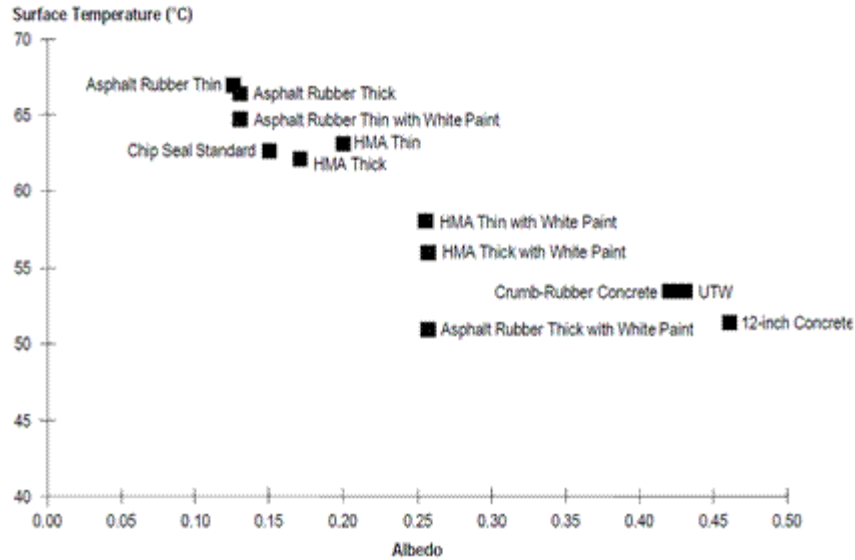
Fig. 1.4 Surface Temperature and Solar Reflectance (Albedo) for Selected Types of Pavements in Phoenix, Arizona (Golden and Kaloush 2004).

1.4 Technical Concept and Feasibility

Figure 1.5 shows a standard solar spectrum. Approximately, five (5) percent of solar energy is in the UV spectrum (200-400 nm), 43 percent of solar energy is visible light (400nm-700nm), and the remaining 52 percent of solar energy is in the infrared range (700nm-5000nm). Considering the fact that nearly half of solar energy is from infrared radiation, increasing the solar reflectance/absorbance in the infrared range would reduce the surface temperature of asphalt pavements without changing their visual appearance. This is the key of the proposed innovation in this project.
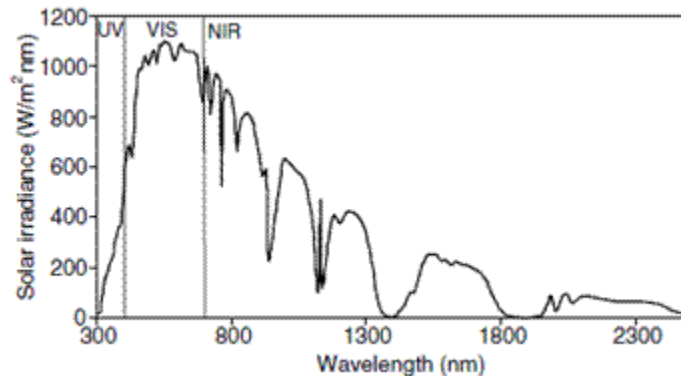
Fig. 1.5 The solar spectrum (ASTM Standard G159-91)

6

Thermochromic materials are smart materials whose optical properties change with temperature. There are a few types of materials demonstrating thermochromic properties. Traditional thermochromical materials are typically based on metallic oxide paints. For example, vanadium dioxide (VO_2) is able to undergo a reversible transition at a critical temperature, below this temperature the material is monoclinic, semiconducting and relatively infrared transparent; above the critical temperature, it is tetragonal, metallic and infrared reflecting. The transition temperature of pure bulk VO_2 is 68°C, which can be changed by doping with a few other metals (Granqvist 2007). Figure 1.6 shows the solar transmittance (which is inversely related to solar absorbance) changed significantly in the infrared range while the transmittance spectra in the visible range are not affected.
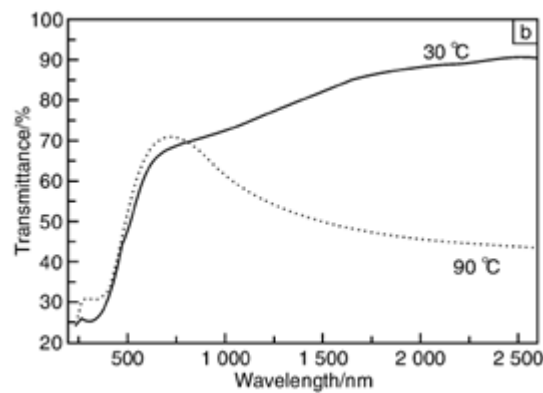
Fig. 1.6 Thermochromic transmittance spectra of solution derived VO_2 film (Luo and Gao 2009)

These traditional thermochromic materials based on metallic powder or crystal salt, while functioning as a solar modulator, have poor compatibility with asphalt binders. Therefore, they can accelerate bonding deterioration in the asphalt binder.

Thermochromic polymers are an emerging group of smart materials that achieve temperature-dependent solar modulation. An example is shown in Figure 1.7. In addition, as they are made of polymeric materials, thermochromic polymers feature excellent compatibility with asphalt binders. Therefore, they are promising to be effective in modulating the surface temperature of pavement.
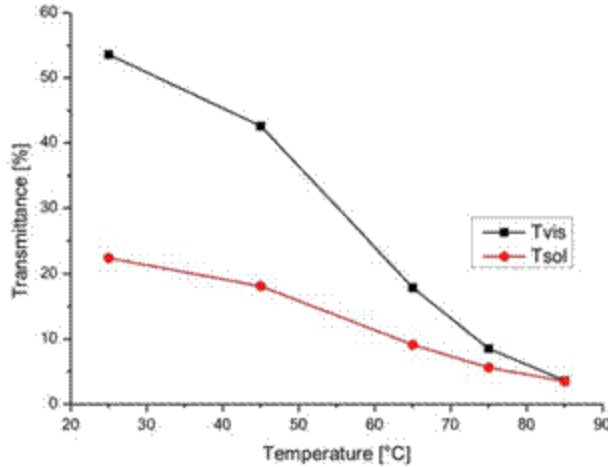
Fig. 1.7 Temperature dependent transmittance behavior of a Ligant-Exchange Thermochromic System (Tvis: Total light transmittance in the visible range 380–770 nm, Tsol: Total solar transmittance range 300–2,500 nm) (Seeboth et al. 2010).

1.5 Organization of the Report

This report presents the development of innovative thermochromic asphalt technology to dynamically modulate the surface temperature of pavement (i.e.-to make pavement cooler during summer and warmer during winter). It is organized into six chapters as follows:

- Chapter one provides background information pertaining to this research. It contains research motivation, background information, and technical feasibility analyses.
- Chapter two reviews the literature discussing the common types of thermochromism. In particular, the literature review focuses on identifying technologies that have potential for applications in asphalt.
- Chapter three presents the preliminary design and thermal performance evaluation of thermochromic asphalt binders.
- Chapter four describes the experimental characterization of the optical properties of thermochromic asphalt binders.
- Chapter five describes the mechanical characterization of the asphalt binders. Superpave binder performance tests were conducted to evaluate the mechanical performance of asphalt binders.
- Chapter six characterizes the thermal properties of thermochromic asphalt binder. Recommendations are provided on the production conditions for different thermochromic

asphalt binders.

- Chapter seven describes the evaluation of thermochromic asphalt binders' performance via an extended outdoor evaluation program. The performance of thermochromic asphalt binders was determined.

- Chapter eight summarizes the research activities. It also provides conclusions and recommendations of future study.

1.6 References

(1) ASTM Standard E903-96. (1996). Standard Test Method for Solar Absorptance, Reflectance and Transmittance of materials using integrating spheres. Standard Book of ASTM Annual Book, ASTM publisher.

(2) ASTM Standard G159-91. (1991). Standard Tables for References Solar Spectral Irradiance at Air Mass 1.5: Direct Normal and Hemispherical for a Tilted Surface, Standard Book of ASTM Annual Book, ASTM publisher.

(3) Bentz, D.P. (2000). A computer model to predict the surface temperature and time-of-wetness of concrete pavements and bridge decks, NIST Research Report. U.S. Department of Commerce. 29p.

(4) Environmental Protection Agency (EPA). 2005. Cool Pavement Report, Cambridge Systematics, Inc., 63p.

(5) EOL-LCA (2010). http://www.eiolca.net/Method/index.html.

(6) Golden, J.S., Kaloush, K.E. (2004). SMART Program, and Arizona State University, July 24, 2004.

(7) Granqvist, G.C. (2007). Transparent conductors as solar energy materials: a panoramic review, Sol. Energy Mater. Sol. Cells 91, 1529–1598.

(8) Huang, X.M., Li, H., Zhang, J.P. (2008). Simulation of Rutting Behavior of Asphalt Pavement Based on Real Temperature Field, Transportation Research Board Annual Meeting 2008 Paper #08-0372.

(9) Luo, H.J., Gao, Y.F. (2009). Solution processing and optical properties of VO2 Thermochromic Materials, Materials China, 28(1): 38-42.

(10) National Asphalt Pavement Association (NAPA). http://www.hotmix.org/index.php?option=com_content&task=view&id=379&Itemid=862.

(11) Shami H.I., Lai, J.S., D'Angelo J.A. and Harman, T.P. (1997). Development of temperature-effect model for predicting rutting of asphalt mixtures using Georgia loaded wheel tester, TRB Annual Meeting, Washington, DC , paper No. 1590.

(12) Synnefa, A., Santamouris, M., Apostolakis, K. (2007). On the development, optical properties and thermal performance of cool colored coatings for the urban environment, Solar Energy, 81: 488–497.

(13) Yu, X. (2009). Thermal exchange at surface of pavements using NIST model, unpublished data.

(14) Seeboth, A., R. Ruhmann, O. Mühling (2010). Thermochromic and Thermtropic Polymer Based Materials for Adaptive Solar Control, Materials, 3(12): 5143-5168.

(15) Lucht, B.L., Euler, W.B. (2009). Development of Thermochromic Paints, Plastics, and Rubbers for Rapid Visual Assessment of Temperature, URITC Project Report No. 536152-536183.

(16) Ma, Y.P., Zhu, B.R. (2009). Research on the preparation of reversibly thermochromic cement based materials at normal temperature, Cement and Concrete Research, 39(2): 90-94.

CHAPTER TWO

LITERATURE REVIEW: PROGRESS ON THERMOCHROMIC MATERIALS AND APPLICATIONS

Thermochromic materials change their colors and spectral properties when exposed to appropriate temperature or temperature range. Polymer, organic and inorganic thermochromic materials were summarized together with their mechanisms in the present paper. Recently, inorganic-organic hybrid became a promising category, which combines advantages of both inorganic and organic thermochromic materials. A large number of research and commericial application focuses on VO_2. An extensive discussion on challenges of VO_2 films is detailed, including high phase transition temperature, low luminous transmittance, small solar modulation (change in solar transmittance), unattractive color, long-term stability, wide temperature hysteresis, high emissivity, and low reflection to far-infrared region of the spectrum. These issues can be partially addressed by introducing dopants, additional layers, using nanostructure, controlling thickness or roughness of films, or adjusting the preparation process. Nanostructured VO_2 particles and their synthesis methods will also be discussed. The advantages of polymeric thermochromic materials for use in asphalt are highlighted at the end of the review.

2.1 Introduction

Chromogenic materials, one particular smart material, are substances that exhibit changes in their colors and spectral properties in response to external stimulus. Such chromogenic materials involve thermochromic (Seeboth et al. 2014), photochromic (Zhang et al. 2014), electrochromic (Wang et al. 2010), gasochromic (Han et al. 2014), piezochromic (Li, W. et al. 2013), ionochromic (Minkin et al. 2014), and biochromic (Sharkany et al. 2005) materials, which are sensitive to temperature, light, electric field, oxidizing or reducing gas, pressure, ion concentration, and biochemical reaction, respectively. Among these chromogenic materials, the thermochromic materials, which turn at a definite temperature or in a temperature range into a white and reflective state, have been known for decades, many based on transition oxides like VO_2. One potential application is used in smart windows, which can intelligently change their spectral properties when triggered by an external stimulus (Granqvist 2007). The present review

is to introduce various kinds of thermochromic materials and their mechanisms. The former and ongoing improvement strategies of VO_2 films and nanoparticles will be summarized. Finally, the application of thermochromic materials and performance will be presented, especially in smart windows.

2.2 Categories and Mechanisms

A wide variety of materials have been found to exhibit thermochromic properties, including polymers, organic, inorganic compounds. Inorganic and polymer based thermochromic materials have been extensively reviewed in studies (Granqvist 2007, Li et als. 2011, Seeboth et al. 2008 and 2010), providing information on the current progess in material science developments, switching characteristics of the various material formulations, and an assessment of market maturity. Depdending on the mechanism that causes the color change, thermochromic materials can be devided into: phase transitions (e.g., in an organic chromophore), changes in ligand geometry, variation in the crystal field or the number of solvent molecules in the coordination sphere (e.g., in a pure transition metal complex that derives its color from crystal field effects, and other more complex mechanisms. Fig. 2.1 summarized various thermocromic materials and their mechanisms. Recently, Seeboth et al. (Seeboth et al. 2014) detailed the thermochromism for polymers, including temperature runnable photonic crystals, nanoparticle based effects (surface plasmon absorption and quantum dots), and dye-dye or polymer-dye aggregation-disaggreagation mechanisms. Additonaly, Naumov (Naumov et al. 2011) proposed a new thermochromism that the thermochromism of overcrowded polycyclic aromatic enes stems from large molecular distortions due to increased thermal oscillations of the two halves of the molecules around the central bridge.
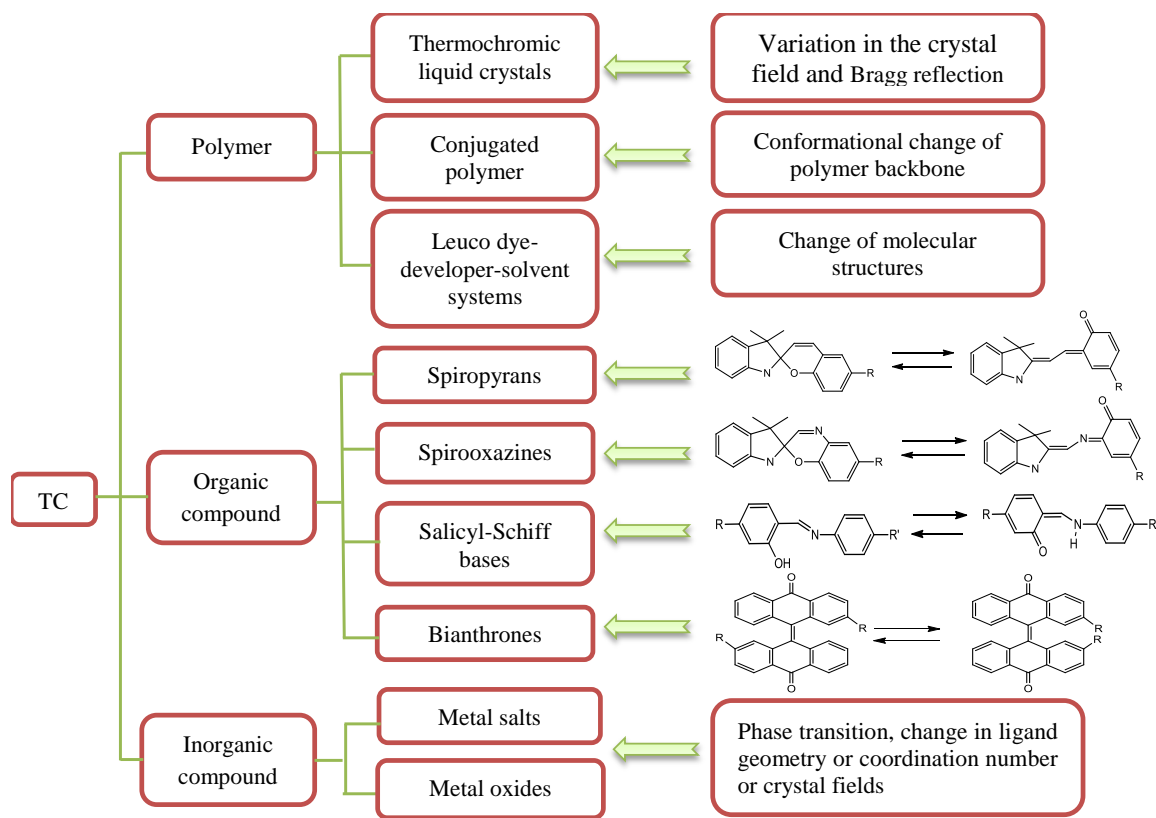
Fig. 2.1. Classifications and mechanisms of thermochromic (TC) materials.

Organic compounds containing spiropyrans, spirooxazines, salicyl-Schiff bases, or overcrowded ethylens, show thermochromic phenomena (Chen and Yan 2009, Crano and Guglielmetti 1999, Lee et al. 2006). Some polymers, thermochromic liquid crystals (like polypeptide vinyl monomer liquid crystals, cholesterol ester), conjugated polymers (like polysilane, polythiophene, polydiacetylene, poly (phenylene vinylene), and leuco dye-developer-solvent system, exhibit thermochromic properties (Seeboth and Lötzsch 2008, Park et al. 2007, Yu et al. 2008, Yarimaga et al. 2010, Chen et al. 2011, Karlessi et al. 2009, Tang et al. 2010). Polymers and organic compounds and systems present adjustable switching temperature, relatively low switching temperature, non-toxic features, with poor light stability.

Metal salts and metal oxides are typically inorganic thermochromic compounds, e.g. Cu_2HgI_4, ZnO and In_2O_3, $Cr_2O_3-Al_2O_3$), $Et_2NH_2)_2CuCl_4$, $CoCl_2$. Inorganic thermochromic compounds display thermochromic behavior upon exceeding a wide range of temperature, generally at 70-500°C (Seeboth and Lötzsch 2008). With a view to application of thermochromic materials in buildings, VO_2 is the most suitable inorganic compounds since their switching temperature could

14

be lowered from 68°C to room temperature, which will be elaborated in the following context. Inorganic themrochromic materials feature thermostability above 200 °C and light stability while are toxic, have relatively high and fixed switching temperatures, and show irreversibly thermochromic transition. To combine advantages of organic, polymer and inorganic compounds, organic-inorganic hybrid thermochromic materials were proposed and have been considered as one of the most likely candidates for new functional materials. Table 2.1 shows some recent examples of hybrided thermochromic materials.

Table 2.1. Examples of organic-inorganic hybrid thermochromic materals

Organic-inorganic hybrid	Properties	Ref.
$K_{12.5}Na_{1.5}[NaP_5W_{30}O_{110}]$	Color changes gradually from yellowish to blue when heating from 120 °C to 180 °C	Jiang et al. 2004
Poly (vinyl alcohol)-cobalt	Thermochromic behavior is observed	Srivastava et al. 2006
$(C_{12}H_{25}NH_3)_2FeCl_4$	A reversible phase transition near 60 °C	Guo et al. 2006
$\{[Cu_2I_2(Hgtsc)]\cdot 2DMF\}n$ (1A) (Hgtsc=glyoxal-dithiosemicarba-zone)	Color change of organge to yellow at 120 °C, irreversible	Li et al. 2012
Cobalt(II) chloro-complexes	Color changes from pale pink to dark blue based on the geometry change from octahedral to tetrahedral	Gadžurić et al. 2012
Ag/polydiacetylene (PDA)	Only exhibits a red phase	Yokoyama et al. 2009
PDA/ZnO	Color changes from blue to purple at about 90 °C, and irreversibly changes from purple to red at 145 °C.	Traiphol et al. 2011
PDA/SiO$_2$	Reversible blue/purple color transition and high thermal stability	Chanakul et al. 2013

2.3 Thermochromic Films and Nanocomposite

VO₂ Films

Vanadium dioxide (VO_2) is the most interesting and extensively studied thermochromic material since it was found to exhibit phase transition from monoclinic VO_2 (M) (semiconductor) to tetragonal rutile VO_2 (R) structure (metal), accompaning a significant reversible change in its electrical and optical properties occurring at transition temperature T_c (approximate 68 °C) (Morin 1959). Optically, VO_2 films exhibit good infrared transmission in the insulating monoclinic phase below the transition temperature, while the metallic phase is highly reflective in the infared region of the spectrum. Therefore, VO_2 can be employed as thin films in smart windows that inhibit a near infrared spectra transmission at high temperature, and permits the transmission at low temperature to control solar/heat automatically without extra energy input (Manning et al. 2002). However, VO_2 is not immediately applicable to windows and commercialization in large scale due to the following three main challenges (Granqvist 2007, Mlyuka et al. 2009, Li et al. 2012, Warwick and Binions 2014, Gao et al. 2012): (i) The switching temperature (τ_c) of VO_2 is typically 68 °C, which is higher than the comfort temperature of approximate 25 °C in buildings; (ii) Solar modulation, expressed by $\Delta T_{sol}=T_{sol}$ ($\tau<\tau_c$) $- T_{sol}$ ($\tau>\tau_c$), is not usually larger than 10%. (iii) Luminous transimission (T_{lum}) in the visible range is typically lowered to 43% (Xu et al. 2004, Jin et al. 2003, Lappalaninen et al. 2008). Films suitable for use in architectural windows should possess visible transmittance values in excess of 60% (Sobhan et al. 1996, Blackman et al. 2009).

Substantial strategies have been investigated to address all of these challenges, including doping various elements, formation of composite, regulation of roughness and thickness of VO_2 film, deposition of anti-reflective layers, nanostructured, and control of processing conditions of VO_2 particle. The results of recent progesses on these techniques are summarized in Table 2. 2-4. To reduce the transition temperature, the doping of W is found to be the most promising strategy, lowering about 27 °C per 1 at % W doping (Shi et al. 2007). Besides the transition temperature, the luminous transmittance (T_{lum}) and solar transmittance modulation (ΔT_{sol}) can be enhanced with a relative balance by using the multilayer structure containing anti-reflecting layers based on oxides of Si, Ti, Zr, Ce and Al. It is expected that some of theses oxide layers are also able to protect VO_2 from oxidation and generate new functions such as photocatalysis.

Table 2.2. Strategies for decrease of phase transition temperature (τ_c) of VO$_2$ composite.

Solutions		Transition Temperature (τ_c)	Refs.
Doping	W	Reduction of 22 °C per atomic%	Manning et al. 2004
	W	Reducing of 27 °C per 1 at.% doping	Shi et al. 2007
	W	Reduction of 20 °C per 1 at.%	Fu et al. 2006; Blackman et al. 2009
	W	Reducing of 19.8 °C per 1 at.% doping	Yan et al. 2008 (a)
	W	Reducing from 63 °C to 28 °C	Batista et al. 2009
	W	Reducing from 69.5 °C to 37.8 °C doping 1.58 mol% W	Ye et al. 2010
	W	Reduction of 21.96 °C per at % of W in the doping range from 0 to 2.5 at. % W	Ji et al. 2011
	W	Decresing from 64 to 54 °C	Luo et al. 2011
	W	30 °C	Huang et al. 2011
	W	Reduction of 15.5 °C/mol	Cho et al. 2012
	W	Decreases from 62 °C to 37 °C at a doping level of 1 at.%	Zhao et al 2013
	W	33.5 °C by 1.8 at% tungsten doping	Xiao et al. 2014
	Mg	Reducing of 3 °C per 1 at.% Mg	Mlyuka et al.2009 (a)
	Mo	Reducing of 15 °C per 1 at.% Mo	Hanlon et al. 2003
	Mo	47 °C	Manning et al. 2005
	W, Mo, Nb	Reduciong of 7 °C per at.% W, 3 °C per at.% Mo, 2 °C per at.% Nb	Batista et al. 2010
	W, Mo	40.8 °C with 4% W, 56.6–63.6 °C with 1% Mo	Zhang et al. 2012
	W, Mo, F	53, 56 and 53 °C with the doped W, Mo and F atoms	Zhang et al. 2013

	F-W co-doping	Reduction of 15 °C/at.%	Burkhardt et al. 2002
	Mo-W co-doping	36 °C with 0.5 at.% of Mo and 0.25 at.% of W	Yan et al. 2008 (a)
	F	~60 °C	Kiri et al. 2011
	Ce	Reducing 4.5 °C per 1 at.% doping	Song et al. 2013
	Mo–W co-doping	15.69 °C (cooling) and 19.5 °C (heating)	Lv et al. 2014
Multi-layer	Pt/VO$_2$ double-layered films	Decreasing from 67.8 to 58.5 °C	Kang et al. 2010
	ZnO: Al/VO$_2$/substrate film		Kang et al. 2011(a)
	VO$_x$-W-VO$_x$ sandwich structure	54 °C	Luo et al. 2011
Applying thermal stress	VO$_2$/c-sapphire, VO$_2$/MgO(111)	44.8 °C, 57.8 °C	Koo, et al 2012
Nanocomposite	VO$_2$ film	35 °C	Chen et al. 2007
	W-doped nanocrystals	24.2 °C with 2.5 at% W doping	Kong et al. 2011
	Nano-structured porous film	58.3 °C	Xu et al. 2013
	Nanopowder	55.5 °C	Ji et al. 2011
	Nanopowder	-14.5–5 °C	Dai et al. 2011
	Nanostructured VO$_2$ film	35 °C	Chen et al. 2012
	Mg-doped	Reduction of 2 °C per at% Mg	Zhou et al. 2013

	VO$_2$ nanoparticle			
	W-doped VO$_2$ nanoparticle	Reduction of 20 °C per W at%		Li et al. 2009
	W-doped VO$_2$ nanoparticle	26.46 °C		Peng et al. 2007
Processing conditions	Annealing at 440 °C	42.7 °C		Zhang et al. 2010 (a)

Table 2.3. Strategies for enhancement of solar modulation (ΔT_{sol})

Strategies		ΔT_{sol}	Refs.
Doping	W	37.3% at 2000 nm	Xiao e tal. 2013
	W, Mo, Nb	35% with 5% W, 36 to 25% with Mo from 3 to 11%	Batista et al. 2010
Composite	VO2/ Sb : SnO$_2$/polymer	6.9%	Gao et al. 2012 (b)
Multi-layers	substrate/VO$_2$/TiO$_2$	highest 15.1%	Chen, Z. et al. 2011
	CeO$_2$/VO$_2$	55% at 2500 nm	Saitzek et al. 2007
	TiO$_2$/VO$_2$/F-doped SnO$_2$/substrate	8.8%	Zhang et al. 2011
	Si-Al coating/VO$_2$	7.7%	Liu et al. 2013
	TiO$_2$/VO$_2$/TiO$_2$/VO$_2$/TiO$_2$	12.1%	Mlyuka, et al 2009 (b)
	ZnO/VO$_2$/ZnS with thickness of 3/4-1/4-3/4	13.01%	Zhao et al. 2013
	VO2/ZnO:Al double-layer film	27% at 2000nm	Chu et al. 2014
Nanocomposite	VO$_2$ nanoparticles in dielectric hosts	>20%	Li et al. 2010
	Nanoporous films	14.1%	Kang et al.

			2011(b)
	SiO$_2$/VO$_2$ core/shell structures	13.6%	Gao et al. 2012 (a)
	VO$_2$(M)@SiO$_2$ foil	8.4%	Li, R. et al. 2013
	Mg-doped VO$_2$ foil	10.6%	Zhou et al. 2013
	indium tin oxide–VO$_2$-based nanocomposites	10%	Granqvist et al. 2014
	Mg-doped VO$_2$ film	10%	Li et al. 2014
	Nanoporous VO$_2$ film	~14.7%	Cao et al. 2014
Processing conditions	Annealling at 450 °C	8.8%	Zhao et al. 2013
Microghness of film	Zn/V=0.08, Zn/V=0.1	11.3%, 10.5% at room temperature	Du et al. 2013

Table 2.4. Strategies for enhancement of luminous transition (T$_{lum}$) of VO$_2$ films.

Strategies		T$_{lum}$	Refs.
Doping	F	Increas from 34.8% to 38.6%	Khan and Granqvist, 1989
	F	Increase 15% at 2500 nm	Kiri et al. 2011
	Mg	Increase from 41% to 51%	Mlyuka, et al 2009 (a)
	W	48% at 2000 nm	Xiao e tal. 2013
Composite	VO$_2$/SiO$_2$	75% at 700 nm with Si/V ratio of 0.05	Chen et al. 2004
	VO$_2$/ Sb : SnO$_2$/polymer	51–55% at $\tau<\tau_c$ and 49–55% at $\tau>\tau_c$	Gao et al. 2012 (b)
Multi-layers	TiO$_2$/VO$_2$/TiO$_2$	Increase from 31% to 58%	Jin, et al 2003
	VO$_2$/ZrO$_2$	Increase from 32% to 55%	Xu et al. 2004

	TiO$_2$/VO$_2$/TiO$_2$/VO$_2$/TiO$_2$	45% at $\tau<\tau_c$ and 42% at $\tau>\tau_c$	Mlyuka, et al 2009 (b)
	Pt/VO$_2$	37.9% at room temperature	Kang et al. 2010
	substrate/VO$_2$/TiO$_2$	61.5% at room temperature	Chen, Z. et al. 2011
	TiO$_2$/VO$_2$/F-doped SnO$_2$/substrate	44.0% at room temperature	Zhang et al. 2011
	Si-Al coating/VO$_2$, F-Si AR coating/VO2	47.5%, 39.5%	Liu, et al 2013
	ZnO/VO$_2$/ZnS with thickness of 3/4-1/4-3/4	63.24% at T<Tc and 57.39% at T>Tc	Zhao et al. 2013
	TiO$_2$/VO$_2$	about 48% at 630 nm and 20 °C, about 30% at 630 nm and 85 °C	Wang et al. 2013
	VO$_2$/ZnO:Al double-layer film	48% at 80 °C and 43% at 20 °C	Chu et al. 2014
Nanocomposite	Nanoporous VO$_2$ films	43.3% at $\tau<\tau_c$ and 39.9% at $\tau>\tau_c$	Kang et al. 2011 (b)
		45–60%	Ji et al. 2011
	VO$_2$ nanoparticles in dielectric hosts	59%	Li et al. 2010
	Nanostructured VO$_2$ film		Chen et al. 2012
	ITO–VO$_2$-based nanocomposites	59.7% at $\tau<\tau_c$ and 51.1% at $\tau>\tau_c$	Granqvist et al. 2014
	VO$_2$(M)@SiO$_2$ foil	35.9%	Li et al. 2013
	Mg-doped VO$_2$ foils	54.2%	Zhou et al. 2013
	Mg-doped VO$_2$ film	about 82% at $\tau<\tau_c$ and 77.5% at $\tau>\tau_c$	Li et al. 2014
	Nanoporous VO$_2$ film	~50%	Cao et al. 2014
Processing conditions	Annealing at 450 °C	41.5%	Zhao, et al 2013
	Annealed at 750 °C	>40%	Wang et al. 2013

Thickness of film	59 nm thick single-layer VO$_2$ film	54.1% at $\tau < \tau_c$ and 49.1% at $\tau > \tau_c$	Zhang et al. 2010 (a)
Microghness of film	Zn/V=0.08, Zn/V=0.1	50.5%, 59.3% at room temperature	Du et al. 2013

Additional drawbacks of VO$_2$-based films also restrict their practical implementation, listed in Table 5. Pure vanadium dioxide is a yellow/brown color, which is unpleasant to the human eye (Manning et al. 2002). This issue can be tackled by doping high concentration of tungsten (Blackman et al. 2009), gold nanoparticles (Binions et al. 2008, Saeli et al. 2010) and fluorine (Kiri et al. 2011). However, doping with gold nanoparticles is not practical due to the high cost of gold and the surface plasmon resonance of the gold nanoparticles, which changes with the dielectric constant and hence the films are different colors in the hot and cold states. Another issue is the long-term stability since thermodynamically unstable VO$_2$ oxides to V$_2$O$_5$ when it is exposed to the air for a long period (Lindstrom et al. 2006). The long-term durability of VO$_2$ films was trying to improve by depositing a top coating to serve as chemical protection, such as CeO$_2$, ZnO: Al, and TiO$_2$.

Besides the above mentioned issues, the VO$_2$ films with wide hysteresis of phase transition temperature began to be taken into account recently. In principle, 20~26°C is considered to be a favorable temperature range for human comfort, so hysteresis higher than ~6°C will be inappropriate for real applications. However, films prepared using powders in reported studies commonly exhibited a very wide hysteresis (Zhang et al. 2010 (a), Gao et al. 2012 (c)).

For application of VO$_2$ films in winter, the emissivity of films should be low to prevent heat loss. However, in the wavelength range for thermal radiation of objects at room temperature (3–50 μm), the emissivity for VO$_2$ films is too high, i.e., 0.85 for monoclinic and 0.84 for rutile phase (Kang et al. 2011). The deposition of anti-reflection layer and the increase in microroughness of the film have been found to reduce emissivity of VO$_2$ films (Zhang et al. 2011, Du et al. 2013).

Recently another proposed problem is that the VO$_2$ film has little reflective capacity to far-infrared region, like 3–50 μm (Granqvist 1981 and 2007). They come from objects in or outside the room, like human body, air condition, electric heater, furniture, ground, and building. To reduce energy consumption in far-infrared region (>3 μm), a new glazing with VO$_2$/3% Al$_2$O$_3$–

ZnO double-layer film was manufactured and showed improved reflecting capacity and lower emissivity (Chu et al. 2014).

Table 2.5. Other challenges and Solutions of VO_2 films.

Drawbacks	Strategies	Results	Refs.
Unattractive film color	Dope W	blue tinge	Blackman et al. 2009
	Dope Au	a variety of greens and blues	Binions et al. 2008, Saeli et al. 2010 (b)
	Dope F	lighter color	Kiri et al. 2011
	Mg	Shift from yellow to blue	Zhou et al. 2013
Wide hysteresis		8 °C	Wu et al. 2013
		5 °C	Wang et al. 2013
		10 °C	Gao et al. 2012 (d)
Long-term stability	Deposite CeO_2 film	limiting the chemical evolution under aggressive wet atmospheres	Saitzek et al. 2007
	Deposite ZnO:Al coating	strong thermochromic properties after oxidization	Kang et al. 2011 (a)
	DepositeTiO_2 film	enhanced resistance to chemical deterioration	Evans et al. 2007
	SiO_2/VO_2 core/shell structure	Enhanced chemical stability	Gao et al. 2012
	Deposite 30 nm Al oxide	delayed the oxidation	Ji et al. 2014
High emissivity	VO_2/ F-doped SnO_2/glass, TiO_2/ VO_2/ F-doped SnO_2/glass	0.19 at $\tau<\tau_c$ and 0.27 at $\tau>\tau_c$, 0.13 at $\tau<\tau_c$ and 0.24 at $\tau>\tau_c$	Zhang et al. 2011
	Increase roughness by using $ZnCl_2$	0.20 at $\tau<\tau_c$ and 0.33 at $\tau>\tau_c$	Du et al. 2013
Low reflecting capacity in the far-	VO_2/Al_2O_3–ZnO double-layer film	reflecting capacity of 49.2%, lower emissivity of	Chu et al. 2014

infrared region		0.66	

Properties of VO₂ films are also influenced by their prepation techniques. Until now, two basic methods have been developed to fabricate VO₂ films, inclcuding gas-phase deposition method and solution based deposition method. The gas-phase depositon method is the most commonly used and studied method for the fabrication of VO₂ films, including chemical vapor deposition (Takei and Soide 1966, Manning et al. 2002 and 2004, Mathur et al. 2007, Vernardou et al. 2004 and 2008, 2006 and 2011, Blackman et al.2009, Kiri et al. 2011), physical vapor deposition (Guinneton 2004), pulse laser deposition (Lysenko et al. 2009, Chen, B. et al. 2009, Soltani et al. 2006), RF sputter deposition (Li et al. 2014), ion implantation (Lopez et al. 2002), atomic layer deposition (Rampelerg et al. 2011, Blanquart et al. 2013, Povey et al. 2007, Zhang, K. et al. 2013, Madhavi et al. 2014, Kim et al. 2014) and recently new proposed high power impulse magnetron sputtering (Fortier et al. 2014). These methods yield superior quality films with precise control over process parameters such as oxygen partial pressure (typically in the range 0.06–0.13 Pa), and film features, including thickness and microstructure. However, these methods are not suitable for practical manufacturing because of complex control parameter, unstable technology, the necessity of special and expensive equipment, and high costs (Peng et al. 2007).

Alternatively, a solution based deposition method (e.g. sol-gel) to prepare VO₂ films has also received great attention in recent years (Gao et al. 2012 (c), Pergament et al. 2008, Wu et al. 2013, Cho et al. 2012, Shi et al. 2011, Kang et al. 2010 and 2011, Chen et al. 2011, Zhang et al. 2010 (b), Jin et al. 2009, Yan et al. 2008 (b), Tsuyumoto and Nawa 2008, Yang et al. 2007, Mai et al. 2006, Pan et al. 2004), including organic and inorganic sol-gel method. Compared with the gas phase deposition method, solution based deposition method is cost-effective, easy doping of other elements, large-scale deposition and flexible on complex shape or large substrate surface (Chae and Kim 2010, Binions et al. 2007, Ye et al. 2010). Also, the inorganic sol-gel method facilitates use of ordinary raw materials. Furthermore, sol-gel method was reported to prepare VO₂ films with narrow temperature hysteresis width. For instance, the hysteresis width of 8 °C at 500 °C was exhibited in VO₂ thin films on mica substrates (Wu et al. 2013) and less 5 °C was found in another study (Wang et al. 2013). However, this method requires complex treatment,

like annealing at high temperature (Kang et al. 2010). More information about these methods is referenced in original literatures.

VO$_2$ Nanocomposites

In the last few years nanostructured VO$_2$ has been gaining interests which provides another promising way to incorporate thermochromic materials into windows and auto devices. As summarized in Table 2-4, VO$_2$ nanocomposite can offer significant properties, e.g. lower transition temperature (Xu et al. 2013, Dai et al. 2011, Chen et al. 2012, Zhou et al. 2013, Kong et al. 2011, Chen et al. 2007, Peng et al. 2007), simultaneously enhanced luminous transmission and solar modulation (Li et al. 2010, Kang et al. 2011 (b), Li et al. 2013, Zhou et al. 2013, Li et al. 2014, Cao et al. 2014), improved stability (Melnik et al. 2012) and preferred color (Saeli et al. 2010). Various types of nanostructured VO$_2$ have been prepared, including nanoparticles (Ishiwata et al. 2010. Son et al. 2010, Zhang et al. 2010, Zhou et al. 2013), nanowires (Chen et al. 2004), nanorods (Gui et al. 2002, Guiton et al. 2005, Ji et al. 2010 (a) and (b), Rama and Rao 2010, Dai et al. 2011), nanobelts (Liu et al. 2004), nanotube (Liu and Taschner 2005) (X. Liu, C. Taschner, A. Leonhardt, M.H. Rummeli, T. Pichler, T. Gemming, B. Buchner, M. Knupfer, Phys. Rev. B 72 (2005) 115407.) and nanoplatelets (Tselev et al. 2010) as well as on VO$_2$(B) nanoparticles (Li and Liu 2010), nanorods (Chen et al. 2010), and nanobelts (Zakharova et al. 2010, Ye et al. 2010), element doped VO$_2$ nanoparticles (Gao et al. 2010, Chen and Huang et al. 2012).

More attention has also been given to the synthetic techniques of VO$_2$ nanocomposites, such as thermolysis method (Zheng et al. 2001, Peng et al. 2007), reduction-hydrolysis method (Xu and Ma et al. 2004), and hydrothermal method (Li et al. 2006, Whittaker et al. 2011, Ji et al. 2010 and 2011, Cao et al. 2008, Son et al. 2010, Cao et al. 2010, Gui et al. 2001, Zhang et al. 2013, Liu et al. 2004, Li et al. 2009, Gao et al. 2012 (b) and 2013). Among them, the hydrothermal synthesis has gained increasing attention due to its uncomplicated route, low cost, large-scale and mass production. Fig. 2.2 displays the typical procedure of hydrothermal synthesis.
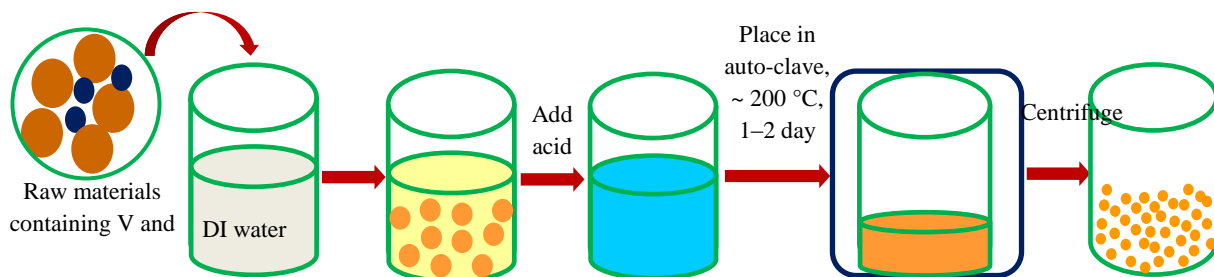
Fig. 2.2. Typical process for hydrothermal synthesis.

One issue for these methods is long-time treatment at high temperature. Therefore, $VO_2(M)$ nanoparticles were prepared by transforming from $VO_2(B)$ since $VO_2(B)$ can be synthesized at much lower temperatures with shorter time compared to $VO_2(M)$ (Li et al. 2009, Liu et al. 2007 and 2010, Ji et al. 2011). Recently, one rapid method proposed by Phoempoon and Sikong formed uniform monoclinic phase $VO_2(M)$ using microwave heating at 500 °C for 1h (Phoempoon and Sikong 2014). Another issue is that VO_2 nanoparticle formed by these methods is not thermodynamically stable under air and after a long time it transforms to V_2O_5, which lacks thermochromic properties. Furthermore, the high reactivity of VO_2 nanoparticles tends to have various reactions with reductant or oxidant agents. The chemical instability of VO_2 naoparticles limits their board applications. Thus, core–shell structures with VO_2 cores were fabricated by the sol-gel method and using shells comprised of SiO_2 (Gao et al. 2012 (a), Zhou et al. 2013, Li et al. 2013 (a) and (b), Huang et al. 2013) or TiO_2 (Li et al. 2013 (a)-(c)), or C (Zhang et al. 2012). These top layers serve as oxidation protection.

Nanostructured VO_2 films are also very promising for optical data storage systems, fiber-optical switching devices, thermal relays and ultrafast optical switching (Yin et al. 1996, Whittaker et al. 2009). This film is generally prepared by dispersing VO_2 nanoparticles or VO_2 core-shell particles in a polymer matrix (Mlyuka et al. 2009 (b), Granqvist et al. 2010, Zhou et al. 2013, Gao et al. 2012 (b)).

2.4 Application of Thermochromic Materials

Thermochromic Windows

Chromogenic materials based smart windows can control the amount of solar irradiation in response to the external environmental stimulus intelligently (Granqvist 2013, Li et al. 2011). This environmental factor can be light in case of photochromic windows; or temperature and

heat in thermochromic windows. Thus, thermochromic smart windows allow the visible day light, block undesired solar radiation in the hot season, while allow desirable solar heat gain in the cold season. In this way, thermochromic windows are capable of curtailing the building energy consumption. Thermochromic windows are usually manufactured by depositing thermochromic films on a glass substrate. VO_2 films, featuring a constant visible spectrum but a change of reflection/transmission in the infrared region of the spectrum, have been considered for energy efficient windows for decades (Smith and Granqvist 2010, Li et al. 2012, Saeli et al. 2010 (a), (b) and 2011, Ye et al. 2012, 2013 and 2014, Baetens et al. 2010, Gao et al. 2012 (b) and (c)).

There are number of studies by experimental measurements and modelling which discussed the energy performance of VO_2 thermochromic windows. For example, Gao et al. tested the applied properties of different types of VO_2 films in two model houses of 34 cm × 27 cm × 29 cm, shown in Fig. 3(a) (Gao et al. 2012 (b)). The results showed that compared with the control window, the windows coated with VO_2-polyurethane (PU) and VO_2-antimony-doped tin oxide-PU composite foils cause the temperature reduction of 17 °C and 20.5 °C, respectively. However, this test was conducted under the infrared irradiation in static air. Recently, Ye et al. (Ye et al. 2013) conducted field measurement on the roof of a building by applying VO_2 film with phase transition of 41.3 °C to the sourthern window (1.65 m × 1.65 m) of a room with a size of 2.9 m × 1.8 m × 1.8 m, shown in Fig. 2.3(b). The field measurement in July demonstrated that room with VO_2 glazing save 10.2–19.9% cumulative cooling load than that with an ordinary glazing. Furtheremore, the performance of VO_2 glazing in different regions was evaluated by BuldingEnergy. The simulation results showed that the application of VO_2 glazing could save approximate 9.4% electricity consumption.
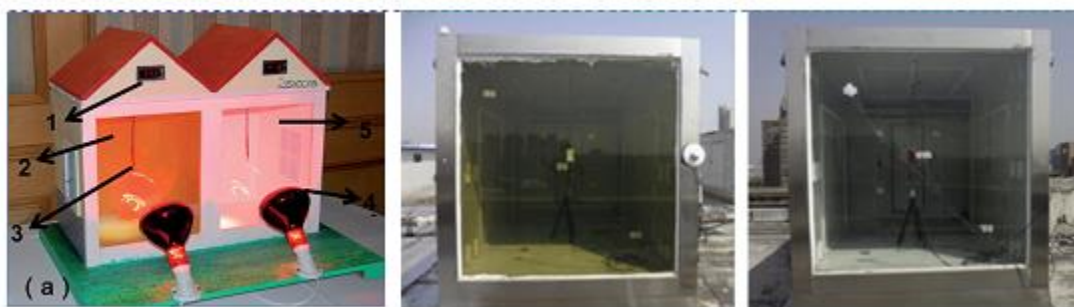
Fig. 2.3. Photographs of the testing system with thermochromic window (Gao et al. 2012, Ye et al. 2013)

Saeli et al. firstly simulated the energy consumption of the rooms with thermochromic glazing using Energy Plus (Saeli et al. 2010 (a) and 2011) and demonstrated the potential of VO_2 glazing in saving energy. According to the conclusions, the total energy consumption reduced more for commercial windows (100% of wall area glazing) than the residential case (25% of wall area glazing). It is found that the glazing works best in cities with warmer climates but is not applicable in cold climate region due to its low solar transmittance, which decreases the indoor heat gain from the solar radiation and leads to an increase in heating energy consumption. Similarily, Xu et al. (Xu et al. 2012) found the cooling energy consumption of the double glass coated with VO_2 films outside is 85% lower than white glass, while the heating consumption of the VO_2 glazing is the highest. The result of this study also shows that thermochromic windows are more suitable for cooling demand climates. Again, Lee et al. (Lee et al. 2013) evaluated large-area polymer thermochromic laminated windows in a full-scale tested office. The film had a broad switching temperature range and when combined to make an insulating window unit had center-of-glass properties of T_{sol}=0.12–0.03, T_{vis}=0.28–0.03 for a glass temperature range of 24–75 °C. The EnergyPlus simulation results demonstrated that annual energy savings in the south, east, and west perimeter zones are 20–43% in the hot/cold climate of Chicago compared to the ASHRAE 90.1-2004 Standard prescriptive window. Compared to code, energy saving in hot climates is lower, e.g. 4–22% in Houston. What's more, Hoffmann (Hoffmann et al. 2014) conducted EnergyPlus simulations on a prototypical large office building with a hypothetical thermochromic glazing with variable solar transimission in the near-infrared region of the solar spectrum: T_{sol}=0.10–0.50 and T_{vis}=0.30–0.60. This glazing coupled with a low-e glazing layer (e=0.04) could reduce the total site annual energy use of 14.0–21.1 kW h/m^2-floor-yr or 12–14% for moderate- to large-area windows (WWR≥0.30) in Chicago and 9.8–18.6 kW h/m^2-floor-yr or 10–17% for WWR≥0.45 in Houston compared to an unshaded spectrally-selective, low-e window in south-, east-, and west-facing perimeter zones.

However, Ye et al. (Ye eet al. 2012) evaluated the energy consumption of different thermochromic windows by an energy analysis program "BuildingEnergy" and found that VO_2 glazing has no apparent energy saving benefit and solar control advantage over conventional glazing. It was concluded that, the energy saving effect of thermochromic windows in summer is due to low transmittance of solar radiation and the higher absorptivity in the metal state results in

higher energy consumptions which consequently makes the phase transition useless to the energy saving performance. They even found that the dropped phase transition temperature causes higher cooling energy consumption in some types of VO_2 glazing. Therefore, recently Ye's group presented the concept of the material's smart regulation capacity, which is related to the VO_2 glazing's spectrum properties. Whether the VO_2 film is smart is judged by the relative variations in solar radiation properties during phase transition. They concluded that VO_2 glazing is capable of smart regulation when it undergoes a high decrease in solar transmittance and a low increase in solar absorptivity after the VO_2 changes into its metallic state (Ye et al. 2014). They also reported that when in its metallic state, the VO_2 glazing should have low solar transmittance and absorptivity and a high infrared emissivity, and when in the semiconductor state, it should have high solar transmittance and low infrared emissivity (Long and Ye 2014).

Construction Fields

In addition to the application of thermochromic materials in windows, they could be used in other positions, like wall and roof. Ma et al. (Ma et al. 2000, 2001, 2002 and 2009) prepared chameleon-type building coatings by incoporating 20 wt.% microencapsulated thermochromic pigments to conventional white building coatings, which could change their colors from red, blue etc. below 20°C to white above 20°C. It is found that at high outdoor temperatures the coatings could reduce 4°C temperature than the ordinary colored coating. They also prepared novel cements by combining thermochromic materials with the conventional cement with transition temperature of 42°C and 58°C, respectively. It is reported that below the switching temperature, the temperature of thermochromic cement is higher by 3 °C than that of normal white cement. Above the switching temperature, the temperature of theromchromic cement is close to that of normal white cement, which means that this cement prevents buildings from over-heating in summer. Recently a novel thermochromic roof system was proposed employing aqueous solution of poly (N-isopropylacrylamide) (PNIPAM) by Ye et al. (Ye and Luo et al. 2012). It is observed that this system features the maximum reflection ratio of 33% and decreases the cell temperature by 6°C, implying the potential to cut energy consumption of buildings and other urban structures. In addition, thermchromic materials were also incorporated into conventional asphalt binder (Hu and Yu 2013 and 2014). It is found that the use of thermochromic materials can reduce the surface temperature of asphalt binder up to 6.6°C in hot weather and increase the

29

surface temperature in cold weather. This implies that the application of thermochromic materials can potentially improve the durability of asphalt pavement as well as mitigate the urban heat island effects.

2.5 Conclusions and Recommendations

The common types of thermochromic materials were summarized, including classifications, thermochromisms, VO_2 films and nanoparticles, applications and their performances.

Among the organic, polymer and inorganic thermochromic materials, vanadium dioxide is the most studied thermcohromic materials, due to its transition temperature close to the room temperature, and as such features the greatest potential for application in thermochromic devices and smart windows. However, significant challenges impede the large scale application and commercialization of VO_2 films, including high transition temperature, low solar modulation (change of solar transmission during phase transition), low visible transmission, unattractive color, long-term durability, and low reflecting capacity in the far-infrared region. Some of them can be addressed by doping elements (W, Mo, Mg, F, Au), forming composite, adjusting thickness of film, designing multilayer, using nanoparticles, or controlling processing conditions and surface roughness. However, no one strategy can address all of the challenges simultaneously. For instance, the doping with tungsten always decreases solar modulation. Therefore, a novel material, a new solution or a combination of these existing solutions is urgently needed for future study.

Nanostructured VO_2 particles and films have recently attracted much attention due to their distinguished features, including reduced phase transition temperature, simultaneously enhanced T_{lum} and ΔT_{sol}, and narrow hysteresis. Several methods have been proposed to synthesize VO_2 nanoparticles, including thermolysis, hydrothermal method, and core-shell structure. One key point is to fabricate high quality nanostructured VO_2 in a simple, low cost and large-scale approach.

Thermochromic smart windows, typically based on VO_2 films, have been widely studied for energy saving in buildings. In theory, with an appropriate transition temperature, the adoption of VO_2 glazing could reduce both cooling and heating energy consumption by regulating heat gain in buildings. However, some experimental and modelling results showed that thermochromic smart windows only save cooling energy, have no benefits or even increase heating energy

consumption.The inconsistency between theory and modelling about the energy performance of thermochromic windows emphasizes the necessity of more comprehensive research in this field. Therefore, phase transition temperature and temperature range, changes of transmission, absorption, reflection and emissivity need be carefully designed to maximize the smart regulation capacity of thermochromic glazing systems. Specifically, the ideal transition temperature should be as low as possible to maximize the time the film spends in the hot and infrared reflective state. Thermochromic films with a narrow switching range about 1–2 °C is also encouraged to produce small temperature gradient and exhibit even appearance, which is desirable from the architectural esthetic perspective. Besides, the change in the infrared optical properties should be as large as possible to maximize the benefit of the hot and reflective state. The larger the change of reflection and transmission between hot and cold state, the higher the energy saving performance can be achieved. The film with high emissivity in both the cold and hot state is not suitable for cold region. Summarily, above the transition temperature, the glazing should have low solar transmittance and absorption, higher reflection and infrared emissivity, while below the transition temperature, it should feature high transmittance and absorption, low reflection and infrared emissivity.

Besides these characteristics, future glazing system for buildings should possess multiple functions from the viewpoints of energy-efficiency and environmental friendship, such as self-protecting based on CeO_2, ZnO:Al, and TiO_2, light control, energy conversion, and so on. Furthermore, the combination of thermochromic windows with photo-, electro- and/or gaso-chromic windows offers a new and promising energy saving application in buildings.

The most widely used thermochromic materials, VO_2, can undergo a sharp, reversible metal-to-insulator transition, accompanying by dramiatic changes in electric and near-infrared optical properties. These unique characteristics make VO_2 a promising material for a variety of potential applications such as the aforementioned energy-efficient windows, thermal sensors (Sella et al. 1998), cathode materials for reversible lithium batteries (Ni et al. 2011), electrical and infrared light switching device (Chen et al. 2008. Viswanath et al. 2011), electronic and gas sensing devices (Strelcov et al. 2009, Bae et al. 2013) and electromechanical actuators (Lee et al. 2013). New applications and other promising thermochromic materials are needed to further explore.

Traditional thermochromic materials based on metallic powder or crystal salt, while functioning as a solar modulator, have poor compatibility with asphalt binders. Therefore, they can accelerate bonding deterioration in the asphalt binder. Polymeric thermochromic dyes feature excellent compatibility with asphalt binders. Therefore, they are promising to be effective in modulating the surface temperature of pavement.

2.6 References

(1)   Baetens, R., Jelle, B.P., Gustavsen, A. Properties, requirements and possibilities of smart windows for dynamic daylight and solar energy control in buildings: a state-of-the-art review. Solar Energy Materials and Solar Cells, 2010, 94(2): 87–105.

(2)   Bae, S.H., Lee, S., Koo, H., Lin, L., Jo, B.H., Park, C., Wang, Z. L. The memristive properties of a single VO2 nanowire with switching controlled by self-heating. Advanced Materials, 2013, 25(36):5098-103

(3)   Batista, C., Teixeira, V., Ribeiro, R.M. Synthesis and Characterization of V1- xMoxO2 Thermochromic Coatings with Reduced Transition Temperatures. Journal of nanoscience and nanotechnology, 2010, 10(2): 1393–1397.

(4)   Batista, C., Carneiro, J., Ribeiro, R., Teixeira, V. Reactive Pulsed-DC Sputtered Nb-doped VO_2 coatings for smart thermochromic windows with active solar control. Journal of Nanoscience and Nanotechnology, 2011, 11(10): 9042–9045(4).

(5)   Berezina, O.Ya., Velichko, A.A., Lugovskaya, L.A., Pergament, A.L., Stefanovich, G.B. Metal-semiconductor transition in nonstoichiometric vanadium dioxide films. Inorganic Materials, 2007, 43(5): 505–511.

(6)   Binions, R., Hyett, G., Piccirillo, C., Parkin, I.P. Doped and un-doped vanadium dioxide thin films prepared by atmospheric pressure chemical vapour deposition from vanadyl acetylacetonate and tungsten hexachloride: the effects of thickness and crystallographic orientation on thermochromic properties. Journal of Materials Chemistry, 2007, 17(44): 4650–4652.

(7)   Binions, R., Piccirillo, C., Palgrave, R.G., Parkin, I.P. Hybrid Aerosol Assisted and Atmospheric Pressure CVD of Gold-Doped Vanadium Dioxide. Chemical Vapor Deposition, 2008, 14(1-2): 33–39.

(8)   Blackman, C.S., Piccirillo, C., Binions, R., Parkin, I.P. Atmospheric pressure chemical vapour deposition of thermochromic tungsten doped vanadium dioxide thin films for use in architectural glazing. Thin Solid Films, 2009, 517(16): 4565–4570.

(9)   Blanquart, T., Niinisto, J., Gavagnin, M., Longo, V., Heikkila, M., Puukilainen, E., Pallem, V.R., Dussarrat, C., Ritala, M., Leskela, M. Atomic layer deposition and characterization of vanadium oxide thin films. RSC Advances, 2013, 3(4): 1179–1185.

(10) Burkhardt, W., Christmann, T., Franke, S., Kriegseis, W., Meister, D., Meyer, B.K., Niessner, W., Schalch, D., Scharmann, A. Tungsten and fluorine co-doping of vanadium dioxide films. Thin Solid Films, 2002, 402 (1-2): 226–231.

(11) Cao, X., Wang, N., Law, J.Y., Loo, S.C.J., Magdassi, S., Long, Y. Nanoporous Thermochromic VO_2 (M) Thin Films: Controlled Porosity, Largely Enhanced Luminous Transmittance and Solar Modulating Ability. Langmuir, 2014, 30(6): 1710−1715.

(12) Cao, C.X., Gao, Y.F., Luo, H.J. Pure single-crystal rutile vanadium dioxide powders: synthesis, mechanism and phase-transformation property. Journal of Physical Chemistry C, 2008, 112(48): 18810–18814.

(13) Cao, C.X., Y.F. Gao, L.T. Kang, H.J. Luo. Self-assembly and synthesis mechanism of vanadium dioxide hollow microspheres. CrystEngComm, 2010, 12(12): 4048–4051.

(14) Chae, B.G., Kim, H.T. Effects of W doping on the metal-insulator transition in vanadium dioxide film. Physica B, 2010, 405(2): 663–667.

(15) Chanakul, A., Traiphol, N., Traiphol, R. Controlling the reversible thermochromism of polydiacetylene/zinc oxide nanocomposites by varying alkyl chain length. Journal of Colloid and Interface Science, 2013, 389(1): 106–114.

(16) Chen, H.-K., Hung, H.-C., Yang, T.C.K., Wang, S.-F. The preparation and characterization of transparent nano-sized thermochromic VO_2–SiO_2 films from the sol–gel process. Journal of Non-Crystalline Solids, 2004, 347(1-3): 138–143.

(17) Chen, C.H., Wang, R.F., Shang, L., Guo, C.F. Gate-field-induced phase transitions in VO_2: monoclinic metal phase separation and switchable infrared reflections. Applied Physics Letters, 2008, 93(17): 171101–171101-3.

(18) Chen, L.H., Huang, C.M., Xu, G., Miao, L., Shi, J.F., Zhou, J.H., Xiao, X.D. Synthesis of Thermochromic W-Doped VO_2 (M/R) Nanopowders by a Simple Solution-Based Process. Journal of Nanomaterials, 2012, 2012(3), 8 pages.

(19) Chen, J.R., Yan, D.Y. Design and Synthesis of an α-Hydroxyphenyl-Containing Spiropyran Thermochromic Colorant. Organic Letters, 2009, 11(8): 1769–1772.

(20) Chen, X., Yoon. J.Y. A thermally reversible temperature sensor based on polydiacetylene: Synthesis and thermochromic properties. Dyes and Pigments, 2011, 89(3): 194–198.

(21) Chen, X., Lv, Q., Yi, X. Smart window coating based on nanostructured VO_2 thin film. Optik - International Journal for Light and Electron Optics, 2012, 123(13): 1187–1189.

(22) Chen, S., Ma, H., Dai, J., Yi, X. Nanostructured vanadium dioxide thin films with low phase transition temperature. Applied Physics Letters, 2007, 90(10):101117– 101117-3.

(23) Chen, Z., Gao, S., Jiang, L., Wie, M., Wie, K. Crystalline VO_2 (B) nanorods with a rectangular cross-section. Materials Chemistry and Physics, 2010, 121(1-2): 254–258.

(24) Chen, Z., Gao, Y., Kang, L., Du, J., Zhang, Z., Luo, H., Miao, H., Tan, G. VO_2-based double-layered films for smart windows: optical design, all-solution preparation and improved properties. Solar Energy Materials and Solar Cells, 2011, 95(9): 2677–2684.

(25) Chen, B., Yang, D., Charpentier, P.A., Zeman, M. Al3+-doped Vanadium Dioxide Thin Films Deposited by PLD. Solar Energy Materials and Solar Cells, 2009. 93(9): 1550–1554.

(26) Chen, W., Peng, J.F., Mai, L.Q., Xu, Q., Zhu, Q.Y. Syntheses and characterizations of two kinds of one-dimensional nanostructure vanadium oxide. Chinese J Inorg Chem , 2004, 20(2004): 147.

(27) Cho, J.-H., Byun, Y.-J., Kim, J.-H., Lee, Y.-J., Jeong, Y.-H., Chun, M.-P., Paik, J.-H., Sung, T.H. Thermochromic characteristics of WO_3-doped vanadium dioxide thin films prepared by sol–gel method. Ceramics International, 2012, 38S (1): S589–S593.

(28) Chu, X.H., Tao, H., Liu, Y., Ni, J., Bao, J., Zhao, X. VO_2/AZO double-layer films with thermochromism and low-emissivity for smart window applications. Journal of Non-Crystalline Solids, 2014, 383(1): 121–125.

(29) Crano, J.C., Guglielmetti, R.J. Organic Photochromic and Thermochromic Compounds. vol. 2, Kluwer Academic/Plenum Publishers, New York, 1999.

(30) Dai, L., C. Cao, Gao, Y., Luo, H. Synthesis and phase transition behavior of undoped VO2 with a strong nano-size effect, Solar Energy Materials and Solar Cells, 2011, 95(2): 712–715.

(31) Du, J. Gao, Y., Chen, Z., Kang, L., Zhang, Z., Luo, H. Enhancing thermochromic performance of VO_2 films via increased microroughness by phase separation. Solar Energy Materials and Solar Cells, 2013, 110: 1–7.

(32) Evans, P., Pemble, M.E., Sheel, D.W., Yates, H.M. Multi-functional self-cleaning thermochromic films by atmospheric pressure chemical vapour deposition. Journal of Photochemistry and Photobiology A: Chemistry, 2007, 189(2–3): 387–397.

(33) Fortier, J.-P., Baloukas, B., Zabeida, O., Klemberg-Sapieha, J.E., Martinu, L.

Thermochromic VO$_2$ thin films deposited by HiPIMS. Solar Energy Materials and Solar Cells, 2014, 125: 291–296.

(34) Fu, G.H., Polity, A., Volbers, N., Meyer, B.K. Annealing effects on VO2 thin films deposited by reactive sputtering. Thin Solid Films, 2006, 515(4): 2519–2522.

(35) Gadžurić, S., Vraneš, M., Dožić, S. Thermochromic cobalt(II) chloro-complexes in different media: Possible application for auto-regulated solar protection. Solar Energy Materials and Solar Cells, 2012, 105: 309–316.

(36) Gao, Y., Wang, S., Luo, H., Dai, L., Cao, C., Liu, Y., Chen, Z., Kanehira, M. Enhanced chemical stability of VO2 nanoparticles by the formation of SiO2/VO2 core/shell structures and the application to transparent and flexible VO2-based composite foils with excellent thermochromic properties for solar heat control. Energy and Environmental Science, 2012, 5 (3): 6104–6110.

(37) Gao, Y.F., Wang, S., Kang, L., Chen, Z., Du, J., Liu, X., Luo H., Kanehira, M. VO2–Sb:SnO2 composite thermochromic smart glass foil. Energy & Environmental Science, 2012, 5(8): 8234–8237.

(38) Gao, Y., Luo, H., Zhang, Z., Kang, L., Chen, Z., Du, J., Kanehira, M., Cao, C. Nanoceramic VO2 thermochromic smart glass: a review on progress in solution progressing. Nano Energy, 2012, 1(2): 221–246.

(39) Gao, Y., Cao, C., Dai, L., Luo, H., Kanehira, M., Ding, Y., Wang, Z.L. Phase and shape controlled VO2 nanostructures by antimony doping. Energy Environ. Sci., 2012, 5(9): 8708–8715.

(40) Granqvist, C.G. Radiative heating and cooling with spectrally selective surfaces. Applied Optics, 1981, 20: 2606–2615.

(41) Granqvist, C.G. Transparent conductors as solar energy materials: a panoramic review. Solar Energy Materials and Solar Cells, 2007, 91: 1529–1598.

(42) Granqvist, C. G., Green, S., Niklasson, G.A., Mlyuka, N.R., von Kraemer, S., Georen, P. Advances in chromogenic materials and devices.Thin Solid Films, 2010, 518(11): 3046–3053.

(43) Granqvist, C.G. Chromogenic windows. Advances in Science and Technology, 2013, 77: 108–117.

(44) Granqvist, C. G., Pehlivan, B., Ji, Y.-X., Li, S.-Y., Niklasson, G.A. Electrochromics and

thermochromics for energy efficient fenestration: Functionalities based on nanoparticles of In$_2$O$_3$:Sn and VO$_2$. Thin Solid Films, 2014, 559: 2–8.

(45) Gui, Z., Fan, R., Chen, X.H., Wu, Y.C. A new metastable phase of needle-like nanocrystalline VO2 center dot H2O and phase transformation. Journal of Solid State Chemistry, 2001, 157(2): 250–254.

(46) Gui, Z., Fan, R., Mo, W.Q., Chen, X.H., Yang, L., Zhang, S.Y., Hu, Y., Wang, Z.Z., Fan, W.C. Precursor Morphology Controlled Formation of Rutile VO2 Nanorods and Their Self-Assembled Structure. Chem. Mater., 2002, 14(12): 5053–5056.

(47) Guo, L.L., Dai, Y.D., Liu, H.X., Ouyang, S.X. Phase Transition and Thermochromism of the Hybrid (C12H25NH3)2FeCl4. Solid State Phenomena, 2006, 111: 55–58.

(48) Guinneton, F. Optimized infrared switching properties in thermochromic vanadium dioxide thin films: role of deposition process and microstructure.Thin Solid Films, 2004, 446(2): 287–295.

(49) Guiton, B.S., Gu, Q., Prieto, A.L., Gudiksen, M.S., Park, H. Single-crystalline vanadium dioxide nanowires with rectangular cross sections. Journal of the American Chemical Society, 2005, 127(2): 498-499.

(50) Hanlon, T.J., Coath, J.A., Richardson, M.A. Molybdenum-doped vanadium dioxide coatings on glass produced by the aqueous sol–gel method. Thin Solid Films, 2003, 436(2): 269–272.

(51) Hoffmann, S., Lee, E.S., Clavero, C. Examination of the technical potential of near-infrared switching thermochromic windows for commercial building applications. Solar Energy Materials and Solar Cells, 2014, 123: 65–80.

(52) Huang, Z., Chen, S., Wang, B., Huang, Y., Liu, N., Xu, J., Lai, J. Vanadium dioxide thin film with low phase transition temperature deposited on borosilicate glass substrate. Thin Solid Films, 2011, 519(13): 4246–4248.

(53) Huang, A., Zhou, Y., Li, Y., Ji, S., Luo, H., Jin, P. Preparation of VxW1-xO2(M)@SiO2 ultrathin nanostructures with high optical performance and optimization for smart windows by etching.

(54) Journal of Materials Chemistry A, 2013, 1(40): 12545–12552.

(55) Hu, J.Y., Yu, X. Experimental Study of Sustainable Asphalt Binder. Journal of the Transportation Research Board, 2013, 2372(1): 108-115.

(56) Hu, J.Y., Gao, Q., Yu, X. Characterization of the Optical and Mechanical Properties of Innovative Multifunctional Thermochromic Asphalt Binders. Journal of Materials in Civil Engineering, 2014.

(57) Ishiwata, Y., Suehiro, S., Hagihala, M., Zheng, X.G., Kawae, T., Morimoto, O., Tezuka, Y. Unusual low-temperature phase in VO2 nanoparticles. Physical Review B, 2010, 82(1182): 115404.

(58) Ji, S.D., Y. Zhao, F. Zhang, P. Jin. Direct formation of single crystal VO2(R) nanorods by one-step hydrothermal treatment. Journal of Crystal Growth, 2010, 312(2): 282–286.

(59) Ji, S.D., Zhao, Y., Zhang, F., Jin, P. Synthesis and phase transition behavior of w-doped VO2(A) nanorods. Ceramic Society of Japan, 2010, 118(1382): 867–871.

(60) Ji, Y.X., Li, S.-Y., Niklasson, G.A., Granqvist, C.G. Durability of thermochromic VO2 thin films under heating and humidity: Effect of Al oxide top coatings. Thin Solid Films, 2014, 562: 568–573.

(61) Ji, S., Zhang, F., Jin, P. Preparation of high performance pure single phase VO2 nanopowder by hydrothermally reducing the V2O5 gel. Solar Energy Materials and Solar Cells, 2011, 95(12): 3520–3526.

(62) Jiang, M., Wang, E., Xu, L., Kang, Z., Lian, S. The first example of multilayer films with thermochromic properties. Journal of Solid State Chemistry, 2004, 177(4–5): 1776–1779.

(63) Jin, P., Xu, G., Tazawa, M., Yoshimura, K. Design, formation and characterization of a novel multifunctional window with VO2 and TiO2 coatings. Applied Physics A, 2003, 77(3-4): 455–459.

(64) Jin, A., Chen, W., Zhu, Q., Yang, Y., Volkov, V., Zakharova, G. Structural and electrochromic properties of molybdenum doped vanadium pentoxide thin films by sol-gel and hydrothermal synthesis. Thin Solid Films, 2009, 517(6): 2023–2028.

(65) Kang, L., Gao, Y., Chen, Z., Du, J., Zhang, Z., Luo, H. Pt/VO2 double-layered films combining thermochromic properties with low emissivity. Solar Energy Materials and Solar Cells, 2010, 94(12): 2078–2084.

(66) Kang, L.T., Gao, Y., Luo, H., Wang, J., Zhu, B., Zhang, Z., Du, J., Kanehira, M., Zhang, Y. Thermochromic properties and low emissivity of ZnO:Al/VO2 double-layered films with a lowered phase transition temperature. Solar EnergyMaterials & Solar Cells, 2011, 95(12): 3189–3194.

(67) Kang, L.T., Gao,Y.F., Luo, H.J., Chen, Z., Du, J., Zhang, Z.T. Nanoporous thermochromic VO2 films with low optical constants, enhanced luminoustransmittance and thermochromic properties. ACS Applied Materials and Interfaces, 2011, 3(2): 135–138.

(68) Karlessi, T., Santamouris, M., Apostolakis, K., Synnefa, A., Livada, I. Development and testing of thermochromic coatings for buildings and urban structures. Solar Energy, 2009, 83(4): 538–551.

(69) Khan, K.A., Granqvist, C.G. Thermochromic sputter-deposited vanadium oxyflu-oride coatings with low luminous absorptance. Applied Physics Letters, 1989, 55(1): 4–6.

(70) Kim, C.-Y., Kim, S.H., Kim, S.J., An, K.-S. VO2(1 1 0) film formation on TiO2 (1 1 0) through post-reduction of ALD grown vanadium oxide. Applied Surface Science, 2014, 313: 368–371.

(71) Kiri, P., Warwick, M.E.A., Ridley, I., Binions, R. Fluorine doped vanadium dioxide thin films for smart windows. Thin Solid Films, 2011, 520(4): 1363–1366.

(72) Koo, H., Yoon, S., Kwon, O.J., Ko, K.E., Shin, D., Bae, S.H., Chang, S.H., Park, C. Effect of lattice misfit on the transition temperature of VO2 thin film. Journal of Materials Science, 2012, 47(17): 6397–6401.

(73) Kong, F.Y., Li, M., Pan, S.S., Zhang, Y.X., Li, G.H. Synthesis and thermal stability of W-doped VO2 nanocrystals. Materials Research Bulletin, 2011, 46(11): 2100–2104.

(74) Lappalainen, J., Heinilehto, S., Saukko, S., Lantto, W., Jantunen, H. Microstructure dependent switching properties of VO2 thin films. Sensors and Actuators A: Physics, 2008, 142(1): 250–255.

(75) Lee, S. C., Jeong, Y.G., Jo, W.H., Kim, H.J., Jang, J., Park, K. M., Chung, I. H. Thermochromism of a novel organic compound in the solid state via crystal-to-crystal transformation. Journal of Molecular Structure, 2006, 825(1-3): 70–78.

(76) Lee, E.S., Pang, X., Hoffmann, S., Goudey, H. Thanachareonkit, A. An empirical study of a full-scale polymer thermochromic window and its implications on material science development objectives. Solar Energy Materials and Solar Cells, 2013, 116: 14–26.

(77) Lee, S., Cheng, C., Guo, H., Hippalgaonkar, K., Wang, K., Suh, J., Liu, K., Wu, J. Axially engineered metal-insulator phase transition by graded doping VO2 nanowires. Journal of the American Chemical Society, 2013, 135(12): 4850–4855.

(78) Lee, K.W., Kweon, J.J., Lee, C.E., Gedanken, A., Ganesan, R. Infrared-wave number-

dependent metal–insulator transition in vanadium dioxide nanoparticles. Applied Physics Letters, 2010, 96: 243111.

(79) Li, J., Liu, C.-Y., Mao, L.-J. The character of W-doped one-dimensional VO2(M). Journal of Solid State Chemistry, 2009, 182(10): 2835–2839.

(80) Li, S.Y., G.A. Niklasson, C.G. Granqvist. Nanothermochromics: calculations for VO2 nanoparticles in dielectric hosts show much improved luminous transmittance and solar energy transmittance modulation. J. Appl. Phys., 108 (6) (2010), pp. 063525–063528.

(81) Li. S.-Y., Niklasson, G.A., Granqvist, C.G. Thermochromic fenestration with VO2-based materials: Three challenges and how they can be met. Thin Solid Films, 2012, 520(10), 10.1016.

(82) Li, S.Y., G.A. Niklasson, C.G. Granqvist, Nanothermochromics with VO2-basedcore–shell structures: calculated luminous and solar optical properties, Journalof Applied Physics 109 (2011) 061102.

(83) Li, S.-Y., G.A. Niklasson, C.G. Granqvist, Thermochromic undoped and Mg-doped VO2 thin films and nanoparticles: optical properties and performance limits for energy efficient windows, J. Appl. Phys. 115 (2014) 053513/1.

(84) Li, S., Y. Li, M. Jiang, S. Ji, H. Luo, Y. Gao, P. Jin, Preparation and characterization of selfsupporting thermochromic films composed of VO2(M)@SiO2 nanofibers, ACS Appl. Mater. Interfaces 5 (2013) 6453.

(85) Li, S.-Y., G.A. Niklasson, C.G. Granqvist. Thermochromic fenestration with VO2-based materials: three challenges and how they can be met, Thin Solid Films, 2012, 520(10): 3823–3828.

(86) Li, H.H., Wang, Y.-J., Dong, H.-J., Chen, Z.-R., Wu, Y.-L., Wang, M., Huang, S.-W. An organic–inorganic hybrid heterobridging luminescent copper(I) polymer exhibiting thermochromic behavior. CrystEngComm , 2011, 13(6): 1778–1781.

(87) Li, W., Yan, D., Gao, R., Lu, J., Wei, M., Duan, X. Recent Advances in Stimuli-Responsive Photofunctional Materials Based on Accommodation of Chromophore into Layered Double Hydroxide Nanogallery. Journal of Nanomaterials, 2013, 2013, 14 pages.

(88) Li, R., Liu, C.Y. VO2(B) nanospheres: hydrothermal synthesis and electrochemical properties. Materials Research Bulletin, 2010, 45(6): 688–692.

(89) Li, R., Ji, S., Li, Y., Gao, Y., Luo, H., Jin, P. Synthesis and characterization of plate-like

VO2(M)@SiO2 nanoparticles and their application to smart window. Materials Letters, 2013, 110(1): 241–244.

(90) Li, Z.Y., Cao, D.M., Zhou, K.C. Review on synthetic technology of vanadium dioxide powder. Rare Metal Materials and Engineering, 2006, 35(2): 316–320.

(91) Li, Y., Ji, S., Gao, Y., Luo, H., Kanehira, M. Core–shell VO2/TiO2 nanorods that combine thermochromic and photocatalytic properties for application as energy-saving smart coatings. Scientific Reports, 2013, 3, 1370/1.

(92) Li, Y., Ji, S., Gao, Y., Luo, H., Jin, P. Modification of Mott phase transition characteristics in VO2@TiO2 core/shell nanostructures by misfit-strained heteroepitaxy. ACS Appl. Mater. Interfaces, 2013, 5(14): 6603–6614.

(93) Li, Y., Ji, S., Gao, Y., Luo, H., Li, S., Jiang, M., Zhou, Y., Li, R., Wang, B., Jin, P. Core-regenerated vapor–solid growth of hierarchical stem-like VOx nanocrystals on VO2@TiO2 core–shell nanorods: microstructure and mechanism. CrystEngComm, 2013, 15(41): 8330–8336.

(94) Lindstrom, R., Maurice, V., Zanna, S., Klein, L., Groult, H., Perrigaud, L., Cohen, C., Marcus, P. Thin films of vanadium oxide grown on vanadium metal: oxidation conditions to produce V2O5 films for Li-intercalation applications and char-acterisation by XPS, AFM, RBS/NRA. Surface and Interface Analysis, 2006, 38(1): 6–18.

(95) Liu, C., Wang, N., Long, Y. Multifunctional overcoats on vanadium dioxide thermochromic thin films with enhanced luminous transmission and solar modulation, hydrophobicity and anti-oxidation. Applied Surface Science, 2013, 283: 222–226.

(96) Liu, J.F., Li, Q.H., Wang, T.H., Yu, D.P., Li, Y.D. Metastable vanadium dioxide nanobelts: Hydrothermal synthesis, electrical transport, and magnetic properties. Angewandte Chemie International Edition, 2004, 43(38): 5048–5052.

(97) Lopez, R., Boatner, L.A., Haynes, T.E., Feldman, L.C., Haglund, R.F. Synthesis and characterization of size-controlled vanadium dioxide nanocrystals in a fused silica matrix. Journal of Applied Physics, 2002, 92(7): 4031–4036.

(98) Liu, X., Huang, C., Yi, S., Xie, G., Li, H., Luo, Y. A new solvothermal method of preparing VO2 nanosheets and petaloid clusters. Solid State Communications, 2007, 144: 259–263.

(99) Long, L.S., Ye, H. Discussion of the performance improvement of thermochromic smart

glazing applied in passive buildings. Solar Energy, 2014, 107: 236–244.

(100) Luo, Z.F., Wu, Z., Xu, X., Du, M., Wang, T., Jiang, Y. Microstructures and thermochromic properties of tungsten doped vanadium oxide film prepared by using VOX–W–VOX sandwich structure. Materials Science and Engineering B, 2011, 176(9): 762–766.

(101) Lv, W.Z., Huang, D., Chen, Y., Qiu, Q., Luo, Z. Synthesis and characterization of Mo–W co-doped VO2(R) nano-powders by the microwave-assisted hydrothermal method. Ceramics International, 2014, 40(8):12661–12668.

(102) Lysenko, S., Rua, A., Fernandez, F., Liu, H. Optical nonlinearity and structural dynamics of VO2 films. J. Appl. Phys., 2009, 105(4): 043502.

(103) Ma, Y., Zhu, B., Wu, K. Preparation and solar reflectance spectra of chameleon-type building coatings. Solar Energy, 2001, 70(5): 417–422.

(104) Ma, Y., Zhu, B., Wu, K. Preparation of Reversible Thermochromic Building Coatings and Their Properties. Journal of Coatings Technology, 2000, 72(911): 67–71.

(105) Ma, Y., Zhang, X., Zhu, B., Wu, K. Research on reversible effects and mechanism between the energy-absorbing and energy-reflecting states of chameleon-type building coatings. Solar Energy, 2002, 72(6):511–520.

(106) Ma, Y., Zhu, B. Research on the preparation of reversibly thermochromic cement based materials at normal temperature. Cement and Concrete Research, 2009, 39(2): 90–94.

(107) Mai, L.Q., Hu, B., Hu, T., Chen, W., Gu, E.D. Electrical Property of Mo-Doped VO2 Nanowire Array Film by Melting−Quenching Sol−Gel Method. J. Phys. Chem. B, 2006, 110(39): 19083–19086

(108) Manning, T.D., Parkin, I.P., Clark, R.J.H., Sheel, D., Pemble, M.E., Vernadou, D. Intelligent window coatings: atmospheric pressure chemical vapour deposition of vanadium oxides.

(109) Journal of Materials Chemistry, 2002, 12(10): 2936–2939.

(110) Manning, T.D., Parkin, I.P., Pemble, M.E., Sheel, D., Vernardou, D. Intelligent window coatings: atmospheric pressure chemical vapor deposition of tungsten-doped vanadium dioxide. Chemistry of Materials, 2004, 16(4): 744–749.

(111) Manning, T.D., Parkin, I.P., Blackman, C., Qureshi, U. APCVD of thermochromic vanadium dioxide thin films - solid solutions V2-xMxO2 (M = Mo, Nb) or composites VO2: SnO2. Journal of Materials Chemistry, 2005, 15(42): 4560–4566.

(112) Mathur, S., Ruegamer, T., Grobelsek, I. Phase-selective CVD of vanadium oxide nanostructures. Chemical Vapor Deposition, 2007, 13(1): 42–47.

(113) Melnik, I. Khatsevych, V., Kladko, A., Kuchuk, V., Nikirin, B., Romanyuk. Low-temperature method for thermochromic high ordered VO2 phase formation. Materials Letters, 2012, 68(1): 215–217.

(114) Minkin, V.I., Bren', V.A., Dubonosov, A.D., Tikhomirova, K.S., Shepelenko, E.N. Photo- and ionochromic properties of aza crown derivatives of enamino 1-benzothiophen-2-ones. Russian Journal of Organic Chemistry, 2014, 50(4): 540–543.

(115) Mlyuka, N.R., Niklasson, G.A., Granqvist, C.G. Thermochromic VO2-based mul-tilayer films with enhanced luminous transmittance and solar modulation. Physica Status Solidi A, 2009, 206(9): 2155–2160.

(116) Mlyuka, N.R., Niklasson, G.A., Granqvist, C.G. Mg doping of thermochromic VO2 films enhances the optical transmittance and decreases the metal–insulatortransition temperature. Applied Physics Letters, 2009, 95:171909.

(117) Morin, F. Oxides Which Show a Metal-to-Insulator Transition at the Neel Temperature. Phys. Rev. Lett., 1959, 3(1): 34.

(118) Naumov, P., Ishizawa, N., Wang, J., Pejov, L., Pumera, M., Lee, S. C. On the Origin of the Solid-State Thermochromism and Thermal Fatigue of Polycyclic Overcrowded Enes. Journal of Physical Chemistry A, 2011, 115(30): 8563–8570.

(119) Ni, J., Jiang, W.T., Yu, K., Gao, Y. F., Zhu, Z.Q. Hydrothermal synthesis of VO2 (B) nanostructures and application in aqueous Li-ion battery. Electrochim Acta, 2011, 56(5): 2122–2126..

(120) Park, H., Lee, J.S., Choi, H., Ahn, D. J. Kim, J.M. Advanced Functional Materials, 2007, 17, 3447-3455.

(121) Peng, Z.F., Jiang, W., Liu, H. Synthesis and electrical properties of tungsten-doped vanadium dioxide nanopowders by thermolysis. Journal of Physical Chemistry C, 2007, 111(3): 1119–1122.

(122) Perdew, J. P., Burke, K., Ernzerhof, M. Generalized Gradient Approximation Made Simple. Physical. Review Letters, 1996, 77: 3865-3868.

(123) Pergament, A.L., Velichko, A.A., Berezina, O.Ya., Kazakova, E.L., Kuldin, N.A., Artyukhin, D.V. Influence of doping on the properties of vanadium oxide gel films.

Journal of Physics: Condensed Matter, 2008, 20(42): 422204.

(124) Phoempoon, P., Sikong, L. Phase Transformation of VO2 Nanoparticles Assisted by Microwave Heating. The Scientific World Journal, 2014, 2014, 8 pages.

(125) Povey, I.M., Bardosova, M., Chalvet, F., Pemble, M.E., Yates, H.M. Atomic layer deposition for the fabrication of 3D photonic crystals structures: growth of Al2O3 and VO2 photonic crystal systems. Surface and Coatings Technology, 2007, 201(22-23): 9345–9348.

(126) Rama, N., M.S.R. Rao. Synthesis and study of electrical and magnetic properties of vanadium oxide micro and nanosized rods grown using pulsed laser deposition technique. Solid State Communications, 2010, 150, 1041.

(127) Rampelberg, G., Schaekers, M., Martens, K., Xie, Q., Deduytsche, D., De Schutter, B., Blasco, N., Kittl, J., Detavernier, C. Semiconductor-metal transition in thin VO2 films grown by ozone based atomic layer deposition. Applied Physics Letters, 2011, 98(16): 162902–162903.

(128) Saitzek, S., Guinneton, F., Sauques, L., Aguir, K., Gavarri, J.R. Thermochromic CeO2– VO2 bilayers: role of ceria coating in optical switching properties. Optical Materials, 2007, 30(3): 407–415.

(129) Saeli, M., Piccirillo, C., Parkin, I.P., Binions, R., Ridley, I. Energy modeling studies of thermochromic glazing. Energy and Buildings, 2010, 42(10): 1666–1673.

(130) Saeli, M., Piccirillo, C., Parkin, I.P., Ridley, I., Binions, R. Nano-composite thermochromic thin films and their application in energy-efficient glazing. Sol. Energy Mater. Sol. Cells, 2010, 94 (2): 141–151

(131) Saeli, M., Vincenzini, P., Ginley, D.S., Bruno, G. Optimisation of thermochromic thin films on glass; design of intelligent windows. Advances in Science and Technology, 2011, 75 (2011): 79–90

(132) Seeboth, A., Lötzsch, D.Thermochromic Phenomena in Polymers. Shawbury, Smithers Rapra Technology Limited, 2008.

(133) Seeboth, A., Ruhmann, R., Mühling, O. Thermotropic and thermochromic polymer based materials for adaptive solar control. Materials, 2010, 3(12): 5143-5168

(134) Seeboth, A., Lo tzsch, D., Ruhmann, R., Muehling, O. Thermochromic Polymers-Function by Design. Chemical Review, 2014, 114(5): 3037–3068.

(135) Sella, C., Maaza, M., Nemraoui, O., Lafait, J., Renard, N., Sampeur, Y. Preparation, characterization and properties of sputtered electrochromic and thermochromic devices. Surface and Coatings Technology, 1998, 98(1–3): 1477–1482.

(136) Sharkany, J.P., Korposh, S.O., Batori-Tarci, Z.I., Trikur, I.I., Ramsden, J.J. Bacteriorhodopsin-based biochromic films for chemical sensors. Sensors and Actuators B: Chemical, 2005, 107(1): 77–81.

(137) Sharoni, A., Ramirez, J.G., Schuller, I.K. Multiple Avalanches across the Metal-Insulator Transition of Vanadium Oxide Nanoscaled Junctions. Physical review letter, 2008, 101(2): 026404–026407.

(138) Shi, J., Zhou, S., You, B., Wu, L. Preparation and thermochromic property of tungsten-doped vanadium dioxide particles. Solar Energy Materials & Solar Cells, 2007, 91(19): 1856–1862.

(139) Shi, Q., Huang, W., Zhang, Y., Yan, J., Zhang, Y., Mao, M., Zhang, Y., Tu, M. Giant phase transition properties at terahertz range in VO_2 films deposited by sol-gel method. ACS Appl. Mater. Interfaces, 2011, 3(9): 3523–3527.

(140) Smith, G.B., Granqvist, C.G. Green Nanotechnology: Solutions for Sustainability and Energy in the Built Environment. CRC Press, Boca Raton, USA (2010).

(141) Sobhan, M.A., Kivaisi, R.T., Stjerna, B., Granqvist, C.G. Thermochromism of sputter-deposited $WxV1-xO2$ films. Solar Energy Materials and Solar Cells, 1996, 44 (4): 451–455.

(142) Soltani, M., Chaker, M., Haddad, E., Kruzelesky, R. V. Thermochromic vanadium dioxide smart coatings grown on Kapton substrates by reactive pulsed laser deposition. Journal of Vacuum Science Technology A Vacuum Surfaces and Films, 2006, 24(3): 612.

(143) Son, J.H., Wei, J., Cobden, D., Cao, G.Z., Xia, Y.N. Hydrothermal synthesis of monoclinic $VO2$ micro- and nanocrystals in one step and their use in fabricating inverse opals. Chemistry of Materials, 2010, 22 (10): 3043–3050.

(144) Song, L.W., Zhang, Y., Huang, W., Shi, Q., Li, D., Zhang, Y., Xu, Y. Preparation and thermochromic properties of Ce-doped $VO2$ films. Materials Research Bulletin, 2013, 48(6): 2268–2271.

(145) Strelcov, E., Lilach, Y., Kolmakov, A. Gas Sensor Based on Metal-Insulator Transition in $VO2$ Nanowire Thermistor. Nano Letters, 2009, 9(6): 2322–2326.

(146) Srivastava, J., Srivastava, J.N., Alam, S., Mathur, G.N. Quantification of response time in poly(vinyl alcohol)-metal complex thermochromic polymeric systems. Journal of Applied Polymer Science, 2006, 100(6): 4832–4834.

(147) Takei, H., Koide, S. Growth and Electrical Properties of Vanadium-Oxide Single Crystals by Oxychrolide Decomposition Method. Journal of the Physical Society of Japan, 1966, 21(5): 1010.

(148) Tan, X., Yao, T., Long, R., Sun, Z., Feng, Y., Cheng, H., Yuan, X., Zhang, W., Liu, Q., Wu, C., Xie, Y., Wei, S. Unraveling metal– insulator transition mechanism of VO2 triggered by tungsten doping. Sci. Rep., 2012, 2, 466–471.

(149) Tang, H., MacLaren, D.C., White, M.A. New insights concerning the mechanism of reversible thermochromic mixtures. Canadian Journal of Chemistry, 2010, 88(11): 1063-1070,

(150) Tangirala, M., Zhang, K., Nminibapiel, D., Pallem, V., Dussarrat, C., Cao, W., Adam, T.N., Johnson, C.S., Elsayed-Ali, H.E., Baumgart, H., Physical Analysis of VO2 Films Grown by Atomic Layer Deposition and RF Magnetron Sputtering. ECS J. Solid State Sci. Technol. 2014, 3(6): N89-N94.

(151) Traiphol, N., Rungruangviriya, N., Potai, R., Traiphol, R. Stable polydiacetylene/ZnO nanocomposites with two-steps reversible and irreversible thermochromism: The influence of strong surface anchoring. Journal of Colloid and Interface Science, 2011, 356(2): 481–489.

(152) Tselev, A., Strelcov, E., Luk'yanchuk, I.A., Budai, J.D., Tischler, J.Z., Ivanov, I.N., Jones, K., Proksch, R., Kalinin, S.V., Kolmakov, A. Symmetry Relationship and Strain-Induced Transitions between Insulating M1 and M2 and Metallic R phases of Vanadium Dioxide. Nano letters, 2010, 10(11): 4409–4416.

(153) Tsuyumoto, I., Nawa, K. Thermochromism of titanium–vanadium oxide thin films prepared from peroxotitanate and peroxovanadate solution. Solid State Ionics, 2008, 179(21–26): 1227–1229.

(154) Vernardou, D., Pemble, M.E., Sheel, D.W. Vanadium oxides prepared by liquid injection MOCVD using vanadyl acetylacetonate. Surface and Coatings Technology, 2004, 188–189: 250–254.

(155) Vernardou, D., Pemble, M.E., Sheel D.W. The growth of thermochromic VO2 films on

glass by atmospheric-pressure CVD: a comparative study of precursors, CVD methodology and substrates. Chemical Vapor Deposition, 2006, 12(5): 263–274.

(156) Vernardou, D., Paterakis, P., Drosos, H., Spanakis, E., Povey, I.M., Pemble, M.E., Koudoumas, E., Katsarakis, N. A study of the electrochemical performance of vanadium oxide thin films grown by atmospheric pressure chemical vapor deposition. Solar Energy Materials and Solar Cells, 2011, 95(10): 2842–2847.

(157) Vinogradova, O.P., Sidorov, A.I., Klimov,V.A., Shadrin, E.B., Nashchekin, A.V., Khanin, S.D., Lyubimov, V.Y. Specific features of the formation of vanadium oxide micro- and nanocrystals during gas-phase synthesis. Physics of the Solid State, 2008, 50(7): 1227– 1233.

(158) Viswanath, B., Ko, C., Ramanathan,cS. Thermoelastic switching with controlled actuation in VO2 thin films. Scripta Materialia, 2011, 64(6): 490–493.

(159) Wang, J., Sun, X.W., Jiao, Z. Application of Nanostructures in Electrochromic Materials and Devices: Recent Progress. Materials, 2010, 3(12): 5029–5053.

(160) Wang, H., He, W., Yuan, G., Wang, X., Chen, Q. Large change of visible transmittance with VO2 phase transition in VO2/TiO2 polycrystalline films. Thin Solid Films, 2013, 540: 168–172.

(161) Wang, M.H., Lei, H., Sawada, Y., Hoshi, Y., Uchida, T., Hou, Z.X. Recent Progress in Gasochromics of Nano-Structured WO3 Film and its Applications. Advanced Materials Research, 2014, 941-944: 1298-1301.

(162) Wang, N., Magdassi, S., Mandler, D., Long, Y. Simple sol–gel process and one-step annealing of vanadium dioxide thin films: Synthesis and thermochromic properties. Thin Solid Films, 2013, 534: 594–598.

(163) Warwick, M.E.A., Binions, R. Advances in thermochromic vanadium dioxide films. Journal of Materials Chemistry A, 2014, 2(10): 3275–3292.

(164) Whittaker, L., Jaye, C., Fu, Z., Fischer, D.A., Banerjee, S. Depressed Phase Transition in Solution-Grown VO2 Nanostructures. J. Am. Chem. Soc., 2009, 131(25): 8884–8894.

(165) Whittaker, L., Wu, T.L., Patridge, C.J., Sambandamurthy, G., Banerjee, S. Distinctive finite size effects on the phase diagram and metal–insulator transitions of tungsten-doped vanadium (IV) oxide. Journal of Materials Chemistry, 2011, 21(15): 5580–5592.

(166) Wu, J., Huang, W., Shi, Q., Cai, J., Zhao, D., Zhang, Y., Yan, J. Effect of annealing

temperature on thermochromic properties of vanadium dioxide thin films deposited by organic sol–gel method. Applied Surface Science, 2013, 268: 556– 560.

(167) Xiao, X.D., Zhang, H., Chai, G., Sun, Y., Yang, T., Cheng, H., Chen, L., Miao, L., Xu, G. A cost-effective process to prepare VO2 (M) powder and films with superior thermochromic properties. Materials Research Bulletin, 2014, 51: 6–12.

(168) Xu, C.-L., Ma, L., Liu, X., Qiu, W.-Y., Su, Z.-X. A novel reduction-hydrolysis method of preparing VO2 nanopowders. Materials Research Bulletin, 2004, 39(7-8): 881–886.

(169) Xu, G, Jin, P., Tazawa, M., Yoshimura, K. Optimization of antireflection coating for VO2-based energy efficient window. Solar Energy Materials & Solar Cells, 2004, 83(1): 29–37.

(170) Xu, X. et al. Simulation and improvement of energy consumption on intelligent glasses in typical cities of China. Science China Technological Sciences, 2012, 55(7): 1999–2005.

(171) Xu, Y.J., Huang, W., Shi, Q., Zhang, Y., Wu, J., Song, L. Shape-dependent thermochromic phenomenon in porous nanostructured VO2 films. Materials Research Bulletin, 2013, 48(10): 4146-4149.

(172) Yan, J.Z., Zhang, Y., Huang, W.X., Tu, M.J. Effect of Mo–W co-doping on semiconductor-metal phase transition temperature of vanadium dioxide film. Thin Solid Films, 2008, 516(23): 8554–8558.

(173) Yan, J.Z., Huang, W., Zhang, Y., Liu, X., Tu, M. Characterization of preferred orientated vanadium dioxide film on muscovite (001) substrate. Physica Status Solidi (A), 2008, 205(10): 2409–2412.

(174) Yarimaga, O., Im, M., Choi, Y.-K., Kim, T.W., Jung, Y.K., Park, H.G., Lee, S., Kim, J.-M. A color display system based on thermochromic conjugated polydiacetylene supramolecules. Macromolecular Research, 2010, 18(4): 404–407.

(175) Yang, T., Hung, B., Chen, Y., Lai, M., Chung, T. Manufacture and characterization of sol–gel V1−x−yWxSiyO2 films for uncooled thermal detectors. Sensors and Actuators A, 2007, 140 (2): 194–199.

(176) Ye, H., Meng, X., Xu, B. Theoretical discussions of perfect window, ideal near infrared solar spectrum regulating window and current thermochromic window. Energy and Buildings, 2012, 49: 164–172.

(177) Ye, H.L., Long, S., Zhang, H.T., Xu, B., Gao, Y.F., Kang, L.T., Chen, Z. The demonstration and simulation of the application performance of the vanadium dioxide

single glazing. Solar Energy Materials and Solar Cells, 2013, 117: 168–173.

(178) Ye, H., Long, L. Smart or not? A theoretical discussion on the smart regulation capacity of vanadium dioxide glazing. Solar Energy Materials and Solar Cells, 2014, 120 B: 669–674.

(179) Ye, J., Zhou, L., Liu, F., Qi, J., Gong, W., Lin, Y., Ning, G. Preparation, characterization and properties of thermochromic tungsten-doped vanadium dioxide by thermal reduction and annealing. Journal of Alloys and Compounds, 2010, 504 (2): 503–507.

(180) Ye, X.W., Luo, Y., Gao, X., Zhu, S. Design and evaluation of a thermochromic roof system for energy saving based on poly(N-isopropylacrylamide) aqueous solution. Energy and Buildings, 2012, 48:175–179.

(181) Yokoyama, T., Masuhara, A., Onodera, T., Kasai, H., Oikawa, H. Development of fabrication process for Ag/polydiacetylene (core/shell) hybridized nanocrystals. Synthetic Metals, 2009, 159(9-10): 897–899.

(182) Yu, X., Luo, Y., Wu, W., Yan, Q., Zou, G., Zhang, Q. Synthesis and reversible thermochromism of azobenzene-containing polydiacetylenes. European Polymer Journal, 2008, 44(9): 3015–3021.

(183) Zakharova, G.S., Hellmann, I., Volkov,V.L., Täschner, C., Bachmatiuk, A., Leonhardt, A., Klingeler, R., Büchner, B. Vanadium dioxide nanobelts: Hydrothermal synthesis and magnetic properties. Materials Research Bulletin, 2010, 45(9): 1118–1121.

(184) Zhang, Y.F., Li, W., Fan, M.J., Zhang, F.F., Zhang, J.C., Liu, X.H., Zhang, H.N., Huang, C., Li, H.B. Preparation of W- and Mo-doped VO2(M) by ethanol reduction of peroxovanadium complexes and their phase transition and optical switching properties. Journal of Alloys and Compounds, 2012, 544: 30–36.

(185) Zhang, Y.F., Zhang, J., Zhang, X., Deng, Y., Zhong, Y., Huang, C., Liu, X., Liu, X., Mo, S. Influence of different additives on the synthesis of VO2 polymorphs. Ceramics International, 2013, 39(7): 8363–8376.

(186) Zhang, J., Eerdemutu, Y.C., Feng, J., Di, X., Liu, Z., Xu, G. Size- and shape-controlled synthesis of monodisperse vanadium dioxide nanocrystals. J Nanosci Nanotechnol., 2010, 10(3): 2092–2098.

(187) Zhang, J., Wang, J., Tian, H. Taking orders from light: progress in photochromic bio-materials.

(188) Materials Horizons, 2014, 1(2): 169–184.

(189) Zhang, K., Tangirala, M., Nminibapiel, D., Cao, W., Pallem, V., Dussarrat, C., Baumgart, H. Synthesis of VO2 Thin Films by Atomic Layer Deposition with TEMAV as Precursor. ECS Trans., 2013, 50(13): 175–182.

(190) Zhang, Y.F., Fan, M., Wu, W., Hu, L., Zhang, J., Mao, Y., Huang, C., Liu, X. A novel route to fabricate belt-like VO2(M)@C core-shell structured composite and its phase transition properties. Materials Letters, 2012, 71: 127–130.

(191) Zhang, Y., Zhang, J., Zhang, X., Huang, C., Zhong, Y., Deng, Y. The additives W, Mo, Sn and Fe for promoting the formation of VO2(M) and its optical switching properties. Materials Letters, 2013, 92: 61–64.

(192) Zhang, Z., Gao, Y., Chen, Z., Du, J., Cao, C., Kang, L., Luo, H. Thermochromic VO2 thin films: solution-based processing, improved optical properties, and lowered phase transformation temperature. Langmuir, 2010, 26(13): 10738–10744.

(193) Zhang, Z.T., Gao, Y., Kang, L., Jing, D., Luo, H. Effects of a TiO2 Buffer Layer on Solution-Deposited VO2 Films: Enhanced Oxidization Durability. Journal of Physical Chemistry C, 2010, 114(50): 22214–22220.

(194) Zhang, Z., Gao, Y., Luo, H., Kang, L., Chen, Z., Du, J., Kanehira, M., Zhang, Y., Wang, Z.L. Solution-based fabrication of vanadium dioxide on F: SnO2 substrates with largely enhanced thermochromism and low-emissivity for energy-saving applications. Energy and Environmental Science, 2011, 4: 4290–4297.

(195) Zheng, C.M., Zhang, X.M., Zhang, J.H., Liao, K.R. Preparation and characterization of VO2 nanopowders. Journal of Solid State Chemistry, 2001, 156(2): 274–280.

(196) Zhao, L.L., Miao, L., Tanemura, S., Zhou, J., Chen, L., Xiao, X., Xu, G. A low cost preparation of VO2 thin films with improved thermochromic properties from a solution-based process. Thin Solid Films, 2013, 543: 157–161.

(197) Zhao, Y., Xu, R., Zhang, X., Hu, X., Knize, R.J., Lu, Y. Simulation of smart windows in the ZnO/VO2/ZnS sandwichedstructure with improved thermochromic properties. Energy and Buildings, 2013, 66: 545–552.

(198) Zhou, J., Gao, Y., Liu, X., Chen, Z., Dai, L., Cao, C., Luo, H., Kanehira, M., Sun, C., Yan, L. Mg doped VO2 nanoparticles: hydrothermal synthesis, enhanced visible transmittance and decreased metal–insulator transition temperature. Physical Chemistry Chemical Physics, 2013, 15(20): 7505–7511.

(199) Zhou, Y., Huang, A., Li, Y., Ji, S., Gao, Y., Jin, P. Surface plasmon resonance induced excellent solar control for VO2@SiO2 nanorods-based thermochromic foils. Nanoscale, 2013, 5(19): 9208–9213.

CHAPTER THREE

PRELIMINARY EXPERIMENTAL STUDY OF THERMOCHROMIC ASPHALT BINDER

This chapter investigates the potential of using a commercially available polymeric dye to produce thermochromic asphalt binder, which reflects solar energy at high temperature and absorbs solar energy at low temperature. Therefore, it will reduce the surface temperature of asphalt pavement during summer and lead to improved durability. The thermal and phase transition properties of thermochromic materials were characterized by Differential Scanning Calorimetry (DSC) and modulated DSC. Comparison measurements found that the surface temperature of thermochromic asphalt binder is lower than that of the conventional asphalt binder with maximum decrease as high as 6.6°C during a typical summer day in the northeast U.S. (i.e. Cleveland, OH). Moreover, experimental results indicated that the temperature dropped slower in thermochromic asphalts than in regular asphalt when subjected to simulated winter temperature. This means thermochromic asphalt can delay ice formation on the surface of road, which is an important potential benefit for road safety in cold regions.

3.1 Introduction

Asphalt pavements are widely used in highways due to their good performance and relatively low construction and maintenance costs. However, the black color of asphalt binder has large solar absorption that leads to high surface temperature of asphalt pavement. Studies (i.e., (1-3)) measured surface temperature as high as 48-67°C during summer. The increased temperature in summer impacts durability of asphalt pavement by accelerating various distress mechanisms (i.e., rutting, shoving, aging, fatigue damage, bleeding) (4). A potential way to improve durability that has gained attention is the use of materials that present high solar reflectivity. Cool pavement has been consequently developed by using these cool materials with high reflectivity and emissivity to the solar radiation. Studies (5-9) show that cool pavement results in increased service life (durability) of the pavement. However, the reduced temperature of asphalt pavement exacerbates low temperature cracking during the winter period (10-11), which is quite harmful to the service life of the road. Furthermore, the lower temperature causes ice formation

in cold weather. So it is necessary to develop a new method to keep asphalt pavement cool during summer and warm during winter.

The strategy we undertake is to use thermochromic materials to create new materials possessing desirable solar reflectance, i.e., they reflect more solar energy at high temperature and reflect less solar energy at low temperature. To avoid any visual impact on road users, we hope to restrain such effects in the infrared range only. Thermochromic materials are substances that can change their colors in response to temperature. The specific temperature that causes the transition is called the transition temperature. The reversible temperature-dependent transformation of thermochromic materials is attributed to the variations of the molecular structures associated with temperature, such as phase transition in a compound (e.g., in an organic chromophore), changes in ligand geometry, variation in the crystal field or the number of solvent molecules in the coordination sphere (e.g., in a pure transition metal complex that derives its color from crystal field effects), and more complex factors in multicomponent mixtures (12). Thermochromic materials are characterized by high solar reflectance in summer and high solar absorption in winter. These properties make them attractive for building applications (13-16). Ma and Zhu (17) studied thermochromic cement and its potential use in building applications.

The objective of this paper is to study the performance of new thermochromic asphalt binders in reducing the pavement surface temperature during summer and therefore extend pavement service life. The study also aims to assess the materials' thermal performance under cold weather conditions. For this purpose, we firstly developed thermochromic asphalt binders by incorporating three selected organic thermochromic pigments into the conventional pure asphalt binder. The properties and performance of thermochromic asphalts were experimentally measured against that of the conventional pure asphalt. The results indicated that the use of thermochromic asphalt brings performance and safety benefits under both hot and cold weather conditions.

3.2 Experimental Design

Materials

The conventional asphalt binder used in this study is Superpave grade, PG64-22, produced by Kokosing Materials Inc. The organic thermochromic pigments were selected from those manufactured by Hali Industrial Corporation Ltd. Red, blue and black thermochromic pigments

with transition temperature around 31°C were chosen for this study. These pigments are microencapsulated with an average particle size of 3 ~ 10 μm. Figure 3.1 shows the color of the pigments below and above the transition temperature.

Thermochromic powders	Below the transition temperature	Above the transition temperature
Red		
Blue		
Black		
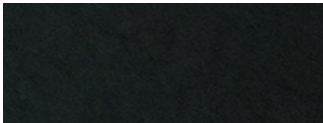
Figure 3.1. The colors of thermochromic microcapsule powders below and above the transition temperature.

Preparation of Thermochromic Asphalt Binder

Preparation procedure of thermochromic asphalt binder is as follows: Pure asphalt binder was heated at 150°C for 5 minutes; thermochromic materials with tentative content of 10% by weight or 11% by volume of pure asphalt binder, were then added into the melted asphalt binder; mixed for five minutes and poured into casting molds. The size of molds is 0.075 m × 0.042 m × 0.002 m. The black, blue and red thermochromic based asphalt binder were named as black, blue and red asphalt binder, respectively in this paper for simplicity in the nomenclature.

In principle, with the characteristics of thermochromic materials, thermochromic asphalt binder should display different response to solar radiation than regular asphalt. Solar energy consists of a spectrum of wavelengths, including ultraviolet, visible, and infrared light (almost 50% of the entire solar energy). Above the transition temperature, thermochromic asphalt binder should reflect more solar energy (mainly infrared radiation); under that temperature, it should reflect less (and therefore absorb more) solar energy (illustrated in Figure 3.2). Both energy-reflecting and energy-absorbing properties of thermochromic asphalt binder help to maintain pavement at an appropriate temperature range desirable for its longevity and performance.
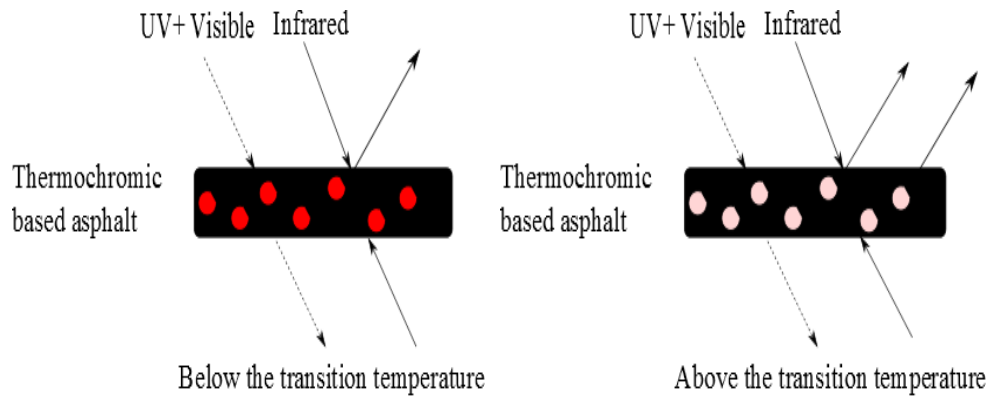
Figure 3.2. Schematic principle of thermochromic based asphalt.

3.3 Experimental Design to Measure the Properties and Performance of Thermochromic Asphalt Binder

Asphalt Binder Density

The density was determined using Archimedes' principle. Pure de-ionized water was used as the immersion fluid. The density of pure water is 0.99719 at 24.4°C. The density ρ of the sample could be calculated by the expression:

$$\rho = 0.99719 \frac{m_1}{m_1 - m_2}$$

(1)

where m_1 is the sample weight measured in air, m_2 is the sample weight measured in water.

Thermal Properties

Phase transition temperature and latent heat of asphalt binder were determined by the Differential Scanning Calorimetry (DSC). DSC is a thermal analysis technique to determine the temperature and heat flow associated with material transitions as a function of time and temperature. In this study, the phase transition temperature and latent heat during melting and freezing were measured by Q200 DSC from TA Instruments under N_2 atmosphere. Samples were encapsulated in aluminum pans. The scanning rate was 2°C/min and the temperature range was between 10°C and 40°C.

Heat capacity and thermal conductivity of asphalt binder were measure by MDSC. Modulated DSC (MDSC) is an expanded DSC in which a sinusoidal oscillation (temperature modulation) is imposed on a linear or isothermal heating or cooling programme (18). MDSC has obtained good

results of specific heat capacity and thermal conductivity (19-21). In this study, the heat capacity (Cp) and thermal conductivity (λ) of materials were measured in a MDSC (Q2000, TA Instruments) at 15, 25 and 35°C. The detailed experimental procedure and calculations referred to ASTM E1958-98 (22).

Cylindrical specimens of polystyrene were previously used to calibrate the MDSC. The measurement was performed by keeping the specimen for 20 minutes at each temperature of interest, with modulation amplitude of ±0.5 °C every 80 seconds. The experimental thermal conductivity was calculated using the equation:

$$\lambda_0 = \frac{8LC^2}{C_p m d^2 P}$$

(2)

where λ_0 is the experimental thermal conductivity (W/m·K), L is the sample thickness (m), C is the apparent heat capacity (J/K), C_p is the heat capacity (J/kg·K), m is the mass of the sample (kg), d is the sample diameter (m) and P is the oscillation period (s), 80 s.

However, the experimental thermal conductivity must be corrected using a standard specimen, polystyrene. So the calibration constant (D) was generated to determine correct thermal conductivity λ:

$$D = \left(\lambda_0 \cdot \lambda_r\right)^{0.5} - \lambda_r$$

(3)

$$\lambda = \frac{\lambda_0 - 2D + (\lambda_0^2 - 4D\lambda_0)^{0.5}}{2}$$

(4)

where λ_r is the thermal conductivity from the literature (23). The calibration constant should be in a range of 0.01 and 0.05 W/(m·K).

3.4 Thermal Performance of Thermochromic Asphalt Binder

For comparison of the thermal performance, black asphalt binder (asphalt binder incorporated with black thermochromic materials), blue asphalt binder (asphalt incorporated with blue thermochromic materials), red asphalt binder (asphalt incorporated with red thermochromic materials) and pure asphalt binder with dimensions of 0.075 m × 0.042 m × 0.002 m were placed on asphalt concrete tiles. To avoid heat flow from below, these tiles were insulated from below

and surrounding sides (Figure 3.3). The diameter and length of the tiles were 0.10 m and 0.06 m. Surface temperatures were recorded for 24 h during a typical hot summer day in Cleveland, OH in July 2012. The basic experiment setup consists of surface temperature sensors (thermocouples type K) connected to a data logging system. The temperature sensors, with an accuracy of 0.1°C, were mounted on the centers of the surfaces of each tile. Instantaneous values of temperature were measured and saved every 60 seconds. To assess their thermal characteristics during winter, comparison measurement was also performed in a freezer. Details of experimental results are elaborated in the following section.
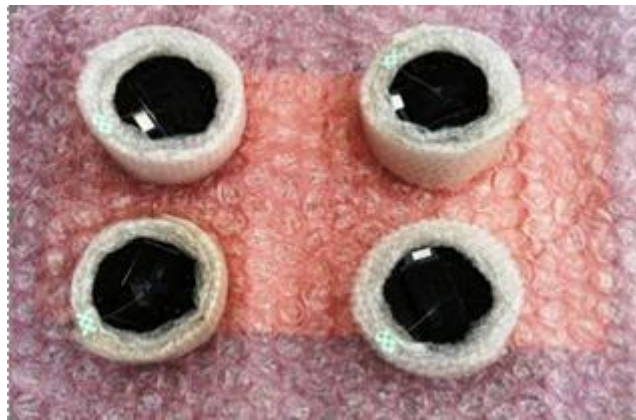
Figure 3.3. View of surface temperature measurement of the samples.

3.5 Results and Analyses

Density

The densities of asphalt binder specimens were measured using Archimedes' principle, each with three repetitions. From this, the average densities and standard deviations of prepared asphalt samples were determined. Results are summarized in Table 3.1.

TABLE 3.1. Density and DSC Results of the Samples

Sample	Density	Melting		Freezing	
	(kg/m3)	Phase change temperature (°C)	Latent heat (J/kg)	Phase change temperature (°C)	Latent heat (J/kg)
Black thermochromic	900	27.28	33,660	20.38	35,680
Blue thermochromic	900	34.41	25,040	23.31	29,370

Red thermochromic	900	31.76	23,270	22.21	38,510
Pure asphalt binder	1013.1±14.1	-7.75	550	43.08	240
Black asphalt binder	1001.6±7.9	27.47	3590	19.83	3120
Blue asphalt binder	1032.7±39.0	34.80	2980	24.14	2970
Red asphalt binder	1022.2±27.8	32.35	1740	23.15	1860

Phase Transition Temperature and Latent Heat

The thermochromic transition behaviors of both raw thermochromic materials and thermochromic asphalt binder were characterized by DSC. The phase transition temperature is determined as the maximum point on the endo- or exotherm, and the latent heat is evaluated from the integrated area of the peak profile. The results are summarized in Table 3.1.

The measured DSC curves of thermochromic materials are shown in Figure 3.4. It can be seen that the melting and freezing temperatures are 27.28 and 20.38°C, 34.41and 23.31°C, as well as 31.76 and 22.21°C for black, blue and red thermochromic powders, respectively. The melting and freezing latent for them are 33,660 and 35,680 J/kg, 25,040 and 29,370 J/kg, as well as 23,270 and 38,510 J/kg, respectively. The phase transition temperature is close to the transition temperature (31 °C) reported by the manufacturer.
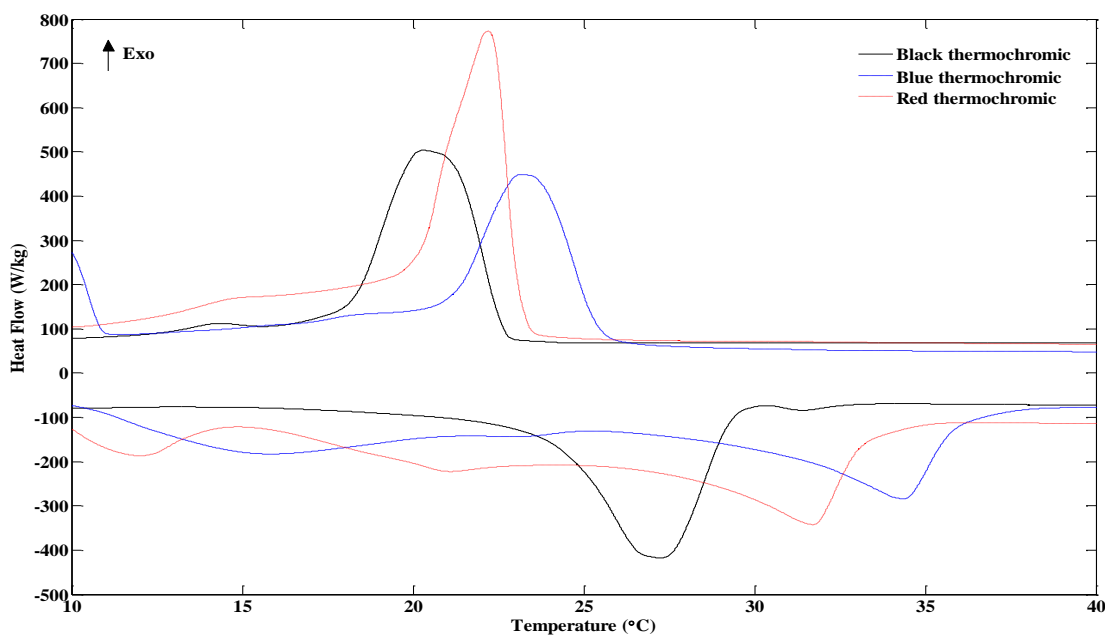
Figure 3.4. DSC curves of raw thermochromic materials.

Figure 3.5 illustrates the DSC curves of thermochromic asphalt binders. The figure shows when incorporated in asphalt binder, the transition temperatures of thermochromic asphalt binders do not change much. However, latent heat of thermochromic asphalt binder is much lower than that of thermochromic powders, possibly due to the low latent heat of pure asphalt. The maximum theoretical values based on parallel model of composite show that melting and freezing latent heat should be 4190 and 4140, 3240 and 3440, 3050 and 4450 J/kg for black, blue and red asphalt binder, respectively. The measured values, as shown in Table 1, are lower than the theoretical predictions. Such difference between theoretical and experimental values might be due to irregular heat dissipation pattern through the samples, which needs to be further investigated.
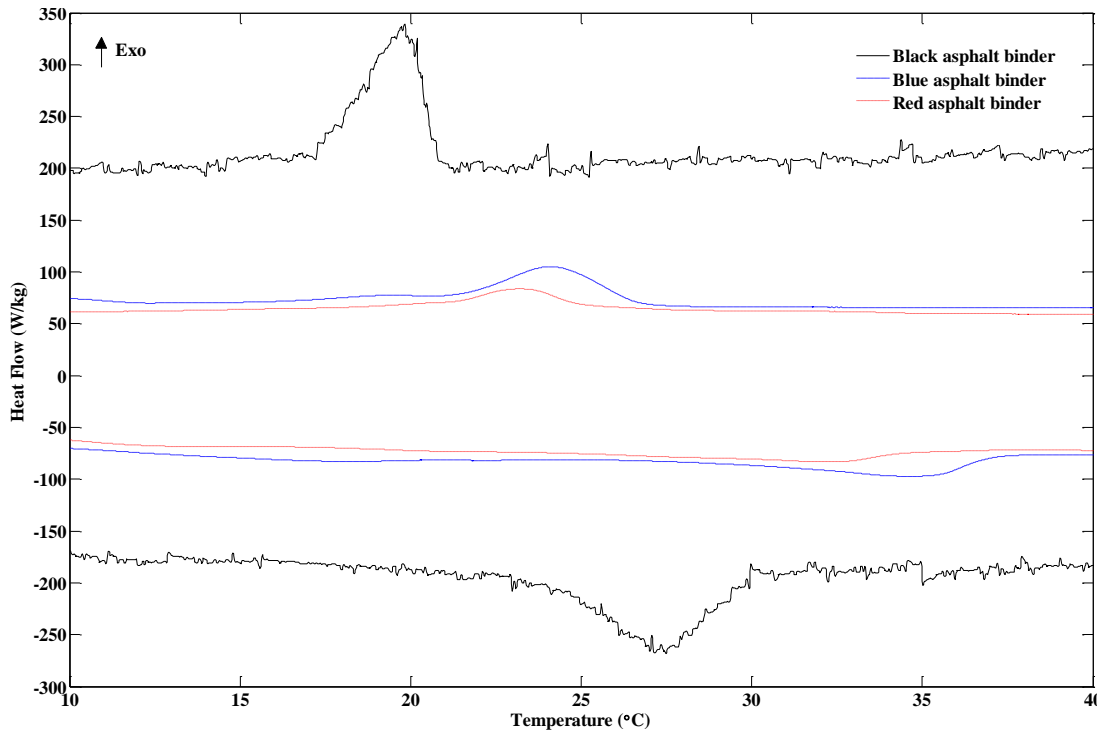
Figure 3.5. DSC curves of thermochromic based asphalt binders.

Heat Capacity and Thermal Conductivity

Modulated DSC tests were performed at 15, 25 and 35 °C to determine the influence of temperature on the thermal properties (i.e. heat capacity and thermal conductivity). These temperatures cover the phase transition temperatures of all samples. The calibration constant at

each temperature was obtained by standard polystyrene sample. The results are listed in Table 3.2.

TABLE 3.2. Calibration Constant, Heat Capacity and Thermal Conductivity Results of the Samples

Temperature (°C)	Calibration constant	Heat capacity (J/kg· K)				Thermal conductivity (W/m·K)			
		Pure asphalt binder	Black asphalt binder	Blue asphalt binder	Red asphalt binder	Pure asphalt binder	Black asphalt binder	Blue asphalt binder	Red asphalt binder
15	0.019966	1392	1479	1447	1.626	0.1498	0.1527	0.1478	0.1657
25	0.018217	1414	1563	1503	1.724	0.1581	0.185	0.1581	0.2210
35	0.017569	1412	1501	1484	1.644	0.1749	0.1801	0.1752	0.2282

Figure 3.6 (a) shows heat capacities obtained using modulated DSC experiments. The dependence of thermal conductivity on temperature is shown in Figure 6 (b). It can be seen from Figure 6 and 7 that heat capacity and thermal conductivity at 25 °C are always higher than those at 15 and 35 °C. This might be attributed to different phases at different temperatures. The heat capacity and thermal conductivity, in the magnitude of values, are red, blue and pure asphalt binders. The difference between values of heat capacity and thermal conductivity could be explained by different structures of thermochromic materials with different colors.
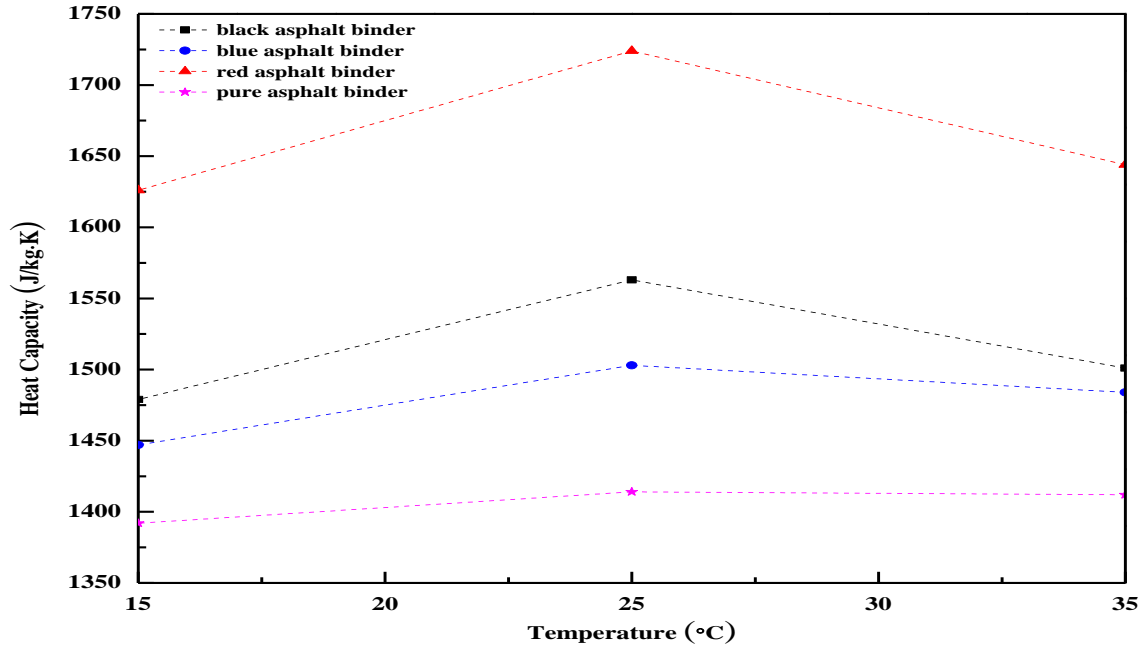
(a)
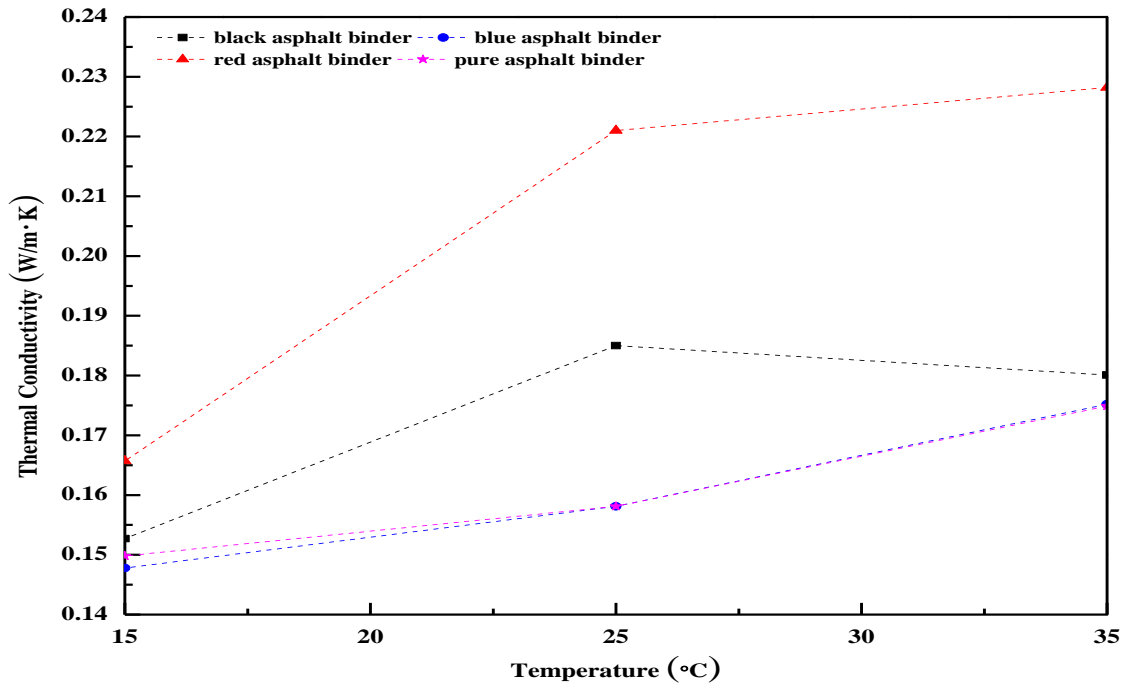
(b)

Figure 3.6. Influence of temperature on heat capacity (a) and thermal conductivity (b) of thermochromic based asphalt binders.

Thermal Performance of Thermochromic Asphalt Binder Samples

Experiments were conducted to evaluate the effects of thermochromic materials on the thermal responses of pavement. The experimental design simulated the surface temperatures of thermochromic asphalt binder samples under typical summer condition. The set up for this comparison study was illustrated in Figure 3.3 and described in the earlier context. Based on the measured surface temperature measurements, the mean, maximum and minimum surface temperatures were calculated for each sample. The results are shown in Table 3.3. The difference between surface temperatures of thermochromic asphalt binders and pure asphalt binder ($T_{thermochromic}$-T_{pure}) with time is shown in Figure 3.7.

TABLE 3.3. Surface Temperature of the Tested Samples during Summer and Winter

Sample	Surface temperature (°C) in summer				Surface temperature (°C) in winter
	Diurnal			Nocturnal	Mean
	mean	maximum	ΔTmax	Mean	
Pure asphalt	51.83	72.11	-	24.79	-6.31
Black asphalt	48.45	68.91	6.6	24.97	-3.54
Blue asphalt	51.74	71.88	2.68	25.36	-3.85
Red asphalt	50.34	70.83	4.96	25.08	-6.12

To explain Table 3.3, during summer, the diurnal surface temperature (07:00-19:00) and the nocturnal surface temperature (00:00-07:00 and 19:00-00:00) were considered respectively. The results show that all thermochromic asphalt binders have lower surface temperature than conventional pure asphalt binder at daytime during summer. The mean diurnal temperature of thermochromic based asphalt binder samples ranges from 48.45°C for black asphalt binder sample to 51.74°C for blue asphalt binder sample. The corresponding temperature for conventional pure asphalt binder is 51.83°C. The maximum diurnal surface temperature of thermochromic based asphalt binders occurred at different time ranges from 68.91°C for black asphalt binder to 71.88°C for blue asphalt binder. The corresponding temperature for conventional pure asphalt binder is 72.11°C. At the same time, the maximum differences of surface temperature between pure asphalt binder and thermochromic based asphalt binders are 6.6°C, 2.68°C and 4.96°C for black, blue and red asphalt binder. These temperature differences between the samples can be explained by the solar reflectance and thermal properties of the

samples. More specifically, the higher the solar reflectance, the lower the surface temperature, as more solar radiation is reflected by the sample. The diurnal temperature difference between the conventional pure asphalt binder and thermochromic asphalt binders is depicted in Figure 3.8. In addition, thermochromic asphalt binders at nocturnal normally keep warmer than pure asphalt binder.

Figure 3.9 presents surface temperature of comparison specimens measured under simulated winter condition. The calculated mean surface temperature ranges from -3.54°C for black asphalt binder to -6.12°C for red asphalt binder. The corresponding temperature of conventional pure asphalt binder is -6.31°C. Therefore, the surface temperature of thermochromic asphalt pavement will be higher than pure asphalt pavement, which will help to mitigate the low temperature crack or icing during winter. Their relatively higher mean surface temperature during winter and nocturnal in summer might be attributed to high solar absorption of thermochromic materials.
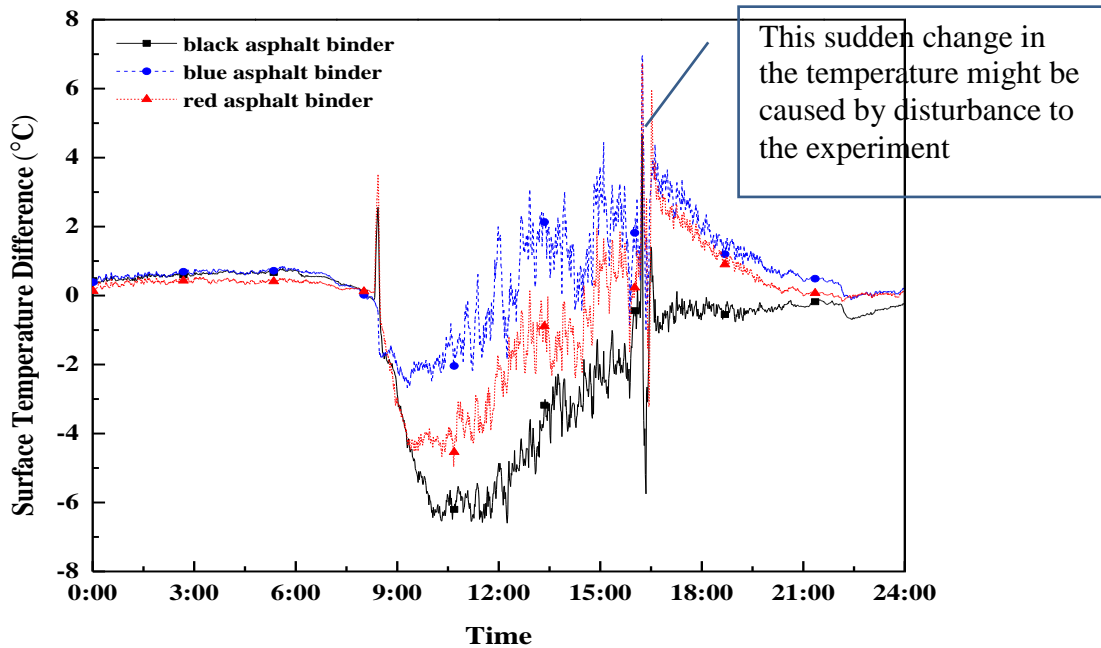
Figure 3.7. Difference between surface temperatures of thermochromic asphalt binders and pure asphalt binder
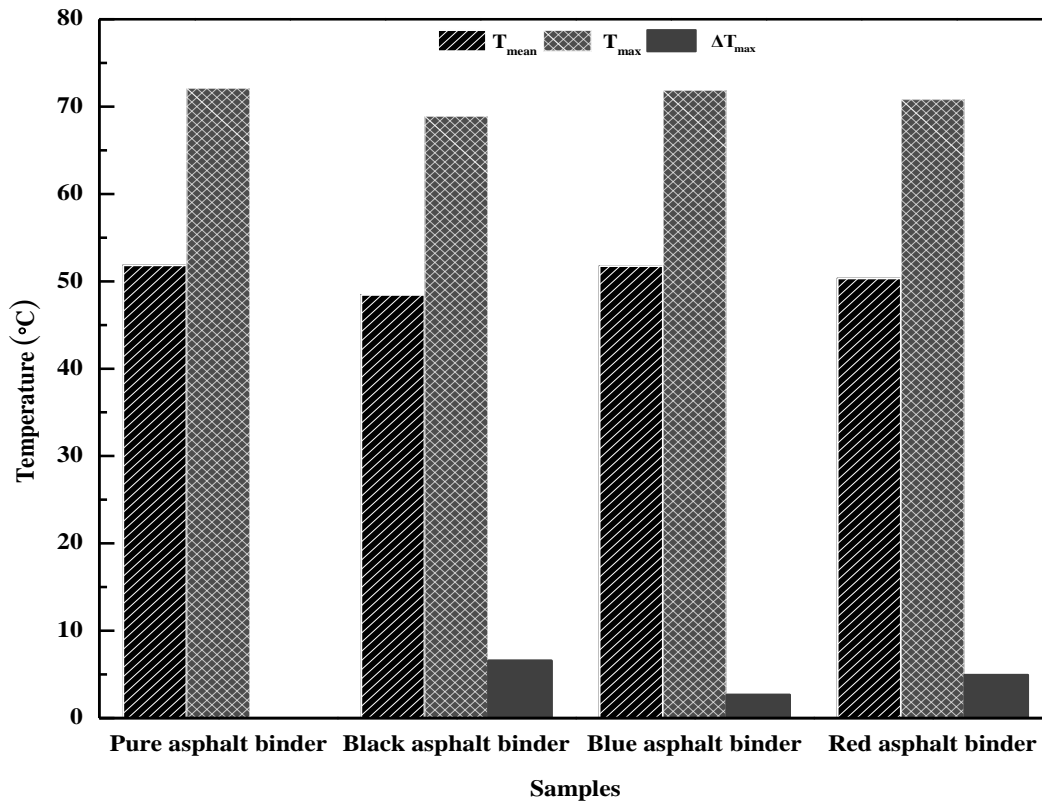
Figure 3.8. Diurnal temperature difference between pure asphalt and thermochromic based asphalt binders.
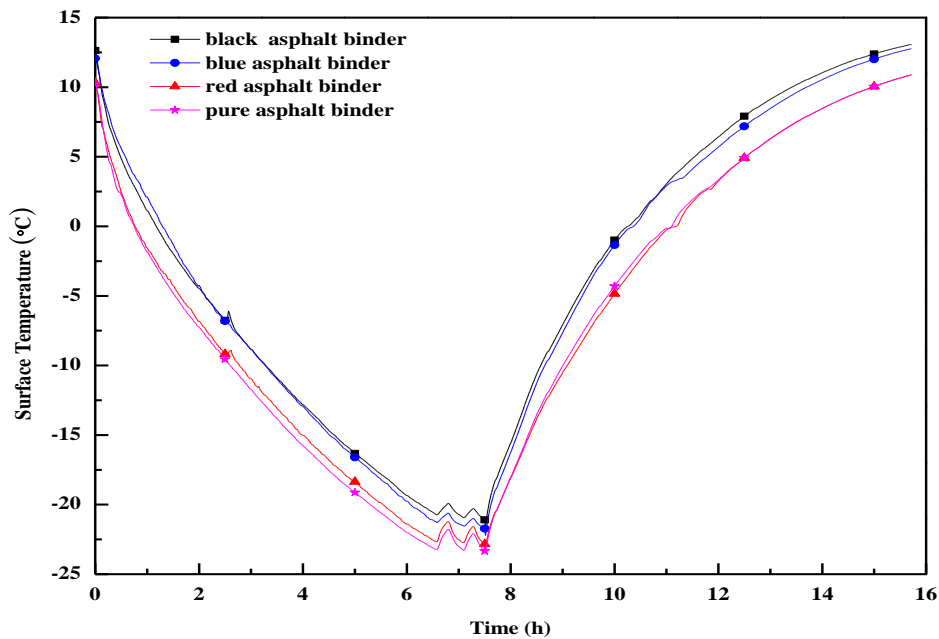
Figure 3.9. Surface temperature of asphalt binder samples during winter.

Discussion

It should be noticed that during evaluation of thermal performance of thermochromic asphalt binder, the rectangular samples with size of 0.075 m × 0.042 m only cover a portion of the surface of the cylinder asphalt specimen (diameter of 0.1 m), or 40% of the surface of the asphalt concrete specimen. Therefore, the net effectiveness of the thermochromic surface is increased in complete surface coverage. It is anticipated that the reduction of the surface temperature will be more significant with 100% coverage of the surface of the comparison specimens. The reduced surface temperature during summer and increased surface temperature during winter both help to reduce temperature related distresses.

Besides the above benefits, it has shown that reduced surface temperature of pavement can mitigate urban heat island, and reduce air pollution and smog formation. The increase of surface temperature during winter conditions helps to mitigate problems such as black ice.

3.6 Summary

This chapter describes the preliminary study to assess the potential of thermochromic materials for improving the performance of asphalt pavement. The key is to use the materials to modulate the surface temperature of asphalt pavement (to make it cooler under high temperature and warmer under low temperature). Experiments were conducted to validate this concept. Thermochromic asphalt binder was prepared by mixing selected thermochromic materials with traditional asphalt binder. Physical and thermal properties of both thermochromic materials and thermochromic asphalt binders were measured.

The effectiveness of thermochromic asphalt binders in changing the surface temperature of asphalt pavement was studied by comparison experiments under typical summer and modeling winter conditions. The results showed that the use of thermochromic asphalt binder (with 40% coverage of pavement surface) can reduce the surface temperature as high as 6.6°C during summer compared with pure asphalt binder. This helps to reduce high temperature related performance degradation. In addition, under winter conditions, the surface temperatures of thermochromic asphalt binders are higher than that of pure asphalt binder. This could help to reduce the low temperature cracking and mitigate ice formation on pavement during winter. Therefore, this innovative thermochromic asphalt binder might potentially help improve the durability and safety of asphalt roads.

3.7 References

(1) Santamouris, M., Pavlou, K., Synnefa, A., Niachou, K., Kolokotsa, D. Recent progress on passive cooling techniques: Advanced technological developments to improve survivability levels in low-income households. Energy and Buildings, 2007, 39(7): 859-866.

(2) Synnefa, A., Dandou, A., Santamouris, M., Tombrou, M., Soulakellis, N. Large scale albedo changes using cool materials to mitigate heat island in Athens. Journal of Applied Meteorology and Climatology, 2008, 47(11): 2846-2856.

(3) Doulos, L., Santamouris, M., Livada, I. Passive cooling of outdoor urban spaces. The role of materials. Solar Energy, 2004, 77(2): 231-249.

(4) Yoder, E. J. and Witzak, M. W. Principles of Pavement Design. New York, NY: Wiley and Sons, 1975.

(5) Pomerantz, M. and Akbari. H. Cooler Paving Materials for Heat Island Mitigation. In 1998 ACEEE Summer Study on Energy Efficiency in Buildings, Asilomar, CA, City: American Council for an Energy-Efficient Economy, 1998.

(6) Pomerantz, M., Akbari, H. Cooler paving materials for heat island mitigation, in: Proceedings of the 1998 ACEEE Summer Study on Energy Efficiency in Buildings, vol. 9, Pacific Grove, CA, 1998, p. 135.

(7) Pomerantz, M., Akbari, H., Chen, A., Taha, H., Rosenfeld, A. Paving Materials for Heat Island Mitigation, Lawrence Berkeley National Laboratory Report LBL- 38074, Berkeley, CA, 1997.

(8) Pomerantz, M., Akbari, H., Harvey, J. T. 2000. Cooler reflective pavements give benefits beyond energy savings: Durability and illumination. Rep. No. LBNL-45370, Berkeley, CA, 14 pp.

(9) Kinouchi, T., Yoshinaka, T., Fukae, N., Kanda, M., 2004. Development of cool pavement with dark colored high albedo coating. Fifth Conference for the Urban Environment, Vancouver, Canada.

(10) Hao, P.W., Zhang, D.L., Hu, X.N., 2000. Evaluation method for low temperature anticracking performance of asphalt mixture. Journal of Xi'an Highway University 20 (3), 1–5.

(11) Kanerva, H.K., VINSON, T.S., Zeng, H., 1994. Low Temperature Cracking Field Validation of the Thermal Stress Rest Rained Specimen Test. R. SHRP-A-401.

(12) White, M. A., LeBlanc, M. Thermochromism in Commercial Products. Journal of Chemical Education, 1999, 76 (9): 1201-1205.

(13) Santamouris, M., Synnefa, A., Kolokotsa, D., Dimitriou, V., Apostolakis, K. Passive cooling of the built environment - use of innovative reflective materials to fight heat island and decrease cooling needs. International Journal Low Carbon Technologies, 2008, 3(2): 71-82.

(14) Karlessi, T., Santamouris, M., Apostolakis, K., Synnefa, A., Livada, I. Development and testing of thermochromic coatings for buildings and urban structures. Solar Energy, 2009, 83(4): 538-551.

(15) Granqvist, C.G. Materials Science for Solar Energy Conversion Systems. Pergamon press, Oxford, 1991.

(16) Saeli, M., Piccirillo, C., Parkin, I. P., Binions, R., Ridley, I. Energy modelling studies of thermochromic glazing. Energy and Buildings, 2010, 42(10): 1666-1673.

(17) Ma, Y. P. and Zhu, B.R. Research on the preparation of reversibly thermochromic cement based materials at normal temperature. Cement and Concrete Research, 2009, 39(2): 90-94.

(18) Reading, M., Luget, A., Wilson, R. Modulated differential scanning calorimetry. Thermochimica Acta, 1994, 238: 295–307.

(19) Marcus, S.M., Blaine, R.L. Thermal-conductivity of polymers, glasses and ceramics by modulated DSC. Thermochimica Acta, 1994, 243(2): 231-239.

(20) Simon, S.L., McKenna, G.B. Measurement of thermal conductivity using TMDSC: solution to the heat flow problem. Journal of Reinforced Plastics and Composites, 1999, 18(6): 559-571.

(21) Isa, I.A.A., Jodeh, S.W. Thermal properties of automotive polymers III—thermal characteristics and flammability of fire retardant polymers. Materials Research Innovations, 2001, 4 (2–3): 135-143.

(22) ASTM E1958-98. Thermal conductivity and thermal diffusivity by modulated temperature differential scanning calorimetry.

(23) Privalko, V.P., Novikov, V.V. The Science of Heterogeneous Polymers: Structure and Thermophysical Properties, John Wiley & Sons, 1995.

CHAPTER FOUR

CHARACTERIZATION AND EMPIRICAL ANALYSIS OF THE OPTICAL REFLECTANCE SPECTRA OF THERMOCHROMIC ASPHALT

This chapter describes the study of the optical reflectance of thermochromic binder. Measurements of spectral reflectance of thermochromic powders indicate that thermochromic materials feature more reflection at higher temperature and more absorption at lower temperature. The spectral reflectance of thermochromic powders as functions of wavelength and temperature are proposed by fitting experimental results. Optical measurements conducted on the asphalt binder mixture show more reflection than conventional asphalt binder and that the reflectance increases with temperature. The relationship between spectral reflectance of asphalt binder mixture and temperature as well as wavelength has been deduced by fitting experimental data. Finally, it is found that the spectral reflectance of the thermochromic asphalt binder mixture increases as the powder content increases. The empirical formulas based on Maxwell, Mori-Tanaka, and effective medium theory (EMT) models are determined between spectral reflectance of the thermochromic asphalt binder mixture and powder content as well as wavelength in the near infrared region by fitting technique. These empirical equations provide a good potential to predict the reflectance spectra of the thermochromic asphalt binder mixture with different contents of thermochromic powders at different temperatures.

4.1 Introduction

Asphalt pavement has been widely used in highways due to the good performance and relatively low construction and maintenance costs. However, the surface temperature of asphalt pavement is reported in studies (i.e., (1-3)) as high as 48-67°C during summer. This is attributed to the black color of asphalt binder, which possesses large solar absorption. The increased temperature in asphalt pavement deteriorates its durability by accelerating various distress mechanisms (i.e., rutting, shoving, aging, fatigue damage, bleeding) (4). A potential way to improve durability that is attractive is to use materials which create high solar reflectivity. Cool pavement has been consequently developed by using these cool materials with high reflectivity and emissivity to solar radiation. Studies (5–9) show that cool pavement exhibits lower surface temperatures,

resulting in increased service life (durability) of pavements. However, the reduced temperature in asphalt pavement exacerbates low-temperature cracking during the winter period (10–11), which is quite harmful to service life of the road. Moreover, the lower temperature is conductive to ice formation in cold weather. So it is necessary to develop a new method to keep asphalt pavement cool during summer and warm during winter.

An innovative strategy in our study is to use thermochromic materials to develop new materials possessing desirable solar reflectance, i.e., they reflect more solar energy at high temperature and reflect less solar energy at low temperature. Thermochromic materials are substances that can change their colors in response to variation in temperature. Materials incorporated with proper thermochromic materials feature high solar reflectance in summer and high solar absorption in winter. The change of their optics in such a dynamic way makes them attractive for applications that improve the urban microclimate, decrease the energy demands of the buildings, and provide a thermally comfortable indoor environment (12–16).

In this study an innovative asphalt binder mixture containing thermochromic materials is designed to modulate the temperature of asphalt pavement. The optical properties are characterized by spectrophotometry measurements. The relationship between reflectance spectra of both of thermochromic powders and asphalt binder mixture and temperature is determined by fitting experimental data. The empirical expressions between reflectance spectra of asphalt binder mixture and content of powders in the near infrared region also are derived. These empirical equations provide good prediction for optical properties of thermochromic asphalt binder mixtures.

4.2 Experimental Design

Raw Materials

Asphalt binder used in this study is Superpave grade, PG 64-22, produced by Kokosing Materials Inc. Thermochromic powders with an average particle size of 3 ~ 10 μm were selected from those manufactured by Hali Industrial Corporation Ltd. Red, blue and black thermochromic powders with transition temperature around 31 °C were chosen for this study. These thermochromic materials are organic mixtures, which consists of lueco dye (electron donor), developer (electron acceptor) and solvent. Below the transition temperature, leuco dye reacts

with the developer, the absorption peaks shifts from the UV to the visible range, and thus the powder becomes colored.

At temperature above the transition temperature, the solvent-developer interactions dominate, and leuco dye is separated from the developer and leads to loss of color. Thermochromic materials are encapsulated by trioctanoinand and therefore at high temperature thermochromic powders become white or light-colored state. The molecular structures of thermochromic materials and their changes with temperature are shown in Fig. 4.1.

(a)

(b)

(c)

Fig. 4.1. Molecular structures of thermochromic powders and their changes with temperature: a) black powder; b) blue powder; c) red powder.

Preparation of Asphalt Binder Mixture with Thermochromic Materials

The following procedures are used to prepare the thermochromic apshalt binder mixture: Pure asphalt binder was first heated to 150°C for a few minutes; Then thermochromic powders at 10% by weight of pure asphalt binder were added into the melted asphalt binder; The materials were mixed for a few minutes before poured into casting molds. The asphalt binder mixtures containing black, blue and red thermochromic powdder are named as black, blue and red asphalt binder, respectively in this paper for simplicity in the nomenclature.

In principle, thermochromic asphalt binder mixture should exhibit a different response to solar radiation than regular asphalt binder. Solar energy consists of a spectrum of wavelengths, including ultraviolet, visible, and infrared light (almost 50% of the entire solar energy). Under the transition temperature (shown in Fig. 4.2(a)), thermochromic powder presents dark color, this innovative binder should reflect less (and therefore absorb more) solar energy; above that temperature (shown in Fig. 4.2(b)), color of thermochromic powder becomes light, thermochromic asphalt binder should reflect more solar energy (mainly infrared radiation). Both energy-reflecting and energy-absorbing properties of the thermochromic asphalt binder mixture help to maintain pavement at an appropriate temperature range desirable for its longevity and performance.

(a) (b)
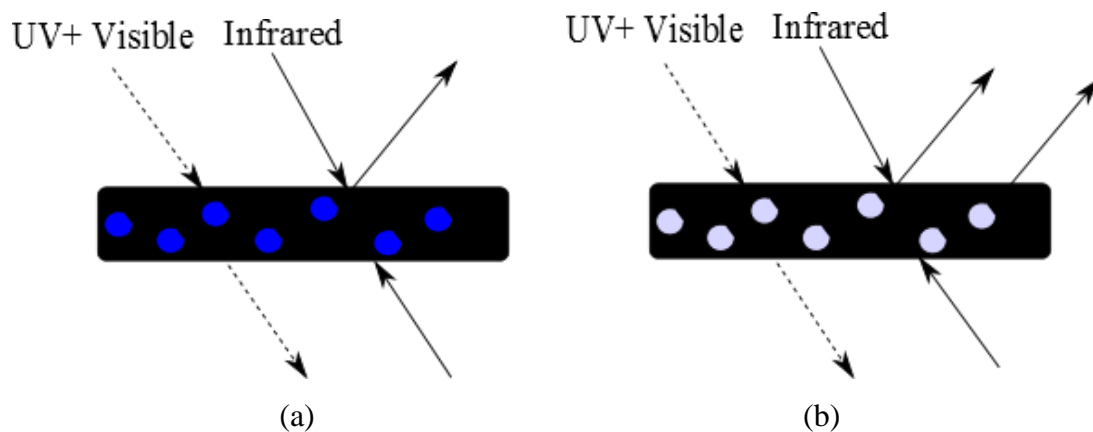
Fig.4.2. Schematic principle of asphalt binder mixture containing blue powders.

Optical Characterization

The spectral reflectance of the samples is measured over the wavelength range of 300-1800 nm by the Agilent Cary 6000i UV-Vis-IR Spectrophotometer with a DRA integrating sphere. The measurements are performed according to ASTM E903-12 (17). During the measurements, thermochromic powders and various asphalt binders are packed between microscopic slides at a thickness of 1mm. Reflectance measurements are conducted through the microscopic slides at 25°C and 35 °C, respectively. To study the influence of powder content on reflectance spectra of asphalt binder mixture, asphalt binder mixtures containing 10%, 20%, 30% and 40% red thermochromic powders by weight are prepared and tested, respectively. All samples are measured with two or three duplicates and the average values are calculated and presented.

4.3 Characterization Results and Empirical Analysis

Reflectance Spectra of Thermochromic Powders

The results from the spectrophotometric measurements of thermochromic powders under different temperatures are presented in Fig. 4.3. As can be seen, in the visible range, reflectance spectra exhibit differences, depending on the specific color. The reflectance curves demonstrate strong absorption in the near-ultraviolet range and high reflection in the near infrared of the spectrum. With the increase of temperature, the values of spectral reflectance of thermochromic powders increase, especially in the visible range. This is attributed to the color change with temperature.
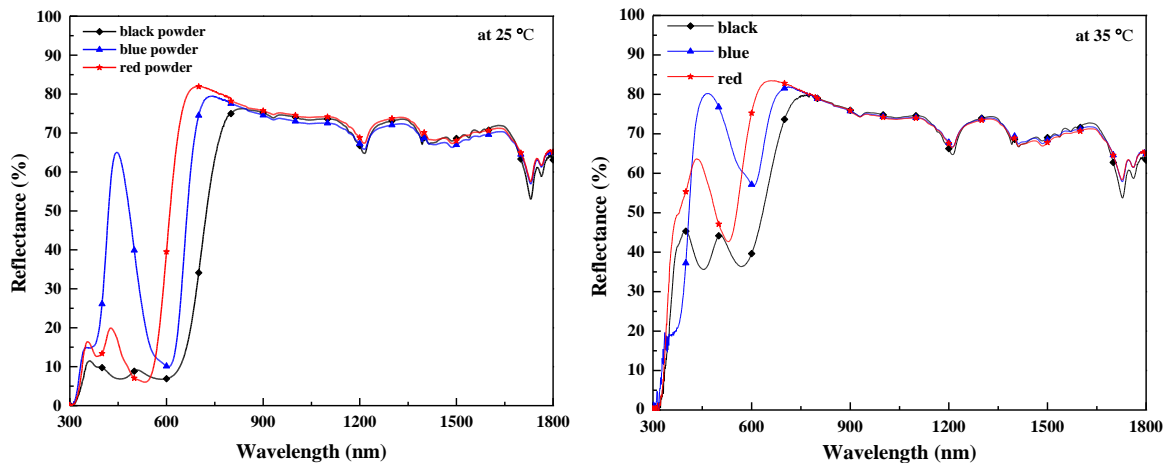
Fig. 4.3. Reflectance spectra of thermochromic powders at 25 and 35 °C.

73

To predict the reflectance spectra of thermochromic powders under a different temperature, the relationship between reflectance and wavelength is first determined by fitting at each temperature. Considered the curve shape in Fig. 4.3, polynomial and Boltzman models are used in different regions to fit experimental data. The fit equations and the values of adjusted R square (R^2) are summarized in Table 4.1. Fig. 4.4 displays the comparison between fitted and measured values. It can be seen that the empirical formulas present good agreement with experimental results. In addition, at higher temperature, the lower bound in Boltzman model increases. In the range of 800–1800 nm, the reflectance spectra of thermochromic powders as a function of temperature can be derived by the interpolation method as follows:

For black thermochromic powder,

$$R_p = 70.65 + \frac{-73.575 + 3.245T - 70.65}{1 + e^{\frac{\lambda - 706.80}{20.50}}} \tag{1}$$

For blue thermochromic powder,

$$R_p = 70.86 + \frac{-108.13 + 4.718T - 70.86}{1 + e^{\frac{\lambda - 655.65}{10.99}}} \tag{2}$$

For red thermochromic powder,

$$R_p = 72.50 + \frac{-83.39 + 3.594T - 72.50}{1 + e^{\frac{\lambda - 599.33}{13.68}}} \tag{3}$$
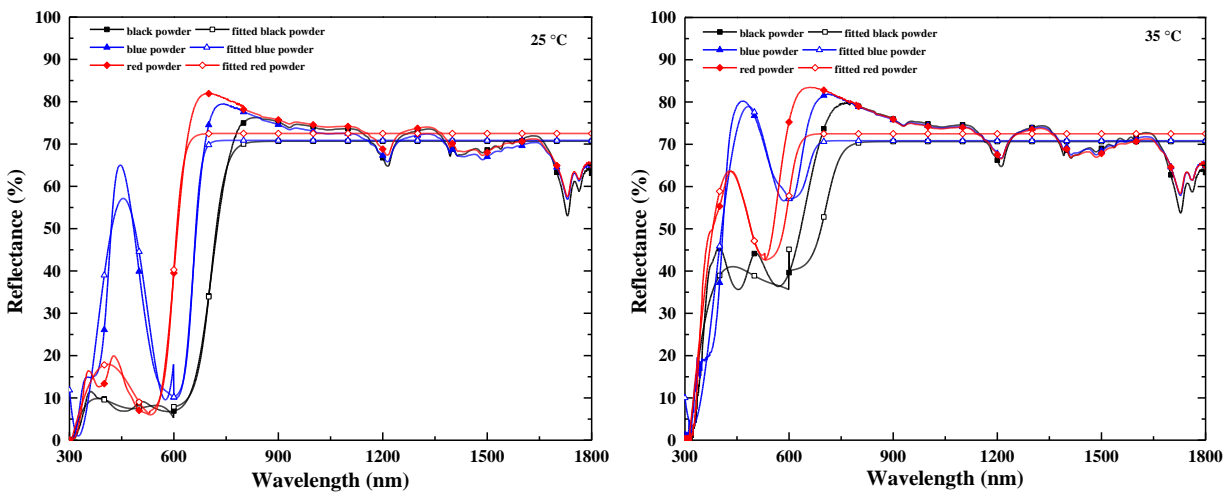
Fig. 4.4. Comparison between experimental and fitted values of reflectance spectra of thermochromic powders at 25 and 35 °C.

Table 4.1. Empirical equations for reflectance spectra of thermochromic powders under different temperatures.

Samples	Range	Temperature (°C)	Empirical Equations	R^2
Black powder	300–599	25	$R_p = -1326.64 + 11.7517\lambda - 0.03829\lambda^2 + 5.4788 \times 10^{-4}\lambda^3 - 2.9082 \times 10^{-8}\lambda^4$	0.816
		35	$R_p = -1944.19 + 15.3839\lambda - 0.0443\lambda^2 + 5.6355 \times 10^{-4}\lambda^3 - 2.6733 \times 10^{-7}\lambda^4$	0.8810
	600–1800	25	$R_p = 70.65 + \dfrac{7.55 - 70.65}{1 + e^{\frac{\lambda - 706.80}{20.50}}}$	0.9343
		35	$R_p = 70.65 + \dfrac{40 - 70.65}{1 + e^{\frac{\lambda - 706.80}{20.50}}}$	0.8640
Blue powder	300–599	25	$R_p = 7526.85 - 72.2084\lambda + 0.2530\lambda^2 - 3.8306 \times 10^{-3}\lambda^3 + 2.1190 \times 10^{-6}\lambda^4$	0.9040
		35	$R_p = 5664.97 - 53.7020\lambda + 0.1850\lambda^2 - 2.7388 \times 10^{-3}\lambda^3 + 1.4785 \times 10^{-6}\lambda^4$	0.9630
	600–1800	25	$R_p = 70.86 + \dfrac{9.82 - 70.86}{1 + e^{\frac{\lambda - 655.65}{10.99}}}$	0.8787
		35	$R_p = 70.86 + \dfrac{57 - 70.86}{1 + e^{\frac{\lambda - 655.65}{10.99}}}$	0.8940
Red powder	300–530	25	$R_p = 344.303 - 5.0938\lambda + 0.024\lambda^2 - 4.5098 \times 10^{-4}\lambda^3 + 2.9583 \times 10^{-4}\lambda^4$	0.8374
		35	$R_p = 4030.98 - 44.3279\lambda + 0.1753\lambda^2 - 2.9578 \times 10^{-3}\lambda^3 + 1.8116 \times 10^{-6}\lambda^4$	0.9734
	531–1800	25	$R_p = 72.50 + \dfrac{6.46 - 72.50}{1 + e^{\frac{\lambda - 599.33}{13.68}}}$	0.886
		35	$R_p = 72.50 + \dfrac{42.4 - 72.50}{1 + e^{\frac{\lambda - 599.33}{13.68}}}$	0.8530

where R_p-reflectance of thermochromic powders (%); λ-wavelength (nm).

Reflectance Spectra of Binary Asphalt Mixtures with Thermochromic Powders

Influence of temperature on reflectance spectra of asphalt binder mixture

The reflectance spectra of asphalt binder mixtures at 25 and 35 °C are shown in Fig. 4.5. It can be noticed that asphalt binder mixtures are more reflective than conventional asphalt binder in the near infrared range. The increase in reflectance in the near infrared region can be explained by the significantly high reflection of thermochromic powders. Small difference between reflectance curves in the visible and near-ultraviolet range might be attributed to the low depth of penetration of the spectrum or light extinction. Besides, the values of spectral reflectance of asphalt binder mixtures increase as temperature increase.
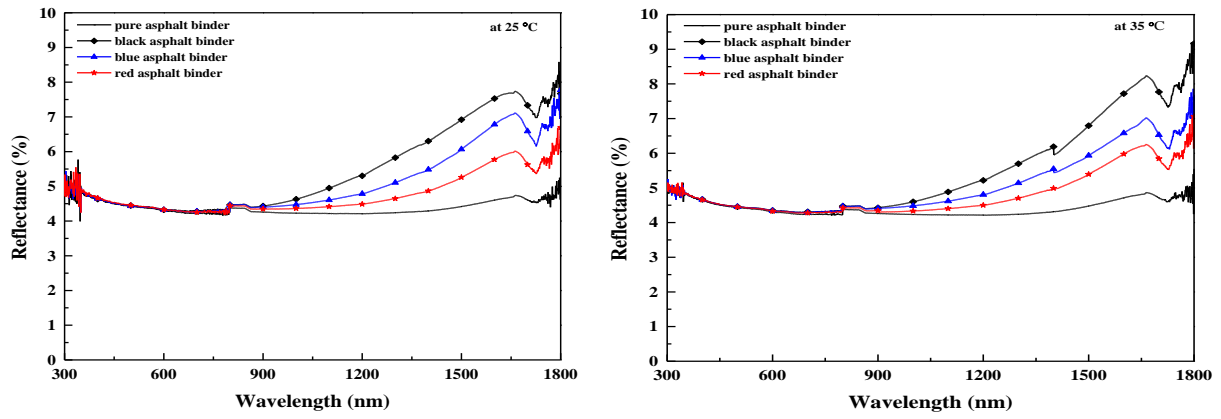
Fig. 4.5. Reflectance spectra of asphalt binder mixtures at 25 and 35 °C.

The relationship between reflectance of asphalt binder mixtures, reflectance of each component and wavelength is fitted by Matlab fitting functions and simple mixing formulas of parallel models. For optical properties, considering the attenuation of the amplitude of the wave for a path of one wavelength in the medium, the parallel model is slightly modified by multiplying the exponential part $e^{(a+b\lambda)}$, where λ is wavelength (nm), a and b are constants, which are determined by fitting experimental data. Fig. 4.6 shows the comparison between fitted and experimental results of reflectance spectra at 25 and 35 °C, respectively. In most of the range shown, the fitted values match the experimental data. As shown in Table 4.2, the considerably high values of R^2 also demonstrate the good fitness. It is noticed that the amplitude of extinction generally decrease with temperature, which means light penetrates more at higher temperature. By interpolating method, the constants as linear functions of temperature can be derived. Then substitute eq. (1)–eq. (3) and the approximate value of R_m (4.37%), the reflectance spectra of

asphalt binder mixture as a function of temperature can be deduced in the wavelength range of 800–1800 nm.

For black asphalt binder, this can be expressed as:

$$R_{mix} = (90\% \times 4.37 + 10\% \times (70.65 + \frac{-73.575 + 3.245T - 70.65}{1 + e^{\frac{\lambda - 706.80}{20.50}}})) \cdot \exp(-1.31085 - 0.01149T + 0.00075\lambda) \quad (4)$$

For blue asphalt binder, the equation is

$$R_{mix} = (90\% \times 4.37 + 10\%(70.86 + \frac{-108.13 + 4.718T - 70.86}{1 + e^{\frac{\lambda - 655.65}{10.99}}})) \cdot \exp(-1.6449 + 0.00364T + 0.0006\lambda) \quad (5)$$

For red asphalt binder, it can be written as:

$$R_{mix} = (90\% \times 4.37 + 10\%(72.50 + \frac{-83.39 + 3.594T - 72.50}{1 + e^{\frac{\lambda - 599.33}{13.68}}})) \cdot \exp(-1.248 - 0.0065T + 0.0005\lambda) \quad (6)$$

Table 4.2. Empirical equations for reflectance spectra of asphalt binder mixture and R^2.

Samples	Temperature (°C)	Empirical Equations	R^2
Black asphalt binder	25	$R_{mix} = (90\% R_m + 10\% R_p)$ $\cdot \exp(-1.5981 + 0.0007\lambda)$	0.9836
	35	$R_{mix} = (90\% R_m + 10\% R_p)$ $\cdot \exp(-1.7130 + 0.0008\lambda)$	0.9866
Blue asphalt binder	25	$R_{mix} = (90\% R_m + 10\% R_p)$ $\cdot \exp(-1.5539 + 0.0006\lambda)$	0.9697
	35	$R_{mix} = (90\% R_m + 10\% R_p)$ $\cdot \exp(-1.5175 + 0.0006\lambda)$	0.9779
Red asphalt binder	25	$R_{mix} = (90\% R_m + 10\% R_p)$ $\cdot \exp(-1.4105 + 0.0005\lambda)$	0.9294
	35	$R_{mix} = (90\% R_m + 10\% R_p)$ $\cdot \exp(-1.4755 + 0.0005\lambda)$	0.9372

where R_{mix}-reflectance of asphalt mixture (%); R_p-reflectance of thermochromic powders (%); R_m-reflectance of pure asphalt binder(%); λ-wavelength (nm); T-Temperature (°C).
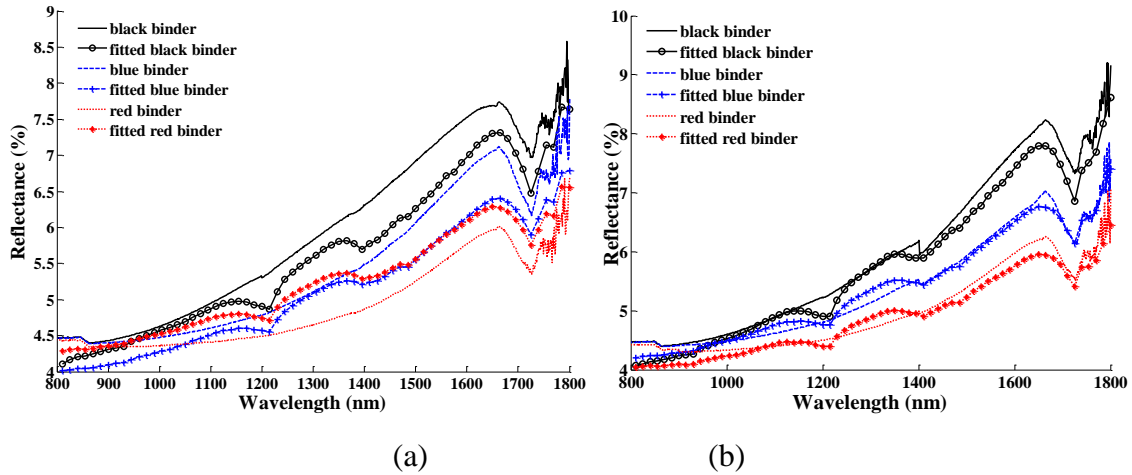
Fig. 4.6. Comparison between experimental and fitting values of reflectance spectra of thermochromic asphalt binders at 25 °C (a) and 35 °C (b).

Influence of content of thermochromic powders on reflectance spectra of asphalt binder mixture
The influence of the fraction of red powders on the reflectance spectra of asphalt binder mixtures at room temperature is exhibited in Fig. 4.7. It is observed that as the content of red powders increases, the value of spectral reflectance increases tremendously, especially in the infrared range. This enhancement is mainly due to more reflection of light radiation from red powders and probably higher light penetration in the infrared range.
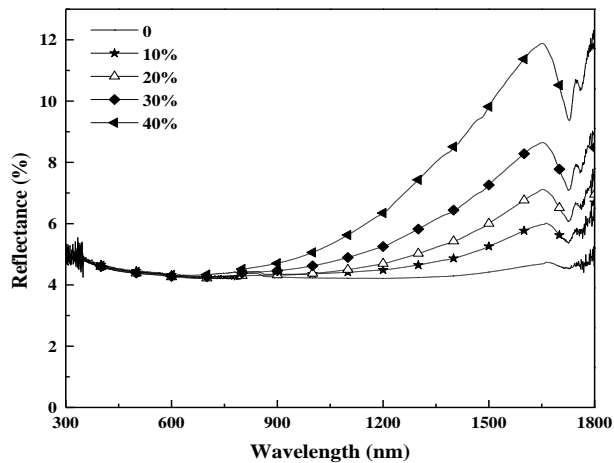
Fig. 4.7. Reflectance spectra of asphalt binder mixture containing different fractions of red powders.

To predict the effective thermal, electrical, mechanical and chemical properties of the composite materials, several models have been developed, such as parallel, serial, Maxwell, effective medium theory (EMT), self-consistent and Mori-Tanaka models. In this paper, these models are applied to predict the effective reflectance spectra of binary asphalt binder mixtures. The schematic models and basic expressions are shown in Table 4.3. In the parallel model, layers of components are placed in the direction of the light radiation. For the serial model, layers of components are normal to the radiation flow. Of the common models, the parallel and serial models are the simplest for two-phase systems and offer upper and lower bounds for many properties of two-phase heterogonous materials (18–19). Based on dielectric theory, Maxwell (20) obtained a simple relationship for the effective properties of the two-component system consisting of a continuous and a randomly, non-interacting dispersed phase. Maxwell model is only applicable to two-phase, dilute composites with spherical powders. EMT model (18, 21) describes the macroscopic properties of a medium based on the properties and the relative fractions of its components. It assumes that for a completely random distribution of components, the local effect caused by individual powders could be averaged such that over a sufficiently large volume the properties within the material could be approximated by a material having a uniform behavior (22). A self-consistent model assumes that each particle is surrounded by the composite material with the effective property rather than by matrix (23). This model is valid for multiphase composites with various inclusion geometries, isotropy or anisotropies, and it has a simple and explicit expression. The Mori-Tanaka (24) model is proposed for the graded microstructure which has a well-defined continuous matrix and a randomly distributed particulate phase. This model takes into account the interaction among neighboring inclusions and assumes that the matrix phase is reinforced by spherical particles. Besides, as above-mentioned, these models need multiply the exponential part $e^{(a+b\lambda)}$, considering light extinction in the medium.

Table 4.3. Summary of models for the effective spectral reflectance of binary mixtures.

Models	Expressions	Remarks
Parallel Model	Light radiation $$R_{mix} = (1-\phi)R_m + \phi R_p$$	Offer upper bound
Serial Model	Light radiation $$R_{mix} = \frac{1}{(1-\phi)/R_m + \phi/R_p}$$	Offer lower bound
Maxwell Model	$$R_{mix} = (1 + \frac{3(\alpha-1)\phi}{(\alpha+2)-(\alpha-1)\phi})R_m$$ $$\alpha = R_p/R_m$$	Limited to two-phase systems; non-interacting, spherical dispersed powders
EMT Model	$$(1-\phi)\frac{R_m - R_{mix}}{R_m + 2R_{mix}} + \phi\frac{R_p - R_{mix}}{R_p + 2R_{mix}} = 0$$	Deals with materials with a completely random distribution of all the components
Self-Consistent Model	particle matrix $$R_{mix} = \frac{\beta + \sqrt{\beta^2 + 4(d-1)R_m R_p}}{2(d-1)}$$ $$\beta = R_m(d(1-\phi)-1) + R_p(d\phi-1)$$	Applicable to multiphase composites containing various inclusion geometries, isotropy or anisotropies; a simple and explicit expression
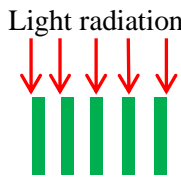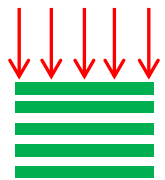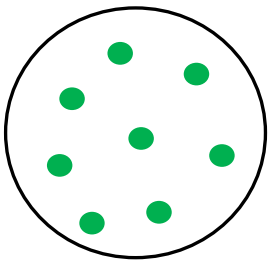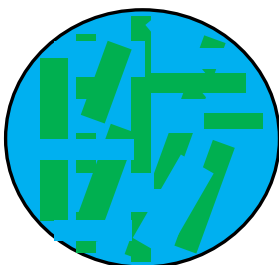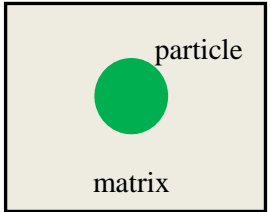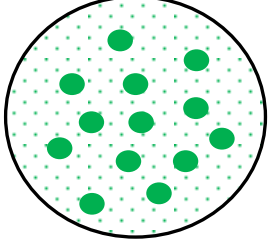
Mori-Tanaka Model		$$\frac{R_{mix}-R_m}{R_p-R_m}=\frac{\phi}{1+(1-\phi)(R_p-R_m)/3R_m}$$	Considered the interaction among neighboring inclusions; valid for multiphase composites; a simple and explicit expression

where Φ–the volume fraction of the dispersed powders (%); R_m–reflectance of pure asphalt binder (%); R_p–reflectance of thermochromic powders (%); R_{mix}–reflectance of asphalt mixture (%); d–dimension of powders.

Fig. 4.8 shows the comparison between experimental and fitted values of reflectance spectra of asphalt binder mixtures filled with different contents of red powders. The empirical equations are given in Table 4.4 with the values of R^2. As seen from Table 4.4, the effective reflectance of the mixture increases with powder content. Also the value of $e^{(a+b\lambda)}$ decreases with the increase of powder content, which could be explained by more interaction between red powder and light radiation, therefore less attenuation of the wave. According to Fig. 4.8 and values of R^2, it can be observed that Maxwell, EMT, and Mori-Tanaka models present relatively better fitting. Specifically, Maxwell and Mori-Tanaka models are more applicable to asphalt binder mixture with lower concentration of thermochromic powders, while EMT model is more accurate to that with higher concentration of powders. The relationship between constants (a and b) and powder content is derived by interpolation method. Then by substituting them and eq. (3) into these models, the effective reflectance spectra of red asphalt binders in the wavelength range of 800–1800 nm is expressed as following:

Based on Maxwell model,

$$R_{mix}=4.37(1+\frac{3(\alpha-1)\phi}{(\alpha+2)-(\alpha-1)\phi})\cdot\exp(-0.1568-3.909\phi+(0.0001+0.002\phi)\lambda) \tag{7}$$

with $\alpha=R_p/R_m=(72.50+\dfrac{6.46-72.50}{1+e^{\frac{\lambda-599.33}{13.68}}})/4.37$

Based on Mori-Tanaka model,

$$\frac{\dfrac{R_{mix}}{\delta} - 4.37}{(72.50 + \dfrac{6.46 - 72.50}{1 + e^{\frac{\lambda - 599.33}{13.68}}}) - 4.37} = \frac{\phi}{1 + (1 - \phi)(72.50 + \dfrac{6.46 - 72.50}{1 + e^{\frac{\lambda - 599.33}{13.68}}} - 4.37) / (3 \times 4.37)} \tag{8}$$

with $\delta = \exp(-0.1568 - 3.909\phi + (0.0001 + 0.002\phi)\lambda)$

Based on EMT model,

$$(1 - \phi)\frac{4.37 - \dfrac{R_{mix}}{\delta}}{4.37 + 2\dfrac{R_{mix}}{\delta}} + \phi\frac{72.50 + \dfrac{6.46 - 72.50}{1 + e^{\frac{\lambda - 599.33}{13.68}}} - \dfrac{R_{mix}}{\delta}}{72.50 + \dfrac{6.46 - 72.50}{1 + e^{\frac{\lambda - 599.33}{13.68}}} + 2\dfrac{R_{mix}}{\delta}} = 0 \tag{9}$$

with $\delta = \exp(-2.7376 - 2.093\phi + (0.0004 + 0.002\phi)\lambda)$

Table 4.4. Summary on empirical equations by fitting various models and R^2.

Model	Content (%)	Empirical Equations	R^2
Parallel Model	10	$R_{mix} = ((1 - \phi)R_m + \phi R_p) \cdot \exp(-1.4105 + 0.0005\lambda)$	0.9294
	20	$R_{mix} = ((1 - \phi)R_m + \phi R_p) \cdot \exp(-2.1627 + 0.0007\lambda)$	0.9594
	30	$R_{mix} = ((1 - \phi)R_m + \phi R_p) \cdot \exp(-2.6213 + 0.0009\lambda)$	0.9708
	40	$R_{mix} = ((1 - \phi)R_m + \phi R_p) \cdot \exp(-3.0265 + 0.0012\lambda)$	0.9638
Serial Model	10	$R_{mix} = \dfrac{1}{(1 - \phi) / R_m + \phi / R_p} \cdot \exp(-0.3905 + 0.0003\lambda)$	0.9654
	20	$R_{mix} = \dfrac{1}{(1 - \phi) / R_m + \phi / R_p} \cdot \exp(-0.6482 + 0.0005\lambda)$	0.9556
	30	$R_{mix} = \dfrac{1}{(1 - \phi) / R_m + \phi / R_p} \cdot \exp(-0.8715 + 0.0007\lambda)$	0.9422
	40	$R_{mix} = \dfrac{1}{(1 - \phi) / R_m + \phi / R_p} \cdot \exp(-1.1440 + 0.0009\lambda)$	0.9249
Maxwell Model	10	$R_{mix} = (1 + \dfrac{3(\alpha - 1)\phi}{(\alpha + 2) - (\alpha - 1)\phi})R_m \cdot \exp(-0.5477 + 0.0003\lambda)$ $\alpha = R_p / R_m$	0.9665
	20	$R_{mix} = (1 + \dfrac{3(\alpha - 1)\phi}{(\alpha + 2) - (\alpha - 1)\phi})R_m \cdot \exp(-0.9386 + 0.0005\lambda)$ $\alpha = R_p / R_m$	0.9589

	30	$R_{mix} = (1 + \dfrac{3(\alpha - 1)\phi}{(\alpha + 2) - (\alpha - 1)\phi})R_m \cdot \exp(-1.2760 + 0.0007\lambda)$ $\alpha = R_p / R_m$	0.9484
	40	$R_{mix} = (1 + \dfrac{3(\alpha - 1)\phi}{(\alpha + 2) - (\alpha - 1)\phi})R_m \cdot \exp(-1.6471 + 0.0010\lambda)$ $\alpha = R_p / R_m$	0.9329
EMT Model	10	$(1-\phi)\dfrac{R_m - R_{mix}/\delta}{R_m + 2R_{mix}/\delta} + \phi\dfrac{R_p - R_{mix}/\delta}{R_p + 2R_{mix}/\delta} = 0$ $\delta = \exp(-2.9585 + 0.0006\lambda)$	0.9115
	20	$(1-\phi)\dfrac{R_m - R_{mix}/\delta}{R_m + 2R_{mix}/\delta} + \phi\dfrac{R_p - R_{mix}/\delta}{R_p + 2R_{mix}/\delta} = 0$ $\delta = \exp(-3.1889 + 0.0008\lambda)$	0.9550
	30	$(1-\phi)\dfrac{R_m - R_{mix}/\delta}{R_m + 2R_{mix}/\delta} + \phi\dfrac{R_p - R_{mix}/\delta}{R_p + 2R_{mix}/\delta} = 0$ $\delta = \exp(-3.3655 + 0.0010\lambda)$	0.9713
	40	$(1-\phi)\dfrac{R_m - R_{mix}/\delta}{R_m + 2R_{mix}/\delta} + \phi\dfrac{R_p - R_{mix}/\delta}{R_p + 2R_{mix}/\delta} = 0$ $\delta = \exp(-3.5748 + 0.0012\lambda)$	0.9647
Self-Consistent Model	10	$R_{mix} = \dfrac{\alpha + \sqrt{\alpha^2 + 4(d-1)R_m R_p}}{2(d-1)} \cdot \exp(-0.5920 + 0.0003\lambda)$ $\alpha = R_m(d(1-\phi)-1) + R_p(d\phi-1)$	0.9669
	20	$R_{mix} = \dfrac{\alpha + \sqrt{\alpha^2 + 4(d-1)R_m R_p}}{2(d-1)} \cdot \exp(-1.1245 + 0.0005\lambda)$ $\alpha = R_m(d(1-\phi)-1) + R_p(d\phi-1)$	0.9625
	30	$R_{mix} = \dfrac{\alpha + \sqrt{\alpha^2 + 4(d-1)R_m R_p}}{2(d-1)} \cdot \exp(-1.6942 + 0.0008\lambda)$ $\alpha = R_m(d(1-\phi)-1) + R_p(d\phi-1)$	0.9602
	40	$R_{mix} = \dfrac{\alpha + \sqrt{\alpha^2 + 4(d-1)R_m R_p}}{2(d-1)} \cdot \exp(-2.3199 + 0.0011\lambda)$ $\alpha = R_m(d(1-\phi)-1) + R_p(d\phi-1)$	0.9528
Mori–Tanaka Model	10	$\dfrac{R_{mix}/\delta - R_m}{R_p - R_m} = \dfrac{\phi}{1 + (1-\phi)(R_p - R_m)/3R_m}$ $\delta = \exp(-0.5477 + 0.0003\lambda)$	0.9665

20	$\dfrac{R_{mix}/\delta - R_m}{R_p - R_m} = \dfrac{\phi}{1 + (1-\phi)(R_p - R_m)/3R_m}$	0.9589
	$\delta = \exp(-0.9386 + 0.0005\lambda)$	
30	$\dfrac{R_{mix}/\delta - R_m}{R_p - R_m} = \dfrac{\phi}{1 + (1-\phi)(R_p - R_m)/3R_m}$	0.9484
	$\delta = \exp(-1.2760 + 0.0007\lambda)$	
40	$\dfrac{R_{mix}/\delta - R_m}{R_p - R_m} = \dfrac{\phi}{1 + (1-\phi)(R_p - R_m)/3R_m}$	0.9329
	$\delta = \exp(-1.6471 + 0.0010\lambda)$	

where ϕ–the mass fraction of the dispersed powders (%); R_m–reflectance of pure asphalt binder (%); R_p–reflectance of thermochromic powders (%); R_{mix}–reflectance of asphalt mixture (%); λ–wavelength (nm); d–dimension of powders.
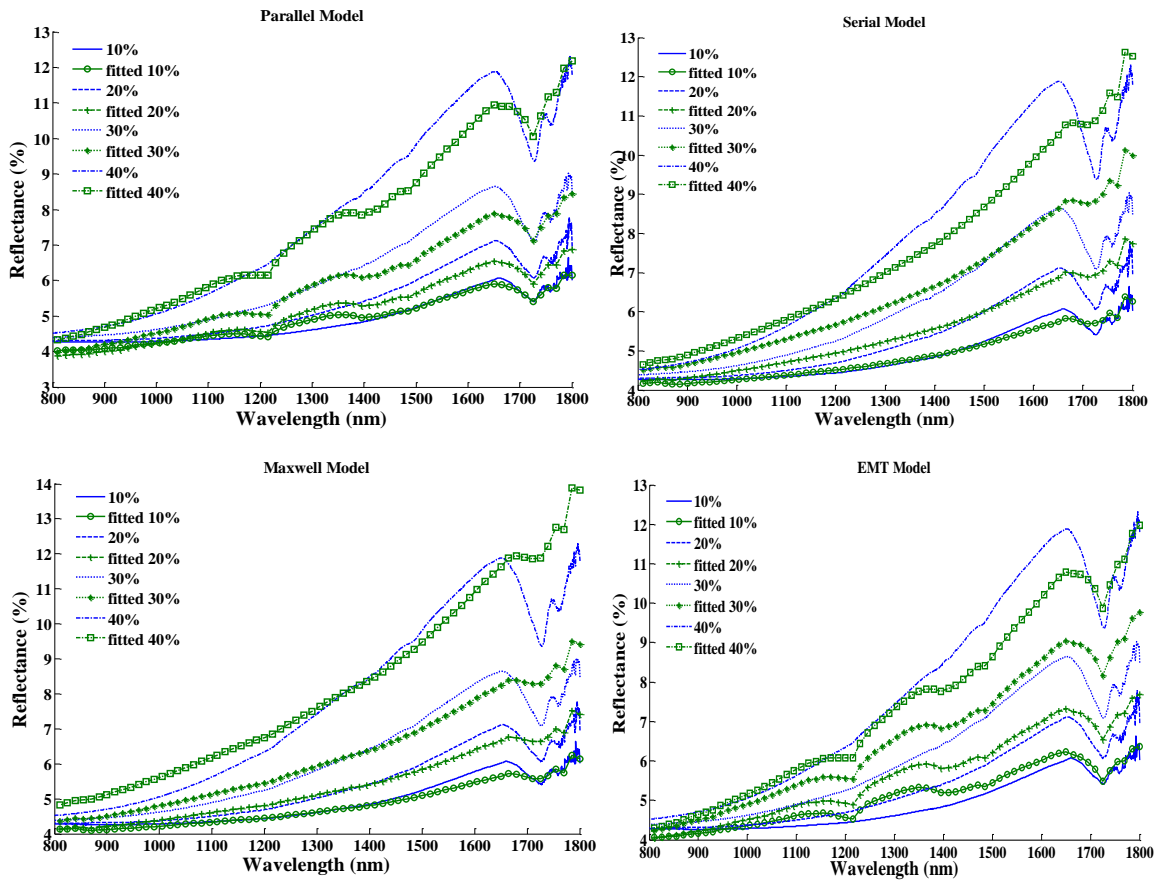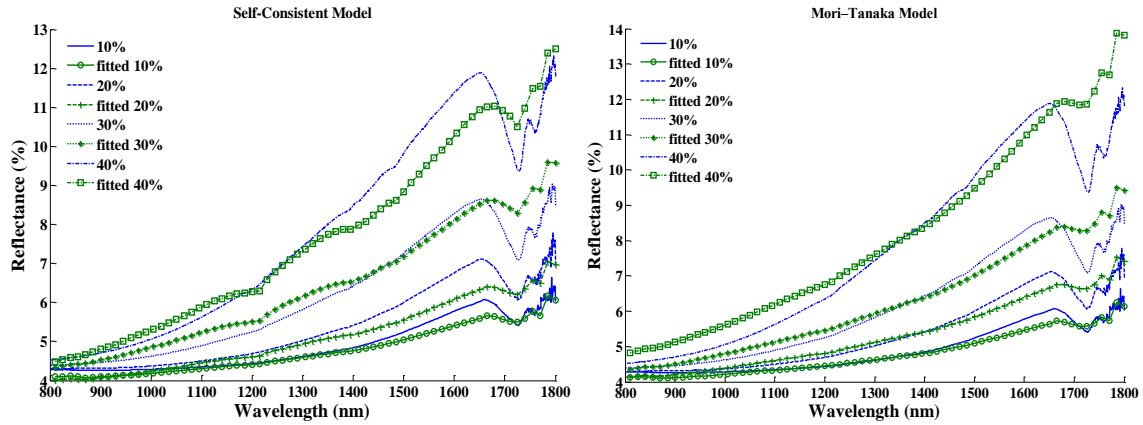
Fig. 4.8. Comparison between experimental and fitted reflectance spectra of asphalt binder mixtures containing different contents of red powder.

4.4 Conclusions

This study characterized the reflectance spectra of both of thermochromic materials and asphalt binder mixture, demonstrating the increase in reflectance of asphalt binder when adding thermochromic materials as well as the potential enhancement in durability of asphalt pavement. The empirical equations between reflectance spectra and temperature have been proposed by fitting experimental data. The comparisons of our fitted results with experimental values show good agreement. These formulas could predict the reflectance spectra of thermochromic powders and asphalt binder mixtures under different temperatures. Furthermore, with the increasing thermochromic powder contents, the spectral reflectance values of asphalt binder mixture increase considerably. Among various models for effective properties of composite, it is found that Maxwell, EMT, and Mori-Tanaka models provide better agreement with reflectance spectra of red asphalt binder. The empirical equations between reflectance spectra of asphalt binder mixture and powder content are presented based on these models. These formulas are of great importance to design asphalt binder mixtures with the desired optical properties. Further studies are needed to refine these equations considering different temperatures, particle size and distribution.

4.5 References

(1) Santamouris, M., Pavlou, K., Synnefa, A., Niachou, K., Kolokotsa, D. Recent progress on passive cooling techniques: Advanced technological developments to improve survivability levels in low-income households. *Energy and Buildings*, 2007, 39(7): 859-866.

(2) Synnefa, A., Dandou, A., Santamouris, M., Tombrou, M., Soulakellis, N. Large scale albedo changes using cool materials to mitigate heat island in Athens. *Journal of Applied Meteorology and Climatology*, 2008, 47(11): 2846-2856.

(3) Doulos, L., Santamouris, M., Livada, I. Passive cooling of outdoor urban spaces. The role of materials. *Solar Energy*, 2004, 77(2): 231-249.

(4) Yoder, E. J. and Witzak, M. W. *Principles of Pavement Design*. New York, NY: Wiley and Sons, 1975.

(5) Pomerantz, M. and Akbari. H. Cooler Paving Materials for Heat Island Mitigation. *In 1998 ACEEE Summer Study on Energy Efficiency in Buildings*, Asilomar, CA, City: American Council for an Energy-Efficient Economy, 1998.

(6) Pomerantz, M., Akbari, H. Cooler paving materials for heat island mitigation, in: Proceedings of the 1998 ACEEE Summer Study on Energy Efficiency in Buildings, vol. 9, Pacific Grove, CA, 1998, p. 135.

(7) Pomerantz, M., Akbari, H., Chen, A., Taha, H., Rosenfeld, A. Paving Materials for Heat Island Mitigation, Lawrence Berkeley National Laboratory Report LBL- 38074, Berkeley, CA, 1997.

(8) Pomerantz, M., Akbari, H., Harvey, J. T. 2000. Cooler reflective pavements give benefits beyond energy savings: Durability and illumination. Rep. No. LBNL-45370, Berkeley, CA, 14 pp.

(9) Kinouchi, T., Yoshinaka, T., Fukae, N., Kanda, M., 2004. Development of cool pavement with dark colored high albedo coating. Fifth Conference for the Urban Environment, Vancouver, Canada.

(10) Hao, P.W., Zhang, D.L., Hu, X.N., 2000. Evaluation method for low temperature anticracking performance of asphalt mixture. Journal of Xi'an Highway University 20 (3), 1–5.

(11) Kanerva, H.K., VINSON, T.S., Zeng, H., 1994. Low Temperature Cracking Field Validation of the Thermal Stress Rest Rained Specimen Test. R. SHRP-A-401.

(12) Santamouris, M., Synnefa, A., Kolokotsa, D., Dimitriou, V., Apostolakis, K. Passive cooling of the built environment - use of innovative reflective materials to fight heat island and decrease cooling needs. *International Journal Low Carbon Technologies*, 2008, 3(2): 71-82.

(13) Karlessi, T., Santamouris, M., Apostolakis, K., Synnefa, A., Livada, I. Development and testing of thermochromic coatings for buildings and urban structures. *Solar Energy*, 2009, 83(4): 538-551.

(14) Granqvist, C.G. *Materials Science for Solar Energy Conversion Systems*. Pergamon press, Oxford, 1991.

(15) Saeli, M., Piccirillo, C., Parkin, I. P., Binions, R., Ridley, I. Energy modelling studies of thermochromic glazing. *Energy and Buildings,* 2010, 42(10): 1666-1673.

(16) Ma, Y. P. and Zhu, B.R. Research on the preparation of reversibly thermochromic cement based materials at normal temperature. *Cement and Concrete Research*, 2009, 39(2): 90-94.

(17) ASTM E903-12. Standard test method for solar absorptance, reflectance, and transmittance of materials using integrating spheres. Book of Standards, Volume: 12.02, American Society for Testing and Materials, 2012.

(18) Bottcher, C. J. F. *Theory of Electric Polarization*. Elsevier, New York, 1952.

(19) Zimmerman, R.W. Thermal conductivity of fluid-saturated rocks. *Journal of Petroleum Science and Engineering* 3, 1989, 3(3): 219–227.

(20) Maxwell, J. C. *A treatise on Electricity and Magnetism*. Oxford University Press, Cambridge, UK, 1904.

(21) Landauer, R. Electrical Transport and Optical Properties of Inhomogeneous Media. *Journal of Applied Physics*, 1952, 23: 779–784.

(22) Davis, H.T., Valencourt, L.R., Johnson, C.E. Transport processes in composite media. *Journal of the American Ceramic Society*, 1975, 58 (9–10): 446–452.

(23) Hashin, Z. Assessment of the self-consistent scheme approximation: conductivity of particulate composites. Journal of Composite Materials, 1968, 2 (3): 284–300.

(24) Mori, T., Tanaka, K. Average stress in matrix and average elastic energy of materials with misfitting inclusions. *Acta Materialia*, 1973, 21 (5): 571-574.

CHAPTER FIVE

CHARACTERIZATION OF THE MECHANICAL PROPERTIES OF THERMOCHROMIC ASPHALT BINDERS

This study investigated the effects of thermochromic materials on the mechanical performance of the asphalt binder. The thermochromic asphalts are characterized using Superpave binder performance tests. Typical testing methods have been conducted on the asphalt binders at three stages: unaged, rolling thin film oven (RTFO) residues, and RTFO + pressure aging vessel residuals. Experimental results indicated that the penetration, phase angle and creep rate of asphalt binder was decreased, while the softening point, viscosity, complex modulus, rutting parameter, fatigue parameter and stiffness of asphalt binder was increased when thermochromic powder was added to conventional asphalt binder. Furthermore, increasing the content of thermochromic powder leads to reduction in the penetration depth and creep rate, and increase of softening point, viscosity, complex shear modulus, rutting parameter, fatigue parameter and stiffness. Additionally, the high temperature performance grades of asphalt binder were enhanced with blending 3–6% black, 6% blue and red themochromic powders. These effects were achieved without considering the benefits of thermochromic asphalt in achieving modulating the surface temperature (i.e., a lower surface temperature during summer and higher surface temperature during winter). Therefore, the incorporation of thermochromic materials into asphalt pavement will potentially improve its performance and durability, especially in hot regions.

5.1 Introduction

Conventional asphalt binder, which consists of residuals from crude oil distillation processes, has been used widely in highway pavement and city roads. However, the black color of asphalt binder causes large solar absorption that leads to high surface temperature of asphalt pavement. Studies (Santamouris et al. 2007, Synnefa et al. 2008, Doulous et al. 2004) reported the surface temperature of asphalt pavement as high as 48–67 °C during summer. The increased temperature in summer impacts durability of asphalt pavement by accelerating various distress mechanisms

(i.e., rutting, shoving, aging, fatigue damage, bleeding) (Yoder and Witzak 1975) as well as causes undesirable environmental issues (i.e., heat island effects, volatile gas emission, etc.) (Gui et al. 2007). A potential way to improve the durability is to use materials with high reflectivity and emissivity to solar radiation. This has led to the development of various cool pavement technologies. Studies (Pomerantz and Akbari 1998, Pomerantz et al. 1997, Pomerantz et al. 2000, Kinouchi et al. 2004) show that cool pavement features low surface temperatures, which increases the service life (durability) of pavements. However, the reduced temperature of asphalt pavement exacerbates the distress of low-temperature cracking during the winter period (Hao et al. 2000, Kanerva et al. 1994), which compromises the service life of road in cold climate. Besides, the lower surface temperature is conductive to ice formation in cold weather, which is a major safety concern. So it is highly desirable to develop new pavement materials and technology to make asphalt pavement cooler during summer and warmer during winter.

An innovative strategy our study pursued is to use thermochromic materials to create new asphalt binders with desirable solar reflectance, i.e., they reflect more solar energy at high temperature and reflect less solar energy at low temperature. To avoid any visual impact on road users, we hope to restrain such effects in the infrared range only. Thermochromic materials, materials changing their colors with temperature, are promising to achieve such functionality as they possess required optical and thermal properties. Materials incorporated with proper thermochromic materials feature high solar reflectance in summer and high solar absorption in winter. The change of their optical and thermal properties in such a dynamic way can lead to applications that improve the urban microclimate, decrease the energy demands of the buildings, and provide a thermally comfortable indoor environment (Santamouris et al. 2008, Karlessi et al. 2009, Granqvist 1991, Saeli et al. 2010, Ma and Zhu 2009, Kinouchi and Santamouris 2013).

In our study, innovative asphalt binder containing thermochromic materials is designed to modulate the temperature of asphalt pavement. The preliminary thermal performance evaluation indicated that the use of thermochromic asphalt binder could reduce the surface temperature of asphalt concrete up to 6.6°C during a typical summer day in Cleveland, Ohio, USA (Hu and Yu 2013). This paper describes the experimental characterization on the effects of thermochromic materials on the optical and mechanical properties of asphalt binder. The optical properties are characterized by spectrophotometry measurements. The mechanical properties are evaluated using complete sets of Superpave binder characterization tests, including needle penetration,

softening point, rotational viscosity (RV), dynamic shear rheology (DSR) and bending beam rheology (BBR). The effects of thermochromic materials on performance grade (PG) of asphalt binders are determined.

5.2 Materials and Experimental Methods

Raw Materials

Asphalt binder used in this study is Superpave grade, PG64-22, produced by Kokosing Materials Inc. Thermochromic powders with an average particle size of 3 ~ 10 μm were selected from those manufactured by Hali Industrial Corporation Ltd. Red, blue, and black thermochromic powders with transition temperature around 31 °C were chosen for this study. These thermochromic materials are organic mixtures, which consists of lueco dye (electron donor), developer (electron acceptor) and solvent. Below the transition temperature, leuco dye reacts with the developer, the absorption peaks shifts from the UV to the visible range and cause the powder becomes colored. At temperature above the transition temperature, the solvent-developer interactions dominate, and leuco dye is separated from the developer and leads to loss of color. Thermochromic materials are encapsulated by trioctanoinand and therefore at high temperature thermochromic powders become white or light-colored state. The molecular structures of thermochromic materials and their changes with temperature are shown in Fig. 5.1.

(a)

(b)

(c)

Fig. 5.1. Molecular structures of thermochromic powders and their changes with temperature: a) black powder; b) blue powder; c) red powder.

Preparation of Thermochromic Asphalt Binders

Thermochromic asphalt binders are prepared by the following procedures: the original asphalt binder was heated to 163 °C in an oven until it completely melted, then thermochromic powders were added. The amount of thermochromic powders by total weight of asphalt binder are 3%, 6% and 10%, respectively. The mixture was mixed using a mixer for 10 minutes and then put them into the oven for 1 hour to ensure the blend became homogenous. The asphalt binders containing black, blue and red thermochromic powders were named as black, blue and red asphalt binder, respectively in this paper for simplicity in the nomenclature.

In principle, with the characteristics of thermochromic materials, thermochromic asphalt binder should exhibit a different response to solar radiation than conventional asphalt binder.

Solar energy consists of a spectrum of wavelengths, including ultraviolet, visible, and infrared light (almost 50% of the entire solar energy). Below the transition temperature of the thermochromic powder, where the powders are less infrared reflective, the binder should reflect less (and therefore absorb more) solar energy, as shown in Fig. 5.2(a); above the transition temperature, where the powders are more reflective to infrared, thermochromic asphalt binder should reflect more solar energy, as shown in Fig. 5.2(b). Both energy-reflecting and energy-absorbing properties of thermochromic asphalt binder help to maintain pavement at an appropriate temperature range desirable for its longevity and performance.
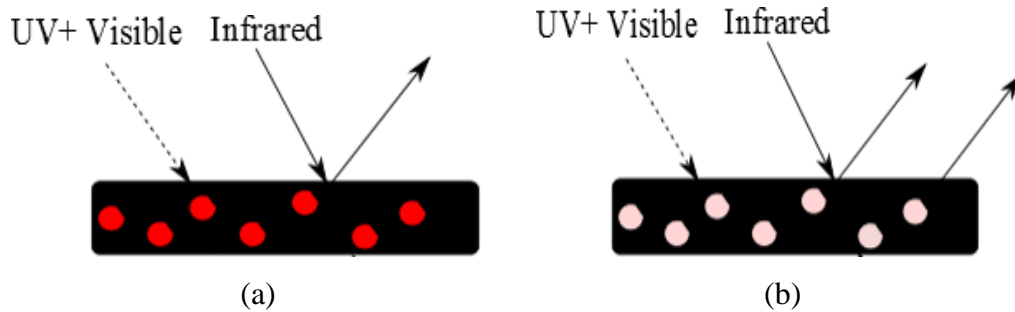
Fig. 5.2. Schematic principle of thermochromic asphalt binder: (a) smaller infrared reflectivity under the transition temperature of thermochromic powders; (b) higher infrared reflectance above the transition temperature.

Optical Characterization of Various Asphalt Binders

The spectral reflectance was measured on various asphalt binders over the wavelength range of 300–1800 nm by the Agilent Cary 6000i UV-Vis-IR Spectrophotometer with a DRA integrating sphere. The measurements were performed according to ASTM E903-12 (ASME E903-12 2012). During the measurements, thermochromic powders and asphalt binders containing different percent of thermochromic powders were packed between microscopic slides with a thickness of 1mm. Reflectance measurements were conducted through the microscopic slides at 25°C and 35 °C, respectively. All samples were measured with two or three duplicates and the average values were calculated and presented.

Superpave Characterizations of Various Asphalt Binders

To study the influence of the thermochromic materials on the binder performance, all the different types of asphalt binders are characterized using Superpave binder classification

experiments. Superpave binder classification is a performance based specification for asphalt binder developed by AASHTO. To achieve the objectives of this study, a number of tests were conducted using Superpave test procedures on original and aged asphalt binders. The experimental design and flow chart is shown in Fig. 5.3. The following subsections detail the procedure for each of these tests. Two or three duplicate samples were prepared for each design recipe. Each sample was measured twice and the average values for each sample was used in the analyses.
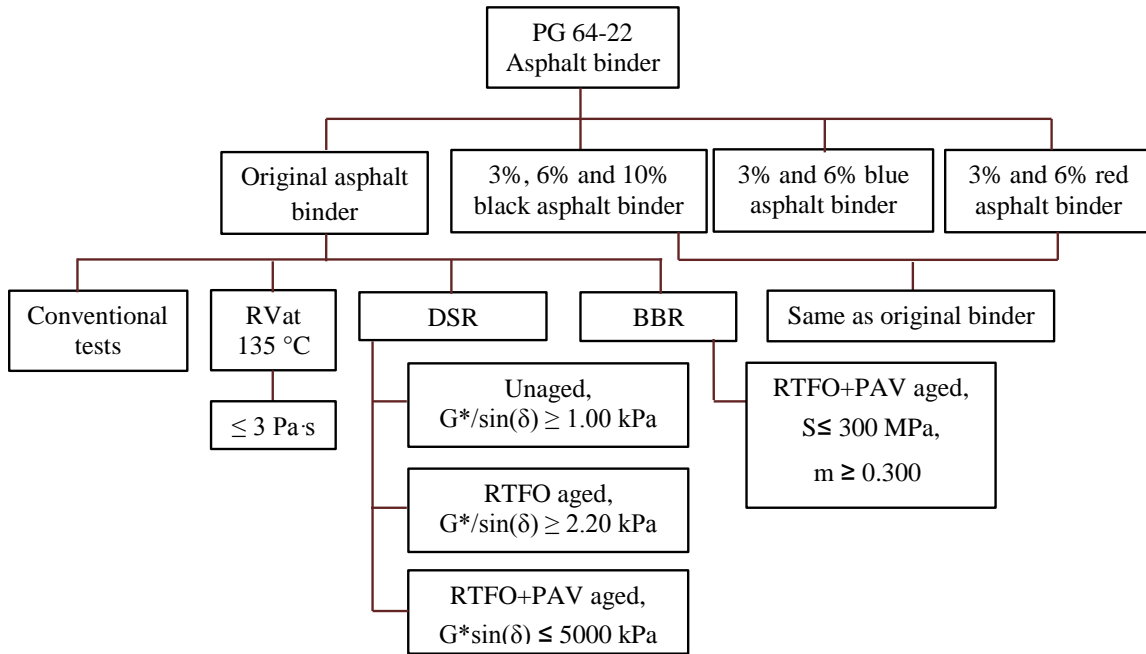
Fig. 5.3. Experimental design to characterize the mechanical properties of binders using Superpave binder performance tests.

Asphalt Binder Aging Procedures

The rolling thin film oven (RTFO) and pressure aging vessel (PAV) were used to accelerate the aging of asphalt binders. The RTFO was employed to simulate the short-term aging of asphalt binder according to AASHTO T 240-06 (AASHTO T240-06 2006). In this test, the asphalt binder was placed in the oven at 163 °C and rotated with rotational speed of 15 rpm for 85 min. The PAV was conducted to simulate the long-term aging of asphalt binder according to AASHTO R28-06 (AASHTO R28-06 2006). To prepare PAV sample, the residue from the

RTFO test was kept in the chamber with the set temperature of 100 °C and pressure of 300 psi for 20 h.

Conventional Physical Properties Tests

The conventional physical properties of asphalt binders, including needle penetration at 25 °C and softening point, were tested in accordance with AASHTO T 49 (AASHTO T 49-06 2006) and AASHTO T 53 (AASHTO T53-06, 2006), respectively.

Rotational Viscosity (RV) Test

Rotation viscosity of asphalt binders were measured with the Brookfield viscometer in according to AASHTO T 316 (AASHTO T 316-06 2006). The RV test was conducted on approximate 8 g of asphalt binders under rotational speed of 20 rpm and the stabilized temperature of 135 °C.

Dynamic Shear Properties Test

Dynamic shear properties were measured with the dynamic shear rheometer according to AASHTO T 315 (AASHTO T 315-06 2006). The DSR measures the complex shear modulus (G^*) and phase angle (δ), both used to evaluate performance of rutting-resistance and fatigue cracking (Asphalt Institute 2003). Rheological tests were performance under controlled strain conditions. There were three test samples using DSR: the unaged, RTFO aged, and PAV aged asphalt binders. The unaged and RTFO aged asphalt binder samples with diameter of 25 mm were tested at high temperature. The PAV aged asphalt binder samples with diameter of 8 mm were tested at intermediate service temperatures. DSR testing was conducted at a frequency of 10 rad/s. The test stopped running until the measured result failed according to the specification.

Low-Temperature Cracking Properties Test

The bending beam rheometer (BBR) tested asphalt binders at low service temperatures to determine the ability of the binder to relax stresses and resist low-temperature cracking (Freddy et al. 2006). The BBR tests were conducted according to AASHTO T 313 (AASHTO T 313-06 2006). Since low temperature cracking occurs only after the pavement undergoes some time, this standard evaluates the low-temperature creep properties using (RTFO+PAV) residues. The asphalt binder beams ($125 \times 12.5 \times 6.25$ mm) were prepared in an aluminum mold. The beam

was then placed on two steel supports after 60 min and subjected to a constant creep load of approximately 980 mN at midspan for 240 s. The deflection of the beam was measured continuously using a linear variable differential transducer. The stiffness (S) and creep rate (m) of the binders were determined at loading time of 60 s.

5.3 Experimental Results and Discussion

Optical Characterization

The results from the spectrophotometric measurements of thermochromic powders at 25 and 35 °C are presented in Fig. 5.4. It can be seen that the thermochromic powders yield high solar reflection, especially in the infrared range of the spectrum. The reflectance curves in the visible range are difference, depending on the specific type of thermochromic powder. Blue powder presents the highest reflectance in the visible part of the spectrum, followed by red and black powder. In addition, compared with those at 25 °C, thermochromic powders at 35 °C present significantly higher reflection in the visible as well as near infrared range. That is because the material changes the color and becomes more solar reflective as temperature increases.
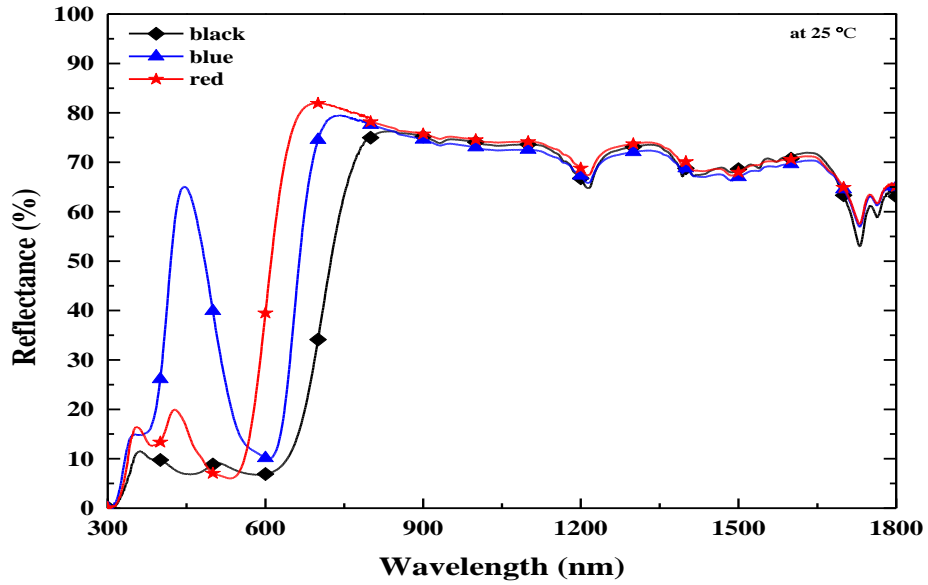
(a)
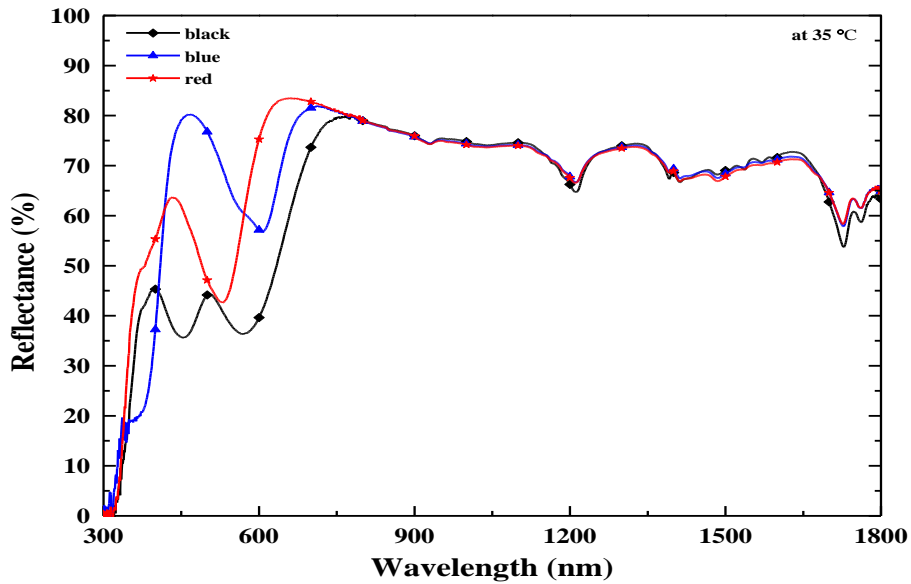
(b)

Fig. 5.4. Spectral reflectance of thermochromic powders at (a) 25 and (b) 35 °C.

Fig. 5.5 shows the measure of the spectral reflectance of different types of asphalt binders, which illustrates the effects of different types of thermochromic powders and temperature on spectral reflectance of asphalt binders. Compared with conventional asphalt binder, thermochromic asphalt binders are more reflective in the near infrared range. The

increase in reflectance is highest for thermochromic asphalt with black thermochromic powders, followed by blue and red thermochromic powders. With the increases of temperature, thermochromic asphalt binders becomes more reflective similar as observed in the reflectance behaviors of thermochromic powder.

The increases in the spectra reflectance of thermochromic binders reduce the solar absorption on the surface of pavement. For comparison of the thermal performance, experiments were conducted where specimens of different types of binders (i.e., pure, black, blue, and red asphalt binders) with dimensions of 0.075 m $\times$ 0.042 m $\times$ 0.002 m were placed the surface of Marshal asphalt concrete specimens. The specimens were completely insulated except the surfaces were exposed to natural sun light. Surface temperatures were recorded using a thermocouple to the accuracy of 0.1°C. The results showed that thermochromic binders reduced the surface temperature up to 6 to 8°C under a typical summer day in Cleveland, Ohio, USA (Fig. 5.6). This is an indication that the use of thermochromic binders can reduce the pavement surface temperature under hot weather and therefore mitigate the rutting and heat island effects. When incorporating aggregates with white color, the reflectance value of the asphalt mixture could be higher than that of asphalt binder. With the same powder content, the reduction in the surface temperature of thermochromic asphalt mixtures is expected to be more than that of thermochromic binder.
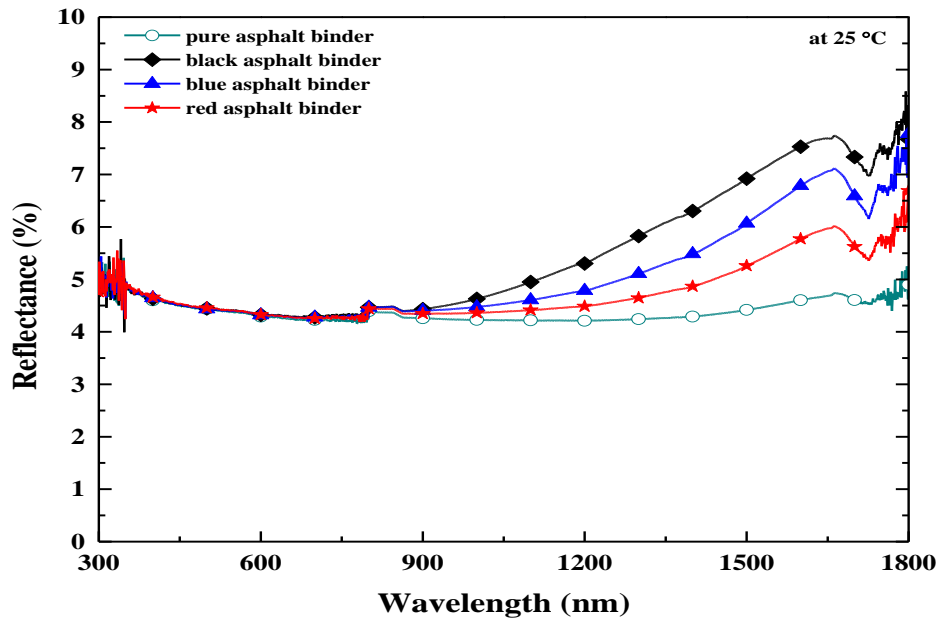
(a)
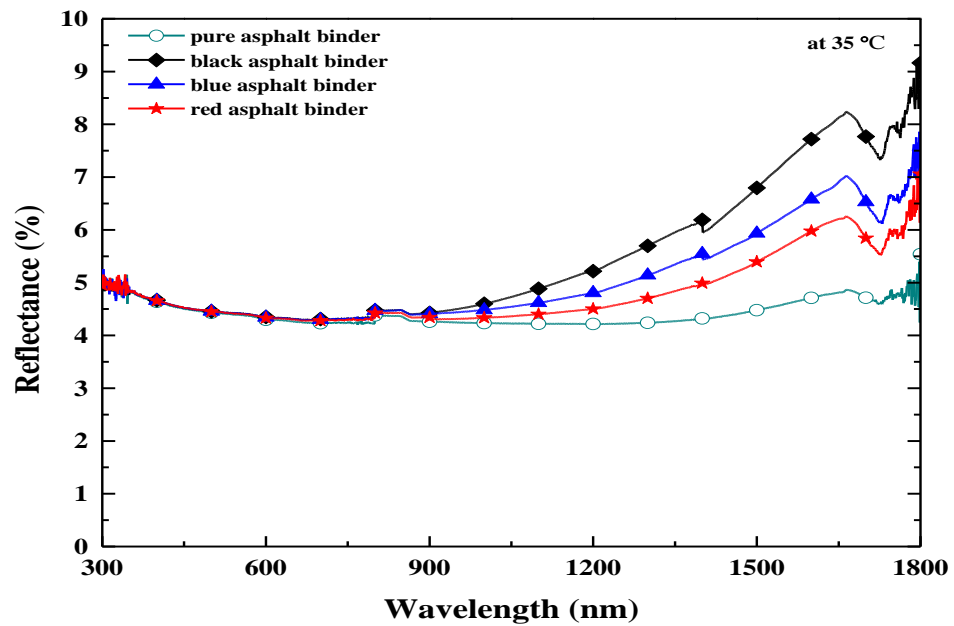
(b)

Fig. 5.5. Spectral reflectance of thermochromic asphalt binders at a) 25 and b) 35 °C.
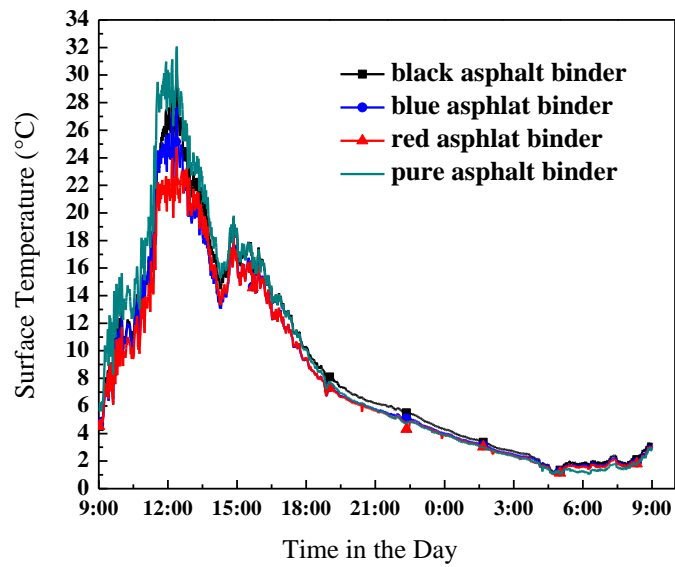
(a)
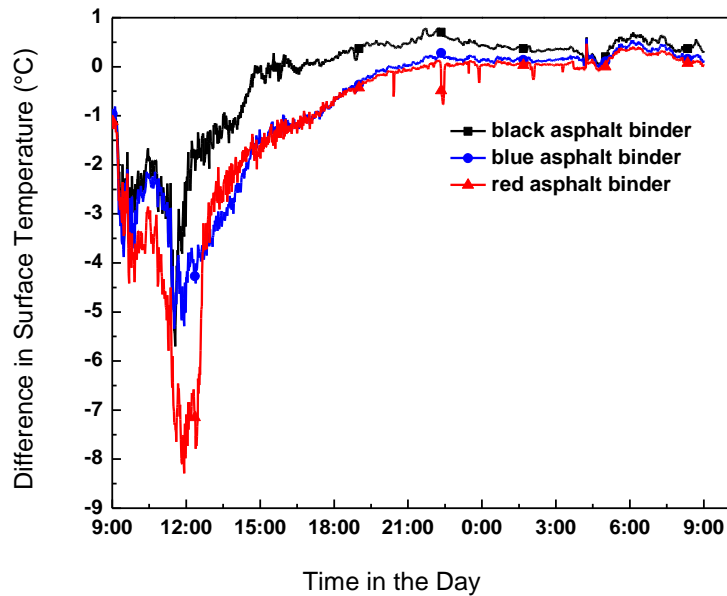
(b)

Fig. 5.6. Measured temperature on the surface of thermochromic asphalt and pure asphalt representing a sunny day in Cleveland, Ohio, USA: a) Surface temperature and b) Differences in the surface temperature with pure asphalt binder as the reference.

Physical Properties

The effects of different thermochromic powders on the conventional physical properties of asphalt binders are presented in Fig. 5.7. As can be seen from Fig. 5.7(a), compared with the control original binder with penetration depth of 60, thermochromic asphalt binders generally possess smaller values, which are between 50 and 56. Among all binders, black thermochromic binder shows the most dramatic decrease, which is up to 16%. In addition, the needle penetrations of thermochromic asphalt binder decrease with increasing powder content. Therefore, the incorporation of thermochromic powders increases the stiffness of the binder at room temperature and asphalt binder containing black powder is the stiffest, followed by red and blue binder.

The softening point test determines the temperature at which the binder softens. Fig. 5.7(b) shows that the addition of thermochromic powder increases the softening point of binder. This implies the addition of thermochromic powders helps to improve the resistance of asphalt to plastic deformation at high temperature. As powder content increases from 3% to 6% and 10%, the softening point of the asphalt binder is increased by 23–104%, 4–21% and 7–15% for black, blue and red binder, respectively.

(a)   (b)
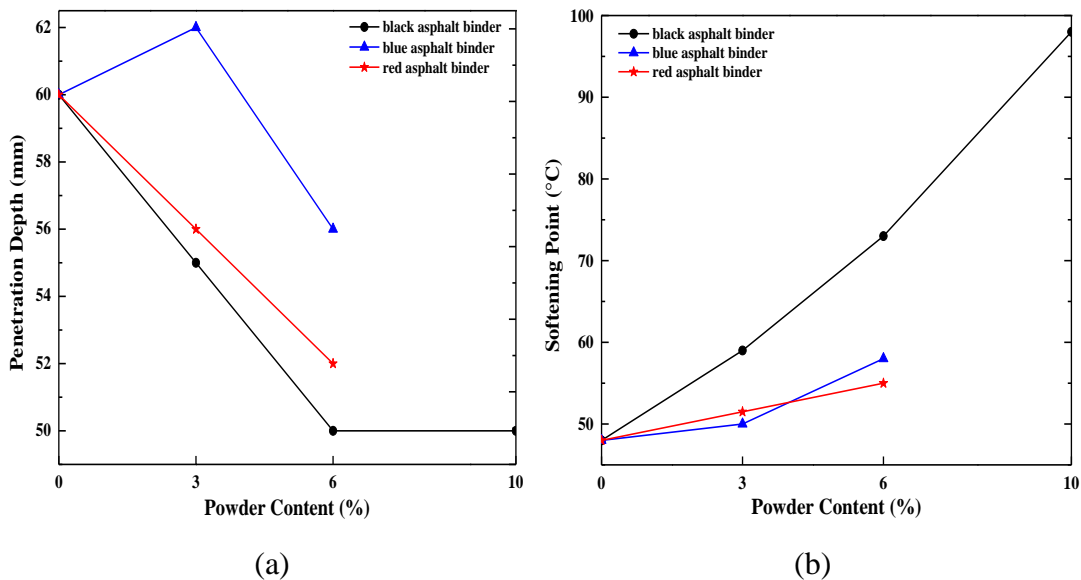
Fig. 5.7. Conventional physical properties of various asphalt binders.

Rotational Viscosity (RV)

The effect of thermochromic powder type and content on the rotational viscosity of asphalt binders at 135 °C is shown in Fig. 8. The results indicated that thermochromic binder containing red thermochromic powder exhibits higher viscosity than original binder; while the binder with blue and black powders however presents lower viscosity than the original asphalt binder. The workability and pumping potential of black and blue binder is better than that of red binder. It is also shown from Fig. 5.8 that with the increasing amount of powders, the viscosity of red and black binder is increased but the viscosity of blue binder is reduced. When considering the Superpave^{TM} specification for asphalt binder viscosity under 3 Pa·s shown in Fig. 5.8, all binders satisfy the performance specification.
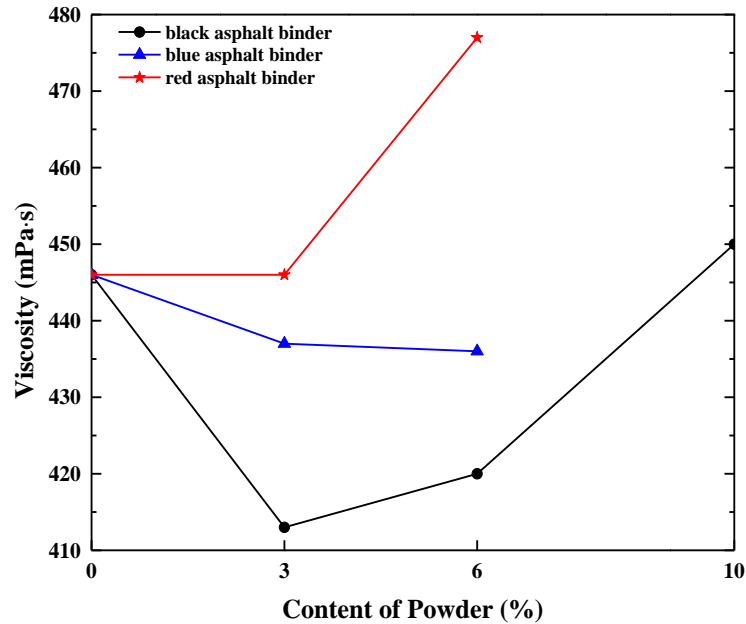
Fig. 5.8. RV test results for various asphalt binders.

Dynamic Shear Rheological (DSR) Properties

Effects of thermochromic powder type, content, and temperature on DSR parameters including G^*, δ and $G^*/\sin \delta$, and $G^*\sin \delta$ are illustrated in Figs. 5.9–5.11. As seen in Figs. 5.9(a)–5.11(a), for unaged and aged asphalt binders, the complex modulus G^* decreases with temperature. Besides, the addition of thermochromic powder increases G^* compared with original asphalt binder. The increasing extent of G^* is different, and black powder has larger effect than blue and

red powder for unaged and RTFO aged binders. As content of thermochromic powder increases, the G* value of asphalt binder is increased at each temperature. The complex shear modulus is a measure of total resistance of a material to deform when exposed to repeated pulses of shear stress (Uddin 2003). Therefore, the rutting resistance of asphalt binder can be improved by adding thermochromic powders.

(a)   (b)

(c)
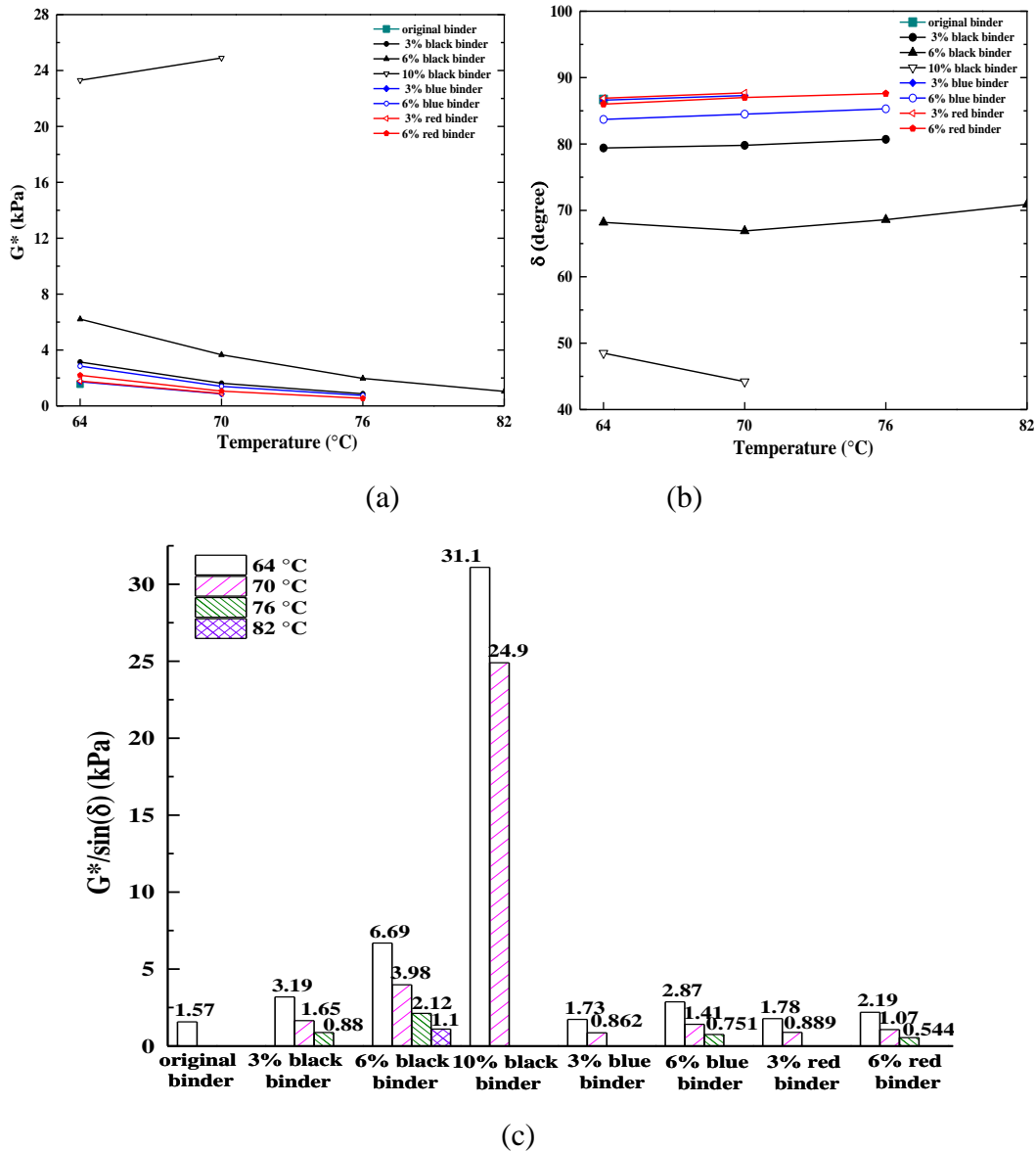
Fig. 5.9. DSR test results for unaged asphalt binders under different temperature.
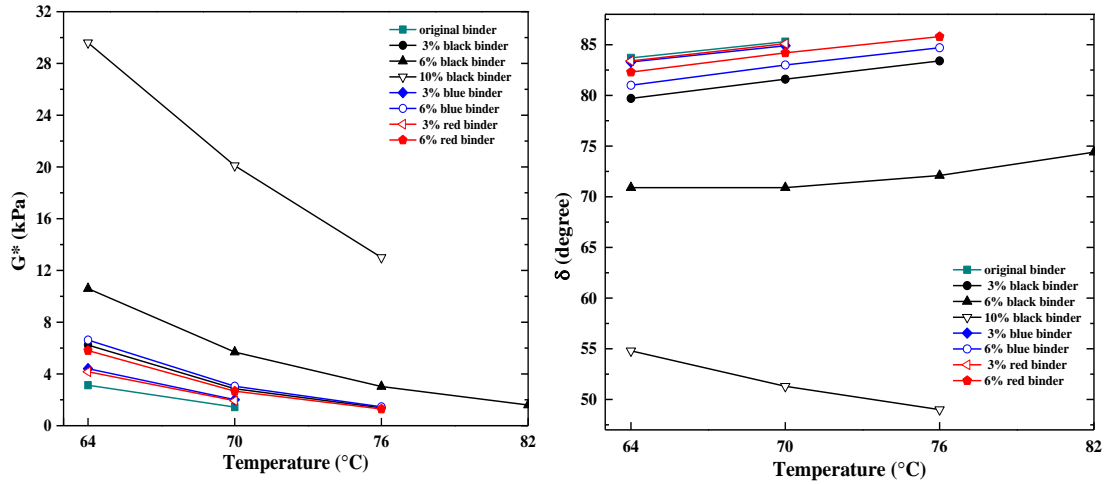
(a) (b)
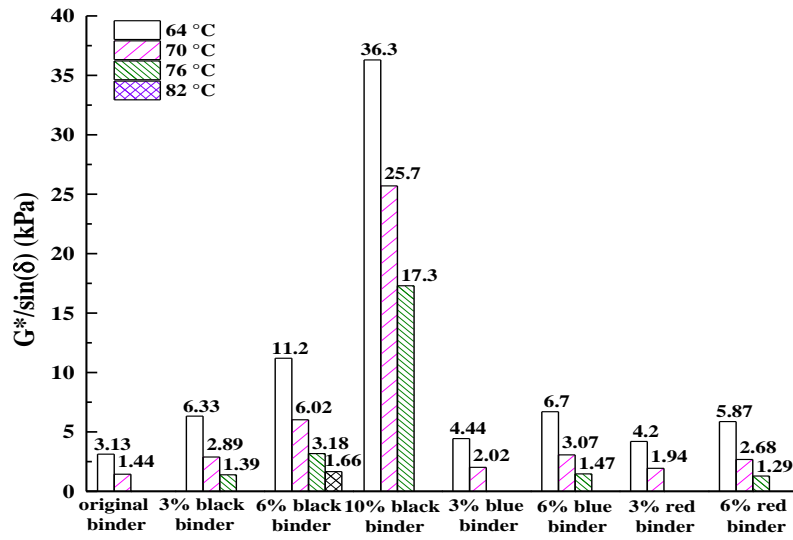
Fig. 5.10. DSR test results for RTFO aged asphalt binders under different temperature.
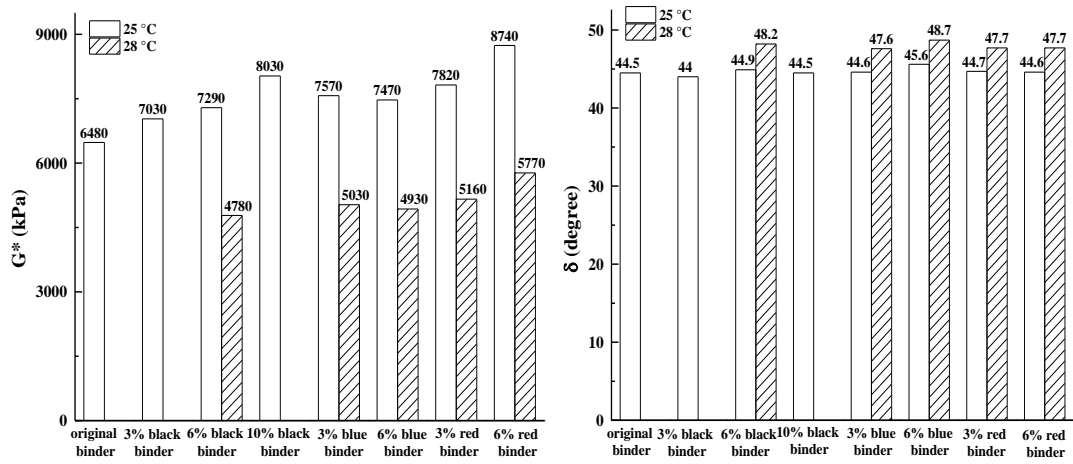
(a)   (b)
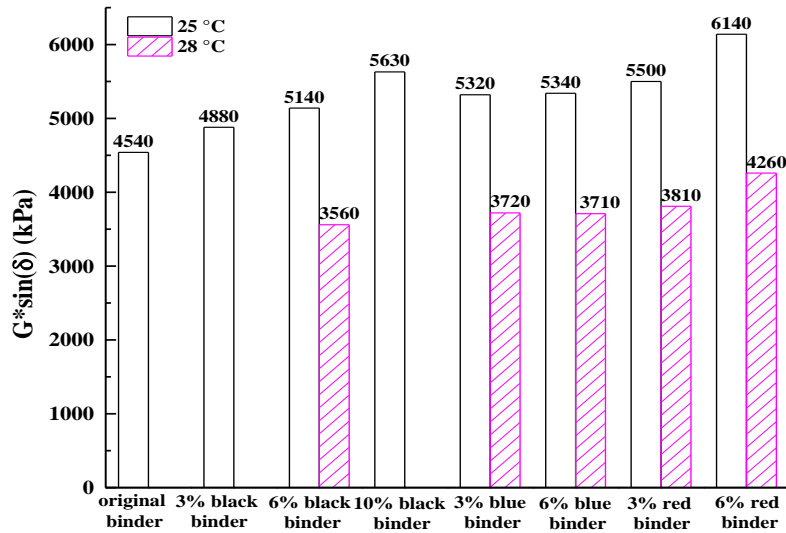
(c)

Fig. 5.11. DSR test results for (RTFO+PAV) aged asphalt binders under different temperature.

As shown in Figs. 5.9(b)–5.11(b), there are small changes in the phase angle with temperature. The small change of δ with temperature indicates a reduction in binder temperature susceptibility and better thermal resistance (Navarro et al. 2009). The δ refers to the ratio between elastic and viscous behaviors during the shearing process. Thermochromic asphalt binder exhibits smaller δ than the control binder, indicating thermochromic asphalt binder shows more elastic behavior than conventional binder. Additionally, with the increasing powder content, the δ of all thermochromic asphalt binders decrease. So the addition of thermochromic

powder increases the viscosity of binder, which is almost consistent with the findings in RV tests.

Figs. 5.9(c) and 5.10(c) show the relationship between rutting resistance parameter, G*/sin δ, and thermochromic powders at different temperature on unaged and RTFO aged binders, respectively. The G*/sin δ of the binder, both in original binder and RTFO residual, decreases with temperature but increases with the incorporation of thermochromic powder. The Superpave criterions specify a minimum value of 1.0 and 2.2 kPa for the G*/sin δ of unaged and RTFO aged asphalt binders at the high performance grade temperature, respectively. Original binder and thermochromic binders containing 3% blue and red powders at 64 °C, binder containing 3% black powder and 6% blue powder at 70 °C, as well as binder containing 10% black powder at 76 °C meet both specifications. Consequently, the use of thermochromic powders in asphalt pavement helps to improve rutting resistance at the corresponding service temperatures.

In addition, with the increasing content, the G*/sin δ increases at different extent. Table 5.1 displays the percentage increase of rutting parameters comparing the results for various unaged asphalt binder. When comparing the G*/sin δ of the unaged control binder, the G*/sin δ is increased by 103–1117%, 10–83% and 13–39% for the unaged binders containing 3–10% black powder, 3–6% blue powder and red powder, respectively. The percentage increases are in the range of 102–1060%, 42–114% and 34–88% for the RTFO aged binders with black, blue and red thermochromic powder, respectively. Table 5.2 displays that the effect of aging on G*/sinδ for various asphalt binders at 64 °C. Compared with the unaged binder, the RTFO aged binder increase the G*/sin δ by 99%, 67–98%, 133–157% and 136–168% for the control binder, black, blue and red binder, respectively. Thus, the stiffness and rutting resistance of asphalt increased after RTFO aging.

TABLE 5.1. Percentage difference comparisons for G*/sin δ of unaged and RTFO aged samples

Aging condition	Mixture comparison	Percentage difference (%)
Unaged	0% vs. 3% black powder	103.18
	0% vs. 6% black powder	326.11
	0% vs. 10% black powder	1117.20
	0% vs. 3% blue powder	10.19

	0% vs. 6% blue powder	82.80
	0% vs. 3% red powder	13.38
	0% vs. 6% red powder	39.49
RTFO aged	0% vs. 3% black powder	102.24
	0% vs. 6% black powder	257.83
	0% vs. 10% black powder	1059.74
	0% vs. 3% blue powder	41.85
	0% vs. 6% blue powder	114.06
	0% vs. 3% red powder	34.19
	0% vs. 6% red powder	87.54

TABLE 5.2. Percentage difference comparisons for G*/sin δ between unaged and RTFO aged samples at 64 °C

Samples	Percent difference %
Original binder	99.36
3% black binder	98.43
6% black binder	67.41
10% black binder	89.95
3% blue binder	156.65
6% blue binder	133.45
3% red binder	135.96
6% red binder	168.04

Fig. 5.11(c) shows the effects of thermochromic powder type and content on the fatigue parameter, G*sin δ, at 25 and 28 °C. The G*sin δ value of (RTFO+PAV) residual decreases with temperature but increases with the content of thermochromic powder. According to the Super pave binder specifications, the G*sin δ should be less than 5000 kPa. The results indicate that original binder and the binder with 3% black powder at 25 °C, the binder with 6% black powder, 3% and 6% blue and red powder at 28 °C satisfy this requirement. This indicates that the low temperature performance grade of binder needs be increased when adding 6% black powder, 3% and 6% blue and red powder. As content increases, the G*sin δ value increases by different

percentage, shown in Table 5.3. The percentage increases are between 7–24%, 17% and 21–35% for RTFO+PAV aged binder containing black, blue and red powder, respectively.

TABLE 5.3. Percentage difference comparisons for G*sin δ of RTFO+PAV aged samples

Aging condition	Mixture comparison	Percentage difference (%)
RTFO+PAV aged	0% vs. 3% black powder	7.49
	0% vs. 6% black powder	13.22
	0% vs. 10% black powder	24.01
	0% vs. 3% blue powder	17.18
	0% vs. 6% blue powder	17.62
	0% vs. 3% red powder	21.15
	0% vs. 6% red powder	35.24

Low-Temperature Cracking Properties

Based on the BBR tests at -12 °C, the creep stiffness modulus (S) and creep rate (m, the rate at which binder stiffness changes with time at low temperatures) of (RTFO+PAV) aged asphalt binders were calculated and shown in Fig. 5.12. Superpave specification of asphalt binder stipulates a maximum S-value of 300 MPa for S and a minimum m-value of 0.300. The decrease in S is expected to result in smaller thermal stresses in asphalt binder and larger m facilitates the binder to relieve thermal stresses (Freddy et al. 2006). Therefore, binders possessing smaller S and larger m value have less chance for low-temperature cracking. In this study, almost all binders meet the requirements at -12 °C, except 10% black binder. Compared with original binder, binder containing thermochromic powders yields higher stiffness and lower m-value as shown in Fig. 5.12(a) and (b). This implies that thermochromic asphalt binder might be less resistant to low-temperature cracking.

To compare the low-temperature cracking performance between thermochromic binders, the coefficient α=S/m is defined. The smaller α value, the better the low-temperature performance is. The influence of thermochromic powder type and content on α is shown in Fig. 5.12(c). It can be observed that with the increase of thermochromic powder content reduces the resistance of thermochromic asphalt binder to low-temperature cracking. Furthermore, at 3% powder content, black asphalt binder displays better performance than blue and red binder; while

at 6%, blue and red binder show better low-temperature performance than black binder. It may be attributed to the different interactions between various thermochromic powders and asphalt binder matrix.
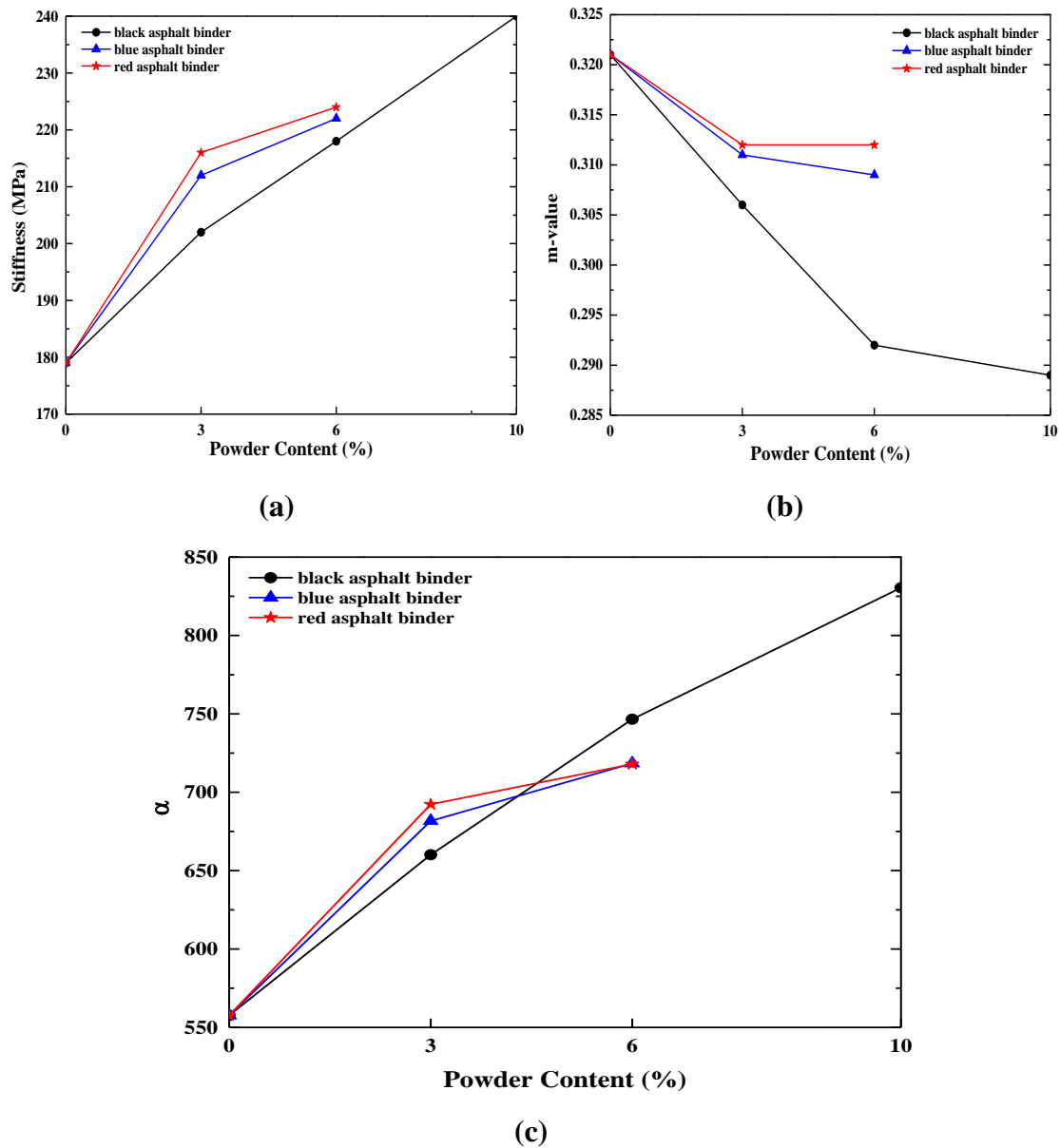
Fig. 5.12. BBR test results for (RTFO+PAV) aged asphalt binders.

Discussion

These series of Superpave binder tests were conducted to determine performance grade (PG) of asphalt binder according to AASHTO M 320 (AASHTM M 320-06 2006). The PG of various

asphalt binders is listed in in Table 5.4. It can be observed that the high temperature of PG can be improved by adding 3–10% black powder, 6 % blue and red powder; the low temperature of PG is however increased by adding 6–10% black powder, 3–6% blue powder and 3% red powder. The results imply that thermochromic asphalt binders can be used in cities under hot climate, e.g. Texas, Florida, etc. Furthermore, the increase in stiffness of thermochromic asphalt binder leads to larger thermal stresses, which could be offset by low reflectance and desirable thermal properties of thermochromic powders at low temperature. In addition, although asphalt binder containing 10% black powder present better optical properties, this binder was found difficult to handle during experiments and shows abnormal testing results. This is possibly due to the fact that at such high concentration, the powders have higher chance to cluster. Consequently, it is more difficult for the thermochromic powder to be uniformly distributed into the host binder matrix. Therefore, we recommend to limit the content of thermochromic powder to less than 5% to 6% and design the optical content of thermochromic powder based on comprehensive considerations of binder performance, cost, and constructability.

TABLE 5.4. Determination of performance grade (PG) of asphalt binder

Samples	PG
Original binder	64–22
3% black binder	70–22
6% black binder	76–16
10% black binder	76–16
3% blue binder	64–16
6% blue binder	70–16
3% red binder	64–16
6% red binder	70–22

5.4 Conclusions

The optical and mechanical properties of thermochromic asphalt binder are characterized in this study. Thermochromic asphalt binder was developed by mixing thermochromic powders with conventional asphalt binder. Optical characterization demonstrated that the reflectance of asphalt

binders is enhanced by incorporating thermochromic powders. Based on the Superpave tests of various asphalt binders, it was found that the addition of thermochromic powder increases the values of softening point, viscosity, complex modulus (G*), rutting parameter (G*/sinδ), fatigue parameter (G*sinδ), stiffness (S) and decreases the values of penetration, phase angle (δ) and creep rate (m-value). Black binder presented the lowest needle penetration depth, highest softening point, lowest viscosity, highest values of G* and G*/sinδ, lowest values of δ, S and m-value, followed by blue and red binder. Furthermore, with increasing thermochromic powder contents, the penetration depth and m-value of thermochromic binders decreased and softening point, viscosity, G*, G*/sinδ, G*sinδ, and S increased. The use of thermochromic powder is found to increase the Superpave high temperature performance grades of asphalt binder. It, however, deteriorates the low temperature performance grade. The use of thermochromic powders is recommended to be less than 5% to 6% from comprehensive considerations of binder performance, cost, and constructability. The use of thermochromic binder could potentially improve performance of asphalt pavement by reducing the surface temperature of pavement, especially in cities under hot climate zone. The lower temperature performance can be improved by use of binder modifier, which is a topic we will continue investigate.

5.5 Reference

(1)　ASTM E903-12 (2012). "Standard test method for solar absorptance, reflectance, and transmittance of materials using integrating spheres". *Book of Standards*, Volume: 12.02, American Society for Testing and Materials.

(2)　AASHTO R 28-06 (1996). "Accelerated Aging of Asphalt Binder Using a Pressurized Aging Vessel (PAV)". *Book of Standards*, American Association of State and Highway Transportation Officials.

(3)　AASHTO T 49-06 (2006). "Standard Method of Test for Penetration of Bituminous Materials". *Book of Standards*, American Association of State and Highway Transportation Officials.

(4)　AASHTO T 53-06 (2006). "Standard Method of Test for Softening Point of Bitumen (Ring-and-Ball Apparatus)". *Book of Standards*, American Association of State and Highway Transportation Officials.

(5)　AASHTO T 240-06 (2006). "Standard Method of Test for Effect of Heat and Air on a Moving Film of Asphalt (Rolling Thin-Film Oven Test)". *Book of Standards*, American Association of State and Highway Transportation Officials.

(6)　AASHTO T 313-06 (2006). "Standard Method of Test for Determining the Flexural Creep Stiffness of Asphalt Binder Using the Bending Beam Rheometer (BBR)". *Book of Standards*, American Association of State and Highway Transportation Officials.

(7)　AASHTO T 316-06 (2006). "Standard Method of Test for Viscosity Determination of Asphalt Binder Using Rotational Viscometer". *Book of Standards*, American Association of State and Highway Transportation Officials.

(8)　AASHTO T 315-06 (2006). "Standard Method of Test for Determining the Rheological Properties of Asphalt Binder Using a Dynamic Shear Rheometer (DSR)". *Book of Standards*, American Association of State and Highway Transportation Officials.

(9)　Asphalt Institute (2003). "Superpave performance graded asphalt binder specification and testing". *Superpave Series No. 1 (SP-1)*. Asphalt Institute, Lexington, KY, USA, 2003. p. 61.

(10)　Doulos, L., Santamouris, M., Livada, I. (2004). "Passive cooling of outdoor urban spaces: the role of materials". *Solar Energy*, 2004, 77(2): 231–249.

(11) Granqvist, C.G. (1991). Materials Science for Solar Energy Conversion Systems. Pergamon Press, Oxford.

(12) Hao, P.W., Zhang, D.L., Hu, X.N. (2000). "Evaluation method for low temperature anticracking performance of asphalt mixture". *Journal of Xi'an Highway University*, 2000, 20 (3):1–5.

(13) Kanerva, H.K., VINSON, T.S., Zeng, H. Low Temperature Cracking Field Validation of the Thermal Stress Rest Rained Specimen Test. R. SHRP-A-401, 1994.

(14) Karlessi, T., Santamouris, M., Apostolakis, K., Synnefa, A., Livada, I. (2009). "Development and testing of thermochromic coatings for buildings and urban structures". *Solar Energy*, 2009, 83(4): 538–551.

(15) Kinouchi, T., Yoshinaka, T., Fukae, N., Kanda, M. (2004). Development of cool pavement with dark colored high albedo coating. *Fifth Conference for the Urban Environment*, Vancouver, Canada, 2004.

(16) Kinouchi, T., Santamouris, M. (2013). "Improving the performance of thermochromic coatings with the use of UV and optical filters tested under accelerated aging conditions". *International Journal of Low-Carbon Technologies*, 2013,0, 1-17.

(17) Ma, Y. P. and Zhu, B.R. (2009). "Research on the preparation of reversibly thermochromic cement based materials at normal temperature". *Cement and Concrete Research*, 2009, 39(2): 90-94.

(18) Hu, J.Y., Yu, X. (2013). "Experimental Study of Sustainable Asphalt Binder: Influence of Thermochromic Materials". *Journal of Transportation Research Record*, 2013.

(19) Pomerantz, M. and Akbari. H. (1998). "Cooler Paving Materials for Heat Island Mitigation". In 1998 *ACEEE Summer Study on Energy Efficiency in Buildings*, Asilomar, CA, City: American Council for an Energy-Efficient Economy, vol. 9, Pacific Grove, 1998, 135.

(20) Pomerantz, M., Akbari, H., Chen, A., Taha, H., Rosenfeld, A. (1997). *Paving Materials for Heat Island Mitigation*. Lawrence Berkeley National Laboratory Report LBL- 38074, Berkeley, CA.

(21) Pomerantz, M., Akbari, H., Harvey, J. T. (2000). *Cooler reflective pavements give benefits beyond energy savings: Durability and illumination*. Report No. LBNL-45370, Berkeley, CA, 14.

(22) Saeli, M., Piccirillo, C., Parkin, I. P., Binions, R., Ridley, I. (2010). "Energy modelling studies of thermochromic glazing". *Energy and Buildings*, 42(10): 1666–1673.

(23) Santamouris, M., Synnefa, A., Kolokotsa, D., Dimitriou, V., Apostolakis, K. (2008). "Passive cooling of the built environment - use of innovative reflective materials to fight heat island and decrease cooling needs". *International Journal Low Carbon Technologies*, 3(2): 71–82.

(24) Yoder, E. J. and Witzak, M. W. (1975). *Principles of Pavement Design*. New York, NY: Wiley and Sons.

(25) Gui, J., Phelan, P. E., Kaloush, K. E., Golden, J. S. (2007). "Impact of Pavement Thermophysical Properties on Surface Temperatures". *Journal of Materials in Civil Engineering*, 19(8): 683–690.

(26) Roberts Freddy L, Kandhal Prithvi S, Brown E Ray. (1996). "Hot mix asphalt materials", *Mixture Design and Construction*. 2nd ed. NAPA Research and Education Foundation; 1996.

(27) Uddin, W. (2003). "Viscoelastic characterization of polymer modified asphalt binders of pavement applications". *Applied Rheology*, 13(4): 191-199.

(28) Navarro, F.J., Partal, P., Garcia, M.M., Martın-Alfonso, M.J., Martınez, B.F., Gallegos. C., Bordado, J.C.M., Diogo, A.C. (2009). "Bitumen modification with reactive and non-reactive (virgin and recycled) polymers: a comparative analysis". *Journal of Industrial and Engineering Chemistry*, 15(4): 458–464.

(29) AASHTO M320-05 (2006). Standard specification for performance graded asphalt binder. American Association of State and Highway Transportation Officials, 2006.

(30) Santamouris, M., Pavlou, K., Synnefa, A., Niachou, K., Kolokotsa, D. (2007). "Recent progress on passive cooling techniques: Advanced technological developments to improve survivability levels in low-income households". *Energy and Buildings*, 39(7): 859–866.

(31) Synnefa, A., Dandou, A., Santamouris, M., Tombrou, M., Soulakellis, N. (2008). "Large scale albedo changes using cool materials to mitigate heat island in Athens". *Journal of Applied Meteorology and Climatology*, 47(11): 2846–2856.

CHAPTER SIX

THERMAL AND PYROLYTIC CHARACTERISTICS OF THERMOCHROMIC ASPHALT BINDER

The research in this chapter studied the thermal kinetic behaviors of the thermochromic asphalt. The goal is to determine the production parameters for thermochromic asphalt. The pyrolytic behavior (more accurate thermolytic behavior, defined as chemical reaction during heating process) and kinetic study of pyrolysis mechanism are important for setting the optimal plant production parameters (i.e., mixing temperature and duration) of thermochromic asphalt binders. This paper reports on the pyrolytic and kinetic characteristics of thermochromic asphalt binder using thermogravimetric analysis (TGA). The results indicate that the mass loss of thermochromic binders are less than 5% when subjected to 200°C for 2 hours. Although the rate of mass losses of asphalt binder is increased, the activation energy of asphalt binder is also increased after adding thermochromic materials, indicating less susceptibility of viscosity of asphalt binder to temperature. The kinetic analysis found that the pyrolytic behaviors of binders are best described by the three-dimensional diffusion function mechanism model, as indicated by the best fits to the experimental data among typical models. Confocal Microscope, Fourier Transform Infrared Spectroscopy (FTIR), and UV-Vis-IR Spectrophotometer are used to characterize the structural and optical behaviors of thermochromic binders before and after thermal treatments. No strong chemical interactions occurs between thermochromic powders and binder matrix. Heat treatment is found to reduce the solar reflectance of thermochromic binders with the effects depending upon the exposure duration. Considering both the pyrolysis characteristics (mass loss) and the performance of solar (infrared) reflectance, blue and red asphalt binders can be produced with temperature ranges covering both hot mix asphalt (HMA) and warm mix asphalt (WMA), while black asphalt binder should be produced with low mixing temperature such as WMA technique.

6.1. Introduction

Asphalt is one of the most widely consumed construction materials worldwide. For example, 96% of the over 10 million kilometers of interstate highway in the U.S. is built with asphalt

pavement. Asphalt binders are produced from the residuals of crude oil distillation processes. It features excellent performance properties. The increases in the price of crude oils experienced in the past decade lead to significant increases in the price of asphalt. As a non-renewable material, improvements of its durability have important sustainability contributions. However, the black color of asphalt binder causes large solar absorption and leads to high surface temperature of asphalt pavement, which has been reported up to 48-67 °C during summer [1-3]. The increased temperature in summer impairs durability of asphalt pavement by accelerating various distress mechanisms (i.e., rutting, shoving, aging, fatigue damage, bleeding) [4] as well as causes undesirable environmental issues (i.e., heat island effects, volatile gas emission, etc.) [5]. A potential way to improve the durability is to use materials with high reflectivity and emissivity to solar radiation. This has led to the development of various cool pavement technologies, or pavement with lower surface temperatures. Studies [6-10] show that cooling the pavement increased the service life (durability) of pavements. However, the reduced temperature of asphalt pavement exacerbates the distress of low-temperature cracking during the winter period [11-12], which compromises the service life of road in cold climate. Besides, the lower surface temperature is inductive to ice formation in cold weather, which is a major safety concern. New pavement materials and technology that make asphalt pavement cooler during summer and warmer during winter will lead to more durable and safe pavement.

An innovative strategy we have pursued is to use thermochromic materials to create asphalt binder with desirable solar reflectance, i.e., they reflect more solar energy at high temperature and reflect less solar energy at low temperature. To avoid visual impacts on road users, such effects are mostly restrained in the infrared range, since infrared accounts for 50% of total solar radiation. Thermochromic materials are materials that change their colors with temperature. Our study has found that thermochromic asphalt binder features high solar reflectance in summer and high solar absorption in winter [13-14]. The change of their optical and thermal properties in such a dynamic way can lead to applications that improve the urban microclimate, decrease the energy demands of the buildings, and provide a thermally comfortable indoor environment [15-20].

To upscale to the plant production, the pyrolysis characteristics and effects of exposure to mixing temperature on the solar reflectance of thermochromic binders need to be evaluated. This paper describes the effects of thermochromic materials on the decomposition kinetics of asphalt

115

binder. This is important to upscale the laboratory study to the field plant production parameters (production temperature, time and the associated thermal stabilities). Kinetic models describe the thermal interactions and help understanding the thermal interaction mechanisms of a material. For example, the kinetic parameters (i.e., activation energy E and pre-exponential factor A) give indication of the reactions' mechanism in solid state, which helps to determine the lifetime of the material, its thermal stability and others [21]. Thermogravimetric research is widely used to determine kinetic parameters and the mechanism of the solid reaction [22-26]. In this study, thermogravimetry (TG) experiments and thermal analysis kinetics are used to discuss the influence of thermochromic materials on pyrolysis characteristics of asphalt binder. Based on the experimental data, pyrolytic reaction mechanism of thermochromic asphalt binder is revealed, which is helpful to understand the thermal interaction mechanism of asphalt binder containing thermochromic materials. In addition, the influence of various production conditions on the morphology, chemical structures, and optical properties of asphalt binders are investigated comprehensively.

6.2 Experiment

Raw Materials

Asphalt binder used in this study is Superpave grade, PG 64–22, produced by Kokosing Materials Inc. Thermochromic powders are selected from those manufactured by Hali Industrial Corporation Ltd. Three types of thermochromic powders (red, blue and black) with transition temperature around 31 °C are chosen for this study. The diameters of powders are in the range of 3-10µm. These thermochromic materials are organic mixtures, which consists of lueco dye (electron donor), developer (electron acceptor) and solvent. Below the transition temperature, leuco dye reacts with the developer, the absorption peaks shifts from the UV to the visible range, and thus the powder becomes colored. At temperature above the transition temperature, the solvent-developer interactions dominate, and leuco dye is separated from the developer and leads to loss of color. Thermochromic materials are encapsulated by trioctanoinand and therefore at high temperature thermochromic powders become white or light-colored state. The molecular structures of thermochromic materials and their changes with temperature are shown in Fig. 6.1.

Fig. 6.1. Molecular structures of thermochromic powders and their changes with temperature: a) black powder; b) blue powder; c) red powder.

Preparation of Thermochromic Asphalt Binder

Thermochromic asphalt binders are prepared by the following procedures: the original asphalt binder is heated to 163 °C in an oven until it completely melted, then thermochromic powders are added. The amount of thermochromic powders is 10% of asphalt binder by weight. The mixture is then mixed using a mixer for 10 minutes. The asphalt binder containing black, blue and red thermochromic powder is named as black, blue and red (thermochromic) asphalt binder, respectively in this paper for simplicity in the nomenclature.

In principle, the thermochromic asphalt binder should exhibit different a response to solar radiation than conventional asphalt binder. Solar energy consists of a spectrum of wavelengths, including ultraviolet, visible, and infrared light (almost 50% of the entire solar energy). Below the transition temperature of the thermochromic powder, where the powders are less infrared reflective, the binder should reflect less (and therefore absorb more) solar energy, as shown in Fig. 6.2(a); above the transition temperature, where the powders are more reflective to infrared, thermochromic asphalt binder should reflect more solar energy, as shown in Fig. 6.2(b). Both energy-reflecting and energy-absorbing properties of thermochromic asphalt binder help to maintain pavement at an appropriate temperature range desirable for its longevity and performance. Another study by the authors have validated that the surface temperature of thermochromic binder is up to around 7 °C lower than regular asphalt at a temperature of around 50 °C [13-14]. The details can be found in the cited papers and are not duplicated here. The kinetic analyses are important to evaluate the thermal stability of thermochromic binder and to set the optimal plant production parameters.

UV+ Visible   Infrared   UV+ Visible   Infrared

(a)   (b)
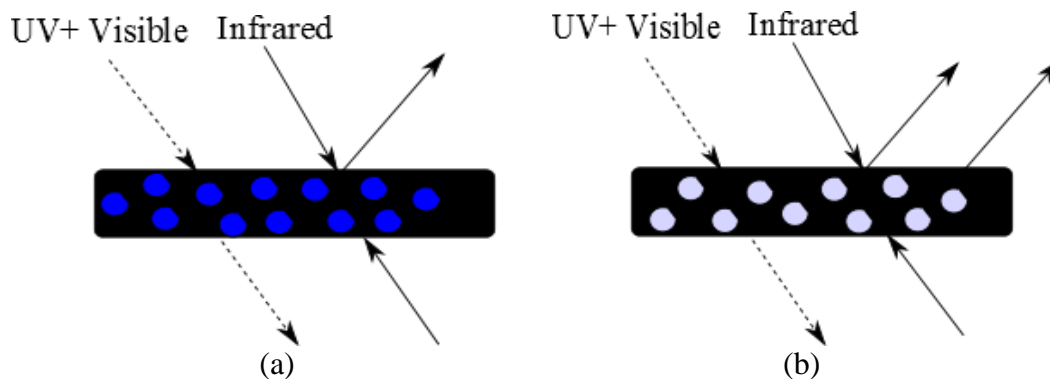
Fig. 6.2. Schematic principle of thermochromic asphalt binder: (a) under the transition temperature of thermochromic powders; (b) higher infrared reflectance above the transition temperature.

Thermal Treatment of Samples

Generally, two technologies are employed to produce asphalt mixtures in plant: hot mix asphalt (HMA) and warm mix asphalt (WMA).Traditional HMA mixtures are typically produced at temperatures ranging from 140 to 170 °C [27]. WMA technology allows significant lower production temperature, which is generally in the temperature range of 105 to 135 °C. To assess

the influence of production processes on the properties of the final binder, thermochromic powders and asphalt binders were heated at 105, 140, 170 and 200 °C for 0.5, 1 and 2 hours, respectively. These thermally treated samples were then analyzed by the following techniques.

Characterizations

The powder distribution in asphalt binder was studied by the Olympus FV1000 Confocal Microscope BX62 based on both surface mapping and depth profiling experiments.

The chemical structures of untreated and treated samples were investigated by Fourier Transform Infrared Spectroscopy (FTIR). The measurements were carried out in the absorption mode in the mid-infrared range (400–4000 cm^{-1}) with a resolution of 4 cm^{-1}.

Thermal degradation of both thermochromic powders, and various regular and thermochromic asphalt binder samples were performance in a thermogravimetric analyzer (Q500 TG, TA Instruments), respectively. Considering the extreme of industrial production conditions, the samples are first heated from ambient temperature to 200 ℃ with the heating rate of 5 °C/min, then kept isothermal at 200 ℃ for 120 min, and finally heated to 400 ℃ with the same heating rate. The continuous records of weight loss and temperature are then used to plot a TG curve and derivative thermogravimetric analysis (DTG) curves.

The reflectance spectra of both thermochromic powders and asphalt binders were measured over the wavelength range of 300–1800 nm by the Agilent Cary 6000i UV-Vis-IR Spectrophotometer with a DRA integrating sphere. The measurements were performed according to ASTM E903-96 [28]. During the measurements, thermochromic powders and asphalt binders were packed between microscopic slides with a thickness of 1mm at room temperature. The change of reflectance spectra between untreated and treated samples was also evaluated.

6.3 Results and Discussion

Confocal surface mapping analyses

Fig. 6.3 shows example of the confocal optical image of the surface of untreated pure asphalt binder as well as untreated and treated red asphalt binders. It is seen that there is a smooth surface in pure asphalt binder (Fig. 6.3(a)). After mixed with thermochromic powders, rough morphology and agglomerated powders appear in the binder matrix as agglomerated particles as can be seen in Fig. 6.3(b). The separation of binder and powders is an indication that the

interactions of binder and thermochromic particles are likely due to physical interactions. There is no significant interface formed in the material matrix. Fig. 6.3(c) shows the surface image of thermally treated red asphalt binder exposed to 200°C for 2 hours. It can be seen that there is an obvious difference in the morphology of red asphalt binder in Fig. 6.3(c) when compared with Fig. 6.3(b). The exposure to high temperature treatment (200°C for 2 hours) might change the interactions of asphalt binder matrix and the embedded thermochromic particles. This, however, can't be determined with confocal microscope.

(a)   (b)   (c)
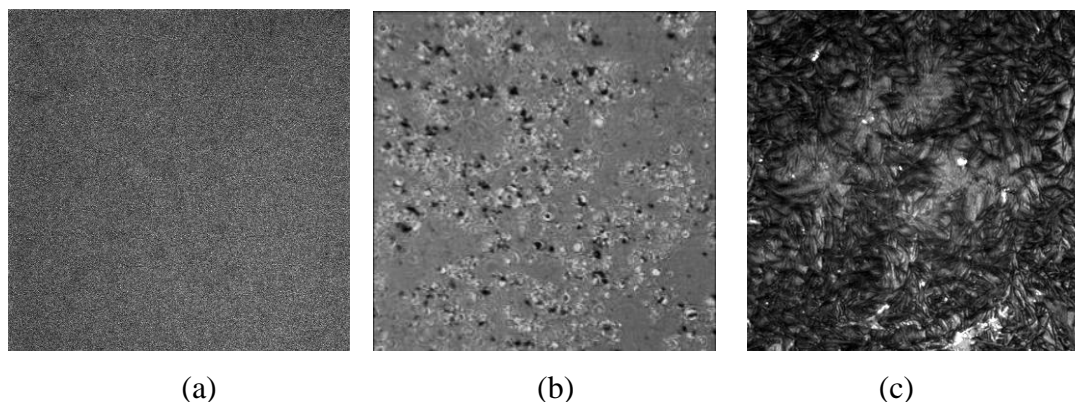
Fig. 6.3. Surface Images of (a) untreated pure asphalt binder; (b) untreated red asphalt binder; (c) treated red asphalt binder after subjected to 200 °C for 2h.

FTIR Spectra

FTIR is used to detect the possible changes in the functional groups of thermochromic powders and powder-binder matrix interactions after being subjected to thermal treatment. The influence of thermal treatment of 200 °C for 2h on the chemical characteristics of both thermochromic powders and thermochromic asphalt binders were studied by FTIR spectroscopy. Fig. 6.4 shows the infrared spectra for black, blue and red powder before and after thermal treatment, respectively. The absorption peak mainly occurs at about 1350, 1470, 1560, 1640, 2850, 2920 and 3300 cm^{-1}, which is attributed to the band of C-O, C=C, C=O, C-H, O-H and N-H, respectively. The absorption peak in the all IR spectra at 2350 cm^{-1} corresponds to the asymmetrical stretch of CO_2. Besides, the comparison of peak positions between untreated and treated powders indicates that there is no significant change of functional group and bands after being subjected to the 200 °C treatment for 2 hours and the powders are considered as thermal stable under this condition.
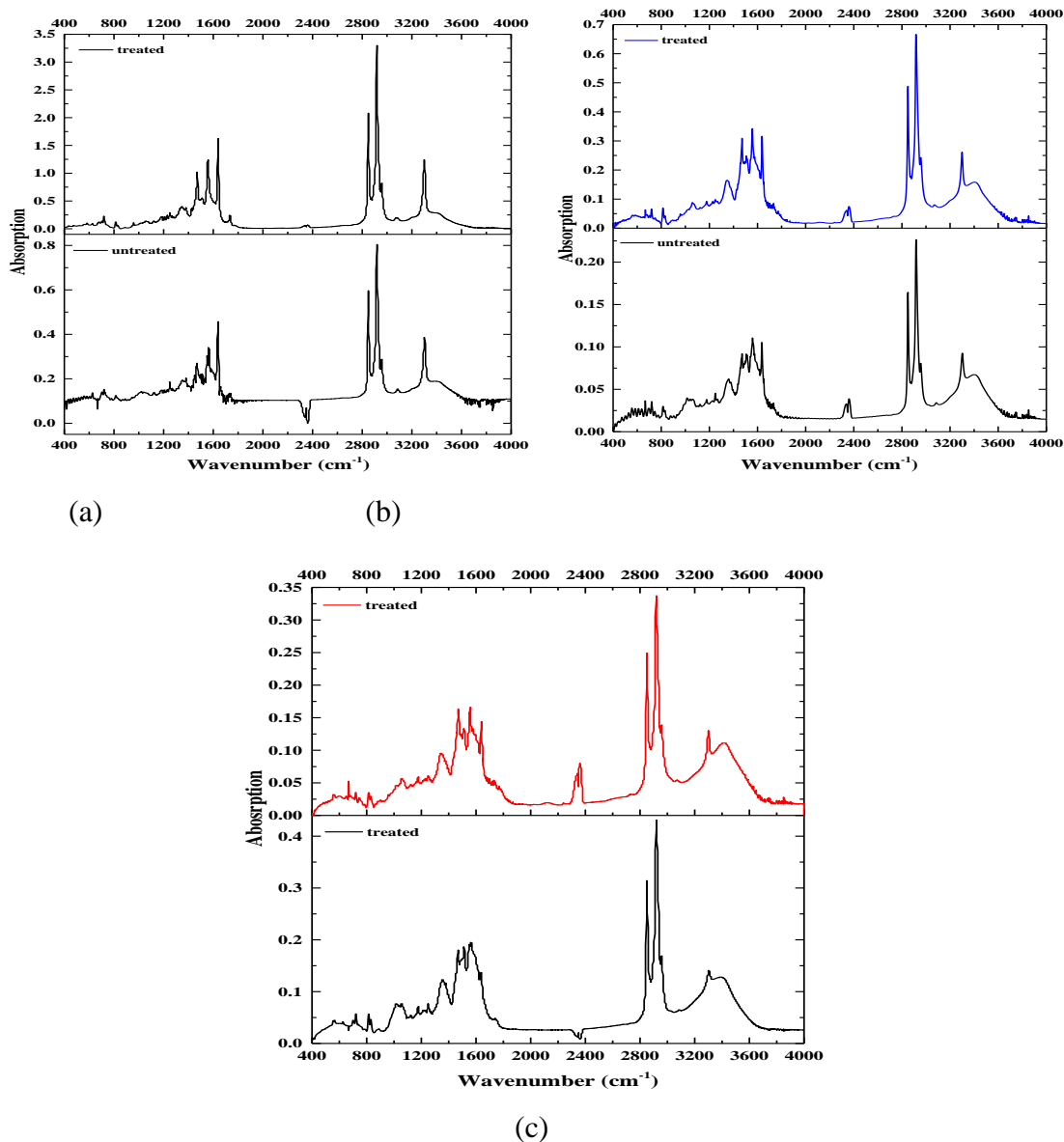
Fig. 6.4. Infrared spectra before and after thermal treatment: (a) black powder, (b) blue powder, (c) red powder.

The FTIR spectra of thermochromic asphalt binders before and after being treated are illustrated in Fig. 6.5. The strong peaks in the range of 2850–3000 cm^{-1} represent typical C-H stretching vibrations in aliphatic chains. Band at 1375 cm-1 and 1455 cm-1is attributed to the C-H symmetric deforming in CH$_3$ vibrations, and C-H asymmetric deforming in CH$_2$ and CH$_3$, respectively. The C=C stretching vibrations in aromatics is observed at about 1575 cm^{-1}. A small number of sulphoxide groups, characterized by the band of S=O at 1030 cm^{-1}, are also noted.

121

Furthermore, the thermochromic asphalt binder shows a tiny peak at 3300 cm⁻¹, which is N-H stretching vibration from thermochromic powders. As shown in Fig. 6.5, thermochromic asphalt binders contain the functional groups similar as the original asphalt binder besides N-H. In addition, compared with untreated binders, treated binders present the similar peak positions in FTIR spectra. This indicates that no chemical major changes occurred after the heat treatment and these asphalt binders are chemically stable under the condition.
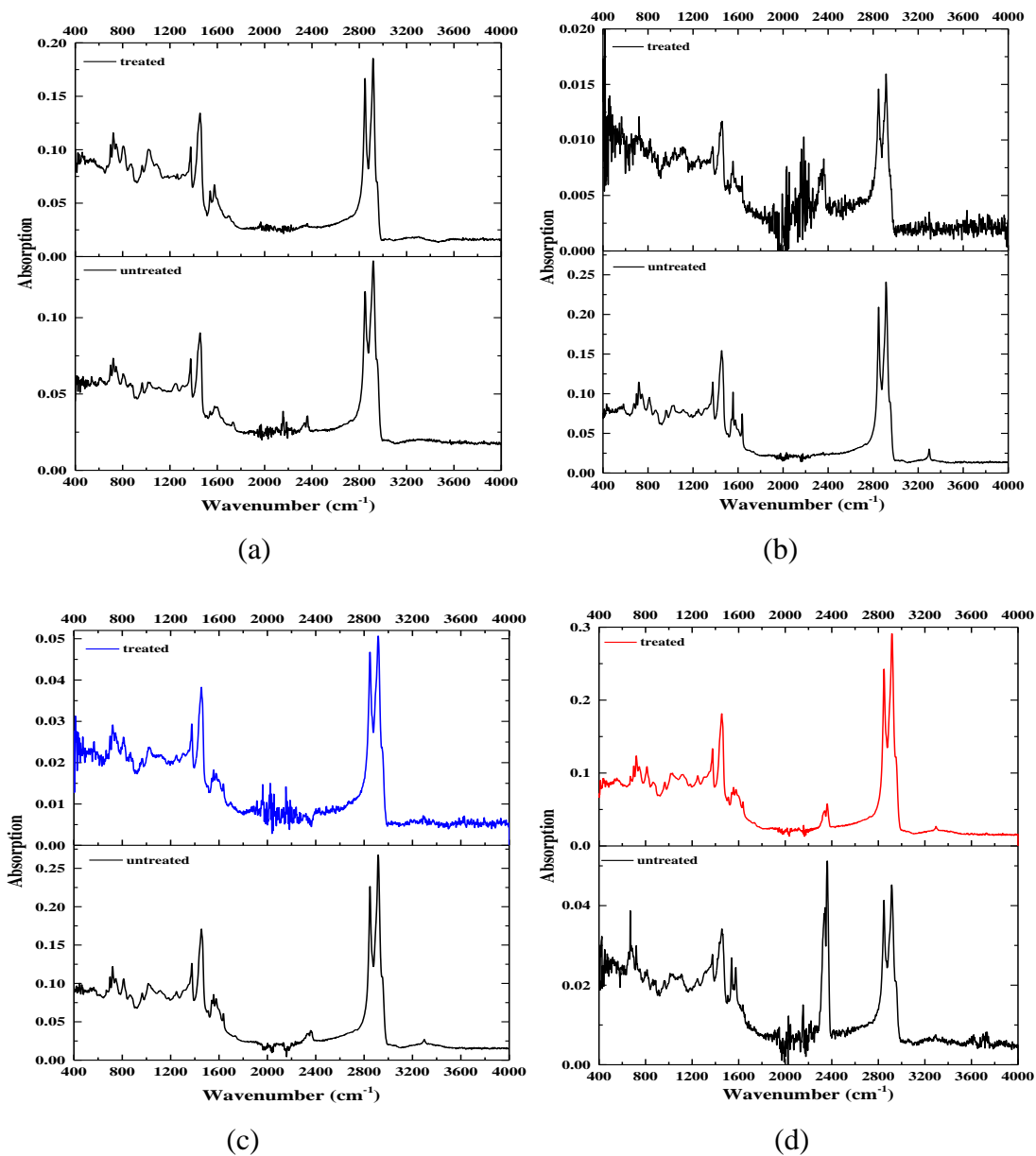
Fig. 6.5. Infrared spectra before and after thermal treatment: (a) pure asphalt binder, (b) black asphalt binder, (c) blue asphalt binder, (d) red asphalt binder.

Table 6.1. Weight losses (%) of the samples at different temperatures.

Samples	105 °C	140 °C	170 °C	200 °C (initial)	200 °C (2 h)
Black powder	1.27	1.89	2.44	3.05	4.64
Blue powder	1.45	2.35	3.14	3.94	5.54
Red powder	1.95	2.93	3.80	4.67	7.79
Pure asphalt binder	0	0	0	0.15	1.89
Black asphalt binder	0.15	0.22	0.4	0.78	3.53
Blue asphalt binder	0.21	0.4	0.73	1.21	3.1
Red asphalt binder	0.19	0.31	0.51	0.85	3.01

The Pyrolysis Characteristics of the Samples

Fig. 6.6 shows the TGA and DTG curves of pure thermochromic powders. The values of the thermal weight losses under different production conditions are summarized in Table 6.1. For temperatures up to 200 °C, weight losses lower than 5% are considered insignificant. This is mostly due to the evaporation of water or capsule materials. Weight loss lower than 5% means the materials are thermally stable during production in industry. From the differentiation on the TGA curve, DTG curves are obtained, which displays the relationship between the mass loss rate and temperature. The DTG curves in Fig. 6.6(b) show two weight loss peaks, indicating that there are mainly 2 stages in the pyrolysis of thermochromic powders. The first stage occurs at the temperature range of 280–300 °C, 265–290 °C, and 283–303 °C for black, blue and red thermochromic powder, respectively. This mass loss peak is probably related to the release and combustion of the weaker chemical bonds and some small gaseous molecules. The second corresponding stage occurred with the highest weight loss between 300–370 °C, 290–360 °C, and 303–360 °C. At the end of second stage, there is 24%, 35% and 32% of residue for black, blue and red powder, respectively. The second peak might be ascribed to the breaking of stronger chemical bonds and large gaseous molecules. To keep their thermal stabilities, the powders should be heated below 200 °C for 2 h or at 200 °C for 30 min.

| (a) | (b) |
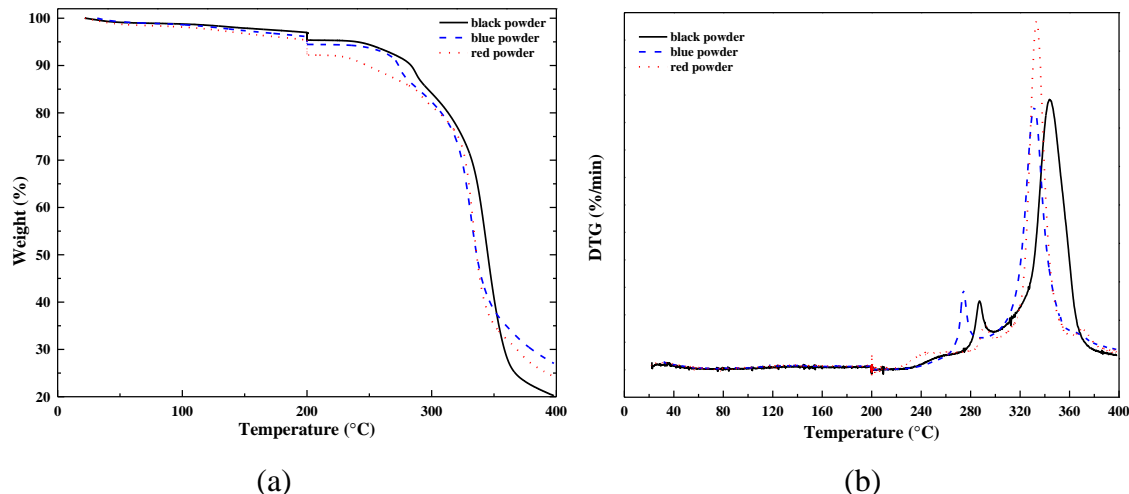
Fig. 6.6. TGA (a) and DTG (b) curves of thermochromic powders.

Fig. 6.7 displays the experimental curves for the measured thermal degradation of various types of asphalt binders. The data at different temperatures is also summarized in Table 6.1. According to Table 6.1, after subjected to 200 °C for 2 hours, all asphalt binder samples present less 5% of weight losses, which implies they should be thermally stable during typical plant production conditions (which is generally less than 200°C). The DTG curve of each asphalt binder sample indicates one main reaction stage in this experiment, which occurs between 280–370 °C. At 370 °C, the amount of residue is 88%, 78%, 83% and 79% of the original pure, black, blue and red asphalt binder, respectively. The relatively high amount of residue implied that during this stage, oil content is mainly released due to its small molecular weight and relatively lower pyrolysis temperature. Additionally, the DTG curves show that compared with conventional asphalt binder, black, blue and red asphalt binder has higher decomposition rate. Therefore, the addition of thermochromic powders increases the thermal decomposition of asphalt binder. This might be attributed to the higher decomposition rate of thermochromic powders than pure asphalt binder.
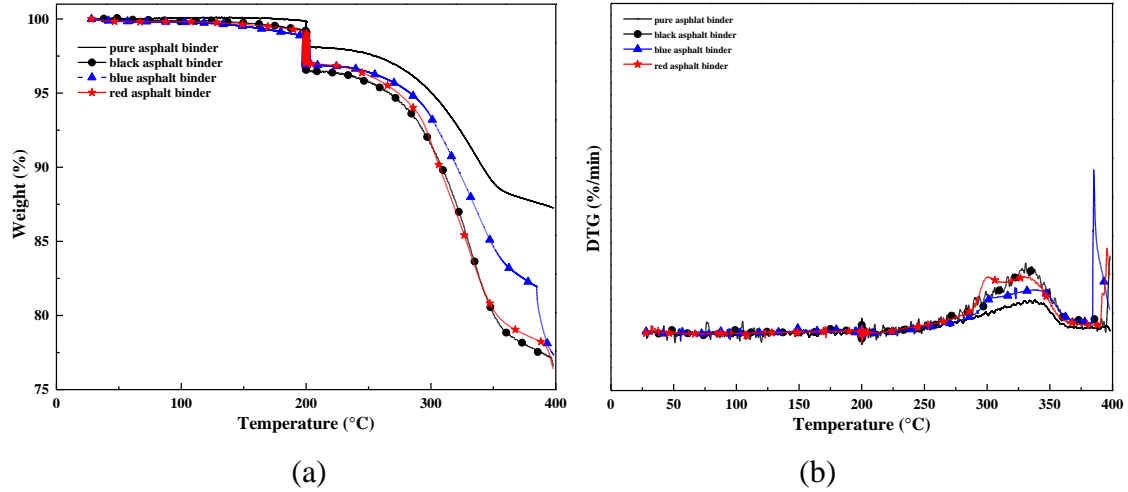
Fig. 6.7. TGA (a) and DTG (b) curves of different asphalt binder samples.

Kinetics Analysis of Pyrolysis Characteristics of the Samples

Pyrolysis reaction rate is controlled by the heating rate, temperature, and pyrolysis products mass. When non-isothermal reaction is assumed to divide into numbers of short time segments, the reaction in each segment is considered as an isothermal procedure. Therefore, the pyrolysis reaction can be described by the Arrhenius method [29]. According to the Arrhenius equation, the pyrolysis reaction of the samples under oxidative atmospheres is governed by

$$\frac{d\alpha}{dt} = kf(\alpha) = A\exp(-\frac{E}{RT})f(\alpha) \tag{1}$$

with $\alpha = 1 - \frac{m}{m_0}$

where k is reaction rate constant, A the frequency factor (min^{-1}), E the activation energy (kJ/mol), R the universal gas constant $(kJ/(mol \cdot K))$, t the time of the pyrolysis process (min), T the pyrolysis temperature at time t (K), α the reaction degree, f(α) function related to the reaction mechanism, m_0 the initial mass (kg), and m the mass at time t.

Substitute the heating rate β (°C/min) of dT/dt, Eq. (1) becomes:

$$\frac{d\alpha}{dT} = \frac{A}{\beta}\exp(-\frac{E}{RT})f(\alpha) \tag{2}$$

125

Define integral function g(α) and get

$$g(\alpha) = \int_0^\alpha \frac{d\alpha}{f(\alpha)} = \frac{A}{\beta} \int_{T_0}^T \exp(-\frac{E}{RT}) dT \qquad (3)$$

where T_0 is the initial temperature.

In this study, the Coats-Redfern method was used to solve the kinetic equation. Based on the approximate integral-type equation, Eq. (3) can be expressed as follows:

$$\ln\left[\frac{g(\alpha)}{T^2}\right] = \ln\left[\frac{AR}{\beta E}(1 - \frac{2RT}{E})\right] - E \cdot \frac{1}{RT} \qquad (4)$$

In this equation, due to 2RT/E<<1, the term 2RT/E can be neglected. So, when the selected f(α) function is appropriate, the plot of $\ln[g(\alpha)/T^2]$ versus 1/RT would yield a straight line whose slope is E, while the intercept determines the frequency factor A.

Table 6.2 shows the most widely used kinetic functions and integral functions for the kinetic analysis [30-31]. They can be classified into four categories: for A2–A4, nucleation and growth are the rate determining process; for D1–D4, diffusion is the rate controlling process; F1–F3 are based on the reaction order; for R2–R3, the geometric nature of the growth of reaction interface is important [32]. Using the TG and DTG data, the functions shown in Table 6.2 are substitute into Eq. (4) respectively to see if they give good linearity with regard to this equation. The regression analysis with the least squares method is employed in the analysis for each pyrolysis stage. The g(α) with maximum correlation coefficient R^2 is considered to be the mechanism function of the pyrolysis reaction for the samples under study.

Table 6.2. Commonly used pyrolysis mechanism functions and integral functions.

Mechanism	f(α)	g(α)	Symbol
Based on nucleation and nuclei growth			
Avrami-Erofeev equ.	$2(1-\alpha)[-\ln(1-\alpha)]^{1/2}$	$[-\ln(1-\alpha)]^{1/2}$	A2
Avrami-Erofeev equ.	$3(1-\alpha)[-\ln(1-\alpha)]^{2/3}$	$[-\ln(1-\alpha)]^{1/3}$	A3
Avrami-Erofeev equ.	$4(1-\alpha)[-\ln(1-\alpha)]^{3/4}$	$[-\ln(1-\alpha)]^{1/4}$	A4
Based on diffusion mechanisms			
One-dimensional (parabolic law)	$1/(2\alpha)$	α^2	D1

Two-dimensional (Valensi equ.)	$-\dfrac{1}{\ln(1-\alpha)}$	$(1-\alpha)\ln(1-\alpha)+\alpha$	D2
Three-dimensional (Jander equ.)	$\dfrac{3(1-\alpha)^{2/3}}{2\left[1-(1-\alpha)^{1/3}\right]}$	$\left[1-(1-\alpha)^{1/3}\right]^{2}$	D3
Three-dimensional (G-B equ.)	$\dfrac{3}{2\left[(1-\alpha)^{-1/3}-1\right]}$	$1-\dfrac{2}{3}\alpha-(1-\alpha)^{2/3}$	D4
	Based on reaction order		
First order	$1-\alpha$	$-\ln(1-\alpha)$	F1
Second order	$(1-\alpha)^{2}$	$(1-\alpha)^{-1}$	F2
Third order	$(1-\alpha)^{3}$	$(1-\alpha)^{-2}$	F3
	Based on geometric models		
Contracting cylinder	$2(1-\alpha)^{1/2}$	$1-(1-\alpha)^{1/2}$	R2
Contracting sphere	$3(1-\alpha)^{2/3}$	$1-(1-\alpha)^{1/3}$	R3

Following the above procedures, fitting results of correlation coefficient for thermochromic powders and asphalt binders at each pyrolysis stage are summarized in Tables 6.3 and 6.4, respectively. By identifying the highest correlation coefficient, it is found that the three-dimensional diffusion function mechanism model (D3 in Table 6.2) leads to the best linearity for all thermochromic powders and asphalt binder samples. This also implies that the diffusion is the rate controlling process in pyrolysis of thermochromic binders.

Table 6.3. Correlation coefficients of the plots of $\ln[g(\alpha)/T^{2}] \sim -1/(RT)$ for thermochromic powders.

$g(\alpha)$	Black powder		Blue powder		Red powder	
	280–300 °C	300–370 °C	265–290 °C	290–360 °C	283–303 °C	303–360 °C
A2	0.9733	0.9535	0.9519	0.945	0.9865	0.9281
A3	0.9635	0.9418	0.9350	0.9285	0.9685	0.9111
A4	0.9474	0.9250	0.9079	0.9034	0.8695	0.8876
D1	0.9807	0.9651	0.9656	0.9607	0.9938	0.9431
D2	0.9812	0.9629	0.9662	0.9612	0.9939	0.9444
D3	**0.9816**	**0.9694**	**0.9668**	**0.9622**	**0.9941**	**0.9454**
D4	0.9813	0.9718	0.9664	0.9629	0.9940	0.9448
F1	0.9798	0.9618	0.9604	0.9574	0.9924	0.9405
F2	0.7499	0.8308	0.1206	0.8592	0.2329	0.8940
F3	0.9809	0.8552	0.9484	0.8879	0.9769	0.9101
R2	0.9789	0.9679	0.9620	0.9579	0.9922	0.9389
R3	0.9791	0.9661	0.9624	0.9575	0.9924	0.9396

Table 6.4. Correlation coefficients of the plots of $\ln[g(\alpha)/T^2] \sim -1/(RT)$ for asphalt binder samples.

$g(\alpha)$	Pure asphalt binder 280–370 °C	Black asphalt binder 280–370 °C	Blue asphalt binder 280–370 °C	Red asphalt binder 280–370 °C
A2	0.9578	0.9602	0.9674	0.9158
A3	0.8929	0.9138	0.9244	0.8228
A4	0.5536	0.7364	0.7332	0.5997
D1	0.9824	0.9800	0.9846	0.9560
D2	0.9829	0.9811	0.9702	0.9577
D3	**0.9833**	**0.9820**	**0.9860**	**0.9593**
D4	0.9830	0.9814	0.9855	0.9582
F1	0.9785	0.9780	0.9826	0.9508
F2	0.0032	0.0827	0.0112	0.0600
F3	0.0653	0.8396	0.2335	0.8817
R2	0.9775	0.9761	0.9812	0.9473
R3	0.9778	0.9767	0.9816	0.9485

After determination of pyrolysis mechanism of the samples, kinetics parameters are calculated based on the slope and intercept of the fitting lines. The kinetic parameters (i.e. A and E values) are summarized in Table 6.5. As shown in Table 6.5, the activation energy is between 152.72–184.42 kJ/mol, 150.48–164.34 kJ/mol, and 79.61–194.29 kJ/mol for black, blue and red powders, respectively. The corresponding range of pre-exponential factor ln(A) value is 25–31, 25–28, and 9–34. It is also found that the values of activation energy (E) and frequency factor (A) of asphalt binder are increased after incorporating thermochromic powder into it. This explains that the reaction rate of thermochromic asphalt binder is higher than that of conventional pure asphalt binder under higher temperature.

Table 6.5. The kinetic parameters under different temperature range for thermochromic powder and asphalt binder samples.

Samples	Temperature range (°C)	E (kJ/mol)	A (min^{-1})
Black powder	280–300	152.72	7.95×10^{10}
	300–370	184.42	4.39×10^{13}
Blue powder	265–290	150.48	8.62×10^{10}
	290–360	164.34	1.05×10^{12}
Red powder	283–303	79.61	1.16×10^{4}
	303–360	194.29	4.62×10^{14}
Pure asphalt binder	280–370	86.93	3.8×10^{3}
Black asphalt binder	280–370	95.31	7.4×10^{4}
Blue asphalt binder	280–370	91.77	2.1×10^{4}
Red asphalt binder	280–370	100.56	2.2×10^{5}

Additionally, the activation energy (E) has strong correlation with the thermal susceptibility of viscoelastic materials [33]. The higher activation energy, the less susceptible the asphalt binder is to change in viscosity with temperature. Therefore, the addition of thermochromic powder helps to decrease the susceptibility of viscosity of asphalt binder to temperature. This agrees with the results reported in our previous study [34], in which all of complex shear modulus (G*), phase angle δ and G*/sinδ of thermochromic asphalt binder decreases with temperature. Consequently, the use of thermochromic powders in asphalt pavement helps to improve rutting resistance at the service temperatures.

Influence of Production Conditions (Temperature and Exposure Duration) on Solar Reflectance

The results of spectrophotometric measurements for both untreated thermochromic powders and asphalt binders at room temperatures are presented in Fig. 6.8. The reflection curves of thermochromic powders demonstrate high solar reflectance, especially in the infrared range (Fig. 6.8a). The specific color of powders determines the reflection spectra in the visible range. It is also found that asphalt binder mixtures are more reflective than conventional pure asphalt binder in the near infrared range (Fig. 8b). The increase in the reflectance of thermochromic binders in the near infrared region can be explained by the high reflectance of thermochromic powders. The effects of thermochromic powders on the reflectance of thermochromic binders are less significant in the visible and near-ultraviolet ranges, which might be due to the smaller penetration depth at shorter wavelengths.

(a)   (b)
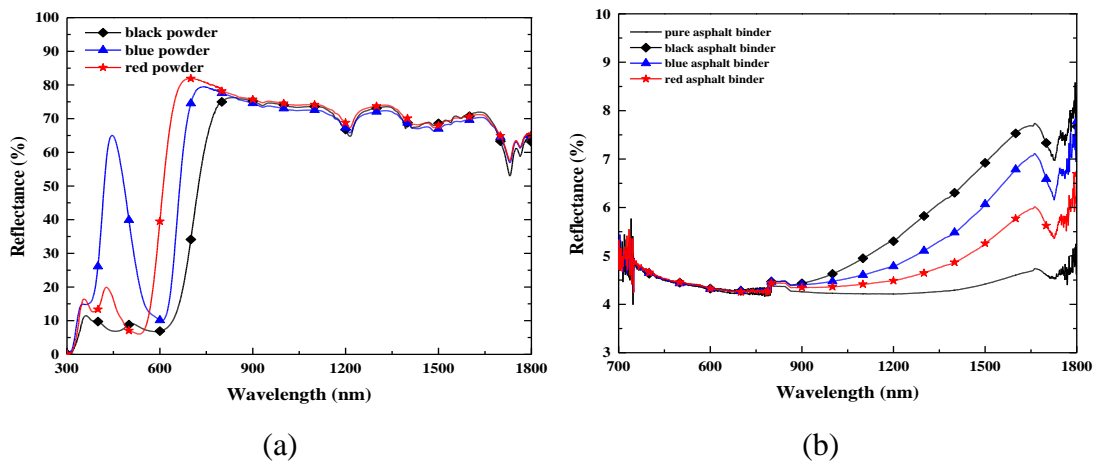
Fig. 6.8. Reflectance spectra of both untreated thermochromic powders (a) and untreated thermochromic asphalt binders (b).
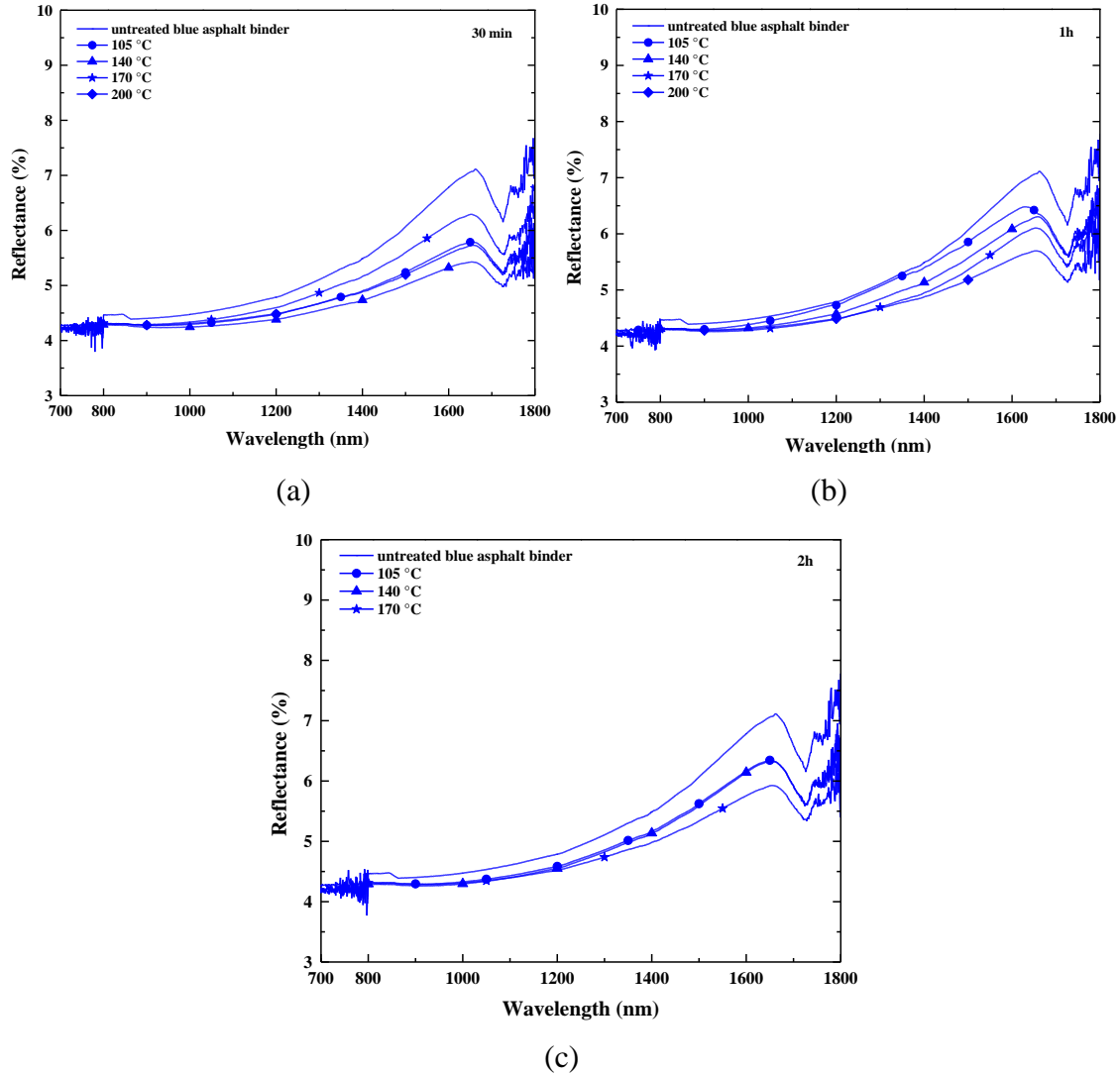
Fig. 6.9. Influence of thermal treatment temperature and time on reflectance spectra of blue asphalt binder a) 30 minutes, b) 1 hour; c) 2 hours.

The solar reflectance of each sample was calculated from the spectral reflectance data by weighted-averaging method (ASTM E903-96 [28]). The standard solar spectrum employed as the weighting function is provided by ASTM E490-00 [35]. The values of solar reflectance of thermally treated samples (i.e., samples subjected to different lengths of exposure to high temperatures) were compared with that of untreated samples. An example of measured solar reflectance spectra for blue asphalt binder is shown in Figure 6.9. As can be seen from this Figure, the solar reflectance of blue asphalt binder reduces with temperature and duration of thermal treatment until becoming relatively stable. The changes of total solar reflectance of

thermochromic powders in UV-VIS-IR range are summarized in Table 6.6. It can be observed that the solar reflectance of thermochromic powders mostly increases upon thermal treatment. For example, the total solar reflectance of blue powder increased up to 14.6% when heat treated at 140°C for 2h. This might be due to the partial melting of the shells of the powders and consequent easier exposure of the colored pigments. However, black powder exhibits appreciable reduction in the total solar reflectance when subjected to extended exposure to high temperature (170°C to 200°C for up to 1 hour), which is in the upper range of production temperatures for HMA. This implies that black powder might not be stable for use in HMA. Instead, it might need to be used with WMA to reduce the high temperature exposure.

Table 6.6. Increase percentage (%) of solar reflectance of treated thermochromic powders compared to that of untreated powders.

Samples	Time	105 °C	140 °C	170 °C	200 °C
Black powder	30 min	2.8%	3.9%	4.5%	-3.3%
	1h	2.7%	3.7%	2.8%	-3.4%
	2h	0.9%	3.8%	-12.2%	-12.0%
Blue powder	30 min	5.6%	3.8%	5.4%	3.9%
	1h	5.3%	5.9%	5.7%	1.3%
	2h	9.2%	14.6%	7.38%	3.2%
Red powder	30 min	2.2%	-0.2%	1.9%	2.6%
	1h	4.2%	3.0%	1.9%	1.3%
	2h	6.2%	6.5%	4.8%	6.2%

Table 6.7 displays the comparison of solar reflectance in the infrared range between untreated and thermally treated asphalt binders. It is observed that the reflectance of thermochromic asphalt binders is generally reduced after thermal treatment, especially the black asphalt binder. The maximum reduction percentage is about 4%, 8.5% and 15.8% for black, blue and red asphalt binder, respectively upon heat treatment under 200°C for two hours. The significant reduction in the solar reflectance in black asphalt binder might be related to the observed reduction in solar reflectance of black asphalt powder. Using the 10% reduction of

solar reflectance as the acceptance criteria, the blue and red asphalt binders meet the requirements.

Table 6.7. Increase percentage (%) of solar reflectance (in the NIR) of treated thermochromic asphalt binders compared to that of untreated binders.

Samples	Time	105 °C	140 °C	105 °C	200 °C
Black asphalt binder	30 min	-14.2%	-12.5%	-13.6%	-14.2%
	1h	-13.9%	-14.8%	-13.7%	-13.9%
	2h	-12.8%	-15.0%	-13.1%	-15.8%
Blue asphalt binder	30 min	-6.7%	-8.5%	-4.4%	-6.7%
	1h	-2.7%	-4.7%	-6.2%	-6.9%
	2h	-4.5%	-4.9%	-5.9%	-7.1%
Red asphalt binder	30 min	-2.2%	-2.4%	-1.6%	-1.5%
	1h	0.8%	-3.7%	-3.9%	-1.6%
	2h	-4.0%	-2.3%	-2.8%	-2.7%

Considering both pyrolysis characteristics and solar reflectance performance, red and blue asphalt binder can be produced under the temperature conditions covering both HMA and WMA technologies. For black asphalt binder, the reduced solar reflectance upon high temperature exposure compromises its higher solar reflectance compared to pure asphalt binder. Therefore, the black asphalt binder should be produced with low mixing temperatures, i.e., the WMA technique.

6.4 Conclusions

In this study, the pyrolysis characteristics of both thermochromic powders and asphalt binders containing theses powders are investigated by thermogravimetric analysis from room temperature to 400°C in air atmosphere. The TGA results showed that thermochromic asphalt binders have less than 5% mass loss when exposed to 200°C for 2 hours. The mass losses and decomposition rates of asphalt binder samples are increased by adding thermochromic powders.

The kinetic mechanism of both thermochromic powder and asphalt binder samples is best described by the three dimensional diffusion mechanism model. The kinetic parameters of activation energy and pre-exponential factor of asphalt binder are increased by adding thermochromic powders. The increase of activation energy helps to reduce susceptibility of viscosity of asphalt binder to temperature, potentially improving the rutting resistance of asphalt pavement.

The confocal image demonstrated the rough morphology of thermochromic asphalt binder and the lack of physical interactions between thermochromic powders and binder matrix. The thermal treatment at 200°C for two hours changed the microstructure of the binder matrix. Meanwhile, FTIR spectra revealed that thermochromic asphalt binder features similar functional groups as the pure asphalt binder except the N-H bond due to thermochromic powders. This implies there are no strong chemical interactions between thermochromic powders and asphalt binder. The optical reflectance spectra of thermochromic binders before and after thermal treatment were measured. In general, the optical reflectance of thermochromic binders reduced after thermal treatment. The blue and red asphalt binders present less percentage reduction of solar reflectance than black asphalt binder under typical production temperature of asphalt. Considering the influence of production temperatures on the morphology, chemical stability, thermal stability, and performance of solar reflectance of thermochromic binders, blue and red asphalt binders can be produced with typical HMA and WMA mixing temperatures, while black asphalt binder has to be produced at lower temperature, i.e., the WMA mixing procedures.

6.5 References

(1)   Santamouris, M., Pavlou, K., Synnefa, A., Niachou, K., Kolokotsa, D. Recent progress on passive cooling techniques: Advanced technological developments to improve survivability levels in low-income households. *Energy and Buildings*, 2007, 39(7): 859-866.

(2)   Synnefa, A., Dandou, A., Santamouris, M., Tombrou, M., Soulakellis, N. Large scale albedo changes using cool materials to mitigate heat island in Athens. Journal of Applied Meteorology and Climatology, 2008, 47(11): 2846-2856.

(3)   Doulos, L., Santamouris, M., Livada, I. Passive cooling of outdoor urban spaces. The role of materials. Solar Energy, 2004, 77(2): 231-249.

(4)   Yoder, E. J. and Witzak, M. W. Principles of Pavement Design. New York, NY: Wiley and Sons, 1975.

(5)   Gui, J., Phelan, P. E., Kaloush, K. E., Golden, J. S. Impact of Pavement Thermophysical Properties on Surface Temperatures. Journal of Materials in Civil Engineering, 2007, 19(8): 683-690.

(6)   Pomerantz, M. and Akbari. H. Cooler Paving Materials for Heat Island Mitigation. In 1998 ACEEE Summer Study on Energy Efficiency in Buildings, Asilomar, CA, City: American Council for an Energy-Efficient Economy, 1998.

(7)   Pomerantz, M., Akbari, H. Cooler paving materials for heat island mitigation, in: Proceedings of the 1998 ACEEE Summer Study on Energy Efficiency in Buildings, vol. 9, Pacific Grove, CA, 1998, 135.

(8)   Pomerantz, M., Akbari, H., Chen, A., Taha, H., Rosenfeld, A. Paving Materials for Heat Island Mitigation. Lawrence Berkeley National Laboratory Report LBL- 38074, Berkeley, CA, 1997.

(9)   Pomerantz, M., Akbari, H., Harvey, J. T. Cooler reflective pavements give benefits beyond energy savings: Durability and illumination. Report No. LBNL-45370, Berkeley, CA, 2000, 14.

(10)   Kinouchi, T., Yoshinaka, T., Fukae, N., Kanda, M. Development of cool pavement with dark colored high albedo coating. Fifth Conference for the Urban Environment, Vancouver, Canada, 2004.

(11)   Hao, P.W., Zhang, D.L., Hu, X.N. Evaluation method for low temperature anticracking

performance of asphalt mixture. Journal of Xi'an Highway University, 2000, 20 (3):1-5.

(12) Kanerva, H.K., VINSON, T.S., Zeng, H. Low Temperature Cracking Field Validation of the Thermal Stress Rest Rained Specimen Test. R. SHRP-A-401, 1994.

(13) Hu, J.Y., Yu, X. Experimental Study of Sustainable Asphalt Binder: Influence of Thermochromic Materials. Journal of Transportation Research Record, 2013, 3(2372): 108-115.

(14) Hu, J.Y., Yu, X. Innovative Chromogenic Materials for Pavement Life Extension: Modeling Study of Surface Temperature of Sustainable Asphalt Pavement. International Journal of Pavement Research and Technology, 2013, 6(2): 141-146.

(15) Santamouris, M., Synnefa, A., Kolokotsa, D., Dimitriou, V., Apostolakis, K. Passive cooling of the built environment - use of innovative reflective materials to fight heat island and decrease cooling needs. International Journal Low Carbon Technologies, 2008, 3(2): 71-82.

(16) Karlessi, T., Santamouris, M., Apostolakis, K., Synnefa, A., Livada, I. Development and testing of thermochromic coatings for buildings and urban structures. Solar Energy, 2009, 83(4): 538-551.

(17) Granqvist, C.G. Materials Science for Solar Energy Conversion Systems. Pergamon press, Oxford, 1991.

(18) Saeli, M., Piccirillo, C., Parkin, I. P., Binions, R., Ridley, I. Energy modelling studies of thermochromic glazing. Energy and Buildings, 2010, 42(10): 1666-1673.

(19) Ma, Y. P. and Zhu, B.R. Research on the preparation of reversibly thermochromic cement based materials at normal temperature. Cement and Concrete Research, 2009, 39(2): 90-94.

(20) Kinouchi, T., Santamouris, M. Improving the performance of thermochromic coatings with the use of UV and optical filters tested under accelerated aging conditions. International Journal of Low-Carbon Technologies, 2013.

(21) Rodriguez, R.P., Sierens, R., Verhelst, S. Thermal and kinetic evaluation of biodiesel derived from soybean oil and higuereta oil. Journal of Thermal Analysis and Calorimetry, 2009, 96(3): 897-901.

(22) Liu, Q., Wang, S.R., Zheng, Y., Luo, Z.Y., Cen K. Mechanism study of wood lignin pyrolysis by using TG–FTIR analysis. Journal of Analytical and Applied Pyrolysis, 2008, 82(1): 170-177.

(23) Aboulkas, A., Harfi, K.E. Bouadili, A.E., Chanâa, M.B., Mokhlisse, A. Pyrolysis kinetics of polypropylene: Morocco oil shale and their mixture. Journal of Thermal Analysis and Calorimetry, 2007, 89(1): 203-209.

(24) Mothe´, M. G., Leite, L.F. M., Cheila, G. Thermal characterization of asphalt mixtures by TG/DTG, DTA and FTIR. Journal of Thermal Analysis and Calorimetry, 2008, 93(1): 105-109.

(25) Xu, T. Huang, X.M. Pyrolysis Properties and Kinetic Model of an Asphalt Binder Containing a Flame Retardant. Journal of Applied Polymer Science, 2011, 119(5): 2661-2665.

(26) Naskara, M., Chaki, T.K., Reddy, K.S. Effect of waste plastic as modifier on thermal stability and -degradation kinetics of bitumen/waste plastics blend. Thermochimica Acta, 2010, 509(1–2): 128-134.

(27) Newcomb, D. An Introduction to Warm-Mix Asphalt. National Asphalt Pavement Association, Accessed from http://fs1.hotmix.org/mbc/Introduction_to_Warm-mix_Asphalt.pdf, August 8, 2007.

(28) ASTM E903-96. Standard test method for solar absorptance, reflectance, and transmittance of materials using integrating spheres. Technical Report, American Society for Testing and Materials, 1996.

(29) Han, X.X., Jiang, X.M., Cui, Z.G. Thermal analysis studies on combustion mechanism of oil shale. Journal of Thermal Analysis and Calorimetry, 2006, 84(3): 631-636.

(30) Liu, N., Fan, W., Dobashi, R., Huang, L.S. Kinetic modeling of thermal decomposition of natural cellulosic materials in air atmosphere. Journal of Analytical and Applied Pyrolysis, 2002, 63(2): 303-325.

(31) Nunez, L., Fraga, F., Nunez, M.R., Villanueva, M. Thermogravimetric study of the decomposition process of the system BADGE (n=0)/1, 2 DCH. Polymer, 2000, 41(12): 4635-4641.

(32) Reading, M., Dollimore, D., Whitehead, R. The measurement of meaningful kinetic parameters for solid state decomposition reactions. Journal of Thermal Analysis, 1991, 37(9): 2165-2188.

(33) Cong, P.L., Wang, J., Li, K., Chen, S.F. Physical and rheological properties of asphalt binders containing various antiaging agents. Fuel, 2012, 97: 678-684.

(34) Hu, J.Y., Gao, Q., Yu, X. Characterization of the Optical and Mechanical Properties of Innovative Multifunctional Thermochromic Asphalt Binders. Journal of Materials in Civil Engineering, 2014.

(35) ASTM E490-00. Standard Solar Constant and Zero Air Mass Solar Spectral Irradiance Tables. American society for Testing and Materials, 2000.

CHAPTER SEVEN

OUTDOOR EVALUATION OF THE PERFORMANCE OF THERMOCHROMIC ASPHALT CONCRETE IN MODULATING PAVEMENT SURFACE TEMPERATURE

This study evaluated the performance of the thermochromic asphalt binder on surface temperatures of pavement to assess its durability and sustainability. Comparison studies were performed that include the outdoor thermal performance of conventional asphalt concrete and asphalt concrete containing black, blue and red thrmochromic materials. The study was operated between spring and summer 2015. Surface temperatures of comparison samples were monitored to investigate the thermal performance of thermochromic asphalt concrete. The results show that the surface temperature of thermochromic asphalt concrete was cooler than conventional asphalt concrete under hot summer conditions up to 6°C, 6.2°C and 3.6°C and warmer during the evening up to 0.4°C, 1.7°C and 1.8°C by using black, blue and red thermochromic materials, respectively. Besides, the temperature fluctuation of asphalt concrete was found to be reduced up to 5°C, 4°C and 3°C by using black, blue and red thermochromic materials, respectively. Furthermore, compared to conventional asphalt concrete, thermochromic asphalt concrete reduced the rate of heating and cooling. These demonstrate the potential of thermochromic asphalt concrete to improve the durability of the pavement, reduce the environmental impacts, and mitigate ice related safety issues on the road. This demonstrates innovation for development of sustainable and environmental benign infrastructure.

7.1 Introduction

The use of asphalt pavement accounts for approximately 94% of US roads (1). As a thermoplastic material, asphalt becomes brittle at low temperatures and becomes soft at high temperatures. Studies (i.e., (2-4)) measured surface temperature as high as 48-67 °C during summer. The increased temperature in summer impacts durability of asphalt pavement by accelerating various distress mechanisms (i.e., rutting, shoving, aging, fatigue damage, bleeding) (5). A potential way to improve durability that aroused interest in the past years is the use of materials that present high solar reflectivity to develop cool pavement. Cool pavement has been developed by using cool materials with high reflectivity and emissivity to the solar radiation.

Studies (6-10) show that cool pavement presents lower surface temperatures, resulting in increased service life (durability) of pavements. However, the reduced temperature of asphalt pavement exacerbates low temperature cracking during the winter period (11-12), which compromise the service life of the road. Additionally, the lower temperature is conductive to ice formation in cold weather. Therefore, it is necessary to develop a new technique to make asphalt pavement cooler during summer and warmer during winter.

An innovative strategy the researchers pioneered is the use of thermochromic materials to create new materials possessing desirable solar reflectance, i.e., they reflect more solar energy at high temperature and reflect less solar energy at low temperature (13-14). Thermochromic materials are substances that can change their colors in response to temperature. They feature high solar reflectance in summer and high solar absorption in winter. These properties make them attractive for urban and building applications (15-19) to improve the urban microclimate, decrease the energy demands of the buildings, and provide a thermally comfortable indoor environment.

The objective of this study is to study the thermal performance of asphalt mixture containing thermochromic materials, which could modulate the pavement surface temperature according to environmental temperatures and therefore extend service life of the pavement. In this study, the surface temperatures of both conventional and thermochromic asphalt concretes are measured on 24 h basis between April and June, 2014. The influence of themochromic materials on surface temperature and temperature fluctuation are evaluated by comparing surface temperature of thermochromic asphalt concrete with that of conventional asphalt concrete under different weather conditions. Example is given to evaluate the influence of thermochromic materials on rate of temperature change of the pavement on a typically summer day.

7.2 Experiment

Materials and Preparation

Asphalt binder used in this study is supplied by Kokosing Materials Inc. and classified as Superpave grade, PG64-22. Thermochromic powders were manufactured by Hali Industrial Corporation Ltd. Red, blue and black thermochromic powders with transition temperature around 31 °C were chosen for this study. The powders have particle sizes in the range of 3 ~ 10 μm. The molecular structures of thermochromic powders and their changes below and above transition temperature are shown in Fig. 7.1. These powders were firstly mixed with asphalt

binder at the concentration of 6% by weight of asphalt binder and then kept them in an oven to get homogeneous binder matrix. The preparation of asphalt concrete follows the Marshall compaction method by mixing thermochromic asphalt binder with aggregates. The samples are cylinders with 0.10 m in diameter and 0.06 m in height. The black, blue and red thermochromic based asphalt concrete were named as black, blue and red asphalt concrete, respectively in this study for simplicity in the nomenclature.

(a)

(b)

(c)
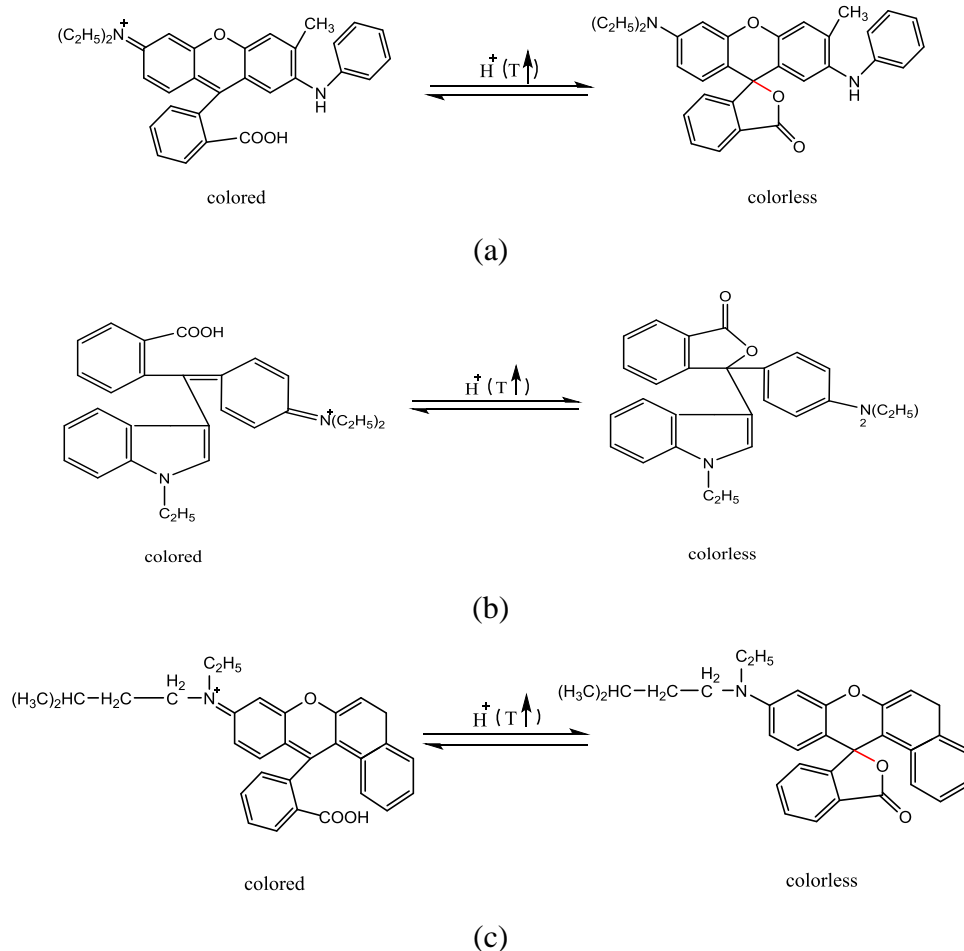
Fig. 7.1. Molecular structures of thermochromic powders and their changes with temperature: a) black powder; b) blue powder; c) red powder.

Experimental Measurements

To compare the thermal performance, the surface temperatures of black, blue and red thermochromic asphalt concrete and conventional asphalt concrete were continuously monitored. The samples were placed on the roof of an office building filled with a layer of stones, shown in

140

Fig. 7.2. To avoid the interferences from environment, i.e., heat flow from surrounding and bottom, these samples were thermally insulated from surrounding except the surface is exposed. The surface temperatures were measured with thermocouples that are connected to a data logging system. The sensors used were thin-wire type K thermocouples, and PicoLog recorder was used for data collection and conversion. The temperature sensors are calibrated to have an accuracy of 0.1°C. Temperature is monitored at 1 second time interval from April 21st to June 15th, 2014.

Fig. 7.2. Photo of the samples on the platform.

The ambient meteorological conditions were recorded from a meteorological station near the experimental sites. Data include the air temperature, wind speed, relative humidity, and solar radiation on a horizontal surface at one minute interval. These parameters were used to characterize the outdoor climatic conditions. The air temperature, the wind speed, the relative humidity and the monthly average daily solar radiation on a horizontal surface during the experimental period are summarized in Table 7.2. The monthly average daily solar radiation (W/m^2) on a horizontal surface, for each month of the experimental period is shown in Fig. 7.3.
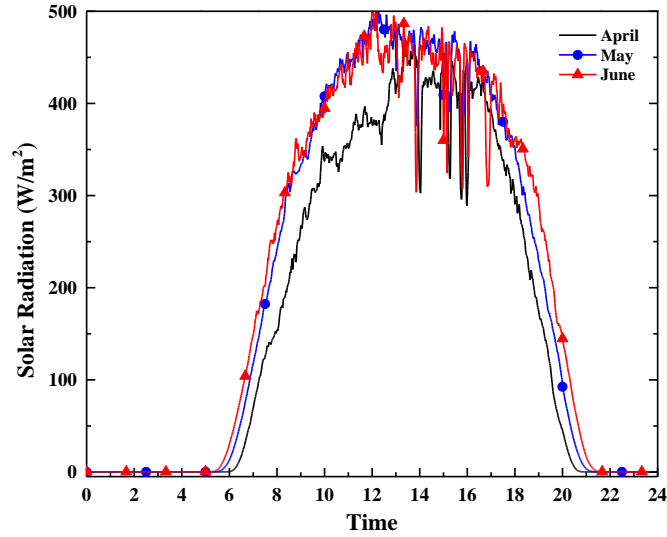
Fig. 7.3. The monthly average solar radiation on a horizontal surface for April, May and June, 2014.

Table 7.1. Air temperature, wind speed, relative humidity and solar radiation during the experimental period.

	Air Temperature (°C)		Wind speed (m/s)		RH (%)	Monthly average daily solar radiation (W/m^2)
	Daily	Nocturnal	Daily	Nocturnal		
April						
Mean	12.1	12.1	3.8	3.2	57.7	
Max	20.8	19.9	6.9	5.4	80.9	330
Min	5.8	7.8	1.6	1.1	49.5	
May						
Mean	17.8	17.8	3.3	2.9	45.3	
Max	25.7	25.3	5.5	4.9	81.0	389
Min	9.1	9.1	1.3	1.0	20.9	
June						
Mean	21.5	21.1	3.1	2.8	43.8	
Max	24.8	25.2	5.2	5.1	60.6	392
Min	17.5	17.8	1.5	1.4	25.1	

7.3 Analysis of the Thermal Performance of Thermochromic Asphalt Concrete

The mean surface temperatures, mean temperature fluctuations, cooling and warming potential by temperature differences during the day period (8:00–20:00LT) and during the night period (22:00–6:00LT) for each month for each sample are summarized in Tables 7.2–7.4. In these tables, ΔT_0 is the surface temperature fluctuation during the daytime or night, and σ is the surface temperature difference between conventional and thermochromic asphalt concrete. They are expressed as:

$$\Delta T_0 = T_{max} - T_{min} \qquad (1)$$

$$\sigma = T_{thermochromic} - T_{conventional} \qquad (2)$$

The negative σ value means thermochromic asphalt concrete is cooler than conventional asphalt concrete, while positive σ value indicates thermochromic asphalt concrete is warmer than conventional asphalt concrete. Details of the experimental results and their implications are elaborated in the following context.

Table 7.2. Daily (8:00–20:00) and nocturnal (22:00–6:00) mean, maximum, minimum surface temperatures temperature fluctuations and differences during April, 2014.

Sample	*April daily*				
	Avg. T_{mean}	Avg. T_{max}	Avg. T_{min}	Avg. ΔT_0	Avg. σ_{min}
Conventional asphalt concrete	18.84	29.83	7.89	21.94	
Black asphalt concrete	18.31	29.69	8.12	21.56	-0.95
Blue asphalt concrete	18.22	29.15	8.06	21.09	-2.57
Red asphalt concrete	18.69	29.30	8.04	21.46	-1.45

	April nocturnal				
	Avg. T_{mean}	Avg. T_{max}	Avg. T_{min}	Avg. ΔT_0	Avg. σ_{max}
Conventional asphalt concrete	8.35	12.38	5.07	7.31	
Black asphalt concrete	8.65	12.59	5.45	7.14	0.76
Blue asphalt concrete	8.77	12.91	5.45	7.26	1.05
Red asphalt concrete	8.74	12.80	5.49	7.31	0.95

Table 7.3. Daily (8:00–20:00) and nocturnal (22:00–6:00) mean, maximum, minimum surface temperatures temperature fluctuations and differences during May, 2014.

Sample	May daily				
	Avg. T_{mean}	Avg. T_{max}	Avg. T_{min}	Avg. ΔT_0	Avg. σ_{min}
Conventional asphalt concrete	29.38	43.68	12.38	31.30	
Black asphalt concrete	27.80	41.65	12.64	29.01	-3.25
Blue asphalt concrete	27.01	41.65	12.58	29.06	-4.20
Red asphalt concrete	27.93	42.86	12.67	30.19	-2.73
	May nocturnal				
	Avg. T_{mean}	Avg. T_{max}	Avg. T_{min}	Avg. ΔT_0	Avg. σ_{max}
Conventional asphalt concrete	12.66	17.13	9.76	7.37	
Black asphalt concrete	13.11	17.17	10.18	6.99	1.30
Blue asphalt concrete	13.27	17.49	10.37	7.11	1.21
Red asphalt concrete	13.08	17.19	10.26	6.93	0.98

Table 7.4. Daily (8:00–20:00) and nocturnal (22:00–6:00) mean, maximum, minimum surface temperatures, temperature fluctuations and differences during June, 2014.

Sample	June daily				
	Avg. T_{mean}	Avg. T_{max}	Avg. T_{min}	Avg. ΔT_0	Avg. σ_{min}
Conventional asphalt concrete	32.25	45.16	17.20	27.96	
Black asphalt concrete	31.91	44.60	16.61	27.90	-2.61
Blue asphalt concrete	30.14	42.85	17.35	25.50	-3.82
Red asphalt concrete	30.77	44.09	17.40	26.69	-2.51
	June nocturnal				
	Avg. T_{mean}	Avg. T_{max}	Avg. T_{min}	Avg. ΔT_0	Avg. σ_{max}
Conventional asphalt concrete	16.75	21.43	14.44	7.00	
Black asphalt concrete	17.38	22.23	14.98	6.59	0.58
Blue asphalt concrete	17.17	21.66	14.84	6.81	0.85
Red asphalt concrete	16.97	21.33	14.72	6.61	0.57

7.4 Influence of Thermochromic Materials on the Surface Temperatures

The Modulation of Surface Temperatures

Comparing Tables 7.2–7.4 with Table 7.1, the daily average temperature of the asphalt concrete samples is higher than the daily average air temperature during daytime, and the average nocturnal temperature of asphalt concrete is lower than that of the nocturnal air temperature. Specifically, during the three month period studied, during the daytime, the average surface temperature of conventional asphalt concrete is 6.7–11.6°C warmer than air temperature, while thermochromic asphalt concrete is 6.1–10.4°C warmer. During the evening, conventional asphalt concrete is 3.8–5.1°C colder than air temperature, and thermochromic asphalt concrete is 3.4–4.7°C colder. The temperature difference between asphalt concrete and ambient air might be attributed to the large solar absorption of asphalt binder at daytime and its large emissivity in the evening.

Interestingly, from Tables 7.2-7.4, the average surface temperature of thermochromic asphalt concrete is lower than that of the conventional asphalt concrete during daytime; while it is higher during evening. For example, during the 2nd month of the experimental period (i.e. May), the average daily surface temperature on black, blue and red asphalt concrete is 3.25, 4.20, 2.73°C lower than traditional asphalt concrete, respectively. This shows that the thermochromic asphalt concrete helps to reduce the surface temperature of pavement during high temperature. On the other hand, during the evening when the air temperature is low, the surface temperature of black, blue and red asphalt concrete is 1.30, 1.21, 0.98°C higher than traditional asphalt concrete, respectively. This indicates that the thermochromic asphalt concrete increases the surface temperature of pavement under low temperature environment. Similar observations can be found during the other study period (i.e., April and June). Among these thermochromic asphalt concrete samples, it is observed higher temperature differences (σ) occur with blue asphalt concrete, exhibiting superior thermal performance. It also needs to be noted that the data shown in Table 7.2-7.4 are the average value of a whole month. The effects of temperature modulation by thermochromic materials are more significant for an individual day/time.

All the above-mentioned cooling and warm effects for thermochromic asphalt concrete can be explained by the higher solar reflectance at high temperature and temperature-dependent thermal properties of thermochromic materials, which have been shown in our previous study (18-19).

Both the capabilities to reduce the surface temperature of pavement under high temperature conditions and to increase the surface temperature of pavement under low temperature conditions are desirable for application purposes. The reduced surface temperature of asphalt pavement might help to reduce the thermal stresses and to mitigate the deterioration. Furthermore, the thermochromic asphalt concrete possess higher temperature than conventional asphalt concrete might help to mitigate the low temperature cracking and to reduce ice formation on the road surfaces under cold weathers.

Additionally, it is also found that the mean maximum temperature reductions (min. σ) and mean surface temperatures of thermochromic asphalt concrete are correlated, shown in Fig. 7.4. The general observation is the higher the mean surface temperature, the larger the effects of surface temperature reduction.

(a)   (b)
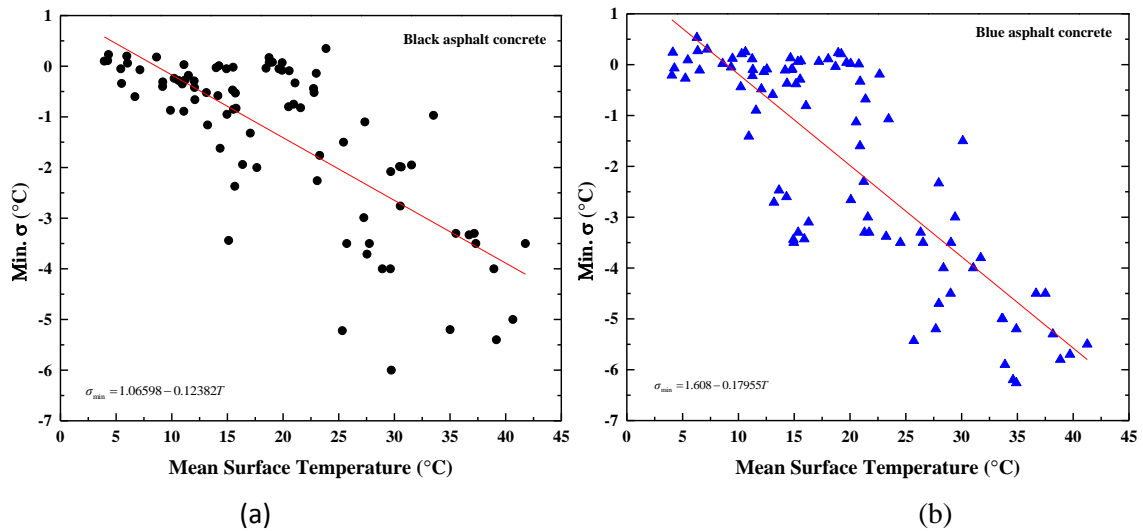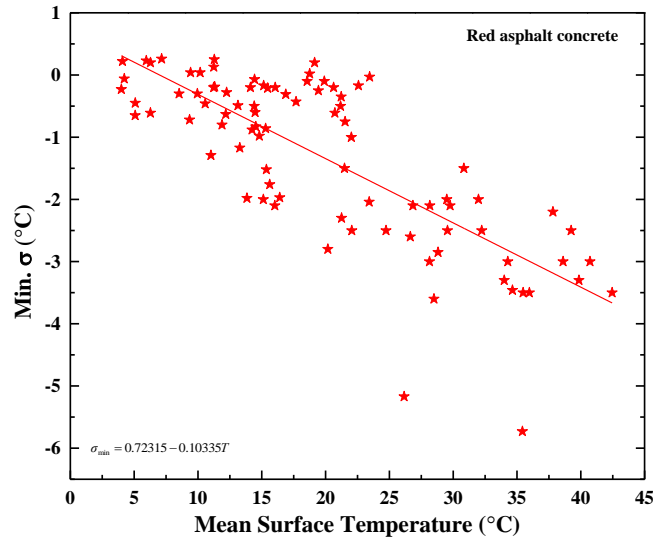
(c)

Fig. 7.4. Temperature reduction versus mean surface temperatures of (a) black, (b) blue and (c) red thermochromic asphalt concrete.

Temperature Fluctuation (ΔT₀) and Temperature Difference (σ)

The temperature fluctuations of asphalt pavement can have drastic impact on the durability and functional lifetime due to thermal expansion and contraction. Fig. 7.5 presents the daily and nocturnal temperature fluctuations (ΔT_0) of various asphalt concrete samples from April to June. It can be observed that the daily temperature fluctuation can decreased up to 5°C, 4°C and 3°C by using black, blue and red asphalt concrete, respectively while the corresponding nocturnal temperature fluctuation is decreased by 1.5°C, 1.1°C and 1.6°C. Such reduction of surface temperature fluctuation of asphalt concrete with thermochromic materials will help to mitigate distresses due to thermal loading including increasing the fatigue resistance of the pavement.

Besides, the factor of weathering is important regarding the thermal performance of the pavement (i.e.-atmospheric pollution and biological growth, and other alterations like UV radiation, sudden temperature swings and precipitation). From Fig. 7.5 it can be seen that for the approximate 2 months of exposures, there is no clear degradation for the reduction function of temperature fluctuations by using thermochromic materials. This might imply that the effect of weathering is insignificant during the period of this study.
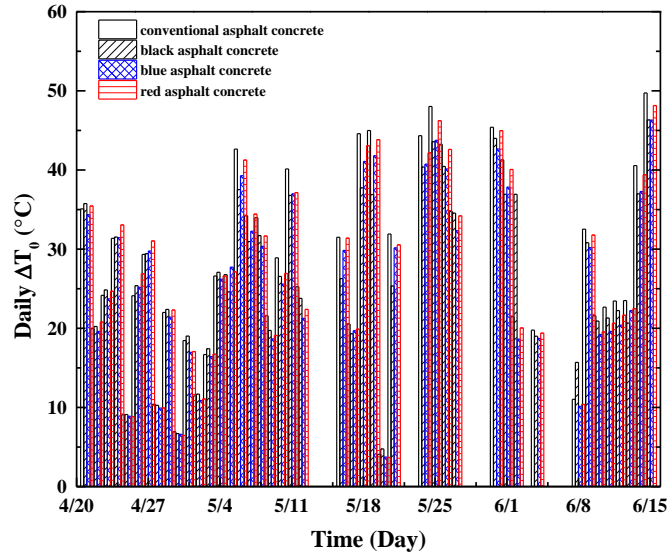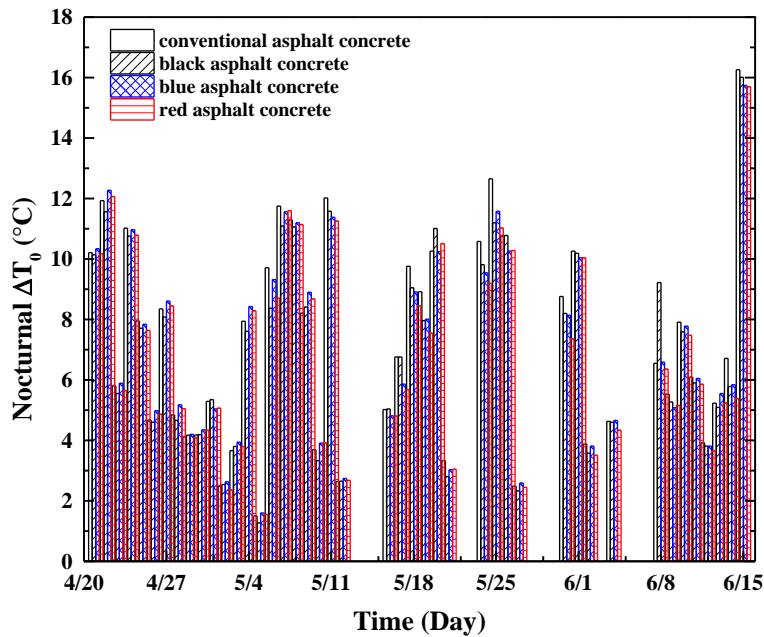
Fig. 7.5. The comparison between daily (a) and nocturnal (b) temperature fluctuations (ΔT_0) of conventional and thermochromic asphalt concrete during the experimental period.

Fig. 7.6 shows the daily temperature reduction during the day and temperature increase at nighttime during the experimental period. It shows that during the day period, the surface temperature of asphalt concrete can be reduced up to 6°C, 6.2°C and 3.6°C by using black, blue and red thermochromic materials, respectively. While during the night period, the corresponding increase of surface temperature of asphalt concrete increased to about 0.4°C, 1.7°C and 1.8°C. In

addition, it seems that the temperature reduction by thermochromic asphalt concrete increases with time during this experimental period. Therefore, the cooling effects of thermochromic asphalt concrete can be significant during hot summer period.
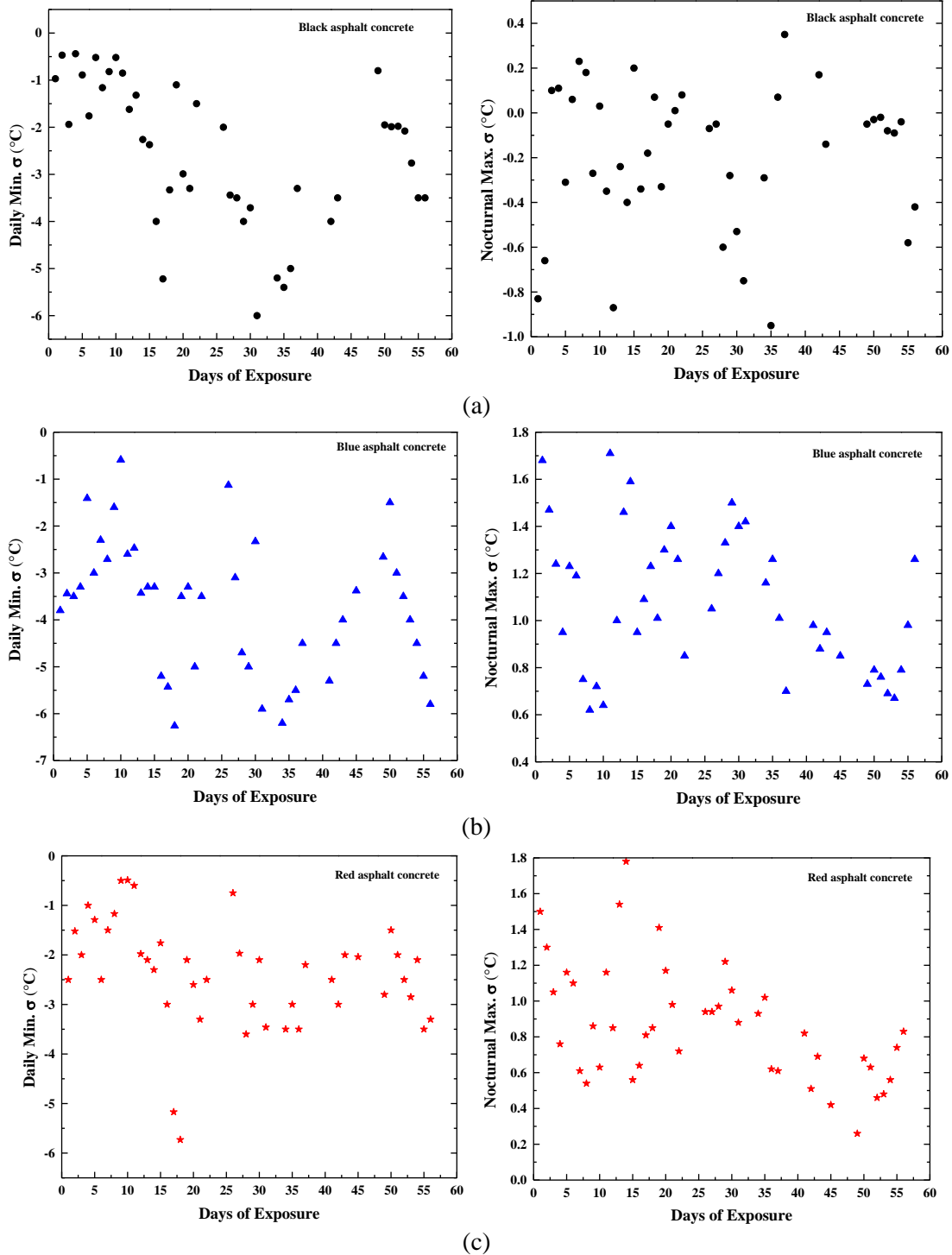
Fig. 7.6. Reduction of surface temperature in the day and increase of surface temperature in the evening by using (a) black, (b) blue and (c) red asphalt concrete.

7.5 Influence of Thermochromic Materials on Rate of Temperature Change of the Samples

Fig. 7.7(a) shows the evolution of surface temperature of various asphalt concretes with time on a typical summer day in May. In general the conventional asphalt concrete has the highest temperature during the daytime. The temperature reduction (ΔT) on this day is up to -5.2°C, -6.2 °C, and -3.5°C for black, blue and red asphalt concrete, respectively compared with regular asphalt concrete. Figs. 7.7b and 7.7c show sections where the surface temperature increase (10:00–13:45LT) and decrease (15:50–0:00LT) with time representing the heating and cooling process, respectively. From Fig. 7.7(b) it can be observed that compared to conventional asphalt concrete, thermochromic asphalt concrete reduces the rate of temperature rise and is maintained at a lower temperature than traditional asphalt concrete. Specifically, the rate of temperature increase is 0.176, 0.140, 0.157 and 0.168 °C/min for conventional, black, blue and red asphalt concrete, respectively. While the corresponding cooling rate in the Fig. 7.7(c) is 0.077, 0.068, 0.070, 0.074°C/min, respectively. The slower rate of temperature change in asphalt concrete by use of thermochromic materials is beneficial as it helps improve performance of the pavement by giving it more time for plastic creep and therefore reduces the stress levels.
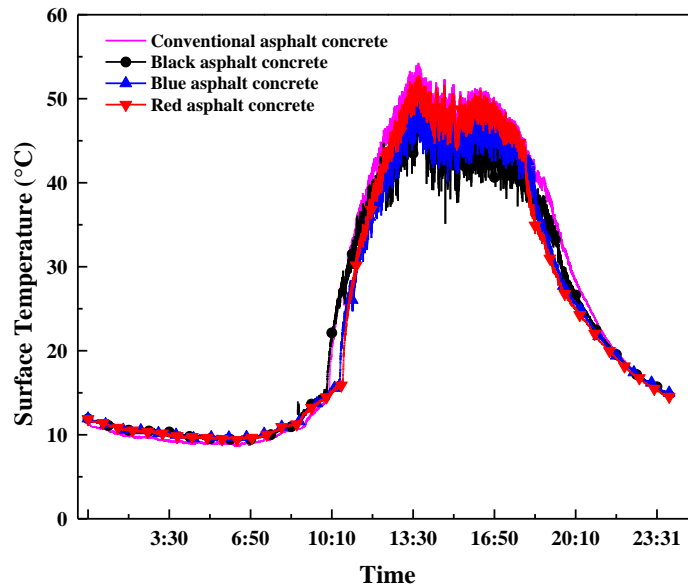
(a)
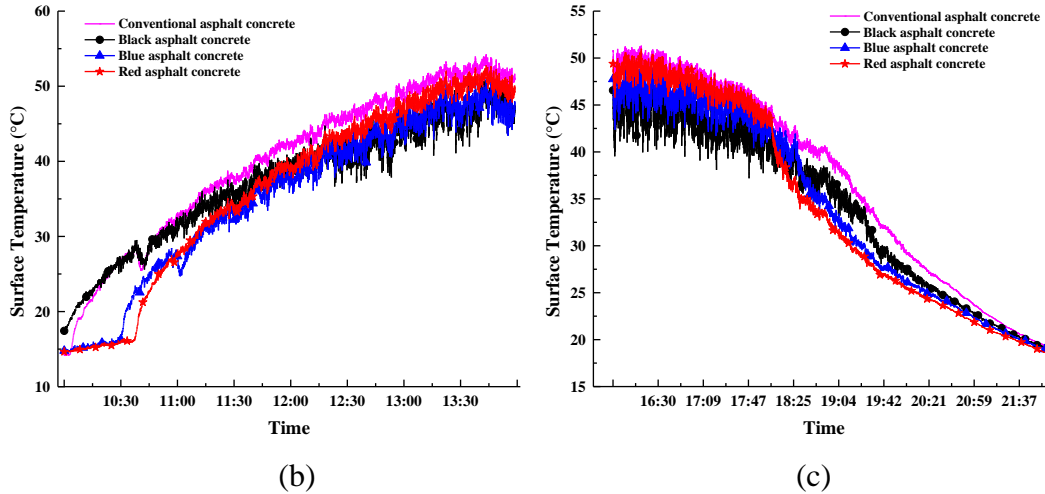
Fig. 7.7. Surface temperature of various asphalt concretes on a typically summer day (a) and its heating (b) and cooling process (c).

7.6 Conclusions

This study evaluated the performance of thermochromic asphalt concretes in modulating the surface temperature of pavement. The outdoor experiments ran from April to June. The following observations are made from the experimental results. 1) The thermochromic asphalt concrete reduced the surface temperature compared with regular asphalt concrete. For example, the average surface temperature of black, blue, and read thermochromic asphalt is 3.25, 4.20, 2.73°C lower than traditional asphalt concrete respectively during daytime in May. 2) With the thermochromic asphalt, the magnitude of temperature variations was reduced. For example, the daily temperature fluctuation during daytime could be decreased up to 5°C, 4°C and 3°C by using black, blue and red asphalt concrete, respectively while the corresponding nocturnal temperature fluctuation was decreased by 1.5°C, 1.1°C and 1.6°C. 3) The amount of surface temperature reduction by thermochromic asphalt concrete increased with the environmental temperature. During the experimental period, the surface temperature of asphalt concrete was reduced up to 6°C, 6.2°C and 3.6°C with the use of black, blue and red thermochromic materials, respectively, while the corresponding evening temperature increased by 0.4°C, 1.7°C and 1.8°C, respectively. 4) The use of thermochromic materials reduced the rate of temperature change of asphalt concrete. The heating rate could be reduced up to 0.036°C/min (2.16°C/h) while the cooling rate was decreased by 0.009°C/min (0.54°C/h).

151

In summary, this study found that the thermochromic asphalt concrete reduces the surface temperatures under high environmental temperature and increase the surface temperature under low environmental temperature. Therefore, the use of thermochromic asphalt concrete helps reduce high temperature related performance degradation (such as rutting, fatigue, etc) as well as mitigate low temperature effects (such as low temperature cracking, ice formation, etc.). These potentially will help improve the durability and safety of asphalt pavement.

7.7 References

(1)   Tripathi, R., Pickett, K.W., Solaimanian M., Kennedy, T.W. Toner-modified asphalt compositions. US pat. 6113681, 2000.

(2)   Santamouris, M., Pavlou, K., Synnefa, A., Niachou, K., Kolokotsa, D. Recent progress on passive cooling techniques: Advanced technological developments to improve survivability levels in low-income households. Energy and Buildings, 2007, 39(7): 859–866.

(3)   Synnefa, A., Dandou, A., Santamouris, M., Tombrou, M., Soulakellis, N. Large scale albedo changes using cool materials to mitigate heat island in Athens. Journal of Applied Meteorology and Climatology, 2008, 47(11): 2846–2856.

(4)   Doulos, L., Santamouris, M., Livada, I. Passive cooling of outdoor urban spaces. The role of materials. Solar Energy, 2004, 77(2): 231–249.

(5)   Yoder, E. J. and Witzak, M. W. Principles of Pavement Design. New York, NY: Wiley and Sons, 1975.

(6)   Pomerantz, M. and Akbari. H. Cooler Paving Materials for Heat Island Mitigation. In 1998 ACEEE Summer Study on Energy Efficiency in Buildings, Asilomar, CA, City: American Council for an Energy-Efficient Economy, 1998.

(7)   Pomerantz, M., Akbari, H. Cooler paving materials for heat island mitigation, in: Proceedings of the 1998 ACEEE Summer Study on Energy Efficiency in Buildings, vol. 9, Pacific Grove, CA, 1998, 135.

(8)   Pomerantz, M., Akbari, H., Chen, A., Taha, H., Rosenfeld, A. Paving Materials for Heat Island Mitigation, Lawrence Berkeley National Laboratory Report LBL- 38074, Berkeley, CA, 1997.

(9)   Pomerantz, M., Akbari, H., Harvey, J. T. Cooler reflective pavements give benefits beyond energy savings: Durability and illumination. Rep. No. LBNL-45370, Berkeley, CA, 2000, 14 pp.

(10) Kinouchi, T., Yoshinaka, T., Fukae, N., Kanda, M. Development of cool pavement with dark colored high albedo coating. Fifth Conference for the Urban Environment, Vancouver, Canada, 2004.

(11) Hao, P.W., Zhang, D.L., Hu, X.N. Evaluation method for low temperature anticracking performance of asphalt mixture. Journal of Xi'an Highway University, 2000, 20 (3):1–5.

(12) Kanerva, H.K., VINSON, T.S., Zeng, H. Low Temperature Cracking Field Validation of the Thermal Stress Rest Rained Specimen Test. R. SHRP-A-401, 1994.

(13) Jianying Hu, Quan Gao, Xiong Yu. Optical and Superpave Characterization of Innovative Asphalt Binder Containing Thermochromic Materials. Journal of materials in civil engineering, 2014.

(14) Jianying Hu, Nandula Wanasekara, Xiong (Bill) Yu. Thermal Properties of Thermochromic Asphalt Binders by Modulated Differential Scanning Calorimetry. Journal of Transportation Research Record, 2014.

(15) Santamouris, M., Synnefa, A., Kolokotsa, D., Dimitriou, V., Apostolakis, K. Passive cooling of the built environment - use of innovative reflective materials to fight heat island and decrease cooling needs. International Journal Low Carbon Technologies, 2008, 3(2): 71–82.

(16) Karlessi, T., Santamouris, M., Apostolakis, K., Synnefa, A., Livada, I. Development and testing of thermochromic coatings for buildings and urban structures. Solar Energy, 2009, 83(4): 538–551.

(17) Granqvist, C.G. Materials Science for Solar Energy Conversion Systems. Pergamon press, Oxford, 1991.

(18) Saeli, M., Piccirillo, C., Parkin, I. P., Binions, R., Ridley, I. Energy modelling studies of thermochromic glazing. Energy and Buildings, 2010, 42(10): 1666–1673.

(19) Ma, Y. P. and Zhu, B.R. Research on the preparation of reversibly thermochromic cement based materials at normal temperature. Cement and Concrete Research, 2009, 39(2): 90-94.

CHAPTER EIGHT

VOLUMETRICS DESIGN OF THERMOCHROMIC HMA AND PERFORMANCE EVALUATION

Both extremely high and low temperature of asphalt pavement impact its long-term durability through high-temperature deformation, accelerated aging, and low-temperature cracking. The innovative strategy proposed in this study is to dynamically control the temperature of asphalt pavement by incorporating thermochromic materials, which can reversibly alter their colors and optical properties in response to change of environmental temperature. This innovative asphalt is designed to module the surface temperature of asphalt pavement, i.e., to reduce the surface temperature of pavement during hot summer days and to increase the surface temperature during cold winter days. The semiconductor of TiO_2 features high absorption of UV light and photocatalytic function. The influence of thermochromic materials and nano-TiO_2 on engineering performance of asphalt mixture was experimentally evaluated by indirect tensile (IDT) strength, accelerated pavement analyzer (APA), and UV-VIS-IR spectrophotometer. It has found that the use of 6% thermochromic materials by weight of asphalt binder considerably increases solar reflectance of asphalt mixture from 6.9% to 10.3%, whereas the combination of 1% thermochromic materials and 3% nano-TiO_2 increases the value from 6.9% to 8.4%. Additionally, the use of nano-TiO_2 powder in asphalt mixture has been demonstrated to improve both resistance to moisture damage and high temperature deformation. Therefore, the incorporation of thermochromic materials and nano-TiO_2 into asphalt pavement will potentially improve its performance and durability, especially in hot regions.

8.1 Introduction

Conventional asphalt binder, which consists of residuals from crude oil distillation processes, has been used widely in highway pavement and city roads. However, the considerable high absorption of black asphalt binder to solar radiation induces extremely high surface temperature of asphalt pavement, which is typically as high as 48–67 °C during summer reported in studies (Santamouris et al. 2007, Synnefa et al. 2008, Doulous et al. 2004). The increased temperature in summer impairs durability of asphalt pavement by accelerating various distress mechanisms (i.e., rutting, shoving, aging, fatigue damage, bleeding) (Yoder and Witzak 1975) as well as causes undesirable environmental issues (i.e., heat island effects, volatile gas emission, etc.) (Gui et al. 2007). A potential way to improve the durability is to use materials with high reflectivity and emissivity to solar radiation. This has led to the development of various cool pavement technologies. Studies (Pomerantz and Akbari 1998, Pomerantz et al. 1997, Pomerantz et al. 2000, Kinouchi et al. 2004) show that cool pavement features low surface temperatures, which increases the service life (durability) of pavements. However, the reduced temperature of asphalt pavement exacerbates the distress of low-temperature cracking during the winter period (Hao et al. 2000, Kanerva et al. 1994), which compromises the service life of road in cold climate. Besides, the lower surface temperature is inductive to ice formation in cold weather, which is a major safety concern. So it is highly desirable to develop new pavement materials and technology to make asphalt pavement cooler during summer and warmer during winter.

An innovative strategy our study pursued is to use thermochromic materials to create new asphalt binders with desirable solar reflectance, i.e., they reflect more solar energy at high temperature and reflect less solar energy at low temperature. To avoid any visual impact on road users, we hope to restraint such effects in the infrared range only. Thermochromic materials, materials

changing their colors with temperature, are promising to achieve such functionality as they possess required optical and thermal properties. Materials incorporated with proper thermochromic materials feature high solar reflectance in summer and high solar absorption in winter. The change of their optical and thermal properties in such a dynamic way can lead to applications that improve the urban microclimate, decrease the energy demands of the buildings, and provide a thermally comfortable indoor environment (Santamouris et al. 2008, Karlessi et al. 2009, Granqvist 1991, Saeli et al. 2010, Ma and Zhu 2009, Kinouchi and Santamouris 2013). In the present study, innovative asphalt binder containing thermochromic materials is designed to modulate the temperature of asphalt pavement. The preliminary study indicated that the use of thermochromic binder could reduce the surface temperature of asphalt concrete up to 6.6°C during a typical summer day in Cleveland, Ohio, USA (Hu and Yu 2013 (a)).

Titanium dioxide (TiO_2) is another attracting material recently which is carried out to develop photocatalytic and self-cleaning asphalt road (Hashimoto et al. 2005, Carneiro et al. 2013, Liu et al. 2015, Chen and Liu 2010). The semiconductor material of TiO_2 is reported to feature powerful oxidation strength, chemical stability, non-toxic properties and availability (Chen et al. 1999, Gouttebaron et al. 2000). Nanosized TiO_2 has been employed by many research groups to improve the light absorption and thus photocatalytic activity through the high surface-to-volume ratio of nanograins (Shannon 1976). It was found that the spraying technique of nano-TiO_2 over the surface of asphalt mixture presents superior photocatalytic capability than volumetric incorporation 25(Gouttebaron et al. 2000). Besides photocatalytic effect, the incorporation of nanoTiO_2 into asphalt mixture was demonstrated to improve the rheological properties of original bitumen, to enhance rutting resistance and fatigue lift of asphalt mixtures (Shafabakhsh

157

and Jafari Ani 2015, Shafabakhsh et al. 2014).

The aim of this study is to fabricate asphalt mixture containing both thermochromic materials and nano-TiO$_2$ and to evaluate the influence of these additives on engineering performance of asphalt concrete mixtures. For this purpose, Superpave volumetric analysis was employed to optimize mixing parameters of the hot-mixing asphalt (HMA) mixtures. Indirect tensile strength, accelerated asphalt pavement analyzer (APA) tests, and optical characterization were performed on HMA mixtures containing different content of thermochromic materials and nano-TiO$_2$.

8.2 Experimental Design

8.2.1 Materials and Mixture Design
Materials

Asphalt binder used in this study is Superpave grade, PG 64-22, produced by Kokosing Materials Inc. The properties of virgin asphalt binder used in this study is illustrated in Table 8.1. The viscosity values at different temperature determine the mixing temperature range of asphalt mixture (153-159 ℃) and compaction temperature range of asphalt mixture (142-146 ℃).

Thermochromic powders with an average particle of 3-10 μm were selected from those manufactured by Hali Industrial Corporation Ltd. Red, blue, and black thermochromic powders with transition temperature around 31°C were chosen for this study. These thermochromic materials are organic mixtures, which consists of lueco dye (electron donor), developer (electron acceptor) and solvent. Below the transition temperature, leuco dye reacts with the developer, the absorption peaks shifts from the UV to the visible range and cause the powder becomes colored. At temperature above the transition temperature, the solvent-developer interactions dominate,

and leuco dye is separated from the developer and leads to loss of color. Thermochromic materials are encapsulated by trioctanoinand and therefore at high temperature thermochromic powders become white or light-colored state. The molecular structures of thermochromic materials and their changes with temperature are shown in Fig. 8.1. Additionally, commercial TiO_2 nanoparticles with density of 4260 kg/m^3 (Titanium (IV) oxide from Sigma-Alorich) were incorporated with thermochromic powder into asphalt binder.

Table 8.6. Characteristics of original asphalt binder.

Performance Grade	PG 64-22
Viscosity (mPa·s) at 135 ℃	425
Viscosity (mPa·s) at 165 ℃	120
Specific Gravity	1.030
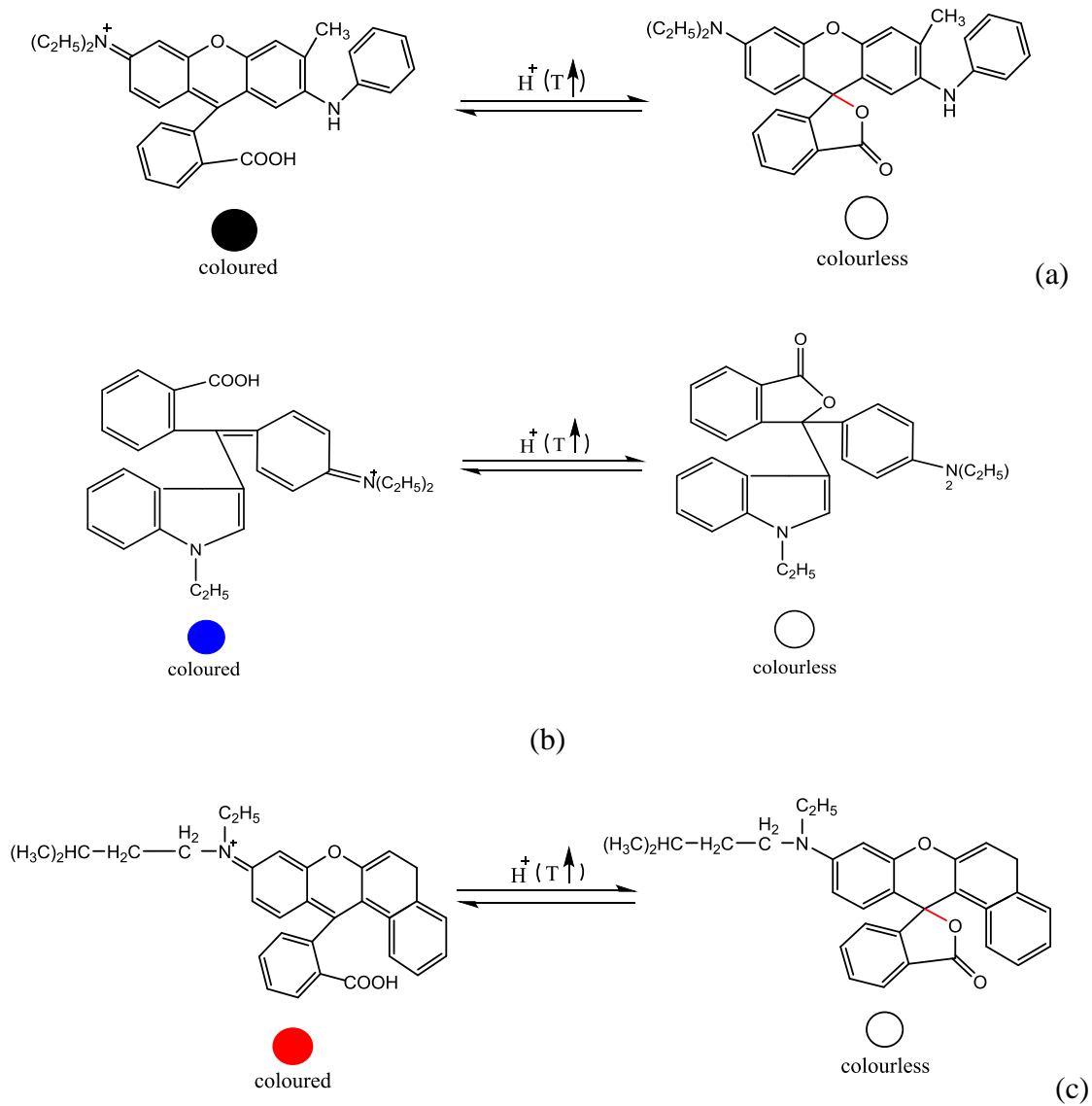
Figure 8.11. Molecular structures of thermochromic powders and their changes with temperature: a) black powder; b) blue powder; c) red powder.

Reclaimed asphalt pavement (RAP) was employed in this study. The characteristics of RAP are summarized in Table 8.2. The average value of asphalt binder content is found to be 5.5% in RAP. The gradation of extracted RAP aggregate is shown in Table 3. The sodium soundness of

RAP aggregated measured according to AASHTO T 104 (AASHTO T104) is 2.60, which satisfies the specifications from ODOT and ASTM.

Combining RAP aggregate with limestone, sand, and Baghous fines, the blended aggregate was designed to meet ODOT specification on aggregation gradation. The gradation and percentage of each aggregate is reported in Table 8.3. The nominal maximum aggregated size was 12.5 mm and effective specific gravity of aggregate (G_{se}) was calculated to be 2.635.

Table 8.7. Characteristics of RAP.

RAP Maximum Specific Gravity	2.438
RAP Binder Specific Gravity	1.050
RAP Binder Viscosity (Pa·s)	5920
RAP Aggregate Soundness Loss	2.60
Binder Content in RAP (%)	5.5

Table 8.8. Aggregate Gradation.

Sieve Size (mm)	Sieve Size	Content and Passing (%)						
		42% #8 Limestone	10% #9 Limestone	18% Limestone Sand	14% Natural Sand	1% Baghouse Fines	15% RAP	Accum ulated
50.8	2 in	100.0	100.0	100.0	100.0	100.0	100.0	100
38.1	1 1/2 in	100.0	100.0	100.0	100.0	100.0	100.0	100
25.4	1 in	100.0	100.0	100.0	100.0	100.0	100.0	100
19	3/4 in	100.0	100.0	100.0	100.0	100.0	100.0	100
12.5	1/2 in	100.0	100.0	100.0	100.0	100.0	100.0	100
9.5	3/8 in	90.0	100.0	100.0	100.0	100.0	90.0	94.3

4.75	#4	23.0	91.0	99.0	99.0	100.0	65.0	61.2
2.36	#8	2.0	15.0	81.0	79.0	100.0	48.0	36.2
1.18	#16	1.0	3.0	48.0	59.0	100.0	35.8	24.0
0.6	#30	1.0	2.0	26.0	40.0	98.0	25.0	15.6
0.3	#50	1.0	2.0	14.0	22.0	93.0	15.3	9.4
0.15	#100	1.0	1.0	8.0	9.0	83.0	10.5	5.6
0.07	#200	1.0	1.0	5.8	2.7	70.0	6.8	3.7

8.3 Mixture Design and Superpave Volumetric Analysis

Hot-mixing asphalt (HMA) mixture were designed and mixed for surface layer following the AASHTO standards (AASHTO R 35, AASHTO M 323). Before preparing powder-modified HMA, the control HMA without powders were designed, prepared and evaluated according to Superpave volumetric design method with an Equivalent Standard Axle Load (ESAL) range of 0.3–3 million ESALs. Four trial HMA samples with varied binder contents from 5% to 6.5% were designed. According to the viscosity of virgin asphalt binder, the mixing and compaction temperatures are set as 154 °C and 143 °C, respectively. Considering the specification on gyration number from AASHTO M 323, shown in Table 8.5, the gyration numbers of $N_{initial}$, N_{design}, and $N_{maximum}$ are 7, 65, and 105, respectively. The trial mixes were prepared using the Superpave gyratory compactor. The experimental evaluation and calculated results of four trail HMA are displayed in Table 4 and Fig. 2. It can be observed that the optimum binder content is 5.8% to produce a targeted 4% air voids (VA) in HMA. Compared to the criteria in Table 8.5, all other factors, void in mineral aggregate (VMA), void filled with asphalt (VFA), unit weight, dust/binder ratio, and percentages of maximum theoretical specific gravity, satisfy the

specifications at the corresponding binder content. The refined design and mixing parameters of

the control HMA are listed in Table 8.6.

Table 8.9. Control HMA mix-design characteristics.

Control HMA	Binder content (wt. %)	G_{mb}	G_{mm}	VA (%)	VMA (%)	VFA (%)	Unit Weight (kg/m^3)	Dust/binder Ratio	% Gmm at $N_{initial}$	% Gmm at N_{design}
1	5.0	2.343	2.503	6.4	15.5	58.8	2342	0.75	84.6	93.6
2	5.5	2.363	2.485	4.9	15.3	67.8	2361	0.68	86.0	95.1
3	6.0	2.383	2.466	3.4	15.0	77.4	2381	0.61	87.3	96.6
4	6.5	2.403	2.488	1.8	14.7	87.5	2402	0.58	88.9	98.2

Table 8.10. Superpave mix design criteria (AASHTO M 323) (AASHTO T166).

20-yr Traffic Loading (in millions of ESALs)	$N_{initial}$	N_{design}	$N_{maximum}$	VFA (%)	VMA (%)	% Gmm at N_{ini}	% Gmm at N_{des}	% Gmm at N_{max}
0.3-3	7	75	115	65-78	≥ 14.0	≤ 90.5	96.0	≤ 98.0
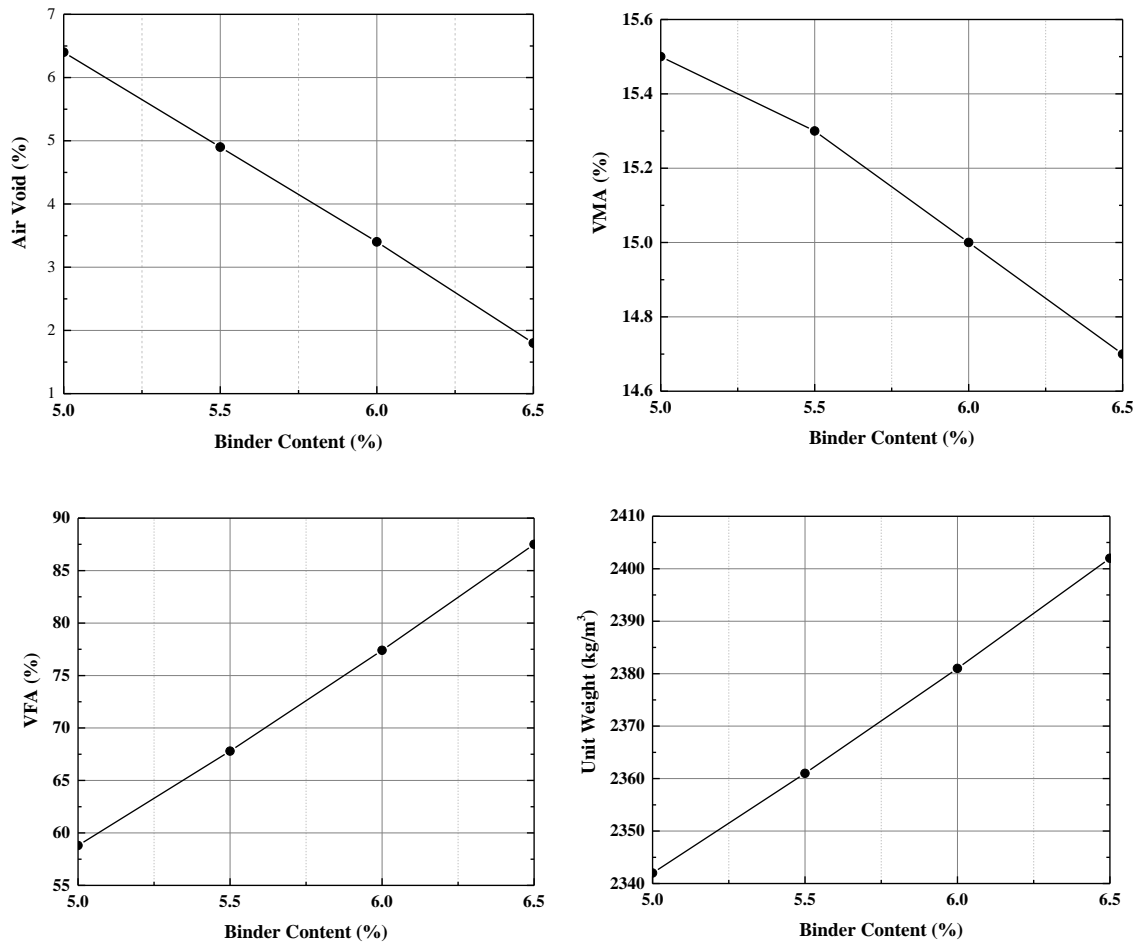
Figure 8.12. Characteristics of trial asphalt mixtures.

Table 8.11. Optimized parameters for preparing control HMA.

Optimum binder content (%)	5.8%
Mixing temperature (°C)	154
Compaction temperature (°C)	143
Initial Gyration Number (N_{ini})	7
Designed Gyration Number (N_{des})	65
Maximum Gyration Number (N_{max})	105

164

Six HMA samples containing black, blue and red thermochromic powder and nano-TiO_2 powder at different percentage levels by weight of virgin asphalt binder were designed in this study. As shown in Table 8.6, the thermochromic powder was employed by adding 6% of asphalt binder, or combing 1% black, blue and red powder with 3% nano-TiO_2 powder of asphalt binder. According to optimized parameters in Table 6, six types of HMA mixtures were prepared, as shown in Fig. 8.3.

Table 8.12. Different combinations percentages of additives.

HMA Sample	Thermochromic Powder	Nano-TiO_2 Powder
6% Black HMA	6% Black	0
6% Blue HMA	6% Blue	0
6% Red HMA	6% Red	0
1%/3% Black/TiO_2 HMA	1% Black	3%
1%/3% Blue/TiO_2 HMA	1% Blue	3%
1%/3% Red/TiO_2 HMA	1% Red	3%

Figure 8.13. Photos of modified HMA samples.

8.4 Performance Evaluation Methods

8.4.1 Specific Gravity and Air Void

Superpave volumetric analysis of compacted HMA mixtures involves two basic tests: bulk specific gravity of the compacted HMA mixture and theoretical maximum specific gravity of the loose HMA mixture. The bulk specific gravity was determined on two cylindrical specimens with diameter of 150 mm and thickness of 115 mm following the procedure in AASHTO T 166 (AASHTO T 166) and was calculated using the following the formula:

$$G_{mb} = \frac{A}{B - C} \tag{8-1}$$

where G_{mb} is the bulk specific gravity of compacted specimen; A the mass of dry specimen in air (g); B mass of saturated surface-dry specimen in air (g); and C the mass of specimen in water (g).

The theoretical maximum specific gravity was determined according to AASHTO T 209 (AASHTO T 2091). The following formula was used to for calculating theoretical maximum specific gravity of the specimen:

$$G_{mm} = \frac{A}{A + D - E} \tag{8-2}$$

where G_{mm} is the theoretical maximum specific gravity of loose specimen; A the mass of oven-dry specimen in air (g); D the mass of container filled with water at 25 °C to calibration mark (g); and E the mass of container with specimen filled with water at 25 °C to calibration mark (g).

Bulk specific gravity features the specific gravity of the compacted specimen, including air voids within the mixture; the theoretical maximum specific gravity gives the specific gravity of the loose compacted with air voids of zero. Both contribute to determining volumetric factor, air void content, which is a good indicator of mixture performance. Air void content (VA, %) was calculated using the following expression:

$$VA = 100 \left[1 - \left(\frac{G_{mb}}{G_{mm}} \right) \right]$$

(8-3)

8.4.2 Moisture Susceptibility

Six cylindrical samples (150 mm diameter by 57.5 mm thickness) were used in finding moisture resistance potential in prepared mixture according to AASHTO T 283 (AASHTO T283). The samples were divided into two groups: the first group is "unconditioned", while the second group is "conditioned". The conditioned samples were saturated with water to between 70-80 percent with water, followed by a freeze-thaw cycle and a warm water soak. The tensile strength of "conditioned" sample St(Conditioned) is compared to the tensile strength of "unconditioned" sample St(Control) to determine tensile strength ratio (TSR) as follows:

$$TSR = 100 \frac{St_{conditioned}}{St_{unconditioned}}$$

(8-4)

The ratio of the average tensile strength of the conditioned to unconditioned samples and a visual assessment of stripping is used to assess moisture sensitivity of HMA. A mixture is considered acceptable if the tensile strength ratio is equal to or greater than 80% and there is no visual evidence of stripping in the conditioned test specimens.

8.4.3 Rutting Resistance

The asphalt pavement analyzer (APA) was employed to evaluate the rutting resistance of HMA mixtures according to AASHTO TP 63 (AASHTO TP 63). In the APA test, a hose pressure of 100 lb/in^2 was placed over the short cylindrical HMA specimen (diameter 150mm, thickness 75 mm) and a wheel load of 100 lb was repeatedly passed over the hose. Schematic view of the manner of implementing APA test is shown In Fig. 8.4. The APA test was carried out at 59 °C for the control HMA mixture and 54 °C for powder-modified HMA mixture. The total deformation was recorded at 5, 500, 1000, and 80000 cycles for each specimen. Rut depth calculated as the average of two tests of two specimens (four specimens total).

Figure 8.14. Schematic view of the APA test.

8.4.4 Optical Characterization

The spectral reflectance of different HMA mixtures was measured over the wavelength range of 350–1800 nm by the Agilent Cary 6000i UV-Vis-IR Spectrophotometer according to ASTM E903 (ASTM 903). The measurements were performed on surface of original cylindrical specimens, rutted surface of cylindrical specimens after APA analysis, and exposed aggregate

surface of cylindrical specimens, which represents the condition of asphalt pavement after long-term abrasion. The photos of rutted surface and exposed aggregate surface of HMA mixtures are shown in Fig. 8.5. Reflectance measurements were conducted on two specimens for each sample at room temperature.

Figure 8.15. Photos of rutted surface (left) and exposed aggregate surface (right) of HMA mixtures.

The total solar reflectance of each sample were calculated from the averaged spectral reflectance data using weighted-averaging method, referred in ASTM E903. Weighted ordinates obtain the solar reflectance R by integrating the spectral reflectance over the standard spectral irradiance distribution, E_λ, as follows:

$$R(\%) = \frac{(\sum_{i=1}^{n} R(\lambda_i) E_{\lambda i}) \Delta \lambda_i}{\sum_{i=1}^{n} E_{\lambda i} \Delta \lambda_i} \tag{8-5}$$

where the standard spectral irradiance distribution, E_λ, and $\Delta \lambda$ as the weighting function are provided by ASTM E490 (ASTM E490).

8.5 Results and Discussion

8.5.1 Specific Gravity and Air Voids

The bulk and theoretical maximum specific gravity as well as air voids of all HMA mixtures were summarized in Table 8.8. It can be seen that the bulk specific gravity is between 2.363 and 2.373 and the theoretical maximum specific gravity is between 2.484-2.491, the air voids are 4.7% to 4.8% for asphalt mixture containing 6% thermochromic powder. With the addition of TiO_2 nanoparticles, they are in the range of 2.363-2.372, 2.483-2.490, and 4.5-5.1%. It can be observed that the combination of nano-TiO_2 with blue and red powder typically decreases void content of asphalt mixture.

Table 8.13. Specific gravity and air void results of HMA mixtures.

Sample	G_{mb}	G_{mm}	Voids (%)
6% Black HMA	2.373	2.491	4.7
6% Blue HMA	2.363	2.484	4.8
6% Red HMA	2.371	2.491	4.8
1%/3% Black/TiO_2 HMA	2.363	2.490	5.1
1%/3% Blue/TiO_2 HMA	2.372	2.483	4.5
1%/3% Red/TiO_2 HMA	2.366	2.483	4.7

8.5.2 Moisture Susceptibility

The moisture resistance of all HMA mixtures were determined through tensile strength ratio and stripping observed in the conditioned specimens. The results of TSR averaged from three replicates and stripping scale are summarized in Table. 8.8. The stripping scale was observed as 1. According to the ASTM D4867 standard, the minimum permissible tensile strength ratio

(TSR) should be 80% in order to have an asphalt mixture that possesses sufficient resistance to moisture and water-related damage. As can be seen from Table 8.8, most of the HMA mixtures possess satisfied TSR values except the mixture containing 6% red thermochromic powders. Additionally, compared to 6% black, blue and red HMA mixtures, the asphalt mixture containing nano-TiO_2 is found to show higher TSR values. This indicates the addition of nano-TiO_2 improve the resistance of HMA mixtures to moisture damage.

Table 8.14. Tensile strength ratio test results of HMA mixtures.

Sample	Unconditioned indirect tensile strength (MPa)	Conditioned indirect tensile strength (MPa)	TSR (%)	Stripping scale (0-5 scale)
6% Black HMA	0.75	0.61	81.4	1
6% Blue HMA	0.99	0.79	80.2	1
6% Red HMA	0.81	0.62	75.7	1
1%/3% Black/TiO_2 HMA	0.97	0.83	85.1	1
1%/3% Blue/TiO_2 HMA	0.92	0.73	80.0	1
1%/3% Red/TiO_2 HMA	0.93	0.80	85.8	1

8.5.3 Rutting Resistance

The results of the rutting resistance of the HMA mixtures using APA tests are plotted in Fig. 8.6. The figure shows that the rutting depth at 8000 cycles is 5.29 mm, 3.22 mm, 4.58 mm, 4.04 mm, 4.05 mm, and 2.73 mm for 6% black HMA, 6% blue HMA, 6% red HMA, 1%/3% black/TiO_2 HMA, 1%/3% blue/TiO_2 HMA, and 1%/3% red/TiO_2 HMA sample., respectively. Most of them satisfy the maximum specification limit for permanent deformation, which is 5 mm specified in

Ohio DOT. Additionally, it can be observed that the use of nano-TiO$_2$ powders increases the resistance to rutting or permanent deformation of asphalt mixture.
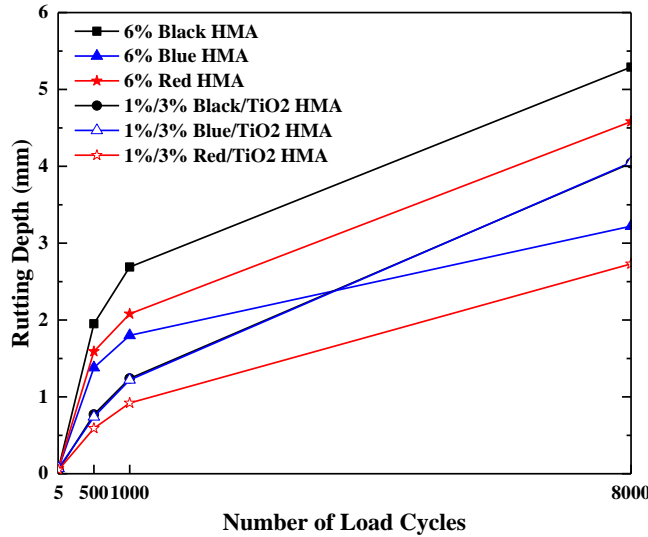
Figure 8.16. Rutting depth of the HMA over 8000 loading cycles.

8.5.4 Optical Reflectance

The results from the spectrophotometric measurements of all HMA mixtures at room temperature are presented in Figs. 8. 7-8.9. The figure 8.7 displays the reflection spectra of original asphalt binder and various HMA mixtures. It can be seen that compared to original asphalt binder, the asphalt mixture containing aggregates, thermochromic materials and/or nano-TiO$_2$ present higher solar reflectance, especially in the infrared range of the spectrum. Additionally, the addition of thermochromic powders considerably increases the reflection of the HMA to solar radiation. Furthermore, the combination of thermochromic and nano-TiO$_2$ relatively enhances the reflectance of the HMA mixtures.

The total solar reflectance values in the range of 800-1800 nm were calculated according to Eq. 8-5 and were summarized in Table 8.9. As seen in Table 8.9, the solar reflectance value is 4.2%, 6.9%, 10.3%, 9.6%, 8.1%, 7.7%, 7.6%, and 8.4% for original asphalt binder, control HMA, 6% black HMA, 6% blue HMA, 6% red HMA, 1%/3% black/TiO_2 HMA, 1%/3% blue/TiO_2 HMA, and 1%/3% red/TiO2 HMA sample, respectively. It can be found that compared to original asphalt binder, the solar reflectance is increased by 64%, 145%, 129%, 93%, 83%, 81%, and 100% by adding 94.2% aggregate, 6% black, 5% blue, 6% red, 1%/3% black/TiO_2, 1%/3% blue/TiO_2, and 1%/3% red/TiO_2 powders, respectively. Compared to control HMA mixture, the use of 6% thermochromic powder increases the solar reflectance by 17-49%, whereas the combination of 1% thermochromic powder and 3% nano-TiO_2 increases the value by 10-22%.
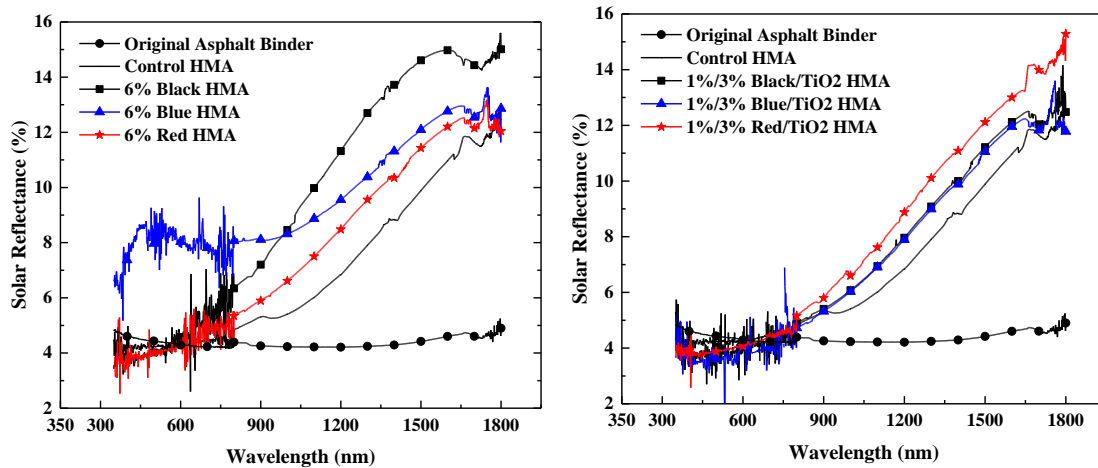
Figure 8.17. Reflection spectra of original HMA samples.

Table 8.15. Solar reflectance (%) on original surface, exposed aggregate surface, and rutted surface of HMA mixtures in the range of 800-1800 nm.

Sample	Original surface	Compared to control	Compared to original	Exposed aggregat	Compared to original	Rutted surface	Compared to original

	HMA (%)	surface (%)	e surface	surface (%)			surface (%)
Original asphalt binder	4.2	-			-	-	-	-
Control HMA	6.9	-	64		-	-	-	-
6% Black HMA	10.3	49	145	24.6	138	7.7	-25
6% Blue HMA	9.6	39	129	25.5	166	7.7	-20
6% Red HMA	8.1	17	93	25.1	210	6.0	-26
1%/3% Black/TiO$_2$ HMA	7.7	12	83	23.7	208	5.6	-27
1%/3% Blue/TiO$_2$ HMA	7.6	10	81	22.2	192	6.3	-17
1%/3% Red/TiO$_2$ HMA	8.4	22	100	22.8	171	7.5	-11

Fig. 8.8 illustrates the reflection spectra on exposed aggregate surfaces of HMA mixtures. It can be found that the reflection is approximately close for all mixtures because of the same content of aggregate in asphalt mixture. The total solar reflectance value, shown in Table 9, is between 22.2% and 25.5% in the near infrared spectrum for the mixtures containing thermochromic and nano-TiO$_2$ powders. This means after long-term pavement/tire interaction, the exposed aggregate increases the solar reflectance of the HMA mixture up to 210% compared to the original asphalt mixture. This is attributed to the light color and thus high solar reflection of aggregate.
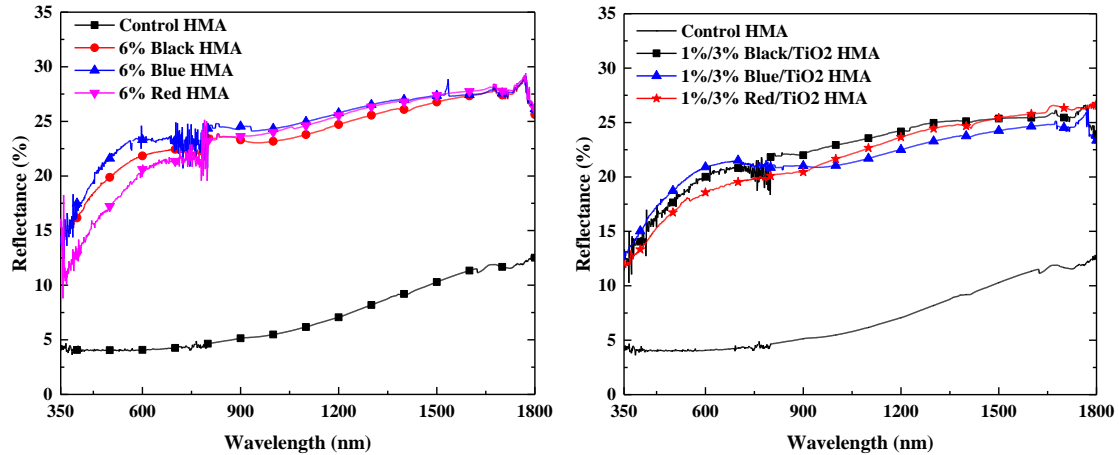
Figure 8.18. Reflection spectra on exposed aggregate surfaces of HMA samples.

Fig. 8.9 presents the comparison of reflection spectra between original surface and rutted surface of the HMA mixture after APA tests. It can be seen after APA testing, the reflection of the rutted surface is reduced in the infrared range compared to original surface of the HMA mixtures. As seen from Table 8.9, the solar reflectance value of rutted surface is 7.7%, 7.7%, 6.0%, 5.6%, 6.3%, and 7.5% for 6% black HMA, 6% blue HMA, 6% red HMA, 1%/3% black/TiO$_2$ HMA, 1%/3% blue/TiO$_2$ HMA, and 1%/3% red/TiO$_2$ HMA sample, respectively. Compared to the original surface, the solar reflectance of rutted surface is correspondingly reduced by 25%, 20%, 26%, 27%, 17%, and 11%, respectively. The considerable reduction in solar reflectance might be attributed to multiple absorption of the diffused light from the rutted surface of the HMA samples, as shown in Fig. 8.10. It is therefore expected that the higher the rutting depth, the lower the total solar reflectance after APA tests. According to Figs. 8.6 and 8.9, the corporation of nano-TiO$_2$ into asphalt mixture enhances the resistance to high temperature deformation and sustain higher solar reflection after long-term traffic loading.
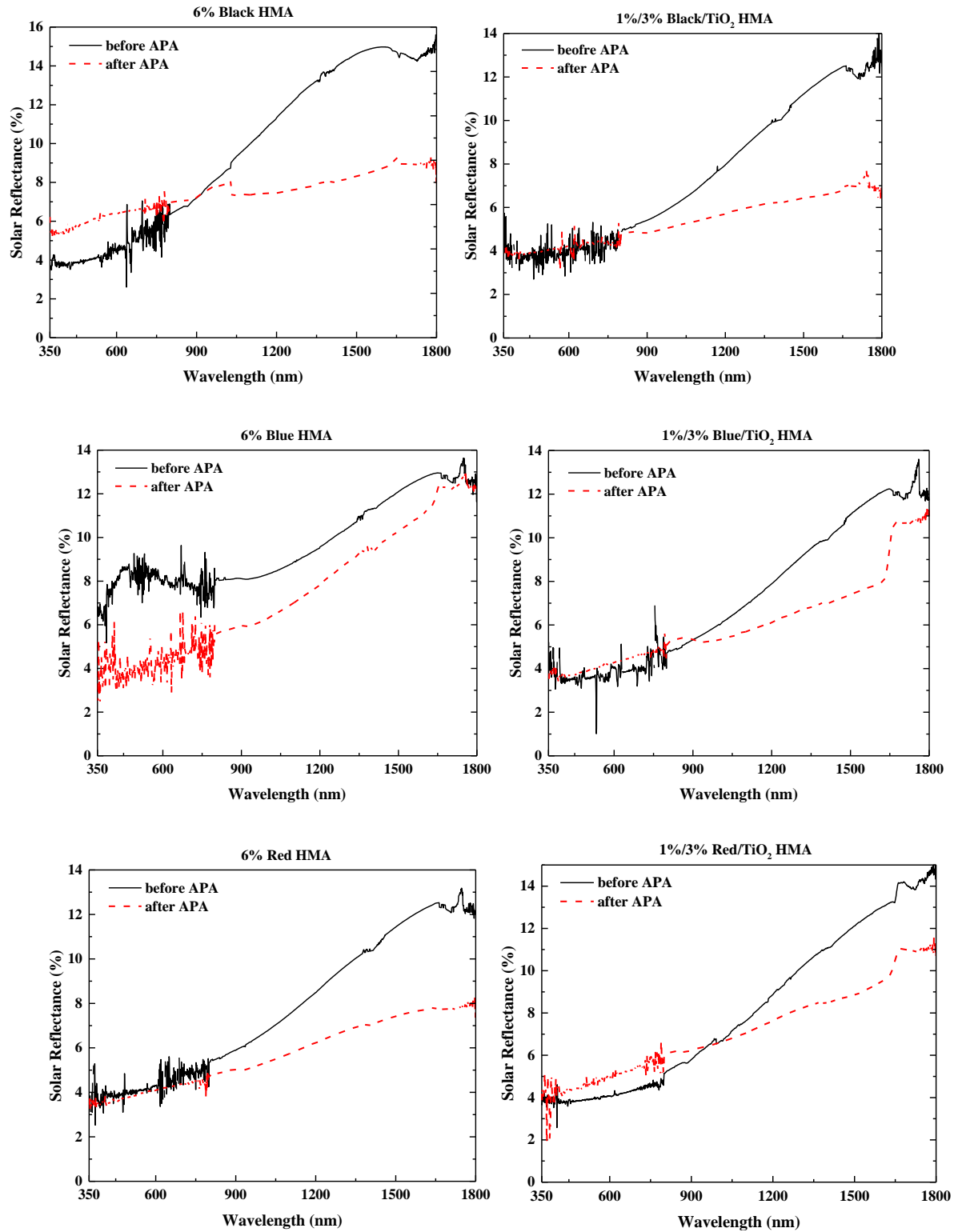
Figure 8.19. Comparison of reflection spectra between original and rutted HMA mixtures.
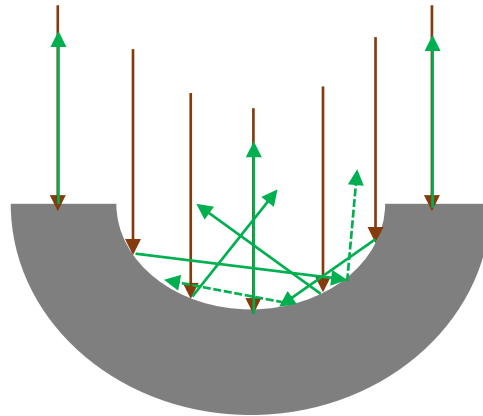
Figure 8.20. Diffusion of light on the rough surface.

8.6 Conclusions and Recommendations

The aim of this study is to design and experimentally evaluate asphalt mixture containing different content of thermochromic and nano-TiO_2 powders. Through laboratory experiments above, the main conclusions are as follows:

1) The asphalt mixtures containing thermochromic powder and nano-TiO_2 were prepared based on Superpave method. The void content of asphalt mixture is around 4.7% with 6% black, blue, and red thermochromic powders and between 4.5%-5.1% with 1% thermochromic powder and 3% nano-TiO_2.

2) The use of 6% red thermochromic powder reduces the moisture resistance of asphalt mixture in terms of indirect tensile strength. The addition of 3% nano-TiO_2 powder improves the resistance of asphalt mixture to moisture damage.

3) The incorporation of 6% black thermochromic powder reduces the rutting resistance of asphalt mixture. The presence of nano-TiO_2 powder increases the resistance of asphalt mixture to rutting or permanent deformation.

177

4) The addition of 6% thermochromic powder increases the solar reflectance in the infrared range from 17% to 49%, whereas the use of 3% nano-TiO_2 increases the value from 10% to 22%. After APA testing, the asphalt mixture containing 6% blue thermochromic powder, 1%/3% blue/TiO_2, and 1%/3% red/TiO_2 powders keeps relatively higher solar reflectance. Additionally, the exposed aggregate surface of all HMA mixtures features considerably high reflectance of around 23%.

Based on these findings, it is recommended to add 6% blue thermochromic powder, 1%/3% blue/TiO_2 powders, and 1%/3% red/TiO_2 powders in asphalt mixture, which has been demonstrated to improve both resistance to moisture damage and high temperature deformation as well as stability of solar reflectance.

CHAPTER NINE

SUMMARY, CONCLUSIONS, AND FUTURE WORK

9.1 Summary and Conclusions

This report consisted of four major components: 1) review of thermochromism and common types of thermochromic materials; 2) preliminary analyses of material production and performance evaluation of thermochromic asphalt binder; 3) advanced characterization of thermochromic asphalt binder in the areas of multifunctional properties (optical, thermal, mechanical properties); and 4) evaluation of performance of thermochromic binder under extended outdoor exposure.

9.1.1   Review of thermochromism and thermochromic materials

Comprehensive literature review was conducted to identify the common types of thermochromic mechanism as well as common types of thermochromic materials. Common types of applications of thermochromic materials in different industries are identified. In particular, the literature review focuses on identifying technologies that have potentials for applications in asphalt. Polymeric thermochromic materials, which feature excellent compatibility with asphalt, are identified. The advantages and limitations of different thermochromisms for applications in asphalt are discussed.

9.1.2   Preliminary analyses of material production and performance evaluation of thermochromic asphalt binder

Activities in this area developed production procedures to introduce thermochromic materials into asphalt binder. Properties of the produce samples were characterized with DSC and other techniques. The performance of the thermochromic binder materials in modulating the surface temperature of pavement were compared with those of the regular asphalt binder. Comparison measurements found that the surface temperature of thermochromic asphalt binder is lower than that of the conventional asphalt binder with maximum decrease as high as 6.6°C during typical

summer day in the northeast U.S. (i.e. Cleveland, OH). Furthermore, experimental results indicated that the temperature dropped slower in thermochromic asphalts than in regular asphalt when subjected to simulated winter temperature. This implies that thermochromic asphalt can delay ice formation on the surface of road than traditional asphalt, which is an important potential benefit for road safety in cold regions such as in Ohio. The preliminary study demonstrated the potential of thermoelectric asphalt and set the tone for further investigations.

9.1.3 Advanced Characterization of Multifunctional Properties of Thermochromic Asphalt Binder

Multifunctional characterizations were conducted to measure the properties of thermochromic asphalt binders to understand the basis of its performance, characterize its mechanical durability, and recommend the production parameters.

Optical properties: The optical reflectance of thermochromic binder was characterized with spectral reflectance measurement. Measurement results indicate that thermochromic materials feature more reflection at higher temperature and more absorption at lower temperature. The spectral reflectance of thermochromic powders as functions of wavelength and temperature are proposed by fitting experimental results. Optical measurements conducted on the asphalt binder mixture show more reflection than conventional asphalt binder and besides, the solar reflectance also increases with temperature. These are desirable for dynamically modulating the surface temperature of pavements.

Thermal properties: The kinetic behaviors of thermochromic asphalt were characterized with thermal analytic instruments such as TGA. The goal is to determine the production parameters for thermochromic asphalt. The pyrolytic and kinetic behaviors are important for setting the optimal plant production parameters (i.e., mixing temperature and duration) of thermochromic asphalt binders. The results indicate that the mass loss of thermochromic binders are less than 5% when subjected to 200°C for 2 hours. Although the rate of mass losses of asphalt binder is increased, the activation energy of asphalt binder is also increased after adding thermochromic materials, indicating less susceptibility of viscosity of asphalt binder to temperature. No strong chemical interactions occur between thermochromic powders and binder matrix. Heat treatment

180

is found to reduce the solar reflectance of thermochromic binders with the effects depending upon the exposure duration. Considering both the pyrolysis characteristics (mass loss) and the performance of solar (infrared) reflectance, the production parameters (temperature and mixing duration) for the thermochromic asphalt binders are determined.

Mechanical properties: The mechanical properties of thermochromic asphalt binder are studied via the Superpave binder performance tests. Experiments were conducted on asphalt binders at three stages: unaged, rolling thin film oven (RTFO) residues, and RTFO + pressure aging vessel residuals. Experimental results indicated that the penetration, phase angle and creep rate of asphalt binder was decreased, while the softening point, viscosity, complex modulus, rutting parameter, fatigue parameter and stiffness of asphalt binder was increased when thermochromic powder were added into conventional asphalt binder. Furthermore, increasing the content of thermochromic powder leads to reduction in the penetration depth and creep rate, and increase of softening point, viscosity, complex shear modulus, rutting parameter, fatigue parameter and stiffness. The percentages of thermochromic powders that improve the high temperature performance grades of asphalt binder were determined. Overall, incorporation of thermochromic materials into asphalt pavement will potentially improve its performance and durability, especially in hot regions.

9.1.4 Evaluation of performance of thermochromic binder under extended outdoor exposure.

Research activities evaluated the performance of thermochromic asphalt binder on modulating the surface temperatures of pavement to assess its durability and sustainability. Comparison studies were performed that include the outdoor thermal performance of conventional asphalt concrete and different types of thermochromic asphalt concrete. The comparison study operated through spring and summer 2014. The results show that the surface temperature of thermochromic asphalt concrete was cooler than conventional asphalt concrete under hot summer conditions up to 6°C, 6.2°C and 3.6°C and warmer during the evening up to 0.4°C, 1.7°C and 1.8°C by using black, blue and red thermochromic materials, respectively. Besides, the temperature fluctuation of asphalt concrete was found to be reduced up to 5°C, 4°C and 3°C by using black, blue and red thermochromic materials, respectively. Furthermore, compared to

conventional asphalt concrete, thermochromic asphalt concrete reduced the rate of heating and cooling. These demonstrate the potential of thermochromic asphalt concrete to improve the durability of the pavement, reduce the environmental impacts, and mitigate ice related safety issues on the road. These are desirable for the development of sustainable and environmental benign infrastructure.

9.1.5   Volumetrics and Performance of Thermochromic HMA

HMA volumetrics design and performance evaluatation were conducted with thermochromic asphalt binder. The asphalt mixtures containing thermochromic powder and nano-TiO_2 were prepared based on Superpave method. The resistance to moisture and rutting of various thermochromic asphalt mixtures satisfied the specification required performance. Furthermore, the addition of nano-TiO_2 powder was found to increase the resistance of asphalt mixture to rutting or permanent deformation. For example, the addition of 6% thermochromic powder increased the solar reflectance in the infrared range from 17% to 49%, whereas the use of 3% nano-TiO_2 increased the value from 10% to 22%. Moreover, the asphalt mixture containing 6% blue thermochromic powder, 1%/3% blue/TiO_2, and 1%/3% red/TiO_2 powders sustained relatively higher solar reflectance after rutting tests. Additionally, the exposed aggregate surface of all HMA mixtures featured considerably high reflectance of around 23%. Recommendations were provided to improve both resistance to moisture damage and high temperature deformation as well as stability of solar reflectance, all of which would lead to longer durability pavement.

9.2 Recommendation for Further Development of the Technology

The research activities so far have conducted comprehensive laboratory characterization of thermochromic asphalt binder. The performance has also been preliminarily evaluated with small scale outdoor testing program. It is recommended that field scale test section be constructed to further evaluate the performance of thermochromic asphalt concrete. This can be achieved via a public private partnership that involve university, Ohio DOT and private industry. Contrast sections can be built with thermochromic HMA as well as ordinary asphalt concrete. A field monitoring program would be implemented to monitor the temperature variation across the pavement layer. The range of temperatures and rate of change of dye modified asphalt concrete

can provide comparison with conventional un-modified asphalt pavement. This will quantify the effectiveness of thermochromic asphalt to positively modulate the surface temperature of pavements.

It is also recommended to develop guidelines for material selection, field construction and maintenance based on the experience from field testing program, guidelines will be developed for materials selection and field construction.